Calcium signalling and differentiation in neuroblastoma cells

Natalie Bell

Thesis submitted for the degree of Doctor of Philosophy

Institute for Cell and Molecular Biosciences
Faculty of Medical Sciences
Newcastle University

September 2011

Abstract

Neuroblastoma is a cancer of the sympathetic nervous system derived from neural crest cells that fail to differentiate during development. Neuroblastoma tumours and cell lines are heterogeneous, comprised of 'neuroblastic' N-type cells, precursors to a neuronal neural crest cell lineage and 'substrate-adherent' S-type cells, precursors to a non-neuronal neural crest cell lineage. Retinoids, such as retinoic acid (RA), cause both N- and S-type cells to switch from proliferation to differentiation. This underlies the use of RA in the treatment of neuroblastoma disease. The aim of this study was to investigate the role of Ca^{2+} signalling in the process of differentiation.

N- and S-type cell populations were enriched from the SH-SY5Y neuroblastoma cell line to allow characterisation of Ca^{2+} signalling and differentiation within the two cell phenotypes. The RA-induced switch from proliferation to differentiation was accompanied by a down-regulation in store-operated Ca^{2+} entry (SOCE) in N-type cells but not in S-type cells. In N-type cells expression of the ER Ca^{2+} sensor protein STIM1 and the channel protein Orai1 also became down-regulated, whilst expression of the channel protein TRPC1 became up-regulated. Knockdown of STIM1 and Orai1 in proliferating N-type cells down-regulated SOCE. Knockdown of Orai1, but not STIM1, induced differentiation and also enhanced differentiation induced by RA. Overexpression of STIM1 and Orai1 in RA-differentiated cells restored SOCE and reduced the extent of differentiation. Knockdown of TRPC1 had no effect on SOCE or differentiation in proliferating N-type cells but reduced the extent of SOCE down-regulation and differentiation induced by RA. These observations suggest that Orai1 may be a negative regulator of differentiation in N-type cells whereas STIM1 down-regulation may be required to maintain the differentiated state. TRPC1 expression may be required for a fully functional differentiated phenotype. These proteins could represent putative drug targets in the multi-modal treatment of neuroblastoma disease.

Acknowledgements

I would like to thank my supervisor Dr Tim Cheek for his help and support during my PhD. Thanks also to my second supervisor Dr Chris Redfern.

I would also like to thank Dr Victoria Hann for her support throughout my PhD. Thanks for teaching me the techniques in the lab, for guidance in the overall plan of my work and being there to help sort out any problems I had on the way.

Thank you also to Alison Gregory and Maureen Sinclair for their assistance with cell culture.

This work was funded by a BBSRC studentship.

Table of Contents

List of Figures

List of Tables

List of Abbreviations

9*c*RA	9-*cis*-retinoic acid
13*c*RA	13-*cis*-retinoic acid
ANOVA	Analysis of variance
ARC	Arachidonate-regulated Ca^{2+}-selective channels
ATRA	all-*trans*-retinoic acid
BSA	Bovine serum albumin
$[Ca^{2+}]_i$	Intracellular free Ca^{2+} concentration
CC	Coiled-coil
CCE	Capacitative Ca^{2+} entry
CICR	Ca^{2+}-induced Ca^{2+} release
CRABPs	Cytosolic retinoic acid-binding proteins
CRACM1	Ca^{2+} release-activated Ca^{2+} modulator 1 (also known as **Orai1**)
DAG	Diacylglycerol
DIC	Differential interference contrast
DMEM	Dulbecco's Modified Eagle's Medium
DMSO	Dimethyl sulfoxide
EDTA	Ethylenediaminetetraacetic acid
ER	Endoplasmic reticulum
ERM	Ezrin-radixin-moesin
EthD-1	Ethidium homodimer-1
EtOH	Ethanol
Fura-2/AM	Fura-2 acetoxymethyl
HRP	Horseradish peroxidise
I_{ARC}	Arachidonate-regulated Ca^{2+}-selective current
I_{CRAC}	Ca^{2+} release-activated Ca^{2+} current
IP_3	Inositol 1,4,5-trisphosphate
IP_3Rs	Inositol 1,4,5-trisphosphate receptors
I_{SOC}	Store-operated Ca^{2+} current
LRDs	Lipid raft domains
mRNA	messenger RNA
NAADP	Nicotinic acid adenine dinucleotide phosphate
NF	Neurofilament

Non-SOCE	Non-store-operated Ca^{2+} entry
O/E	Overexpressed
Opti-MEM	Opti-Modified Eagle's Medium
PBS	Phosphate buffered saline
PIP_2	Phosphatidyl inositol 4,5-bisphosphate
PKC	Protein kinase C
PLC	Phospholipase C
PM	Plasma membrane
PMCA	Plasma membrane Ca^{2+}-ATPase
RA	Retinoic acid
RAREs	Retinoic acid response elements
RARs	Retinoic acid receptors
RISC	RNA induced silencing complex
ROC	Receptor-operated Ca^{2+} channel
RT	Room temperature
RXRs	Retinoid X receptors
RYRs	Ryanodine receptors
SAM	Sterile α-motif
SCID	Severe combined immunodeficiency disorder
SDS-PAGE	Sodium dodecyl sulphate-polyacrylamide gel electrophoresis
SEM	Standard error of the mean
SERCA	Sarco/endoplasmic reticulum Ca^{2+}-ATPase
siRNA	small interfering RNA
SNS	Sympathetic nervous system
SOC	Store-operated Ca^{2+} channel
SOCE	Store-operated Ca^{2+} entry
SR	Sarcoplasmic reticulum
STIM1	Stromal-interaction molecule 1
TG	Thapsigargin
TPCs	Two-pore channels
TRPC1	Transient receptor potential channel 1 (canonical)
VOC	Voltage-operated Ca^{2+} channel

Chapter 1
Introduction

1.1 Neuroblastoma

Neuroblastoma is a cancer of the sympathetic nervous system (SNS) derived from cells of the neural crest (Brodeur *et al*., 1997; Goodman *et al*., 1999). Neuroblastoma is the most common cancer in infancy (Gurney *et al*., 1999) and accounts for 15% of all paediatric oncology deaths (Maris *et al*., 2007). 90% of neuroblastoma cases are diagnosed in patients under the age of 5 (Maris *et al*., 2007).

In the developing embryo neural crest cells migrate and separate into several distinct cell lineages (Ciccarone *et al*., 1989; Ross *et al*., 2003; Nakagawara *et al*., 2004; Walton *et al*., 2004). The sympathoadrenal cell lineage of the neural crest gives rise to sympathetic neurones of the SNS and neuroendocrine chromaffin cells of the adrenal medulla (Ciccarone *et al*., 1989). In neuroblastoma, for unknown reasons, cells derived from the sympathoadrenal cell lineage fail to differentiate. Tumours predominantly consist of immature nerve cells (i.e. neuroblasts) and are most commonly found in the adrenal gland, though they can also be found in the nerve tissues of the spine, chest, neck and pelvis (Ishola *et al*., 2007).

One of the most significant prognostic factors in neuroblastoma is age. The 5-year survival rate from diagnosis in infants (under the age of 1) is 83%, in patients 1-4 years old is 55% and in patients aged 5 years and above is 40% (Goodman *et al*., 1999). Neuroblastoma is unique as advanced metastatic disease can spontaneously regress or mature into benign ganglioneuromas, particularly in infants (Brodeur, 1995).

50% of neuroblastoma patients are classed as high-risk (Maris *et al*., 2007). The 5-year survival rate for high-risk patients is only ~30% (Cotterill *et al*., 2001; Mertens *et al*., 2001). High-risk patients may receive chemotherapy with the retinoid 13-*cis*-retinoic acid (Matthay *et al*., 1999, 2009). RA treatment of neuroblastoma induces differentiation and inhibits proliferation (Sidell, 1982). This effect underlies the use of RA in the treatment of neuroblastoma today (Matthay *et al*., 1999, 2009; Reynolds *et al*., 2003).

1.2 Heterogeneity in neuroblastoma tumours and cell lines

Cellular heterogeneity is a characteristic of both neuroblastoma tumours and their derived cell lines (Biedler *et al*., 1973, 1975; Ross *et al*., 1983, 1995, 2003, 2007; Ciccarone *et al*., 1989; Walton *et al*., 2004). Three morphologically and biochemically distinct cellular phenotypes have been identified; these are N-type, S-type and I-type cells (Ciccarone *et al*., 1989; Ross *et al*., 1995, 2003).

The 'neuroblastic' N-type cells have small round cell bodies, scant cytoplasm and several short neuritic like processes. They are weakly substrate adherent in culture and attach better to each other than to substrate and therefore form cell aggregates (pseudoganglia) (Biedler *et al*., 1973; Walton *et al*., 2004). The N-type cells display neuronal properties such as expression of neurotransmitter enzymes (Biedler et al., 1973, 1978; Ross *et al*., 1983), catecholamine uptake and the presence of neurofilament proteins (Ciccarone *et al*., 1989). They also display neuroendocrine properties as they contain chromogranin A which is characteristic of adrenal medulla cells (Ciccarone *et al*., 1989; Ross *et al*., 2003). The presence of neuronal and neuroendocrine properties is consistent with the concept that N-type cells are multipotent precursor cells of the sympathoadrenal cell lineage of the neural crest (Ross *et al*., 1995, 2003, 2007). In culture N-type cell lines have been described as 'immortal' (Ciccarone *et al*., 1989).

The 'substrate-adherent' S-type cells, originally named E-type for epithelial-like (Biedler *et al*., 1975), are larger and more flattened in appearance with abundant cytoplasm and no neuritic processes. These cells are strongly substrate adherent and show contact inhibition of growth and therefore grow as monolayers (Biedler *et al*., 1973; Walton *et al*., 2004). S-type cells do not display neuronal properties and instead display properties of glial cells, Schwann cells and melanocytes (Ciccarone *et al*., 1989; Ross *et al*., 1995). The presence of tyrosinase is indicative of melanocytes; stromal collagen of glial and Schwann cells and fibronectin and vimentin of all three (Ciccarone *et al*., 1989). The S-type cells display properties of a number of different cell types which is consistent with the concept that they are multipotent precursor cells of a non-neuronal neural crest cell lineage (Ross *et al*., 1995). In culture S-type cells appear to have a limited lifespan and begin to grow extremely slowly and/or stop proliferating (Ciccarone *et al*., 1989; Ross *et al*., 2007).

The ‘intermediate’ I-type cells are intermediate with respect to N- and S-type cells, displaying morphological and biochemical features of both cell phenotypes (Ciccarone *et al*., 1989; Ross *et al*., 1995). As such I-type cells are more difficult to identify and were not identified until over ten years later than N- and S-type cells (Cicarrone *et al*., 1989). I-type cells are small in appearance, may or may not have neuritic processes and have intermediate levels of cytoplasm. They are moderately substrate adherent and grow as multilayers that are able to form cell aggregates (Walton *et al*., 2004).

I-type cells have been hypothesised to be a cancer stem cell as they display the property of self renewal and are potentially progenitors of the N- and S- cell phenotypes as they express both N- and S- markers (Ross *et al*., 1995). I-type cells would therefore have the capacity to give rise to at least two distinct neural crest cell lineages. In contrast N- and S-type cells, although multipotent, appear to be committed to a specific cell lineage of the neural crest (Ross *et al*., 2007). I-type cells could also represent an intermediate stage in the transdifferentiation process between N- and S-type cells. N- and S-type cells can also transdifferentiate into one another without an intermediate (Ross *et al*., 1983, 2003, 2007; Ciccarone *et al*., 1989) (Figure 1.1).

It has been shown that there is a strong correlation between cell phenotype and malignant potential (Piacentini *et al*., 1996; Matthay *et al*., 1999). The N-type cell line SH-SY5Y has a tumour frequency of 22% in athymic mice while the S-type cell line SH-EP1 has a tumour frequency of 0%. In contrast the I-type cell line BE-2-M17 has a tumour frequency of 81% and therefore displays the greatest malignant potential. This is consistent with the hypothesis that I-type cells are cancer stem cells (Ross *et al*., 2003). It has also been shown that aggressive tumours have higher levels of I-type cells (Walton *et al*., 2004).

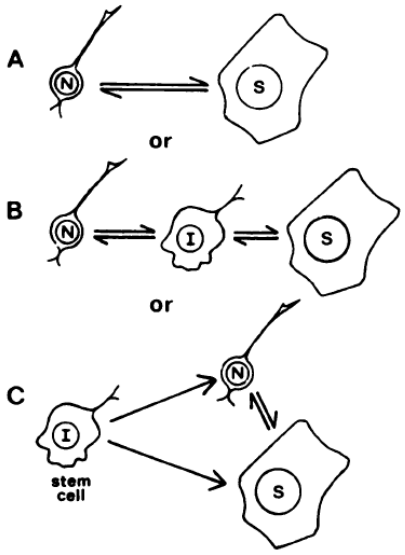

Figure 1.1 Transdifferentiation between cell phenotypes (Ciccarone *et al*, 1989)

Three possible models explaining the process of cellular transdifferentiation as proposed by Ciccarone *et al*., 1989. **A)** N- and S-type cells transdifferentiate into one another directly (as shown by Ross *et al*., 1983). **B)** N- and S-type cells transdifferentiate into one another via a transient intermediate, the I-type cell. **C)** I-type cells are progenitors of both N- and S-type cells and N- and S-type cells can transdifferentiate into one another directly.

1.3 The SH-SY5Y neuroblastoma cell line

The SK-N-SH neuroblastoma cell line was established in 1970 from a bone marrow aspiration of a 4 year old female with metastatic neuroblastoma (Biedler *et al*., 1973). The SK-N-SH cell line is comprised of N- and S-type cells (Biedler *et al*., 1973) and was thrice cloned (SH-SY, SH-SY5, SH-SY5Y) to produce the N-type neuroblastoma cell line SH-SY5Y (Biedler *et al*., 1975; Ross *et al*., 1983). Evidence of the neuronal origin of N-type cells is that cells express tyrosine hydroxylase and dopamine-*β*-hydroxylase activity, enzymes that are specific to noradrenergic neurons (Ross *et al*., 1983). Although predominately composed of N-type cells, the SH-SY5Y cell line remains heterogeneous in nature as N-type cells are able to give rise to S-type cells (Biedler *et al*., 1975; Ross *et al*., 1983). Neuroblastoma cell lines have been identified as prime cell lines for the study of neuronal differentiation (Abemayor & Sidell, 1989). The SH-SY5Y cell line was used in the study of Ca^{2+} signalling and RA-induced differentiation in this thesis.

1.4 Differentiation

In 1982 Sidell first reported that the retinoid, all-*trans*-retinoic acid (ATRA), could induce growth arrest and differentiation in human neuroblastoma cells. The ability of RA to inhibit proliferation and induce differentiation of neuroblastoma cells underlies the use of retinoids in the treatment of high-risk neuroblastoma patients (Matthay, 1999).

1.4.1 Retinoic acid

Vitamin A (retinol) and its derivatives (retinoic acid) play an important role in the regulation of many biological processes, including differentiation, growth, vision, and gene transcription (Niles, 2000). RA plays a prominent role in regulating the transition of cells from proliferation to differentiation (Reynolds, 2000, 2003). Several naturally occurring RA isoforms exist; ATRA, 13-*cis*-retinoic acid (13*c*RA) and 9-*cis*-retinoic acid (9*c*RA) (Lovat *et al*., 1994, 1997a, 1997b; Miller *et al*., 1998) (Figure 1.2).

RA works by binding to two families of retinoid receptor; the retinoic acid receptors (RARs) and the retinoid X receptors (RXRs), each family has an α, β and γ isoform (Miller *et al*., 1998; Ponthan *et al*., 2001). Receptors are members of the steroid/thyroid family of receptors and are located within the cell nucleus (Reynolds *et al*., 2003). RA is transported to the cell nucleus via cytoplasmic retinoic acid-binding proteins (CRABPs). ATRA, 13*c*RA and 9*c*RA all bind to RARs whereas only 9*c*RA can bind to RXRs (Redfern *et al*., 1995). Binding of RA to RARs and RXRs activates the receptors which form heterodimers that bind to regions of the chromosome known as retinoic acid response elements (RAREs). RAREs are linked to RA responsive genes and binding of these regions allows regulation of gene transcription thus enabling RA to regulate biological processes such as differentiation (Reynolds *et al*., 2003).

In vitro RA has been shown to induce differentiation of the immature neuroblastic cells that form the bulk of most tumours into a mature non-proliferating neuronal phenotype (Lovat *et al*., 1994, 1997a, 1997b; Miller *et al*., 1998; Matthay *et al*., 1999; Reynolds *et al*., 2003). Clinical trials therefore began integrating RA as a part of the treatment process for high-risk patients (Matthay *et al*., 1999, 2009). The 13*c*RA isomer is used in

the treatment of high-risk neuroblastoma patients due to the lower levels of toxicity it displays in comparison to the other retinoids (Lovat *et al*., 1997a; Ponthan *et al*., 2001). 13*c*RA has a very low affinity for RAR receptors but in vivo isomerises to ATRA, which is thought to be the main biologically active isomer (Redfern *et al*., 1994; Lovat *et al*., 1997a). 9*c*RA has been shown to be the most effective isoform for the induction of cellular differentiation and inhibition of proliferation which may be attributed to its differential binding of RXR receptors (Lovat *et al*., 1997a; Miller *et al*., 1998; Ponthan *et al*., 2001). Although 9*c*RA would appear to be more effective for neuroblastoma treatment the levels of toxicity it displays are too high for use in a clinical setting (Ponthan *et al*., 2001).

13*c*RA is currently only used as a treatment option for high-risk neuroblastoma patients (Matthay *et al*., 1999, 2009). These patients have already gone through intensive treatments including surgery, chemotherapy, radiotherapy and/or bone marrow transplants (Matthay *et al*., 1999). Although tumour responsiveness to RA treatment was less than anticipated (Lovat *et al*., 1997a, 1997b), a significant increase in 3-year event-free survival was observed in patients administered 13*c*RA (46±6%) following primary treatment (autologous bone marrow transplantation or chemotherapy) compared to patients who were not (29±5 %) (Matthay *et al*., 1999) (Figure 1.3). The results have since been followed up and show that overall survival was significantly higher for patients administered 13*c*RA than for those who were not (Matthay *et al*., 2009).

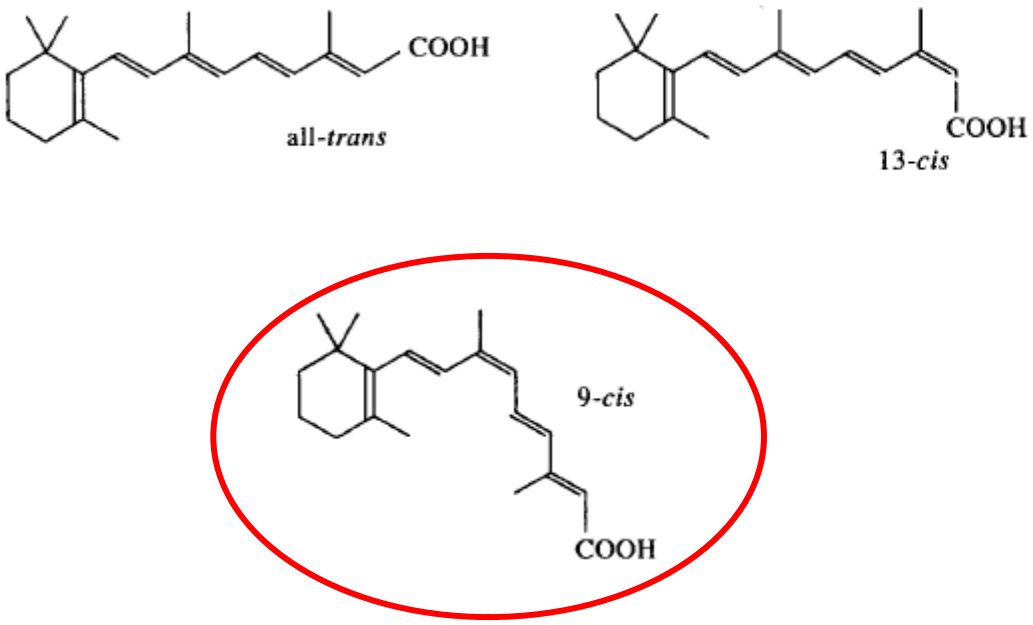

Figure 1.2 RA exists in several naturally occurring isoforms (adapted from Redfern *et al*., 1994)

RA exists in several naturally occurring isoforms; all-*trans* (ATRA), 9-*cis* (9*c*RA) and 13-*cis* (13*c*RA) isomers being the most widely studied. The 9*c*RA isoform was used to induce neuronal differentiation of SH-SY5Y neuroblastoma cells in this thesis.

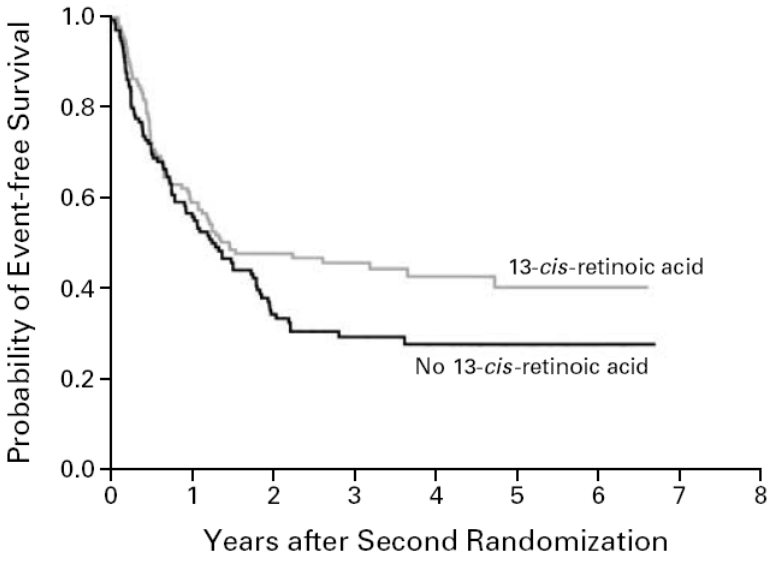

Figure 1.3 Treatment with 13*c*RA (Matthay *et al.*, 1999)

The 3-year event-free survival probability for high-risk neuroblastoma patients was significantly higher in patients who received 13*c*RA treatment compared to those who did not, P=0.027. The first randomisation was whether the patients received continuation chemotherapy or bone marrow transplantation. The second randomisation was whether or not patients received 13*c*RA treatment.

1.4.2 Bcl-2

The proto-oncogene Bcl-2 is expressed throughout the nervous system, particularly in sympathetic and sensory neurones (Garcia *et al*., 1992; Merry *et al*., 1994). As a cancer of the SNS, cells from neuroblastoma tumours express Bcl-2 (Hanada *et al*., 1993; Lasorella *et al*., 1995). The level of Bcl-2 expression in neuroblastoma cell lines is related to how neuronal the cell line is. For example, the N-type neuroblastoma cell line SH-SY5Y expresses high levels of Bcl-2 whereas the S-type neuroblastoma cell line SH-EP has no detectable Bcl-2 expression. SK-N-SH, the parental cell line of SH-SY5Y and SH-EP, comprised of both N- and S-type cells shows intermediate levels of Bcl-2 expression (Reed *et al*., 1991). Furthermore, RA-induced differentiation of SH-SY5Y cells is associated with a further increase in Bcl-2 expression as the cells become more neuronal-like (Hanada *et al*., 1993; Lasorella *et al*., 1995; Riddoch *et al*., 2007). It is unknown whether changes in Bcl-2 expression are due to the direct action of RA or to neuronal differentiation itself. However, as Bcl-2 expression correlates with neuronal phenotype Bcl-2 was considered as a biochemical marker of differentiation in this thesis.

Cells expressing high levels of Bcl-2 are more resistant to apoptosis in response to cytotoxic agents which has implications in the treatment of neuroblastoma (Hanada *et al*., 1993; Lasorella *et al*., 1995). Bcl-2 expression is thought to inhibit apoptosis by interfering with p53 expression (Lasorella *et al*., 1995). Conversely p53 may regulate Bcl-2 expression and it is the low expression of p53 in neuroblasts that increases Bcl-2 expression (Miyashita *et al*., 1994). Differential expression of Bcl-2 and p53 has been identified in N- and S-type cells enriched from the parental neuroblastoma cell line SK-N-BE(2); in N-type cells high Bcl-2 expression and barely detectable p53 expression was associated with a low apoptotic index, whereas in S-type cells low Bcl-2 expression and p53 expression was associated with a high mitotic index (Piacentini *et al*., 1996). The complete role of Bcl-2 in apoptosis is not yet fully understood (Pinton *et al*., 2000).

Bcl-2 may also play a role in store-operated Ca^{2+} entry (SOCE) where increased Bcl-2 expression has been associated with inhibition of SOCE (Pinton *et al*., 2000; Riddoch *et al*., 2007).

1.5 Ca^{2+} signalling

Ca^{2+} is a ubiquitous intracellular second messenger that controls a diverse range of cellular processes, such as proliferation, differentiation, apoptosis and gene transcription (Berridge *et al*., 1998, 2000; Bootman *et al*., 2001). Cells possess a Ca^{2+} signalling 'toolkit' comprised of Ca^{2+} 'on' mechanisms and Ca^{2+} 'off' mechanisms that enables cells to generate Ca^{2+} signals that vary in space, time and amplitude (Berridge *et al*., 1998, 1999, 2000; Bootman *et al*., 2001).

The equilibrium between Ca^{2+} 'on' and 'off' mechanisms maintains the resting level of cytosolic Ca^{2+} at ~100nM. Ca^{2+} sensitive processes are activated when cytosolic Ca^{2+} rises to ~1µM (Berridge *et al*., 2000; Bootman *et al*., 2001). Cells generate Ca^{2+} signals with the use of extracellular and intracellular Ca^{2+}. Extracellular Ca^{2+} enters cells across the plasma membrane (PM) and intracellular Ca^{2+} is released from internal endoplasmic reticulum (ER) stores, or the sarcoplasmic reticulum (SR) in muscle cells (Berridge *et al*., 2000; Bootman *et al*., 2001). These sources are often used simultaneously or sequentially (Putney *et al*., 2001). An additional intracellular Ca^{2+} store is found in endosomes and lysosomes (Calcraft *et al*., 2009; Galione *et al*., 2010).

1.5.1 Ca^{2+} 'on' mechanisms

Channels that mediate Ca^{2+} entry into the cell cytosol are referred to as Ca^{2+} 'on' mechanisms, as they allow the cytosolic Ca^{2+} level to increase, thus generating Ca^{2+} signals. Ca^{2+} 'on' mechanisms are balanced with Ca^{2+} 'off' mechanisms which serve to reduce cytosolic Ca^{2+} levels and thus remove the signal (Bootman *et al*., 2001).

Ca^{2+} 'on' mechanisms located at the PM include, voltage-operated Ca^{2+} channels (VOCs), receptor-operated Ca^{2+} channels (ROCs), and store-operated Ca^{2+} channels (SOCs) (Berridge *et al*., 2000; Bootman *et al*., 2001). VOCs are Ca^{2+} entry channels that open in response to depolarization (Bootman *et al*., 2001). There are several channel types; L, T, N P/Q and R, grouped accordingly due to differences in kinetics and pharmacological properties. VOCs are commonly present in excitable cells (Berridge *et al*., 2000). ROCs are Ca^{2+} entry channels that open in response to binding of extracellular agonists, such as the neurotransmitters glutamate, ATP and

acetylcholine (Berridge *et al*., 2000; Bootman *et al*., 2001). ROCs are commonly present in secretory cells and at nerve terminals. SOCs are Ca^{2+} entry channels that open in response to ER store depletion. The link between ER store depletion and SOC activation is the focus of much current research (see section 1.6 for more detail). Ca^{2+} 'on' mechanisms located on the ER/SR membrane include, ryanodine receptors (RYRs) and inositol 1,4,5-trisphosphate receptors (IP_3Rs) (Berridge *et al*., 2000). Both are sensitive to Ca^{2+} and both are involved in the process of Ca^{2+}-induced Ca^{2+} release (CICR). Depletion of internal stores occurs as a result of CICR, whereby Ca^{2+} self-promotes its own release by activating IP_3Rs and also RYRs (Berridge *et al*., 2000). IP_3Rs must first be primed by IP_3 binding before responding to Ca^{2+} (Berridge *et al*., 2000). RYRs can be directly activated by Ca^{2+} but have also been shown to be primed by the second messenger cyclic ADP ribose (cADPr) (Berridge *et al*., 2000; Bootman *et al*., 2001). The second messenger nicotinic acid adenine dinucleotide phosphate (NAADP) binds to TPCs (two-pore channels) located on endosome and lysosome membranes (Calcraft *et al*., 2009; Galione *et al*., 2010). Subsequent release of Ca^{2+} from stores can generate local Ca^{2+} signals which can be amplified by CICR though activation of IP_3Rs and/or RYRs (Zhu *et al*., 2010).

1.5.2 Ca^{2+} 'off' mechanisms

Ca^{2+} 'off' mechanisms located on the PM include the Na^+/Ca^{2+} exchanger and the PM Ca^{2+} ATPase (PMCA) which actively remove Ca^{2+} from the cytosol into the extracellular environment (Berridge *et al*., 2000). The sarco/endoplasmic reticulum Ca^{2+} ATPase (SERCA) located on the ER/SR membrane actively removes Ca^{2+} from the cytosol and pumps it back into the ER/SR (Berridge *et al*., 2000). Mitochondria are also an 'off' mechanism as they sequester Ca^{2+} during Ca^{2+} signals and then slowly release it back once resting levels have been restored. Ca^{2+} binding proteins are also considered 'off' mechanisms and include Ca^{2+} buffers and Ca^{2+} sensors. Buffers such as parvalbumin in the cytosol bind Ca^{2+} as it enters the cell and sensors such as calmodulin bind Ca^{2+} and in response activate various cellular responses (Berridge *et al*., 2000).

1.5.3 Ca^{2+} signals

The ability of Ca^{2+} to act as a diverse intracellular messenger is due to the generation of highly versatile Ca^{2+} signals that vary in space, time and amplitude (Berridge *et al*., 1998, 1999, 2000; Bootman *et al*., 2001).

Ca^{2+} signals can be highly localised to specific regions of the cell to control highly localised events such as vesicle secretion at the PM (Berridge *et al*., 1998; 1999). An increase in $[Ca^{2+}]_i$ at the mouth of a Ca^{2+} channel allows various cellular responses to occur that differ depending on the type of Ca^{2+} channel opened and its location (Berridge *et al*., 1998). These types of Ca^{2+} signal are called elementary events and are rapidly removed by the process of simple diffusion (Berridge *et al*., 1998). Elementary events are also the 'basic building blocks of Ca^{2+} signalling' (Berridge *et al*., 1998), as they can initiate the generation of global Ca^{2+} signals through the process of CICR (Berridge *et al*., 1998; 1999). In the process of CICR Ca^{2+} promotes release of itself from internal stores by activating IP_3Rs and RYRs. This regenerative process can create an intracellular Ca^{2+} wave that passes throughout the entire cell. Intracellular Ca^{2+} waves are seen in the processes of fertilisation and cell proliferation (Berridge *et al*., 1998). If cells are connected by gap junctions, the wave can propagate into neighbouring cells thereby creating an intercellular Ca^{2+} wave. This allows the coordination of many cells to regulate a specific cellular response, such as ciliary beat frequency at the lung epithelium (Berridge *et al*., 1998; 2000; Bootman *et al*., 2001).

A prolonged increase in the level of $[Ca^{2+}]_i$ is a signal for apoptosis. Elementary and global Ca^{2+} signals therefore occur as brief 'transients' or oscillations. Ca^{2+} signals differ in time by variations in the frequency of transients which can occur seconds, minutes or hours apart. For example, global Ca^{2+} waves seen after fertilisation occur minutes apart, whereas Ca^{2+} transients involved in proliferation occur hours apart (Berridge *et al*., 1998). Differences in the amplitude of Ca^{2+} signals has also been found to induce different cellular responses however, it is the spatial and temporal characteristic of Ca^{2+} signals that are the key to diversity.

Ca^{2+} plays a vital role in processes that are affected in cancerous cells including proliferation, differentiation and apoptosis. It is therefore important that these processes

are central aspects of current cancer research (Bergner and Huber, 2008). In neuroblastoma the process of differentiation is affected leading to the formation of tumours consisting of immature cells. This project therefore concentrates on elucidating the role of Ca^{2+} signals, specifically SOCE, in the process of differentiation.

1.6 Store-operated Ca^{2+} entry (SOCE)

SOCE, originally termed capacitative calcium entry (CCE), is the process whereby IP_3 mediated depletion of ER Ca^{2+} stores activates SOCs in the PM to enable extracellular Ca^{2+} to enter the cell cytosol and replenish depleted stores (Putney *et al*., 1986). SOCE is a major Ca^{2+} entry pathway in both excitable and non-excitable cells (Berridge *et al*., 1998).

In the phosphoinositide signalling pathway, activation of G-protein-coupled receptors located at the PM activates phospholipase C (PLC). PLC catalyses the hydrolysis of phosphatidylinositol 4,5-bisphosphate (PIP_2), a membrane bound phospholipid, into the second messengers IP_3 and diacylglycerol (DAG). DAG remains in the PM and activates protein kinase C (PKC). IP_3 diffuses through the cytosol and binds to and activates IP_3Rs located on the ER/SR membrane. Opening of these channels allows Ca^{2+} to move down its concentration gradient from the ER (~500μM) into the cytosol (~100nM) and deplete ER stores through IP_3Rs and CICR (Bootman *et al*., 2001). Depletion of ER Ca^{2+} stores activates SOCE (Figure 1.4).

STIM1 (stromal interaction molecule 1), Orai1, also known as CRACM1 (Ca^{2+} release-activated Ca^{2+} modulator 1), and TRPC1 (transient receptor potential channel 1) have all been implicated in SOCE. A large body of evidence now supports that STIM1 is the ER Ca^{2+} sensor that signals store depletion to Orai1, the pore forming subunit of the SOC channel, together forming the elementary unit of SOCE (Luik *et al*., 2006). Before the discovery of these proteins TPRC1 was a prime SOC channel candidate, though a role for TRPC1 in SOCE remains controversial (Alicia *et al*., 2008). However, the biophysical properties of SOCE varies between cell types, therefore the composition of SOC channels most likely varies between cell types also (Roos *et al*., 2005; Cheng *et al*., 2008). For example, it is thought that the Ca^{2+} release-activated Ca^{2+} current (I_{CRAC}), a highly selective Ca^{2+} current, is mediated through Orai1 channels (Prakriya *et al*., 2004; Parekh & Putney, 2005), whereas the store-operated Ca^{2+} current (I_{SOC}), a non-selective Ca^{2+} current is mediated through TRPC1 channels (Ambudkar *et al*., 2007b; Liu *et al*., 2007). Furthermore, in some cells complexes between STIM1, Orai1 and TRPC1 have been shown to constitute SOCE (Ong *et al*., 2007; Liao et al., 2008, 2009; Cheng *et al*., 2008).

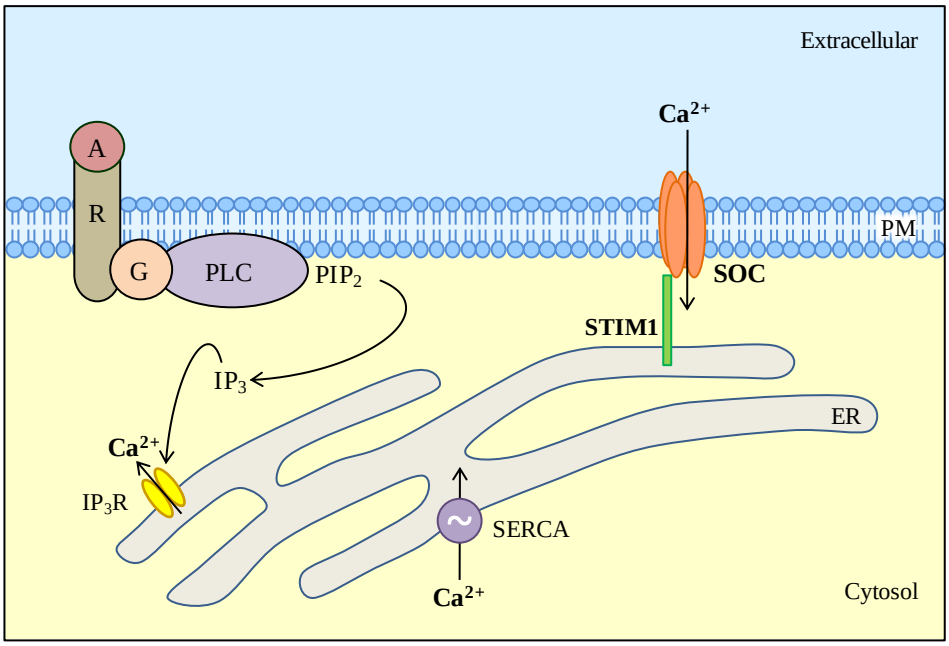

Figure 1.4 Depletion of ER Ca^{2+} stores activates SOCE

Binding of an agonist (A) to a G-protein-coupled receptor (R) activates phospholipase C (PLC) which hydrolyses PIP_2 (anchored in the PM) to generate the second messenger IP_3. IP_3 diffuses through the cell cytosol and binds to IP_3 receptors (IP_3Rs) located in the ER membrane. Opening of IP_3Rs results in ER store depletion. Depletion of ER Ca^{2+} stores is signalled, most likely by STIM1, to SOCs located in the PM. SERCA is a Ca^{2+} ATPase that pumps Ca^{2+} from the cytosol into the ER to replenish depleted stores.

1.6.1 STIM1

In vertebrates there are two STIM homologues; STIM1 and STIM2 (Liou *et al*., 2005).

STIM1 is a 77kDa type 1 membrane protein, the majority of which is located in the ER membrane (Lewis, 2007); though up to 25% of STIM1 expression can be identified in the PM (Zhang *et al*., 2005). STIM1 is composed of multiple domains; an unpaired EF-hand and sterile α-motif (SAM) domain reside within the ER lumen at the N-terminal region of the protein and a coiled-coil (CC)/ezrin-radixin-moesin (ERM), serine/proline-rich and lysine-rich domain reside within the cell cytosol at the C-terminal region of the protein (Manji *et al*., 2000; Williams *et al*., 2001, 2002).

In 2005, STIM1 was first identified as playing a key role in SOCE where knockdown of STIM1 in several cell types inhibited thapsigargin (TG) and agonist induced SOCE (Roos *et al*., 2005; Liou *et al*., 2005). STIM1 was proposed to be a sensor of ER Ca^{2+} stores and the missing link between Ca^{2+} store depletion and SOCE (Zhang *et al*., 2005).

When ER Ca^{2+} stores are replete STIM1 exists as a monomer (Stathopulos *et al*., 2006, 2008), located diffusely throughout the ER membrane (Liou *et al*., 2005; Zhang *et al*., 2005; Wu *et al*., 2006). Following store depletion STIM1 rapidly (<5 seconds) forms oligomers in the ER membrane before more slowly (40 seconds) translocating to form punctae at pre-existing ER-PM junctions located 10-25nm from the plasma membrane, close enough to allow protein-protein interactions between STIM1 and SOCs (Liou *et al*., 2005; Wu *et al*., 2006). SOCE only occurs in the immediate vicinity directly opposite STIM1 puncta (Luik *et al*., 2006). STIM1 does not permanently reside at ER-PM junctions (Luik *et al*., 2006), following replenishment of ER Ca^{2+} stores puncta dissociate and STIM1 returns to its uniform distribution throughout the ER membrane (Liou *et al*., 2007).

STIM1 is predicted to sense the level of Ca^{2+} within the ER through its unpaired EF-hand domain. Consistent with this role is the *in vitro* Ca^{2+} binding affinity of the EF-hand which is 200-600μM (Stathopulos *et al*., 2006), which overlaps with the 250-600μM [Ca^{2+}] reported within the ER (Demaurex *et al*., 2003). EF-hand mutant studies,

in which critical Ca^{2+} binding residues (Nakayama *et al*., 1994) were substituted in order to lower the Ca^{2+} binding affinity of the EF-hand and therefore mimic store depletion, resulted in formation of STIM1 puncta and constitutive activation of SOCE even when ER Ca^{2+} stores were full (Liou *et al*., 2005; Zhang *et al*., 2005; Spassova *et al*., 2006). This provided strong evidence that the EF-hand of STIM1 is the ER Ca^{2+} sensor.

Deletion of several cytosolic STIM1 domains prevents SOCE (Baba *et al*., 2006). The SAM domain is essential in STIM1 oligomerisation as SAM deletion mutants are unable to form inducible puncta. The cytosolic C-terminus of STIM1 is essential in the translocation of STIM1 oligomers to ER-PM junctions (Baba *et al*., 2006; Huang *et al*., 2006; Liou *et al*., 2007) where deletion of the ERM domain prevented translocation of STIM1 to ER-PM junctions (Huang *et al*., 2006). Similarly, mutant STIM1 lacking the polybasic C-terminal (lysine-rich domain) oligomerised following store depletion, but failed to translocate to ER-PM junctions (Liou *et al*., 2007). The lysine-rich domain may interact with lipids in the membrane to facilitate SOCE (Huang *et al*., 2006).

The cytosolic C-terminus of STIM1 activates SOCE in cells expressing Orai1 (Prakriya *et al*., 2006; Muik *et al*., 2008; Zhang *et al*., 2008), interaction between STIM1 and Orai1 may be mediated through coiled-coil interactions (Luik *et al*., 2006).

STIM2 is also a type 1 transmembrane protein which shares 66% sequence homology with STIM1 (Williams *et al*., 2001). Like STIM1, STIM2 also has an EF-hand and SAM domain located within the ER lumen and a CC, serine/proline-rich and lysine-rich domain located in the cell cytosol (Williams *et al*., 2001; Zheng *et al*., 2008). STIM2 however is only expressed in the ER membrane, unlike STIM1 which is also expressed in the PM (Zheng *et al*., 2008).

STIM2, like STIM1, translocates to ER-PM junctions in response to ER store depletion and can activate SOCE through interaction with Orai1, STIM2 however responds to smaller decreases in ER $[Ca^{2+}]$ than STIM1 (Brandman *et al*., 2007). As knockdown of STIM2 reduces basal $[Ca^{2+}]$ and overexpression increases basal $[Ca^{2+}]$ (Brandman *et al*., 2007) and also inhibits SOCE (Soboloff *et al*., 2006a) STIM2 is considered a sensor

and regulator of basal [Ca^{2+}]. Consistent with monitoring changes in basal [Ca^{2+}] is the binding affinity of the EF-hand domain which is ~500μM (Zheng *et al*., 2008, 2011).

As STIM1 activates SOCE following store depletion, the role and expression of STIM1 was investigated in this thesis.

1.6.2 Orai1

In vertebrates there are three Orai homologues; Orai1, Orai2 and Orai3 (Feske *et al*., 2006).

Orai1 is a 33kDa four-transmembrane domain protein located within the PM with both N- and C-termini located within the cell cytosol (Prakriya *et al*., 2006; Gwack *et al*., 2007).

In 2006 Orai1 was first identified as an essential component of SOCE (Feske *et al*., 2006; Vig *et al*., 2006a; Zhang *et al*., 2006). T cells from patients with severe combined immunodeficiency (SCID) syndrome failed to activate SOCE following store depletion (Feske *et al*., 2005) which was later attributed to a single point mutation (R91W) in *Orai1* (Feske *et al*., 2006). Furthermore transfection with wild-type *Orai1* in cells from SCID patients restored SOCE.

Overexpression of both Orai1 and STIM1 reconstitutes I_{CRAC}, suggesting that Orai1 is a component of SOCs (Mercer *et al*., 2006; Peinelt *et al*., 2006; Soboloff *et al*., 2006b; Zhang *et al*., 2006; Yamashita *et al*., 2007). STIM1 is obligatory for the function of Orai1 as a SOC (Mercer *et al*., 2006; Peinelt *et al*., 2006; Zhang *et al*., 2006) and following store depletion STIM1 and Orai1 interact directly with one another as determined by co-immunoprecipitation studies (Yeromin *et al*., 2006; Vig *et al*., 2006b). A domain within the C-terminus of Orai1 is thought to be the interaction site for STIM1 (Li *et al*., 2007). Deletion of lysine-rich region did not prevent the activation of Orai1 (Li *et al*., 2007; Zeng *et al*., 2008) nor did the combined deletion of the serine/proline- and lysine-rich regions (Zeng *et al*., 2008) suggesting that these regions are not involved in the direct activation of Orai1.

When ER Ca^{2+} stores are replete Orai1 exists as a dimer (Penna *et al*., 2008), located diffusely throughout the PM. Following depletion of ER Ca^{2+} stores, STIM1 interacts with Orai1 dimers and induces dimerization to form tetramers that form the pore of the SOCs (Mignen et al., 2008b; Penna *et al*., 2008). Orai1 translocates to ER-PM junction directly opposite STIM1 puncta (Luik *et al*., 2006; Xu *et al*., 2006). SOCE only occurs in the immediate vicinity directly opposite STIM1 puncta (Luik *et al*., 2006). Ca^{2+} entering the cell cytosol is taken up into the ER by the SERCA pump to replenish the depleted stores. Orai1 does not permanently reside at ER-PM junctions (Luik *et al*., 2006) and following replenishment of ER Ca^{2+} stores Orai1 returns to its uniform distribution throughout the PM (Liou *et al*., 2007).

Evidence that Orai1 forms the pore forming subunit of SOCs came from mutant studies in which substitution of acidic residues in transmembrane domains 1 and 3 and in the extracellular loop region between transmembrane domains 1 and 2 altered Ca^{2+} permeability and selectivity of I_{CRAC} (Prakriya *et al*., 2006; Yeromin *et al*., 2006; Vig *et al*., 2006b). Also the R91W point mutation in SCID patients with dysfunctional I_{CRAC} is located in transmembrane domain 1 (Feske *et al*., 2006).

Orai2 co-expression with STIM1 in HEK293 cells enhanced SOCE though to a lesser extent than Orai1 (Mercer *et al*., 2006).

Orai3 does not generally appear to be involved in SOCE as, unlike Orai1 and Orai2, co-expression of Orai3 with STIM1 in HEK293 cells did not enhance SOCE (Mercer *et al*., 2006; DeHaven *et al*., 2007) and expression of a mutant Orai3 in HEK293 cells had no effect on SOCE (Mignen *et al*., 2008a). However Orai3 may be involved in SOCE in some instances as Orai3 expression in Orai1 knockdown cells rescued SOCE (Mercer *et al*., 2006). Orai3 has been identified as an essential component of the store-independent, arachidonic acid regulated Ca^{2+} (ARC) channels (Mingen *et al*., 2008a, 2009, 2012). Though the expression of mutant Orai3 had no effect on SOCE it significantly reduced currents through ARC channels (Mignen *et al*., 2008a). ARC channels are composed of three Orai1 and two Orai3 subunits (Mingen *et al*., 2009, 2012) and their activation is dependent on PM STIM1 (Mignen *et al*., 2007, 2008a, 2009, 2012).

As Orai1 is most strongly associated with SOCE, the role and expression of Orai1 was investigated in this thesis.

1.6.3 TRPC1

TRPC1 is a 90kDa PM protein that has been implicated in SOCE in many cell types (Parekh and Putney, 2005). For example, knockout of TRPC1 in submaxillary acinar mouse cells caused an 80% reduction in SOCE (Liu *et al*., 2007) and in HEK293 cells STIM1 and TRPC1 co-immunoprecipitate when co-expressed (Huang *et al.*, 2006). The role of TRPC1 as a SOC is controversial, as several studies have shown that TRPC1 is not involved in SOCE. Most of the controversy surrounding the role of TRPC1 as a SOC is due to its well established role as a ROC. However, recent studies suggest that TRPC1 can function as both a ROC and a SOC in a STIM1 dependent manner (Alicia *et al*., 2008).

TRPC1 activation is STIM1 dependent where knockdown of STIM1 inhibits TRPC1 channel function (Yuan *et al*., 2007). Store depletion induces translocation of STIM1 and TRPC1 to ER-PM junctions (Huang *et al.*, 2006). Following store depletion the interaction between STIM1 and TRPC1 is increased (Huang *et al*., 2006; Lopez *et al*., 2006; Ong *et al*., 2007; Pani *et al*., 2008; Jardin *et al*., 2008; Alicia *et al*., 2008; Ng *et al*., 2009).

In contrast with Orai1, deletion of STIM1 lysine-rich or serine/proline-rich domains, or both combined, prevents activation of TRPC1 (Zeng *et al*., 2008). The C-terminal lysine-rich tail of STIM1 is essential for gating and activation of TRPC1 channels (Huang *et al*., 2006). Residues ^{684}KK^{685} of STIM1s lysine-rich tail were involved in the gating of the TRPC1 channel through electrostatic interaction with residues ^{639}DD^{640} residues of TRPC1s C-terminal region (Zeng *et al*., 2008).

SOCs may be composed of heteromeric complexes that include TRPC1 and Orai1 (Ambudkar *et al*., 2007b; Liao *et al*., 2007, 2008, 2009; Ong *et al*., 2007; Jardin *et al*., 2008a, 2008b; Cheng *et al*., 2008). Several studies have demonstrated that TRPC1 forms complexes with both STIM1 and Orai1. Complexes are dynamic where TRPC1 only acts as a SOC when in the complex and otherwise is not involved in SOCE (Jardin

et al., 2008a). The interaction between STIM1 and TRPC1 requires Orai1 in some cell types. Prevention of STIM1-Orai1 interactions prevented STIM1-TRPC1 interactions in human platelets (Jardin *et al*., 2008a). Also expression of mutant Orai1 (R91W) reduced STIM1-TRPC1 dependent SOCE in HEK293 cells (Liao *et al*., 2008; Cheng *et al*., 2008). Orai1 interaction with STIM1 may confer sensitivity of TRPC1 channels to SOCE (Liao *et al*., 2007, 2008). However, DeHaven *et al*., 2009, found that TRPC1 channels function independently of STIM1 and Orai1 in HEK293 cells.

Several studies have proposed that lipid raft domains (LRDs) play an essential role in enabling STIM1-TRPC1 interactions. STIM1 can covert TRPC1 from a ROC to a SOC by inserting it into LRDs in HEK293 cells (Alicia *et al*., 2008). Only when TRPC1 is inserted into LRDs can it function as a SOC, otherwise it functions as a ROC (Alicia *et al*., 2008). TRPC1 is anchored in the PM at ER-PM junctions by the cholesterol binding protein caveolin-1. Following store depletion STIM1 puncta formation causes the dissociation of TRPC1 with caveolin-1 enabling STIM1-TRPC1 interactions (Pani *et al*., 2009a, 2009b). STIM1 puncta have been found to be anchored in LRDs (Pani *et al*., 2008). LRDs are also important for Orai1-TRPC1 interactions as disturbance of LRDs reduced Orai1-TRPC1 interactions and SOCE in human platelets (Jardin *et al*., 2008b).

1.7 Aims

The aims of this thesis were;

1. To obtain enriched N- and S-type cell populations from the SH-SY5Y neuroblastoma cell line and characterise them morphologically and biochemically before and after 9*c*RA-induced differentiation (Chapter 3).

2. To characterise SOCE in proliferating and 9*c*RA-differentiated SH-SY5Y, N- and S-type cells (Chapter 4).

3. To investigate the roles played by the three key Ca^{2+} signalling proteins; STIM1 (Chapters 5), Orai1 (Chapter 6) and TRPC1 (Chapter 7) in SOCE and differentiation.

Chapter 2

Materials and Methods

2.1 Materials

All chemicals were from Sigma-Aldrich (Sigma-Aldrich Company Ltd, Dorset, UK) unless otherwise stated.

2.1.1 Cell culture

SH-SY5Y cells were from Professor Robert A Ross (Fordham University, NY, USA). D-MEM with GlutaMAX and Opti-MEM Reduced Serum Medium with GlutaMAX were from Invitrogen (Life Technologies Ltd, Paisley, UK).

2.1.2 Transfection

Silencer Negative Control siRNA and nuclease-free water were from Ambion (Applied Biosystems, Warrington, UK). siGENOME SMARTpool siRNA (human STIM1, ORA1I and TRPC1) was from Thermo Scientific (Thermo Fisher Scientific, Dharmacon Products, Lafayette, CO, USA. Lipofectamine 2000 Transfection Reagent and pcDNA3.1/Zeo$^{(+)}$ were from Invitrogen (Life Technologies Ltd, Paisley, UK). Cherry-STIM1 and GFP-Orai1 were from Professor Richard S Lewis (Stanford School of Medicine, CA, USA).

2.1.3 Immunofluorescence

FluorSave was from Calbiochem (Merck KGaA, Darmstadt, Germany). Suppliers of antibodies used in immunofluorescence experiments are shown in Table 2.1a

2.1.4 Western blotting

Protease cocktail inhibitor tablets were from Roche (Roche Products Ltd, Hertfordshire, UK). Blotting-Grade Blocker nonfat dry milk powder, Protein Assay Dye Reagent Concentrate and Precision Plus Dual Color Protein Standards were from Bio-Rad (Bio-Rad Laboratories Ltd, Hertfordshire, UK). 10% NuPAGE Bis-Tris Gels (1.0mm, 10 well), NuPAGE MOPS SDS Running Buffer and NuPAGE Antioxidant were from Invitrogen (Life Technologies Ltd, Paisley, UK). Suppliers of antibodies used in western blotting experiments are shown in Table 2.1b.

2.1.5 Determination of $[Ca^{2+}]_i$

Fura-2/AM, Ionomycin and Thapsigargin were from Calbiochem (Merck KGaA, Darmstadt, Germany)

a)

Antibody - species raised in	Supplier	Catalogue number
Anti-β-Tubulin III alexa-fluor 488) - Mouse	Covance, Princeton, NJ, USA	A488-435L
Anti-Vimentin (alexa-fluor 647) - Mouse	Santa Cruz Biotechnology Inc, Santa Cruz, CA, USA	sc-6260 AF647

b)

Antibody - species raised in	Supplier	Catalogue number
Anti-β-Actin - Mouse	abcam, Cambridge, UK	ab8226
Anti-Bcl-2 - Mouse	Santa Cruz Biotechnology Inc, Santa Cruz, CA, USA	sc-7382
Anti-β-Tubulin III - Mouse	Covance, Princeton, NJ, USA	MMS-435P
Anti-Orai1 - Rabbit	Sigma, Sigma-Aldrich Company Ltd, Dorset, UK	O8264
Anti-STIM1 - Mouse	BD Biosciences, San Jose, NJ, USA	610954
Anti-TRPC1 - Rabbit	Alomone Labs Ltd, Jerusalem, Israel	ACC-010
Anti-Vimentin - Mouse	Santa Cruz Biotechnology Inc, Santa Cruz, CA, USA	sc-6260
Anti-Mouse (HRP) - Rabbit	Dako, Glostrup, Denmark	PO260
Anti-Rabbit (HRP) - Swine	Dako, Glostrup, Denmark	PO217

Table 2.1 Antibodies used with respective suppliers and catalogue numbers

a) Antibodies used in immunofluorescence experiments (Methods 2.5). **b)** Primary and Secondary antibodies used in western blotting experiments (Methods 2.6). Antibodies were validated by siRNA knockdown, recombinant protein expression and, for TRPC1, peptide block.

2.2 SH-SY5Y cell culture

SH-SY5Y cells were cultured in Dulbecco's Modified Eagle's Medium (D-MEM) with GlutaMAX (L-glutamine substitute - 2.5mM) supplemented with foetal calf serum (10% v/v), penicillin (100IU.ml^{-1}) and streptomycin (100IU.ml^{-1}). Cells were kept at 37°C in a humidified atmosphere consisting of 95% air and 5% CO_2. Cells were grown in 75cm^2 flasks and passaged once a week when 90% confluent. If a 1/40 dilution (i.e. 250µl in 10mls) was used then a 1/30, 1/40 and 1/50 flask would be set up for the following week to account for variation in cell growth rate. Cells were not used beyond passage 28.

In preparation for the passage of cells D-MEM, phosphate buffered saline (PBS) and 0.02% (v/v) ethylenediaminetetraacetic acid (EDTA) were pre-warmed to 37°C. Cells were washed twice with PBS (10ml) and detached from the flask by incubation with EDTA (3ml) for 5 minutes at 37°C. D-MEM (7ml) was added to the flask and the cell suspension was pipetted across the surface of the flask five times to fully remove adherent cells. The cell suspension (10ml) was centrifuged at 1000rpm for 5 minutes, the supernatant was discarded and the cell pellet was re-suspended in D-MEM (10ml). The cell suspension was then centrifuged for a second time at 1000rpm for 5 minutes, the supernatant was discarded and the cell pellet was re-suspended in D-MEM (10ml). The resultant cell suspension was used for seeding of cells into flasks and onto dishes as required (2.2.4).

Typically the SH-SY5Y cell line is predominantly composed of N-type cells, though S-type cells remain present (Introduction 1.3). Due to differences in substrate adherence between the two cell phenotypes it was possible to enrich for N- and S-type cell populations. The method for enrichment, based on differential adherence, was adapted from Piacentini *et al*., 1996. Every passage performed for the enrichment of either N- or S-type cells was done using a flask that was ~80% confluent. Flasks that were 90-100% confluent were not appropriate for the enrichment of N- and S-type populations as the cells peeled off in sheets preventing enrichment by separation.

2.2.1 N-type cell populations

D-MEM and PBS were pre-warmed to 37°C. Cells were washed once with PBS (10ml) and then left to stand for ~60 seconds in PBS (3ml). Flasks were gently tapped to knock off the more weakly adhered cells (~10-20% of cells were knocked off). These cells were transferred to a new flask containing D-MEM (10ml) and were pipetted up and down several times to obtain a uniform cell suspension. The first time this was done the cells were called N1 as the SH-SY5Y cell line had been enriched for N-type cells once. This process was repeated up to N12.

To remove N-type cells from flasks for use in experiments cells were washed once with PBS (10ml) and then left to stand in PBS (3ml) for ~60 seconds. Then ~40% of cells were knocked off. These cells were added to D-MEM (7mls). The cell suspension was pipetted up and down several times to obtain a uniform cell suspension. Cells were counted (Methods 2.2.4) and the required volume plated onto dishes.

2.2.2 S-type cell populations

D-MEM and PBS were pre-warmed to 37°C. Cells were washed once in PBS (10ml) and then left to stand for ~4 minutes in PBS (4ml). Flasks were knocked repeatedly to remove N-type cells. The remaining cells still adhered to the flask (~30%) were washed with PBS (10ml) a second time. D-MEM (10ml) was added to the flask. The first time this was done the cells were called S1 as the SH-SY5Y cell line had been enriched for S-type cells once. This process was repeated up to S12.

To remove S-type cells from flasks for use in experiments cells were washed once in PBS (10ml) and then left to stand in PBS (4ml) for ~5 minutes. Flasks were knocked repeatedly to remove N-type cells. The remaining cells were washed with PBS (10ml) and then scraped into PBS (3ml). D-MEM (7mls) was added to the flask and the cell suspension was pipetted up and down several times to obtain a uniform cell suspension. Cells were counted (Methods 2.2.4) and the required volume plated onto dishes.

2.2.3 Differentiation

Cells were seeded onto dishes at least 24 hours prior to treatment to allow enough time to adhere. 9*c*RA (1mg) was dissolved in AnaLar EtOH to provide a stock concentration of 10mM which was aliquoted and stored at -20°C. Differentiation was initiated by the addition of 1µM 9*c*RA to cells at 10-20% confluency. 1µM 9*c*RA has previously been shown to successfully induce differentiation of SH-SY5Y cells (Lovat *et al*., 1997). Differentiation media (D-MEM with 9*c*RA) was replaced every 2 days and cells were used following 7 days of treatment. Previous data from this laboratory have shown that differentiation reaches a plateau by 7 days of treatment (Brown *et al*., 2005). A new aliquot of 9*c*RA was used each week and a new stock batch was made each month. Control cells (i.e. proliferating cells) were treated identically with an equal volume of vehicle EtOH (0.01% in D-MEM).

2.2.4 Cell counts

An improved Neubauer haemocytometer (VWR International Ltd, Leicestershire, UK) with a chamber depth of 0.1mm was used for counting cells. Prior to each cell count the haemocytometer was cleaned with 70% EtOH and allowed to dry. The glass coverslip was then fixed in place and cell suspension was added to the chamber. Cells in the four corner squares (each square is $1mm^2$) were counted; cells touching the top and left line of each grid were counted and those touching the bottom and right line of each grid were not counted. The average number of cells per square was calculated (total number of cells / 4) and multiplied by 10^4 to obtain the number of cells per ml (the volume of each square is 0.1µl). The required volume of cells was then seeded onto dishes.

Table 2.2 shows the number of cells seeded onto 35mm dishes for use in fluorimetry experiments (35mm dishes contain four wells that hold four 10mm glass coverslips). Corresponding 60mm dishes were set up for harvesting of protein with twice the number of cells seeded as was seeded for fluorimetry experiments. Corresponding 35mm dishes were set up for immunofluorescence or DIC images with half as many cells seeded as was seeded for fluorimetry experiments.

a)

Cell type	EtOH	9*c*RA
SH-SY5Y	5×10^4	2×10^5
N-type	5×10^4	2×10^5
S-type	10×10^4	4×10^5

b)

Experiment	EtOH	9*c*RA
siRNA	6×10^5 (Treatment NA)	
siRNA : 3 day	4×10^5	4×10^5
7 day : Plasmid DNA	2.5×10^4	1×10^5

Table 2.2 Number of cells seeded for fluorimetry experiments

a) Number of cells seeded onto 35mm dishes to obtain ~90% confluency following 7 days EtOH or 9*c*RA treatment for SH-SY5Y, N- and S-type cells (assuming treatment started ~24 hours after seeding). **b)** Number of cells seeded onto 35mm dishes to obtain ~90% confluency following treatment and/or transfection of N-type cells. 3 day indicates 3 days EtOH or 9*c*RA treatment.7 day indicates 7 days EtOH or 9*c*RA treatment. For siRNA transfection assumes transfection started ~48 hours after seeding (to provide enough time for cells to obtain a suitable confluency; ~50-60% for siRNA transfection alone and ~40% for siRNA transfection followed by 3 days EtOH or 9*c*RA treatment). For 7 days treatment followed by plasmid DNA transfection assumes treatment started ~24 hours after seeding.

2.3 Transient transfection

2.3.1 small interfering RNA (siRNA) transfection

siRNA transfection is used as a tool to down-regulate gene expression. siRNA's are double-stranded RNA (dsRNA) molecules of ~19-22 nucleotides in length that can be transfected into cells with Lipofectamine 2000. Lipofectamine is a cationic lipid that forms complexes with the negatively charged siRNA's. The Lipofectamine-siRNA complexes are taken into cells by endocytosis. Once inside the cell cytosol siRNA's bind to the RNA induced silencing complex (RISC) which separates the dsRNA and destroys the sense strand. The antisense strand remains associated with the RISC complex and binds to its corresponding (i.e. target) messenger RNA (mRNA). The mRNA is cleaved by the RISC complex and then degraded and therefore cannot be translated into protein, effectively silencing the gene.

For siRNA transfection of cells siGENOME SMARTpool siRNA was used which consists of 4 nucleotide sequences targeted to the gene of interest (Table 2.3). STIM1, ORAI1 and TRPC1 siRNA (10nmol) were resuspended in nuclease-free water (100µl) to produce a stock concentration of 100µM which was aliquoted and stored at -20°C.

Cells were grown in antibiotic free D-MEM for 24 hours prior to siRNA transfection and were transfected when 40-60% confluent. For 35mm dishes; siRNA (2.5µl) and Opti-MEM (250µl) were mixed together and Lipofectamine 2000 (5µl) and Opti-MEM (250µl) were mixed together for 15 minutes at RT. The diluted siRNA and the diluted Lipofectamine 2000 were mixed together for a further 15 minutes at RT to allow the formation of siRNA-Lipofectamine complexes. Complexes were added to cells (final siRNA concentration of 125nM) which were placed back in the incubator at 37°C for use in experiments following 48 hours. For control cells the equivalent concentration of silencer negative control siRNA was added in place of siRNA.

For experiments in which STIM1, Orai1 and TRPC1 were knocked down by siRNA transfection followed by treatment with 9cRA (5.2.3, 6.2.3 and 7.2.3) a set of cells transfected with STIM1, Orai1 or TRPC1 siRNA followed by EtOH treatment was not

included. To ensure that the changes seen were not due to 9*c*RA treatment alone, knockdown of each protein in proliferating cells was determined beforehand.

siRNA	Target Sequence
Human STIM1	CAUCAGAAGUAUACAAUUG
	AGAAAGAGCUAGAAUCUCA
	AGAAGGAGCUAGAAUCUCA
	GGUGGUGUCUAUCGUUAUU
Human ORAI1	GCUCACUGGUUAGCCAUAA
	GGCCUGAUCUUUAUCGUCU
	GCACCUGUUUGCGCUCAUG
	CAGCAUUGAGUGUGUACUA
Human TRPC1	GAACAUAAAUUGCGUAGAU
	GGACUACGGUUGUCAGAAA
	GAGAAGAACUGCAGUCCUU
	UCAGGUGACUUGAACAUAA

Table 2.3 siGENOME SMARTpool siRNA

siGENOME SMARTpool siRNA from Thermo Scientific consists of 4 sequences targeted to the mRNA of the protein of interest.

2.3.2 Plasmid DNA transfection

Plasmids are small circular double stranded DNA (dsDNA) molecules that are capable of self replication. A gene of interest can be inserted into plasmids which can then transfected into cells with Lipofectamine 2000. Once inside cells the gene of interest is transcribed and the resultant mRNA is translated into protein and thereby the protein of interest is expressed.

A plasmid containing the STIM1 gene and mCherry (Cherry-STIM1) and a plasmid containing the Orai1 gene and green fluorescent protein (GFP-Orai1) were used for overexpression of STIM1 and Orai1 proteins respectively. For construction of Cherry-STIM1 and GFP-Orai1 plasmids see Luik *et al.*, 2006.

Cells were grown in antibiotic free D-MEM for 24 hours prior to plasmid DNA transfection and were transfected when ~80% confluent. For 35mm dishes; plasmid DNA (4µg) and Opti-MEM (250µl) were mixed together and Lipofectamine 2000 (10µl) and Opti-MEM (250µl) were mixed together for 5 minutes at RT. The diluted plasmid DNA and the diluted Lipofectamine 2000 were mixed together for a further 20 minutes at RT to allow the formation of DNA-Lipofectamine complexes. Complexes were added to cells which were placed back in the incubator at 37°C for use in experiments following 24 hours. For control cells the equivalent amount of pcDNA3.1/Zeo$^{(+)}$ was added in place of plasmid DNA.

2.4 Images

Phase contrast images were taken with a Motic AE21 microscope using a 10x objective.

Differential interference contrast (DIC) images were taken with an Axiovert 200M microscope (Carl Zeiss Ltd) coupled to a laser scanning confocal microscope system (LSM 510, Carl Zeiss Ltd) using a 40x objective and helium-neon (HeNe) laser (633nm).

DIC images were taken to determine the percent differentiation of cells following various treatments and transfections (Figure 2.1). To calculate percent differentiation for an *n* of 1, six random images were taken from a single coverslip. The total number of cells from all six images was counted (S-type cells were not counted). The total number of differentiated cells (≥50µm in length) was also counted from the same six images. The total number of differentiated cells was divided by the total number of cells and multiplied by a 100 to convert to a percentage. An example of this is shown in Figure 2.1

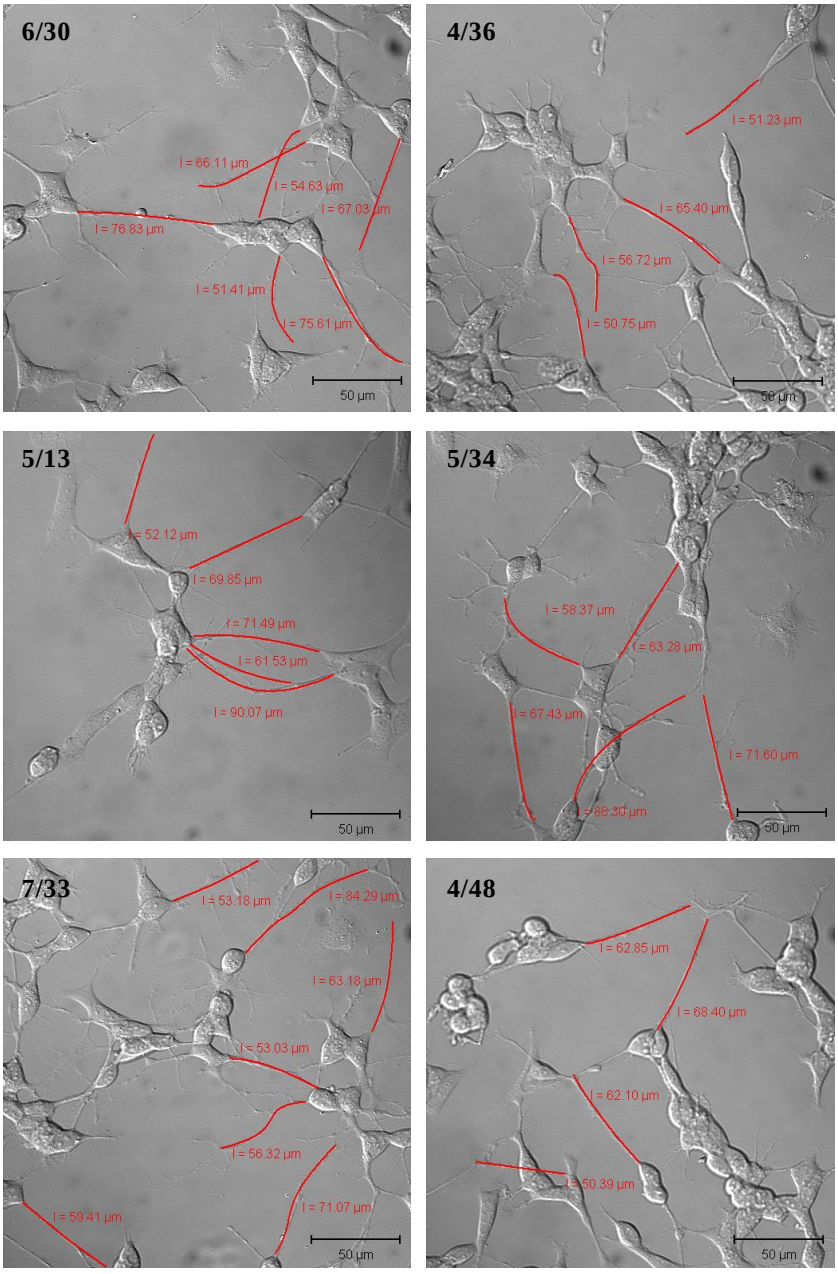

Figure 2.1 DIC images for percent differentiated cells

For *n*=1 six random DIC images were taken of cells on the same coverslip. The total number of differentiated N-type cells was divided by the total number of N-type cells from all six images and multiplied by 100 to convert to a percentage. In the above example the total number of differentiated cells is 31 and the total number of cells is 194 therefore the percent differentiation calculated for this coverslip is 16% [(31/194) x100]. Cells were deemed differentiated if they exhibited neurites of ≥50µm in length (determined using Zeiss LSM Image Browser software). Scale bars represent 50µm.

2.5 Immunofluorescence

PBS, 4% w/v paraformaldehyde (PFA), 0.1% v/v Triton X-100 and 5% w/v bovine serum albumin (BSA) were used at 4°C for the following protocol. Cells on 10mm glass coverslips were washed with PBS (2 x 5 minutes) and then fixed by incubation with PFA for 10 minutes at RT. Fixed cells were washed with PBS (2 x 5 minutes) and then permeabilised with Triton X-100 for 10 minutes at RT. Following permeabilisation cells were washed with PBS (2 x 5 minutes) and then blocked in BSA for 30 minutes at 4°C. Primary antibodies were diluted in BSA (Table 2.4) and then incubated with cells for 2 hours at 4°C in the dark. Control cells were incubated with BSA only. Cells were again washed in PBS (2 x 5 minutes) before incubation with the nucleic acid dye, ethidium homodimer-1 (EthD-1), at a 1/500 dilution, for 10 minutes at RT. Cells were washed in PBS (2 x 5 minutes) and then in dH_20 (1 x 5 minutes) before being mounted onto glass slides with FluorSave. Cells were left to dry overnight at RT in the dark and then stored at 4°C until use.

Cells were viewed using a laser scanning confocal microscope (LSM 510, Carl Zeiss Ltd). The excitation and emission spectra of the fluorophores used in experiments are show in Figure 2.2. The emission wavelengths of alexa-fluor 647 and EthD-1 overlap and were therefore collected separately.

To collect emission wavelengths separately a multi-track configuration was used as when one track is active the other track is switched off thereby preventing cross-talk. Track one was set up to detect the vimentin signal (Figure 2.3) and track two was set up to detect the β-Tubulin III and EthD-1 signals (Figure 2.4). Images were acquired with 12 bit data depth, a frame size of 512 x 512 and a scan speed of 9.

Antibody	Conjugate	Dilution used
Anti-β-Tubulin III	Alexa-fluor 488	1/50
Anti-Vimentin	Alexa-fluor 674	1/50

Table 2.4 Antibodies used in immunofluorescence experiments

Anti-vimentin and anti-β-Tubulin III were both used at a 1/50 dilution. Cells did not require incubation with a secondary antibody as fluorescent tags were directly conjugated to the primary antibodies.

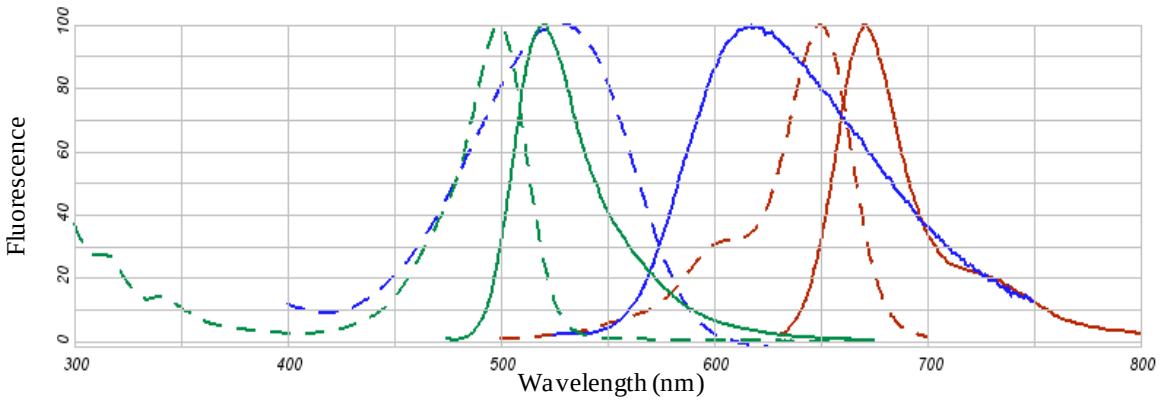

Figure 2.2 Excitation and emission spectra of fluorophores

Excitation (dashed line) and emission (solid line) spectra of ■ alexa-fluor 488, ■ alexa-fluor 647 and ■ EthD-1 (from Invitrogen; Fluorescence SpectraViewer). The emission of alexa-fluor 647 and EthD-1 overlap and were therefore collected separately.

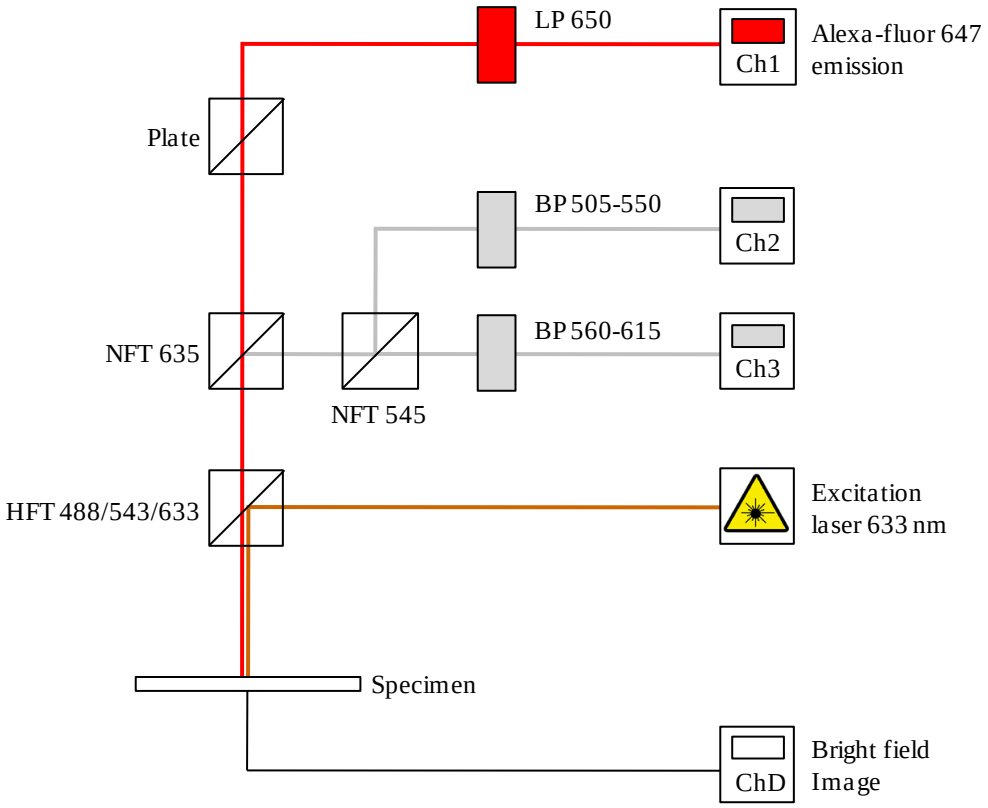

Figure 2.3 Track one set up - Vimentin detection

This track was set up to collect the emission wavelengths of alexa-fluor 647 (peak emission ~670nm). It also takes a bright field image of the cells in channel D (ChD). The HeNe laser sends an excitation wavelength of 633nm to the main dichroic mirror (HFT 488/543/633) which is reflected 90° to the cells. Light emitted from the cells then passes through the main dichroic mirror to a secondary dichroic mirror (NFT 635) which only allows light above 635nm to pass through. The light is then directed to a long pass (LP) filter of 650nm. Only wavelengths above 650nm can pass through to be detected by the photomultiplier tube in channel 1 (Ch1).

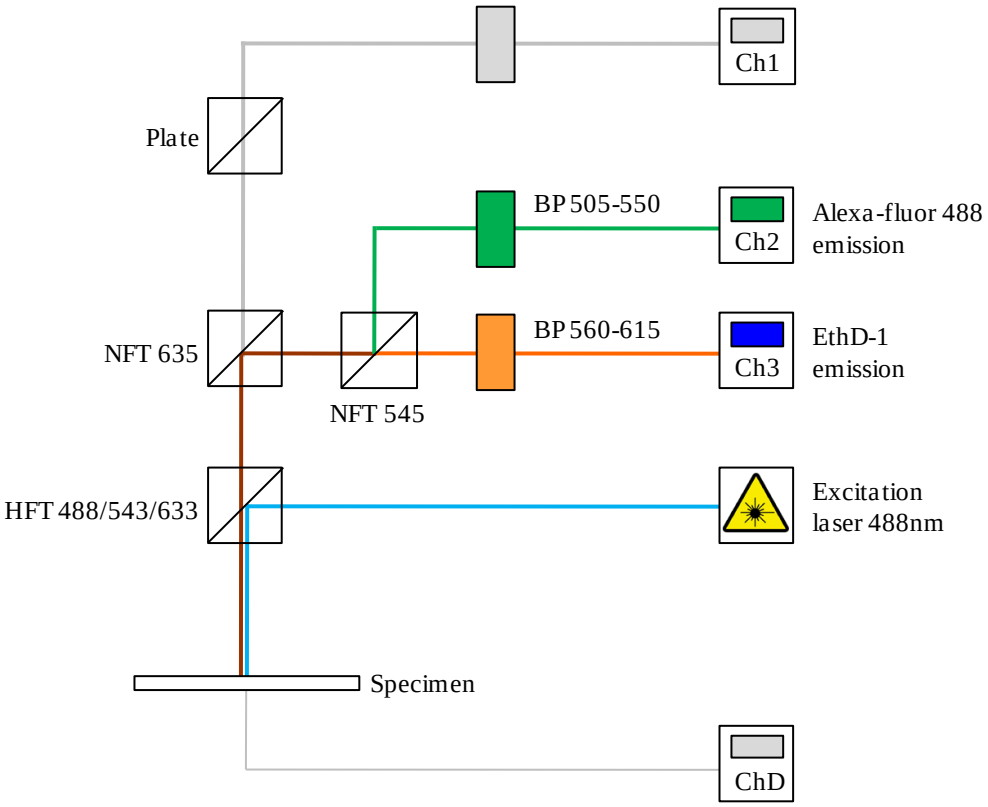

Figure 2.4 Track two set up - β-Tubulin III and EthD-1 detection

This track was set up to collect the emission wavelengths of alexa-fluor 488 (peak emission ~519) and EthD-1 (peak emission ~615nm). The argon (Ar) laser sends an excitation wavelength of 488nm to the main dichroic mirror (HFT 488/543/633) which is reflected 90° to the cells. Light emitted from the cells then passes through the main dichroic mirror to a secondary dichroic mirror (NFT 635) which reflects light below 635nm 90° to another secondary dichroic mirror (NFT 545). Light below 545nm (alexa-fluor 488) is reflected 90° to a band pass (BP) filter of 505-550nm which only allows light of 505-550nm to pass through to be detected by the photomultiplier tube in channel 2 (Ch2). Light above 545nm (EthD-1) passes through the mirror and is directed to a band pass (BP) filter of 560-615nm which only allows light of 560-615nm to pass through to be detected by the photomultiplier tube in channel 3 (Ch3).

2.6 Western Blotting

Western blotting is the process whereby proteins are separated based on their molecular weight by sodium dodecyl sulfate-polyacrylamide gel electrophoresis **(**SDS-PAGE) (2.6.5), transferred onto a membrane (2.6.7), detected with the use of antibodies and x-ray film (2.6.8) and analysed using densitometry (2.6.9).

2.6.1 Extraction of proteins from cells

Cells on 60mm dishes were washed in PBS (4°C) and then lysed by the addition of 200µl lysis buffer (4°C) for ~1 minute; 1mM EDTA (pH 8), 1mM EGTA (pH 8), 1.28mM sucrose, 2mM Tris (pH 7.6), 10% (v/v) Triton X-100, dH_20 and 1 protease inhibitor tablet per 10mls. Cells were scraped off dishes and then broken up by being passed through a 20-gauge needle ~10 times. Cells were spun down at 10,000g for 10 minutes at 4°C to remove cellular debris. The supernatant was aliquoted and stored at -20°C.

2.6.2 Determination of protein concentration (Bradford assay)

The Bradford assay is a colorimetric assay used to determine protein concentration. A stock BSA solution (1mg/ml in lysis buffer) was used to provide a range of protein standards (0µg, 0.05µg, 1µg, 2µg, 5µg, 10µg, 20µg and 40µg). BSA standards and protein samples (3µl) were made up to 40µl with dH_20. Protein Assay Dye Reagent Concentrate (1ml) was then added to the standards and samples which were briefly vortexed and left to stand for 15 minutes at RT. The Coomassie Brilliant Blue G-250 dye within the reagent binds to protein causing a shift in maximum absorption from 465nm to 595nm with a corresponding change in colour from blue to brown. The absorbance measurements from BSA standards at 595nm were plotted to form a standard curve to which a line of best fit was added (Figure 2.5). The absorbance measured from the 0µg BSA standard was subtracted from each reading. The value of the slope (Y), calculated from the line of best fit, was used to calculate the concentration of protein samples which were measured in triplicate. The average absorbance from the protein samples (divided by 3 as 3µl of protein samples) was divided by the slope (Y) of the standard curve. This provided an estimate of protein concentration in µg/µl which was used to calculate the volume required to load 20µg and 40µg samples onto gels.

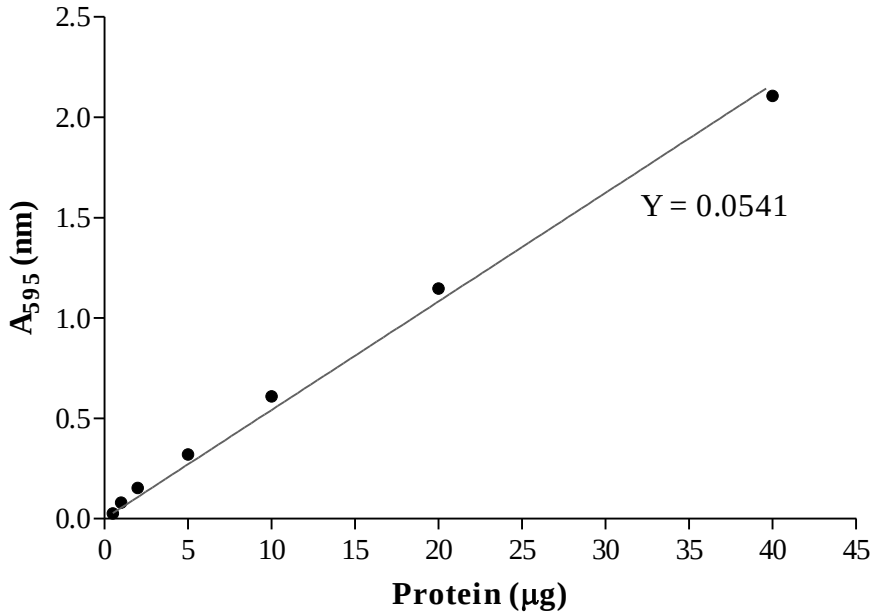

Figure 2.5 BSA standard curve

An example of a standard curve generated from BSA standards of 0.05µg, 1µg, 2µg, 5µg, 10µg, 20µg and 40µg. The absorption of each standard was measured at 595nm. A best fit linear regression line forced through the origin was added using GraphPad Prism software. The value for the slope of the line (Y) was used to calculate the concentration of protein samples.

2.6.3 Chloroform/methanol protein precipitation

The chloroform/methanol method (Wessel and Flugge, 1984) was used to precipitate proteins if concentrations were too low for SDS-PAGE as determined by Bradford assay. To the protein samples (20µg or 40µg in 100µl deionised H_2O) methanol (4 volumes) was added and the samples were vortexed. Chloroform (1 volume) was added and the samples were vortexed. Deionised H_2O (3 volumes) was added and the samples were vortexed and then spun down at 13,000 rpm for 2mins. The supernatant above the protein layer was removed and discarded. Methanol (3 volumes) was then added and the samples were inverted gently to allow mixing. The samples were then again spun at 13,000rpm for 2 minutes. The supernatant was removed and discarded and the protein pellets allowed to air dry for ~5 minutes. 1 x sample buffer (2.6.4) was added to the protein pellets which were then heated for 5 minutes at 95°C. Samples were then spun down for 10 seconds at 13,000rpm to remove condensation on the underside of the lid. Samples could then be loaded directly onto gels or stored at -20°C until required.

2.6.4 Sample buffer

Sample buffer (1x) was composed of 2% w/v sodium dodecyl sulfate (SDS), 5% v/v 2-Mercaptoethanol, 10% w/v glycerol and bromophenol blue (pinch) in 60mM Tris (pH 6.8). SDS is an anionic detergent that denatures proteins by disrupting noncovalent bonds. SDS coats proteins with a negative charge relative to molecular weight. Mercaptoethanol reduces disulfide bonds. Heating of protein with sample buffer for 5 minutes at 95°C helps denature the proteins and aids binding of SDS. Glycerol increases the viscosity of the protein sample which weighs down samples in wells before the current is turned on. Bromophenol blue is a dye used to monitor progression of protein separation in SDS-PAGE as it is a small molecule which migrates through the gel quickly.

2.6.5 SDS-PAGE

When an electric field is applied the negatively charged proteins move toward the positive electrode located at the bottom of the gel. Proteins are separated based on their molecular weight where small proteins move through the porous polyacylamide gel quickly and large proteins move through the gel more slowly.

20µg protein samples (or 40µg for Orai1) were made up to 20µl with dH_20 so that the same volume of sample was loaded into each well. 1x sample buffer was added to each protein sample. Samples were heated for 5 minutes at 95°C and centrifuged for 10 seconds at 12,000g to remove condensation on the underside of the lid.

NuPAGE gels (10% Bis-Tris) were clamped into a gel tank (Invitrogen, Life Technologies Ltd, Paisley, UK). The inner chamber was filled with NuPAGE MOPS SDS buffer (200ml) with antioxidant (500µl). The addition of antioxidant to the inner chamber maintains proteins in a reduced state during electrophoresis. The outer chamber was filled with NuPAGE MOPS SDS buffer (600ml). The comb was removed and each well was washed with buffer from the inner chamber using a Hamilton syringe. Protein samples and the molecular weight marker (10µl) were loaded into the wells using a Hamilton syringe (25µl). Electrophoresis was carried out at a constant voltage of 200V for ~1 hour or until dye front reached the bottom of the gel.

2.6.6 Transfer

Following SDS-PAGE proteins were transferred from gels onto nitrocellulose membranes at 50V (constant) for 2 hours using a wet transfer system. A transfer cassette was set up to transfer the proteins from the gel onto a nitrocellulose membrane. Foam sponges, blotting paper and nitrocellulose membranes were cut to fit transfer cassettes and then pre-equilibrated in transfer buffer (25mM Tris, 192mM glycine, 20% v/v methanol). The gel was removed from its casing. The transfer cassette was then constructed as follows; 1x sponge, 2x sheets of blotting paper, gel, nitrocellulose membrane, 2x sheets of blotting paper and 1x sponge (Figure 2.6). Air bubbles were removed following the placement of the nitrocellulose membrane on the gel by carefully rolling a glass pipette over the surface. Transfer cassettes were placed in the transfer tank (BioRad, Bio-Rad Laboratories Ltd, Hertfordshire, UK) in an orientation so that the gel was closest to the negative electrode and the nitrocellulose membrane was closest to the positive electrode so that when an electric field was applied the negatively charged proteins moved towards the positive electrode and bound to the nitrocellulose membrane. A cooling unit was placed in the transfer tank to prevent overheating during transfer (Bio-Ice Cooling Unit). Transfer tanks were then placed on a magnetic stirplate to ensure the buffer was continuously stirred throughout transfer.

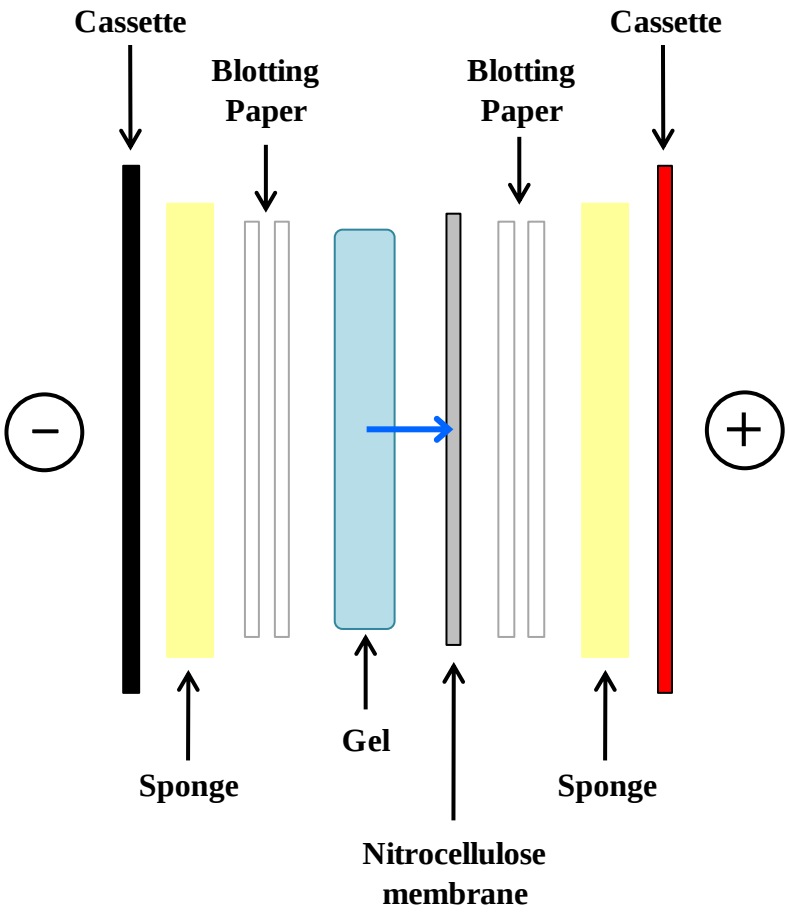

Figure 2.6 Transfer Cassette

Proteins were transferred from gels onto nitrocellulose membranes (represented by blue arrow) using a wet transfer system. The transfer cassette was set up in a 'sandwich' formation; sponge, blotting paper, gel, nitrocellulose membrane, blotting paper, sponge. Transfer cassettes were placed in the transfer tank in an orientation so that the gel was closest to the negative electrode (-) and the nitrocellulose membrane was closest to the positive electrode (+). Application of an electric field causes the negatively charged proteins to move toward the positive electrode and bind to the nitrocellulose membrane. Transfers were performed at a constant voltage of 50V for 2 hours.

2.6.7 Blocking

Following the transfer of proteins onto nitrocellulose membranes the cassette was disassembled and the gel was discarded. Membranes were briefly washed in PBS and then incubated with block (PBS, 5% w/v non-fat dried milk, 0.02% v/v Triton X-100) for 1 hour at RT with gentle agitation to block unoccupied sites on membranes to prevent non-specific binding of antibodies.

2.6.8 Immunodetection

Membranes were placed in 50ml falcon tubes (with the side that was in contact with the gel facing inwards) with 3mls of incubation buffer (PBS, 2.5% w/v non-fat dried milk) containing primary antibody (see Table 2.5a). Membranes were incubated overnight at 4°C on rollers. Following incubation with primary antibody membranes were washed (3 x 5 minutes) in wash buffer (PBS, 2.5% w/v non-fat dried milk, 0.2% v/v Triton X-100) to remove any unbound primary antibody.

Membranes were then incubated with horseradish peroxidise (HRP) conjugated secondary antibody in 5mls of incubation buffer (see Table 2.5b) for 1-2 hours at RT on rollers. Following secondary antibody incubation membranes were washed (3 x 10 minutes) in wash buffer to remove any unbound secondary antibody.

Immunoreactive bands on membranes were developed by processing in a solution containing, 1.25mM luminol in 0.1M Tris (pH 8.5), 0.09mM p-coumaric acid and 0.09% v/v hydrogen peroxide for 1 minute. Membranes were wrapped in saran wrap, placed in a film cassette and exposed to x-ray film (Hyperfilm^{TM}, GE Healthcare, Life Sciences, Amersham, Bucks, UK) for various times (2 seconds - 10 minutes) depending on the primary antibody used. Regions of film exposed to light (i.e. from HRP) darken. Exposed film was placed in Kodak Developer until immunoreactive bands were visible, briefly washed in water and then placed in Kodak fix for 5 minutes.

a)

Primary antibody	Dilution used
Anti-β-Actin	1/10000
Anti-Bcl-2	1/200
Anti-β-Tubulin III	1/20000
Anti-Orai1	1/100
Anti-STIM1	1/200
Anti-TRPC1	1/200
Anti-Vimentin	1/200

b)

Secondary antibody	Conjugate	Dilution used
Anti-Mouse	HRP	1/5000
Anti-Rabbit	HRP	1/5000

Table 2.5 Antibodies used for western blotting

a) Primary antibodies used for western blotting. All primary antibodies were incubated with blots overnight at 4°C. **b)** Secondary antibodies used for western blotting. The appropriate corresponding secondary antibody was used following primary antibody incubation. Secondary antibodies were incubated with blots for 1-2 hours at RT. All antibody dilutions were made up in incubation buffer.

2.6.9 Densitometry analysis

X-ray films were scanned onto a computer where they could be analysed using ImageJ software (Rasband W, 1997-2007). The integrated pixel density (sum of pixel values in selected area) of each band was measured (Figure 2.7). The selection area remained constant for each set of bands analysed. A background value was also subtracted from each band. Values were then expressed as a ratio of β-actin in order to determine the expression levels of proteins.

Figure 2.7 Densitometry analysis of western blots

Blots were analysed using ImageJ software (Rasband W, 1997-2007). The same area was measured for each band using the same box (dashed red).

2.7 Determination of $[Ca^{2+}]_i$

For measurements of $[Ca^{2+}]_i$ cells were seeded onto 10mm diameter glass coverslips and used when ~90% confluent. Ca^{2+} measurements were made on individual coverslips.

Cells were washed two times with Krebs buffer (10mM glucose, 118mM NaCl, 4.7mM KCl, 1.2mM KH_2PO_4, 1.2mM $MgSO_4$, 4.2mM $NaHCO_3$, 10mM HEPES, 2mM $CaCl_2$, 800μM sulfinpyrazone, pH 7.4) and then loaded with the Ca^{2+}-sensitive fluorescent indicator dye, fura-2/AM (3μM) for 45 minutes at RT in the dark.

Fura-2/AM is membrane permeable and insensitive to Ca^{2+} due to acetoxymethyl (AM) esters disguising carboxylate groups. During loading fura-2/AM diffuses across the PM and once inside the cell cytosol is activated by cleavage of AM esters to fura-2. Fura-2 is sensitive to Ca^{2+} (due to exposure of carboxylate groups) and cannot diffuse across the PM as it becomes polar. However, fura-2 can be pumped out of cells or taken up into organelles, such as mitochondria, by organic anion transporters. This results in poor loading and/or inaccurate fluorescent readings. Sulfinpyrazone (an organic anion transport inhibitor) is therefore added to Krebs buffer to prevent this from occurring.

Following loading cells were washed twice in Krebs buffer and incubated for a further 25 minutes at RT in the dark to allow fura-2/AM to fully de-esterify.

Each coverslip was washed twice in Ca^{2+}-free Krebs buffer and then mounted in a coverslip holder (PerkinElmer, Beaconsfield, UK). Coverslip holders were inserted into a Hellma fluorescence UV Quartz 10mm cuvette (Scientific Laboratory Supplies Ltd, Nottingham, UK) containing Ca^{2+}-free Krebs buffer and a magnetic stirrer. The cuvette was then placed into a fluorimeter (PerkinElmer, LS-50B) for measurement of $[Ca^{2+}]_i$ in cells. Before beginning each experiment an excitation wavelength scan (250-450nm) was performed to identify poor confluency and/or dye loading (Figure 2.8). Less than 5% of coverslips were rejected on this basis.

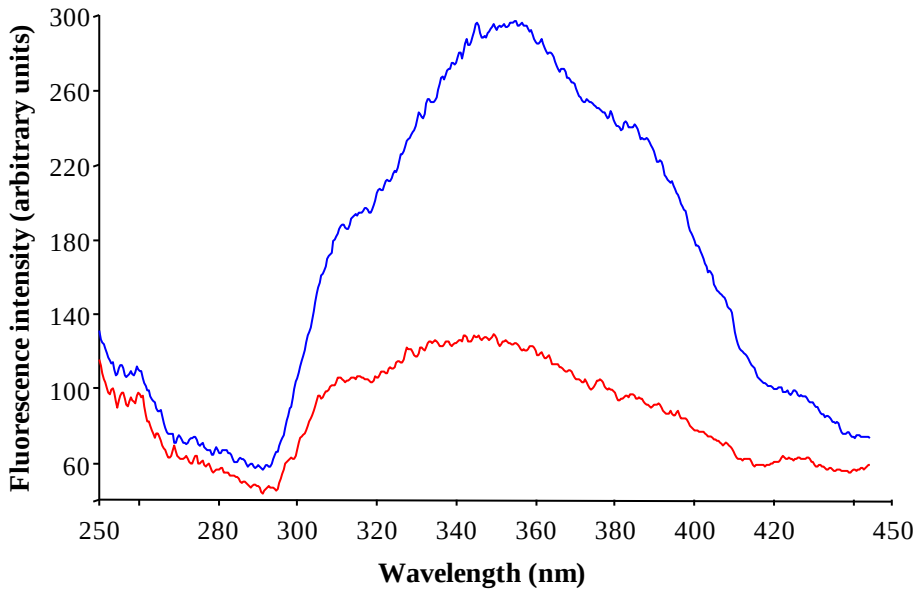

Figure 2.8 Examples of excitation wavelength scans

Blue trace: A scan showing good fura-2 loading and high cell confluency as determined by the high peak of fluorescence intensity (~300) units and the low shoulders either side of the peak. Red trace: A scan showing poor fura-2 loading and low cell confluency as determined by the low peak of fluorescence intensity (~100 units) and the high shoulder to the left of the peak. Coverslips for which such scans were obtained were rejected for use in Ca^{2+} add-back experiments.

Ca^{2+} add-back experiments were performed in order to measure both store depletion and resultant Ca^{2+} entry (i.e. SOCE). Fura-2 fluorescence was monitored continuously using excitation and emission wavelengths of 340nm and 510nm respectively. A typical Ca^{2+} add-back trace is shown Figure 2.9a.

Following the establishment of a steady baseline TG (200nM) was added to the cuvette. TG is a selective inhibitor of the SERCA pump which causes Ca^{2+} to leak from the ER into the cell cytosol. The resultant increase in $[Ca^{2+}]_i$ is observed as an increase in fura-2 fluorescence. Although depletion of ER Ca^{2+} stores activates the SOCE pathway only store depletion is measured as cells are in Ca^{2+}-free buffer.

Following store depletion (TG response), Ca^{2+} ($CaCl_2$, 2mM) was added to the cuvette. An increase in $[Ca^{2+}]_i$ concentration occurs as extracellular Ca^{2+} enters the cells to replenish depleted stores. The increase in $[Ca^{2+}]_i$, observed as an increase in fura-2 fluorescence, reveals the activity of the SOCE pathway.

The Ca^{2+} ionophore ionomycin (50µM) was added to the cuvette. Ionomycin increases cell membrane permeability to Ca^{2+} resulting in a massive influx of Ca^{2+} into the cell. This saturates the fura-2 dye causing a large sharp rise in $[Ca^{2+}]_i$ and therefore fluorescence. This provides a maximum fluorescence (F_{max}) value.

Mn^{2+} ($MnCl_2$, 1mM) was added to the cuvette. Fura-2 has a greater affinity for Mn^{2+} than Ca^{2+} and therefore quenches the dye. This results in a sharp drop in fluorescence, providing an indirect measurement of the minimum fluorescence (F_{min}), known as auto-fluorescence (AF).

The F_{max} and AF values were used to calibrate Ca^{2+} add-back traces to translate changes in fluorescence to changes in $[Ca^{2+}]_i$. Perkin Elmer Winlab software uses the formula of Grynkiewicz *et al,* 1985 which assumes a dissociation constant (K_d) of 224nM and an instrument constant (IC) of 3. To calculate F_{min} and $[Ca^{2+}]_i$ the following equations were used:

$$F_{min} = 1 / IC \ (F_{max} - AF)$$

$$[Ca^{2+}]_i = K_d \ (F - F_{min}) / (F_{max} - F)$$

Each trace was individually calibrated to account for variation in confluency and/or dye loading in cells. A typical calibrated trace is shown Figure 2.10a.

To quantify store depletion and resultant Ca^{2+} entry the areas from TG responses and Ca^{2+} responses were calculated from calibrated traces using Perkin Elmer Winlab software. An example of the regions selected to calculate the area of TG and Ca^{2+} responses is indicated by the dashed lines in Figure 2.10a. For each set of experiments performed data are presented in histograms showing the mean areas obtained.

TG is dissolved in DMSO and therefore control Ca^{2+} add-back traces were performed by adding the equivalent volume of vehicle control DMSO (0.02%) in place of TG. A typical control Ca^{2+} add-back trace is shown in Figure 2.9b. Control Ca^{2+} add-back traces were calibrated; a typical control calibrated trace is shown Figure 2.10b. For each dish (4 coverslips in total) 1 coverslip was used as a control (DMSO: Figure 2.9b) and the other 3 coverslips were used to determine the TG response (Figure 2.9a). The mean areas obtained from calibrated control DMSO traces were subtracted from the mean areas obtained from calibrated TG traces. All histograms presented throughout this thesis are basal-subtracted (i.e. DMSO response) and are therefore response to stimulus only.

To calculate the percentage decrease in $[Ca^{2+}]_i$ following treatments and/or transfections the mean Ca^{2+} response was divided by the control Ca^{2+} response and multiplied by 100 to obtain the treated/transfected mean as a percentage of the control mean. This value was then subtracted from 100 to provide the percentage decrease.

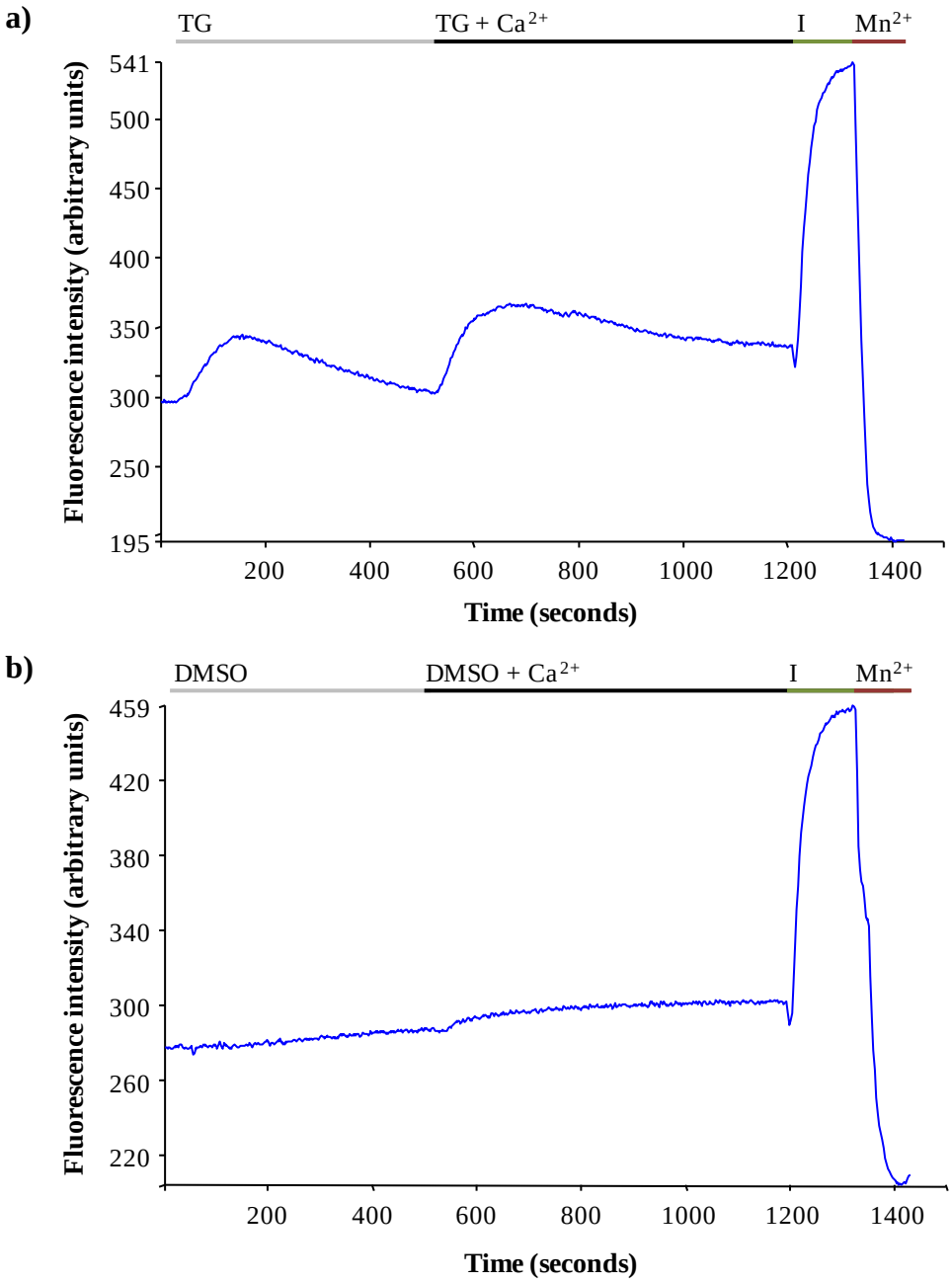

Figure 2.9 Ca^{2+} add-back experiments

a) Typical trace from a Ca^{2+} add-back experiment. An increase in fluorescence is observed following the addition of TG (200nM), due to store depletion, and Ca^{2+} (2mM), due to Ca^{2+} entering the cell cytosol. The addition of ionomycin (I) (50µM) and Mn^{2+} (1mM) provided the maximum and minimum fluorescence respectively and therefore enabled calibration of the trace. **b)** Typical trace from a control Ca^{2+} add-back experiment. Vehicle control DMSO (0.02%) was added in place of TG. The addition of Ca^{2+} (2mM) reveals Ca^{2+} entry not specific to SOCE. Ionomycin (I) (50µM) and Mn^{2+} (1mM) were added to enable calibration of traces.

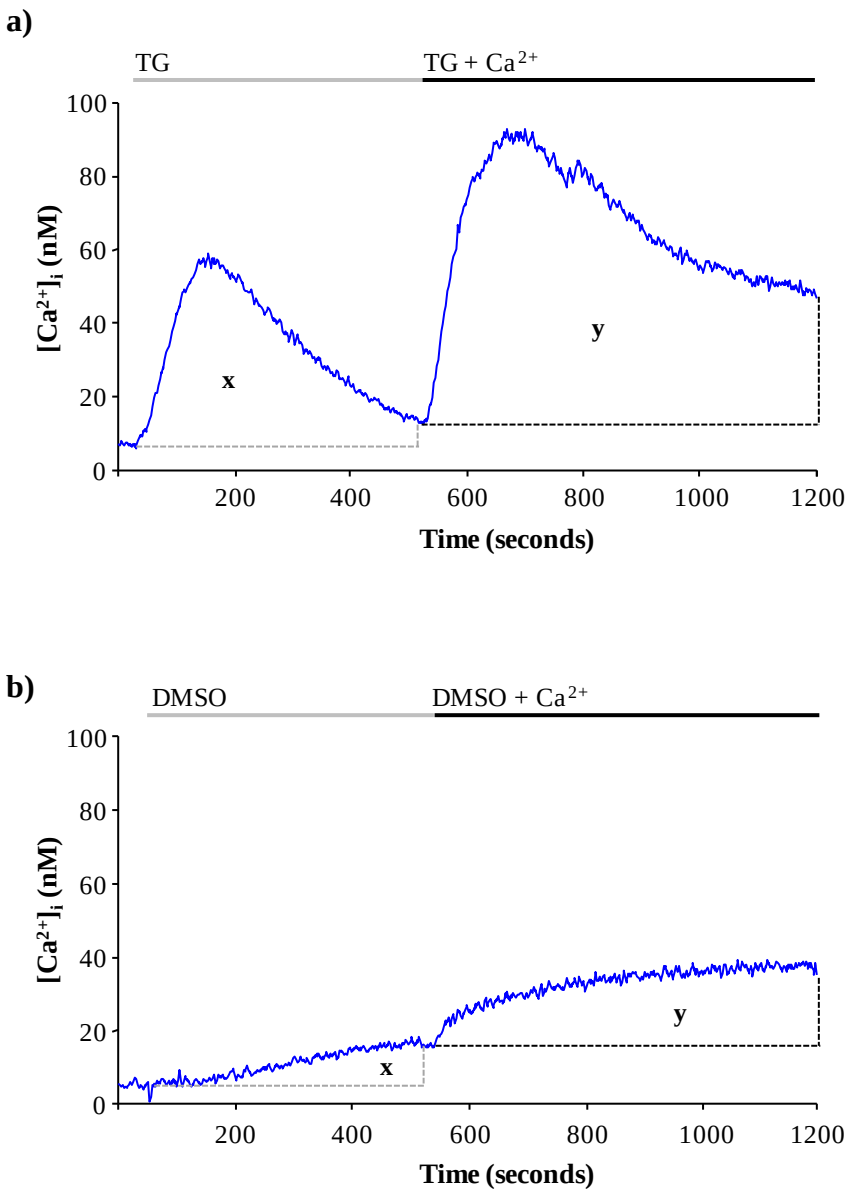

Figure 2.10 Calibrated Ca^{2+} add-back traces

a) Typical calibrated trace from a Ca^{2+} add-back experiment. An increase in $[Ca^{2+}]_i$ is observed following the addition of TG (200nM), due to store depletion, and Ca^{2+} (2mM), due to Ca^{2+} entering the cell cytosol. **x** indicates the area measured to calculate the TG response. **y** indicates the area measured to calculate the Ca^{2+} response **b**) Typical calibrated trace from a control Ca^{2+} add-back experiment. A small increase in $[Ca^{2+}]_i$ is observed following the addition of DMSO (0.02%) and Ca^{2+} (2mM). **x** indicates the area measured to calculate the DMSO response. **y** indicates the area measured to calculate the Ca^{2+} response. Values obtained from DMSO control traces were subtracted from TG traces.

2.8 Statistics

Data are generally presented as mean ± SEM of *n* determinations (Cumming *et al*., 2007). Statistical comparisons of mean values were performed using GraphPad Prism software. For unpaired groups a two-tailed Student's t-test was used. For groups of three or more, one-way analysis of variance (ANOVA) was used. Statistical significance was accepted at $P<0.05$. The level of significance was also indicated on graphs ($P<0.05$*, $P<0.01$**, $P<0.001$***).

Chapter 3

Results I - 9*c*RA-induced differentiation of SH-SY5Y cells and enrichment for N- and S-type cells

3.1 Introduction

SH-SY5Y neuroblastoma cells differentiate into neuronal-like cells following RA treatment (Brown *et al*., 2005). The first aim of this chapter was to define 9*c*RA-induced differentiation of SH-SY5Y cells both morphologically and biochemically.

The SH-SY5Y cell line is composed of two identifiable cell phenotypes; 'neuroblastic' N-type cells and 'substrate-adherent' S-type cells. N-type cells are the predominant cell type of the SH-SY5Y cell line, which itself is classed as an N-type cell line (Introduction 1.3). N-type cells are the neuroblast population that commonly form the bulk of most neuroblastoma tumours. These cells are of the sympathoadrenal neural crest cell lineage and are those that differentiate into neuronal-like cells following 9*c*RA treatment. S-type cells are a population derived from a non-neuronal neural crest cell lineage. These cells are precursors to glial type cells of the SNS. Although the minority cell type in the SH-SY5Y cell line S-type cells can compose 5-15% of the cell population. The second aim of this chapter was to enrich for N- and S-type cell populations from the SH-SY5Y cell line and define these cell populations both morphologically and biochemically prior to and following 9*c*RA-induced differentiation.

N- and S-type cell populations were enriched from the SH-SY5Y cell line which was possible due to differences in substrate adherence between the cells, where N-type cells are weakly adherent and S-type cells are strongly adherent (Methods 2.2). N- and S-type cells were defined biochemically in order to further characterise the two cell types. The neuronal protein β-Tubulin III (a component of microtubules) and the non-neuronal protein vimentin (an intermediate filament protein) were used to provide immunofluorescent profiles for both proliferating and differentiated SH-SY5Y, N- and S-type cells. The level of expression of the proto-oncogene Bcl-2 was also investigated in SH-SY5Y, N- and S-type cells.

3.2 Results

3.2.1 SH-SY5Y cells differentiate into a neuronal like phenotype following 9*c*RA treatment

SH-SY5Y neuroblastoma cells were treated with 1µM 9*c*RA for 7 days in order to induce differentiation. Cells treated with 9*c*RA will henceforth be referred to as differentiated cells. Differentiated cells were characterised by rounded cell bodies and longer, straighter, less branched neurite extensions (Figure 3.1b). Differentiation was quantified morphologically by measuring neurite length, where cells were deemed differentiated if they had one or more neurite extensions of ≥50µm in length (Pahlman *et al*., 1981, 1984; Nicolini *et al*., 1998; Brown *et al*., 2005). Control cells were treated with an equal volume of EtOH as vehicle (0.01% of culture media volume). Cells treated with EtOH will henceforth be referred to as proliferating cells. Proliferating cells were characterised by elongated or rounded cell bodies and many short, branched neurite like processes (Figure 3.1a). The morphological appearance of proliferating cells was the same as before treatment with EtOH.

Differentiated cell populations (Figure 3.1b) were far less confluent compared to proliferating cell populations (Figure 3.1a), demonstrating that 9*c*RA treatment inhibits proliferation. The effect of inhibition of proliferation can be seen when seeding cells for experiments; for differentiated cells to have an equal confluency to proliferating cells after 7 days treatment, 4 times as many cells need to be seeded (Methods 2.2.4). This can also be seen by comparing the cell counts for 7 day treated proliferating (4097 cells) and differentiated cells (1035 cells) where cells were seeded at the same density prior to treatment (Figure 3.2). The growth rate of proliferating cells remained the same as before treatment with EtOH.

Morphologically, as determined by neurite length, there was a significant increase in the percentage of differentiated cells following only 1 day of 9*c*RA treatment; 2.95±0.36% vs. 6.71±1.60%, P=0.0404 (Figure 3.2). By 7 days 9*c*RA treatment 34.79±3.71% of cells were classed as differentiated (compared to 7 day EtOH 2.03±0.19%, P<0.0001). This indicates a heterogeneous response to 9*c*RA treatment where some cells respond more quickly compared with others. The extent of differentiation seen in proliferating

cells did not significantly change throughout the 7 days of EtOH treatment and never exceeded 3%. The percentage of differentiated cells did not increase beyond ~35% even following 8 or more days of 9*c*RA treatment and therefore never reached 100%. It is noteworthy however that the extent of morphological differentiation may actually be higher than that seen (~35%) as only neurites that were fully visible could be counted. Nevertheless cells are clearly heterogeneous in their response to 9*c*RA as cells of a proliferating morphology are always present in 9*c*RA differentiated cell populations.

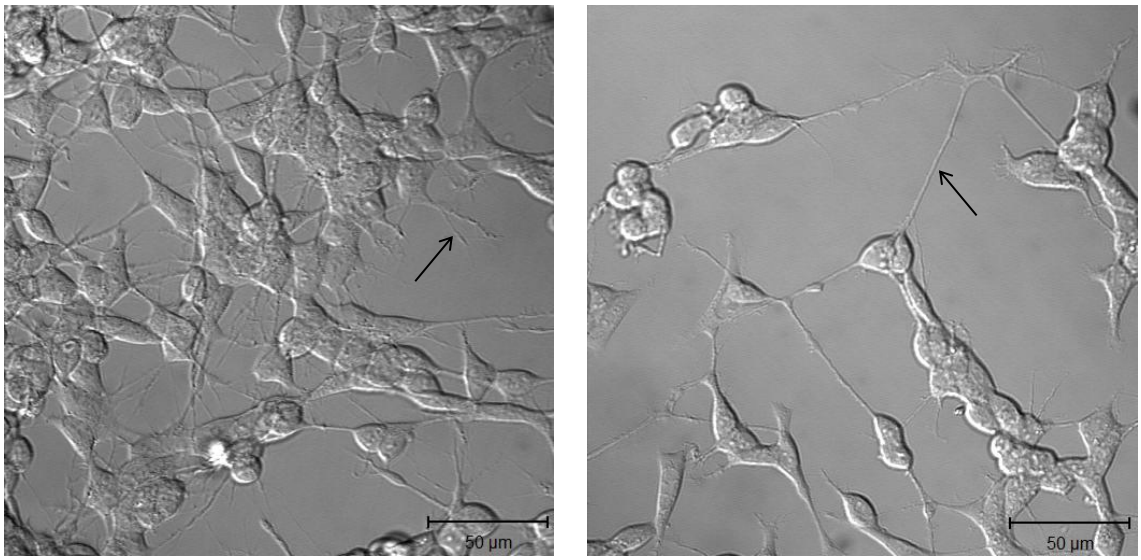

a) Proliferating cells (EtOH) **b) Differentiated cells (9*c*RA)**

Figure 3.1 9*c*RA treatment of SH-SY5Y cells induces morphological differentiation

Cells were treated with either vehicle EtOH or 1µM 9*c*RA for 7 days. DIC images of cells were taken following treatment. **a**) Proliferating cells (vehicle EtOH treated) display many short branched processes (arrow). **b**) Differentiated cells (1µM 9*c*RA treated) exhibit neurite extensions (arrow). Cells were deemed differentiated if they exhibited neurites of ≥50µm in length. The same numbers of cells were seeded onto coverslips prior to treatment. Images are representative of >50 images. Scale bars represent 50µm.

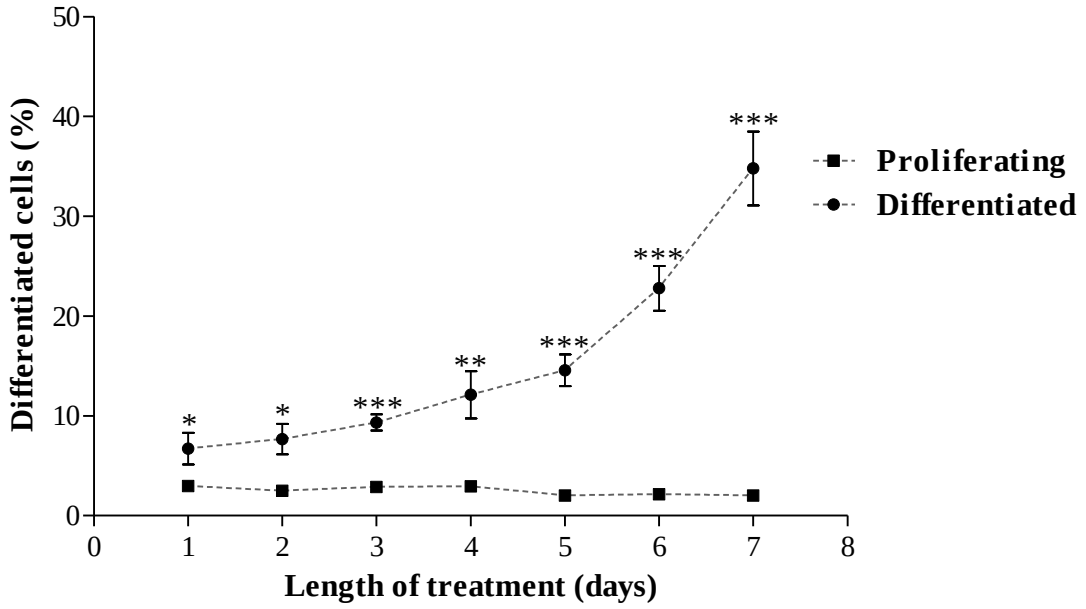

Figure 3.2 9*c*RA treatment of SH-SY5Y cells induces morphological differentiation over 7 days as determined by neurite length

Cells were treated with either vehicle EtOH (proliferating) or 1µM 9*c*RA (differentiated) for 1-7 days. DIC images were taken of cells following treatment. Cells with one or more neurite extensions of ≥50µm in length were classed as differentiated. Differentiated cells were counted and expressed as a percentage of the total cell population. Following 7 days 9*c*RA treatment (i.e. the point at which the cells were used in this study) ~35% of cells were classed as differentiated, compared with only ~2% in 7 day proliferating cells. Day 1; proliferating cells, *n*=7 (101/3373 cells), differentiated cells *n*=7 (176/3417 cells), P=0.0404*. Day 2; proliferating cells, *n*=6 (61/2494 cells), differentiated cells *n*=7 (213/3233 cells), P=0.0107*. Day 3; proliferating cells, *n*=6 (84/2928 cells), differentiated cells, *n*=6 (243/2636 cells), P<0.0001***. Day 4; proliferating cells, *n*=6 (86/2996 cells), differentiated cells *n*=4 (151/1469 cells), P=0.0017**. Day 5; proliferating cells, *n*=6 (62/3193 cells), differentiated cells *n*=6 (253/1721 cells), P<0.0001***. Day 6; proliferating cells, *n*=6 (87/4091 cells), differentiated cells *n*=6 (248/1163 cells), P<0.0001***. Day 7; proliferating cells, *n*=6 (83/4097 cells), differentiated cells *n*=6 (319/1035 cells), P<0.0001***.

3.2.2 Bcl-2 is a biochemical marker of differentiation

Previous studies in this laboratory have shown that the anti-apoptotic proto-oncogene Bcl-2 is expressed in both proliferating and differentiated SH-SY5Y cells (Riddoch *et al*., 2007). Immunolocalisation studies revealed that Bcl-2 expression was up-regulated in differentiated cells compared to proliferating cells, as determined by an increase in fluorescence (Riddoch *et al*., 2007). The same anti-Bcl-2 antibody was used in this study to observe changes in protein expression following 1-7 days of EtOH (proliferating) and 9*c*RA (differentiated) treatment.

Bcl-2 is expressed in both proliferating (Figure 3.3a) and differentiated (Figure 3.3b) SH-SY5Y cells as identified by the presence of a band at 26kDa, the molecular weight for Bcl-2 (Hanada *et al*., 1993). Proliferating cells (EtOH) showed no change in the level of Bcl-2 expression throughout the 7 days treatment whereas differentiated cells (9*c*RA) showed increased Bcl-2 expression. Blots were re-probed with an anti-β-actin antibody which was used as a loading control. The increase in Bcl-2 expression in differentiated cells was confirmed by quantitative analysis where Bcl-2 was expressed as a ratio of β-actin (Figure 3.3c). Bcl-2 expression was significantly up-regulated in differentiated cells compared to proliferating cells following 5 days of 9*c*RA treatment, P=0.0217. Up-regulated Bcl-2 expression in differentiated cells following 7 days 9cRA treatment was used as a biochemical marker for differentiation.

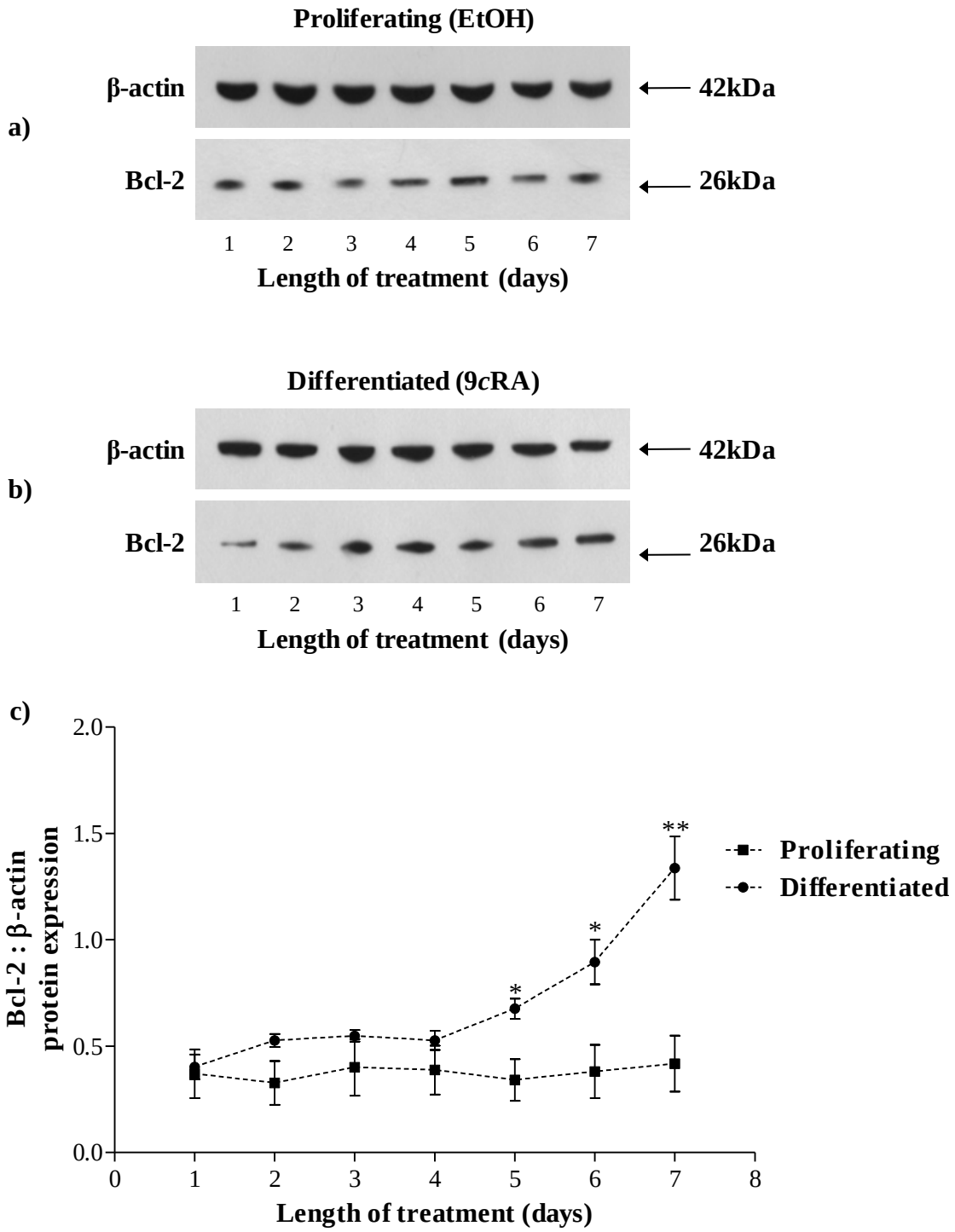

Figure 3.3 Expression of Bcl-2 increases in SH-SY5Y cells following 9*c*RA treatment

Western blots were performed on protein extracted from 1-7 day EtOH (proliferating) and 9*c*RA (differentiated) treated SH-SY5Y cells (Methods 2.6). Blots were probed with anti-Bcl-2 antibody which detected a band of 26kDa. Blots were re-probed with anti-β-actin antibody, used as a loading control, which detected a band of 42kDa.

a) Western blot showing Bcl-2 protein expression in proliferating cells treated with vehicle EtOH for 1-7 days. **b**) Western blot showing Bcl-2 protein expression in differentiated cells treated with 1µM 9*c*RA for 1-7 days. **c**) Quantitative measurements of bands were performed using densitometry (ImageJ software, Methods 2.6.9). Bcl-2 was expressed as a ratio of β-actin for days 1-7 of EtOH and 9*c*RA treatment. Bcl-2 expression increases with 9*c*RA treatment over 7 day and becomes significantly up-regulated by 5 days treatment. Day 1, P=0.8102. Day 2, P=0.1136. Day 3, P=0.3175, Day 4, P=0.3045. Day 5, P=0.0217*. Day 6, P=0.0198*. Day 7, P=0.0036**, *n*=4

3.2.3 Enrichment for N- and S-type cells

The SH-SY5Y cell line is composed of N-type and S-type cells. The two cell types show differences in their substrate adherence where N-type cells are weakly substrate adherent and S-type cells are strongly substrate adherent. It was therefore possible to enrich for an N-type population and an S-type population from the SH-SY5Y cell line (Figure 3.4). Each time the cells types were enriched for they were numbered accordingly (Methods 2.2). N8 and S8 enrichments were used for the experiments performed in this chapter.

The SH-SY5Y cell line is classed as an N-type cell line, although due to the heterogeneous nature of these cells, S-type cells are still present at a level of ~10% (Figure 3.4a) and are usually identified as patches amongst the N-type cells. The morphology of N-type cells is the same as that described for the SH-SY5Y cells. The cells have rounded or elongated cell bodies with many short, branched neurite-like processes (Figure 3.4b). N-type cells grow rapidly and can grow on top of one another. Attached neurospheres can be identified in SH-SY5Y and N-type cell populations (Figure 3.5). These are balls of cells thought to be derived from neural stem cells (Bez *et al*., 2003). S-type cells are larger and flatter than N-type cells. They show contact inhibition of growth (Figure 3.4c) and grow at a slower rate than the N-type cells.

Following 1µM 9*c*RA treatment for 7 days N-type cells differentiate into a neuronal like phenotype with long, straight neurite extensions (Figure 3.6c), as was seen with the SH-SY5Y cell population (Figure 3.1b). S-type cells also change morphology following 9*c*RA treatment and become larger and flatter in appearance (Figure 3.6d).

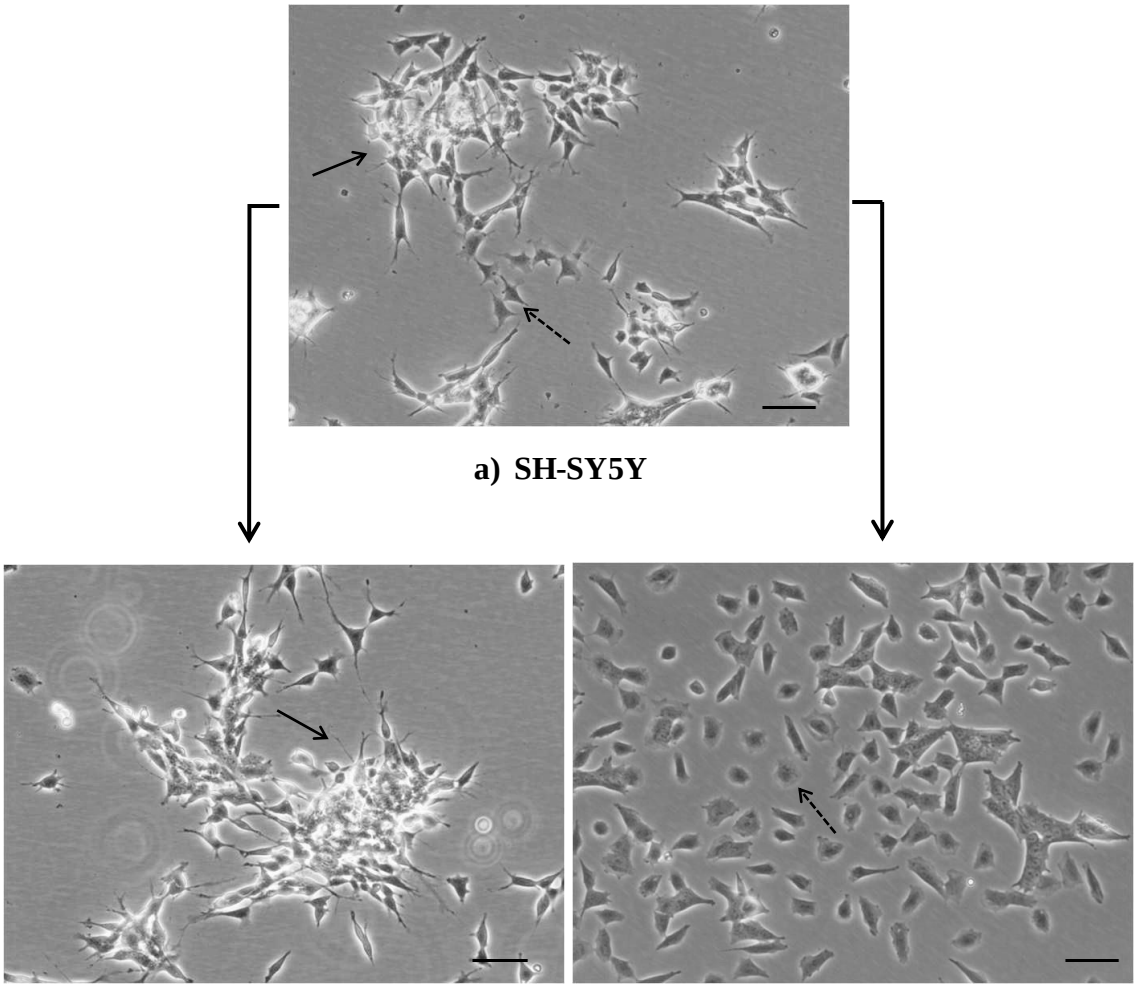

Figure 3.4 Enrichment for N- and S-type cell populations

Phase contrast images were taken of cells using a Motic AE21 microscope. **a**) The SH-SY5Y cell line, although predominantly composed of N-type cells (block arrow) is heterogeneous in nature in that it is also composed of S-type cells (dashed arrow). Due to differences in substrate adherence between the two cell types it is possible to enrich for N- and S-type cell populations (Methods 2.2). **b**) N-type cell population (N8). Cells are small with elongated cell bodies, short processes (block arrow) and are often seen growing as aggregates. **c**) S-type cell population (S8). Cells are flatter and slightly larger (dashed arrow) than N-type cells and grow as a contact inhibited layer. Scale bars represent 50µm.

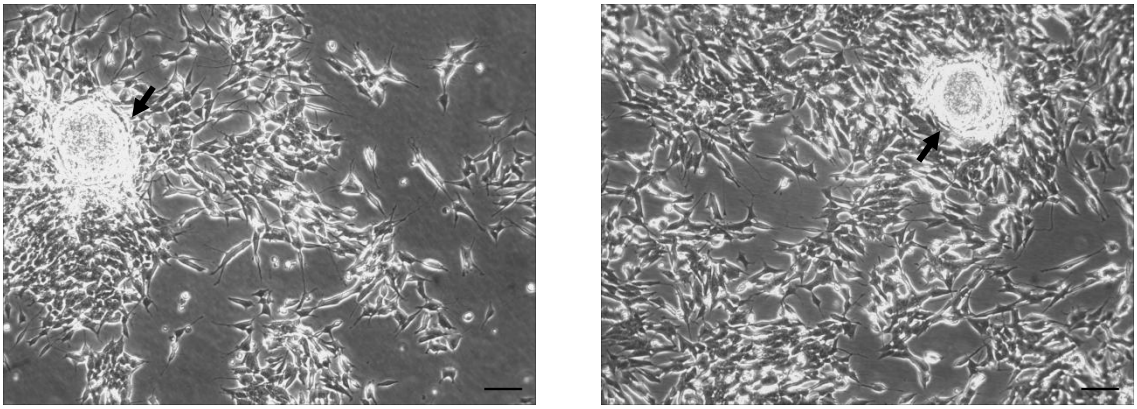

Figure 3.5 N-type cells can form neurospheres

Phase contrast images were taken of cells using a Motic AE21 microscope. Attached neurospheres (black arrows) are occasionally identified in SH-SY5Y and N-type cell populations. Scale bars represent 50µm.

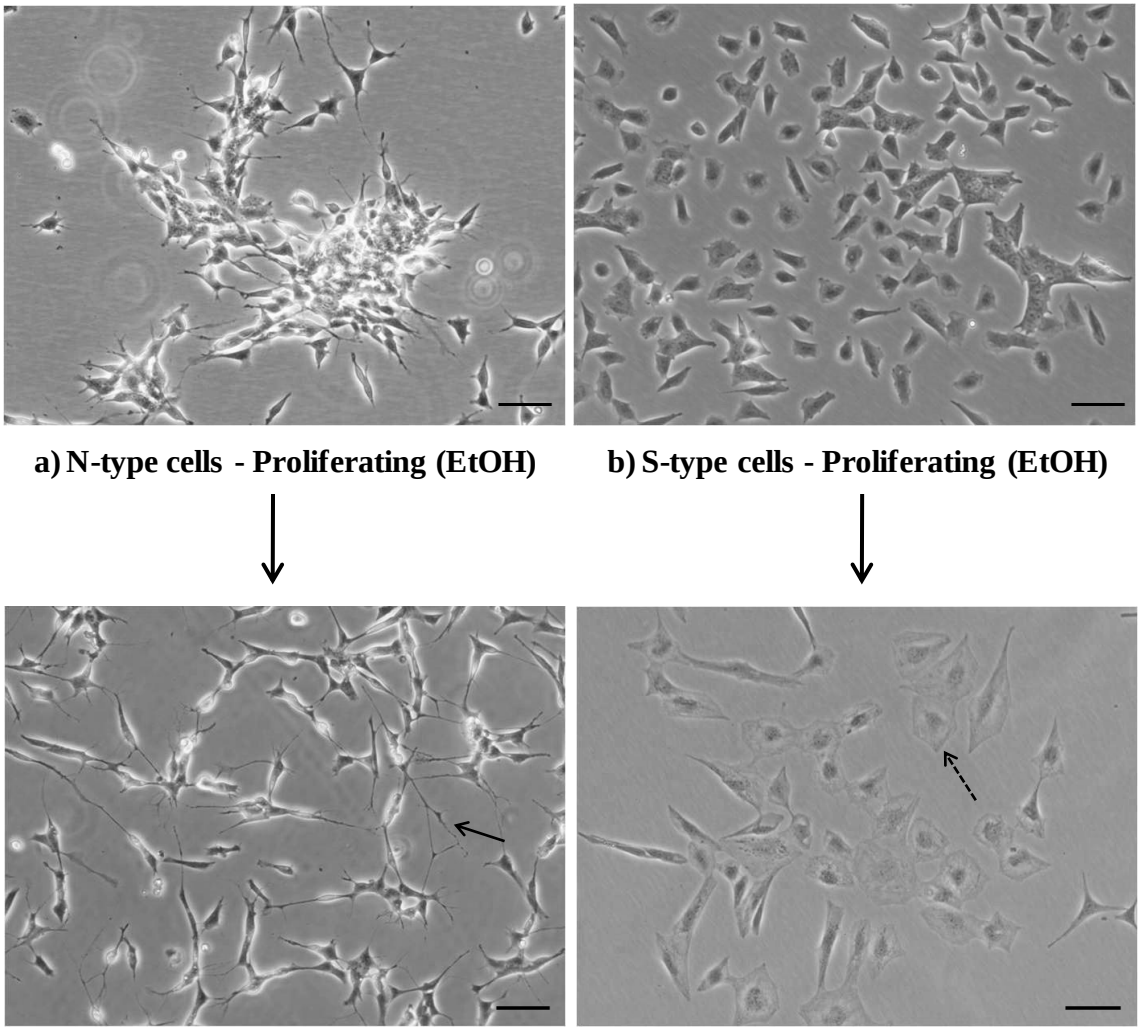

Figure 3.6 9*c*RA treatment of enriched N- and S-type cell populations

Phase contrast images were taken of cells using a Motic AE21 microscope **a**) N-type cell population. **b**) S-type cell population. **c**) N-type cell population differentiated with 1µM 9*c*RA for 7 days. Cells develop neurite extensions of ≥50µm in length (block arrow). **d**) S-type cell population differentiated with 1µM 9*c*RA for 7 days. Cells are more epithelial-like becoming larger and flatter (dashed arrow). Scale bars represent 50µm.

3.2.4 N-type cells are positive to a neuronal marker whereas S-type cells are positive to a non-neuronal marker

Immunofluorescent studies were performed on SH-SY5Y, N- and S-type cells in order to define the cells biochemically. As previously described (Introduction 1.3) the SH-SY5Y cell line is predominantly composed of N-type cells. β-Tubulin III is a component of microtubules in neuronal cells (Draberova *et al*., 1998; Katsetos *et al*., 2003) and was therefore used to determine the neuronal like nature of the N-type cells. Vimentin is an intermediate filament protein that is expressed in non-neuronal cells derived from the neural crest such as Schwann cells and glial cells (Ciccarone *et al*., 1989) and was therefore used to determine the non-neuronal nature of S-type cells.

Proliferating and differentiated SH-SY5Y, N- and S-type cells were stained with an anti-β-Tubulin III antibody (green), an anti-vimentin antibody (red) and the dye EthD-1 (blue), which stains the cell nuclei. The SH-SY5Y cell line is predominantly composed of N-type cells which stain positive for β-Tubulin III (Figure 3.7). However patches of S-type cells, which stain positive for vimentin, are often identified within SH-SY5Y cell populations. This is consistent with the observation that S-type cells are present within the SH-SY5Y population at around 5-15% (nb not all fields of view contain patches of S-type cells).

Both proliferating and differentiated N-type cells stain positive for β-Tubulin III (Figure 3.8). Cells that stain positive for vimentin can be identified in N-enriched cell populations; these are S-type cells that remain present in all N-enriched populations albeit at a very low number. Again the difference in cell morphology following 9*c*RA treatment can be seen. Proliferating cells have elongated cell bodies with short, branched neurite like processes. Differentiated cells have rounded cell bodies and long, unbranched neurites of over 50μm in length. Neurite like extensions stain positive for β-Tubulin III (Figure 3.9 arrow i).Vimentin was identifited in some neurite extensions (Figure 3.9 arrow ii), although a non-neuronal protein, vimentin has been shown to be involved in the initiation of neurite outgrowth and is temporarily present before being replaced with neuronal proteins (Shea *et al*., 1993).

Both proliferating and differentiated S-type cells stain positive for vimentin (Figure 3.10). S-type cells also stain positive for β-Tubulin III throughout their cell cytoplasm, to the extremity of the cells, slightly beyond vimentin staining. The staining however is weak in comparison to vimentin staining and appears also to be weaker again in differentiated cells compared to proliferating cells. Following 9*c*RA treatment differentiated cells are much larger and flatter in comparison to the proliferating controls.

The distinct immunofluorescent profiles of N- and S-type cells are consistent with the morphological differences previously observed between the two cell types (Figures 3.4 and 3.6).

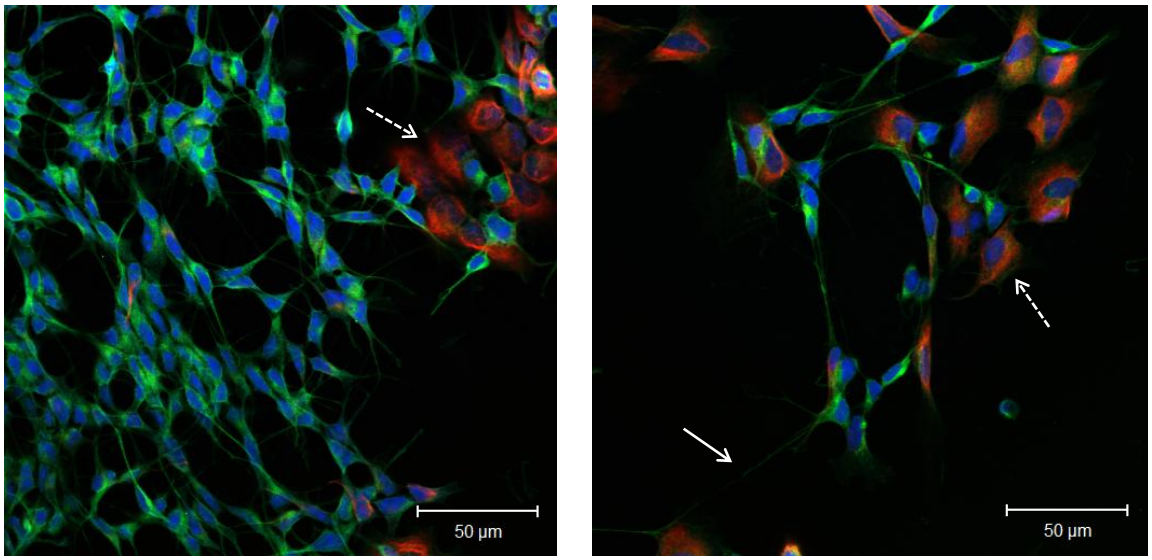

a) Proliferating cells (EtOH) **b) Differentiated cells (9*c*RA)**

Figure 3.7 Immunofluorescent profile of the SH-SY5Y cell line

Cells were stained with β-Tubulin III antibody (green), vimentin antibody (red) and the nuclear stain EthD-1 (blue). N-type cells stain positive for β-Tubulin III and S-type cells stain positive for vimentin. Images were captured using laser scanning confocal microscopy **a**) Proliferating (7 day EtOH treated) SH-SY5Y cells are predominantly comprised of N-type cells which stain positively for β-Tubulin III throughout the cell cytoplasm and down the short neurite like processes. Patches of S-type cells are often identified (dashed arrow). **b**) Differentiated (7 day 9*c*RA treated) SH-SY5Y cells are predominantly comprised of N-type cells which develop neurite extensions of ≥50µm in length that stain positive for β-Tubulin III (block arrow). As with the proliferating cells, patches of S-type cells can often be identified (dashed arrow). Images are representative of over 20 images. Scale bars represent 50µm.

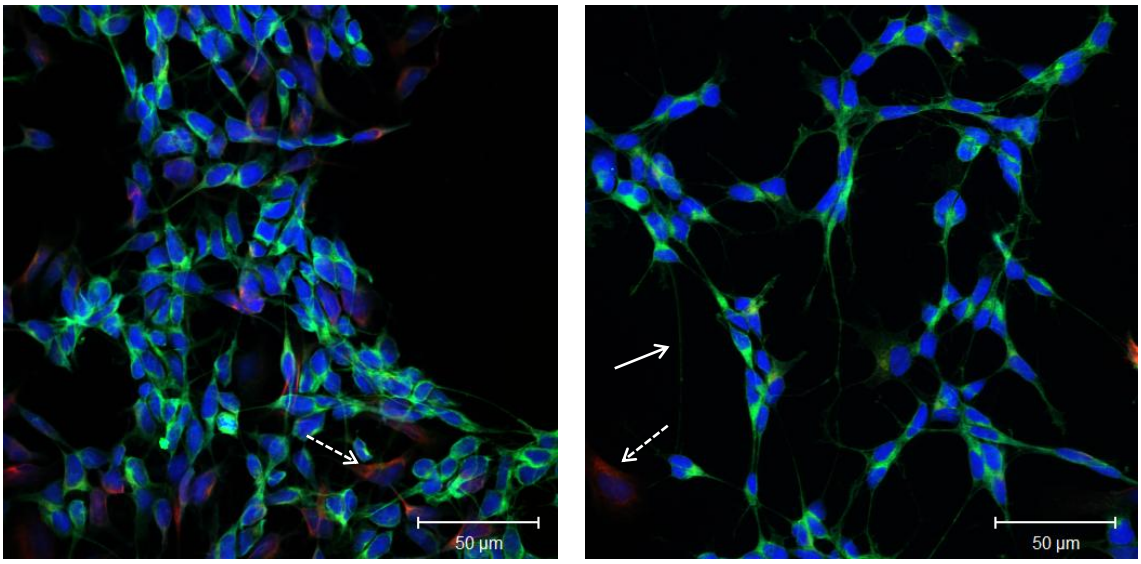

a) Proliferating cells (EtOH) **b) Differentiated cells (9*c*RA)**

Figure 3.8 Immunofluorescent profile of N-type cells

Cells were stained with β-Tubulin III antibody (green), vimentin antibody (red) and the nuclear stain EthD-1 (blue). N-type cells stain positive for β-Tubulin III and S-type cells stain positive for vimentin. Images were captured using laser scanning confocal microscopy **a**) Proliferating (7 day EtOH treated) N-type cells stain positively for β-Tubulin III throughout the cell cytoplasm and down the short neurite like processes. S-type cells are still present in enriched populations (dashed arrow). **b**) Differentiated (7 day 9*c*RA treated) N-type cells develop neurite extensions of ≥50µm in length that stain positive for β-Tubulin III (block arrow). S-type cells again remain present in enriched populations (dashed arrow). Images are representative of over 60 images. Scale bars represent 50µm.

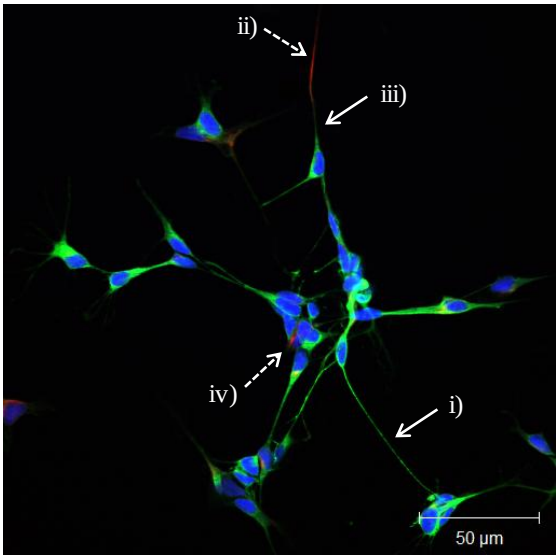

Figure 3.9 Vimentin is present in neurites in some N-type cells

Cells were stained with β-Tubulin III antibody (green), vimentin antibody (red) and the nuclear stain EthD-1 (blue). As indicated by arrow i) neuronal like extensions stain positively for β-Tubulin III. The non-neuronal protein vimentin can however also be identified in developing neurite extensions as indicated by arrow ii). Vimentin is thought to be replaced by β-Tubulin III as neurite extensions develop; arrow iii). Arrow iv) indicates an area positive for vimentin staining which may be the initiation point of a future neurite outgrowth. Scale bar represents 50µm.

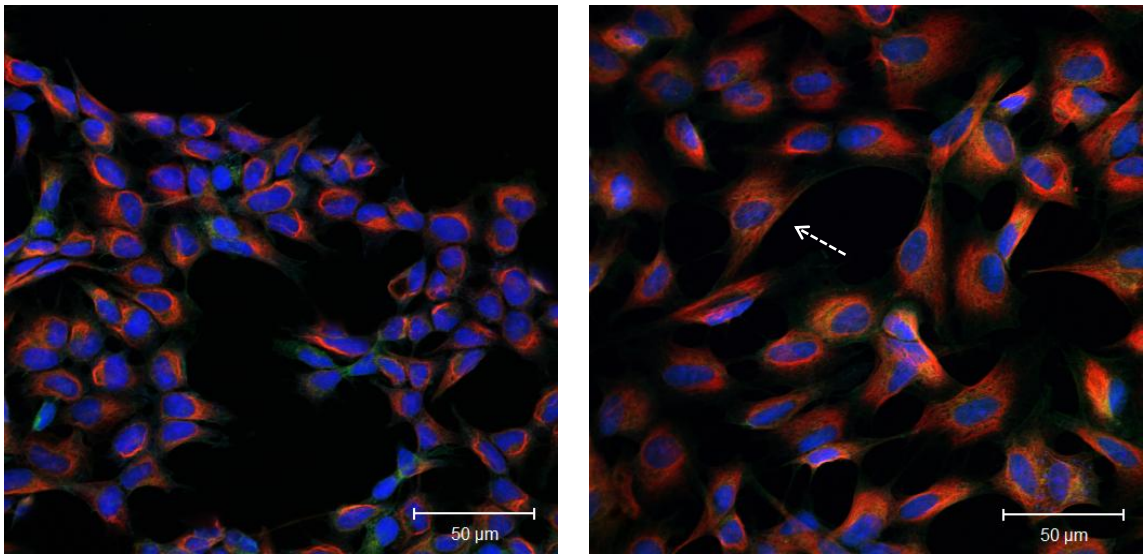

a) Proliferating cells (EtOH) **b) Differentiated cells (9*c*RA)**

Figure 3.10 Immunofluorescent profile of S-type cells

Cells were stained with β-Tubulin III antibody (green), vimentin antibody (red) and the nuclear stain EthD-1 (blue). N-type cells stain positive for β-Tubulin III and S-type cells stain positive for vimentin. Images were captured using laser scanning confocal microscopy **a**) Proliferating (7 day EtOH treated) S-type cells stain positively for vimentin throughout the cell cytoplasm. They also however stain weakly for β-Tubulin III throughout the cell cytoplasm. **b**) Differentiated (7 day 9*c*RA treated) S-type cells become larger and flatter and they too stain positive for both vimentin and β-Tubulin III (dashed arrow). Images are representative of over 50 images. Scale bars represent 50µm.

Western blots were performed on proliferating and differentiated SH-SY5Y, N-type and S-type cell protein extracts to quantify the immunofluorescent profile seen for each cell type.

β-Tubulin III is expressed in proliferating and differentiated SH-SY5Y, N- and S-type cells as determined by the presence of a band at 50kDa in response to anti-β-Tubulin III antibody (Figure 3.11a). The level of β-Tubulin III expression does not appear to be different between SH-SY5Y and N-type cells but appears to be reduced in S-type cells. Quantification of western blots (Figure 3.11b) revealed that β-Tubulin III expression was not altered in SH-SY5Y ($P=0.1672$) or N-type ($P=0.1175$) cells following 9*c*RA induced differentiation. Also β-Tubulin III expression was not significantly different between proliferating SH-SY5Y and N-type cells ($P=0.3504$) and also differentiated SH-SY5Y and N-type cells ($P=0.2179$); which may be expected due to the SH-SY5Y cell line being predominantly composed of N-type cells. Although β-Tubulin III was present in S-type cells, expression was significantly lower in proliferating S-type cells compared to proliferating SH-SY5Y ($P=0.0009$) and N-type cells ($P=0.0017$). Following 9*c*RA treatment of S-type cells the level of β-Tubulin III expression became significantly down-regulated compared to proliferating S-type cells, $P<0.0001$.

Vimentin expression was not detected in SH-SY5Y or N-type cells (Figure 3.12a). Although vimentin positive cells were seen in both SH-SY5Y (Figure 3.7) and N-type (Figure 3.8) cell populations the number of cells and/or the level of expression is presumably too low to be detected by the vimentin antibody used in this study. S-type cells stain positive for vimentin as determined by the presence of a band at 57kDa, the molecular weight of vimentin (Hanada *et al*., 1993), in response to anti-vimentin antibody. Quantification of western blots (Figure 3.12b) revealed that vimentin expression was not significantly different following 9*c*RA treatment, $P=0.8792$. From the morphological profile of S-type cells (Figure 3.6) it can be seen that the cells increase in size following 9*c*RA-induced differentiation however the level of vimentin protein remains unchanged.

The protein Bcl-2 is expressed in proliferating and differentiated SH-SY5Y, N-type cell and S-type cells as determined by the presence of a band at 26kDa, in response to anti-Bcl-2 antibody (Figure 3.13a). Quantification of western blots (Figure 3.13b) revealed

that following 7 days 9*c*RA treatment Bcl-2 protein expression becomes significantly up-regulated in SH-SY5Y cells (P=0.0198) and N-type cells (P=0.0271). Bcl-2 protein expression remains unchanged following 9*c*RA-induced differentiation of S-type cells (P=0.2325) and therefore is solely used as a biochemical marker for SH-SY5Y and N-type cell differentiation and not S-type cell differentiation.

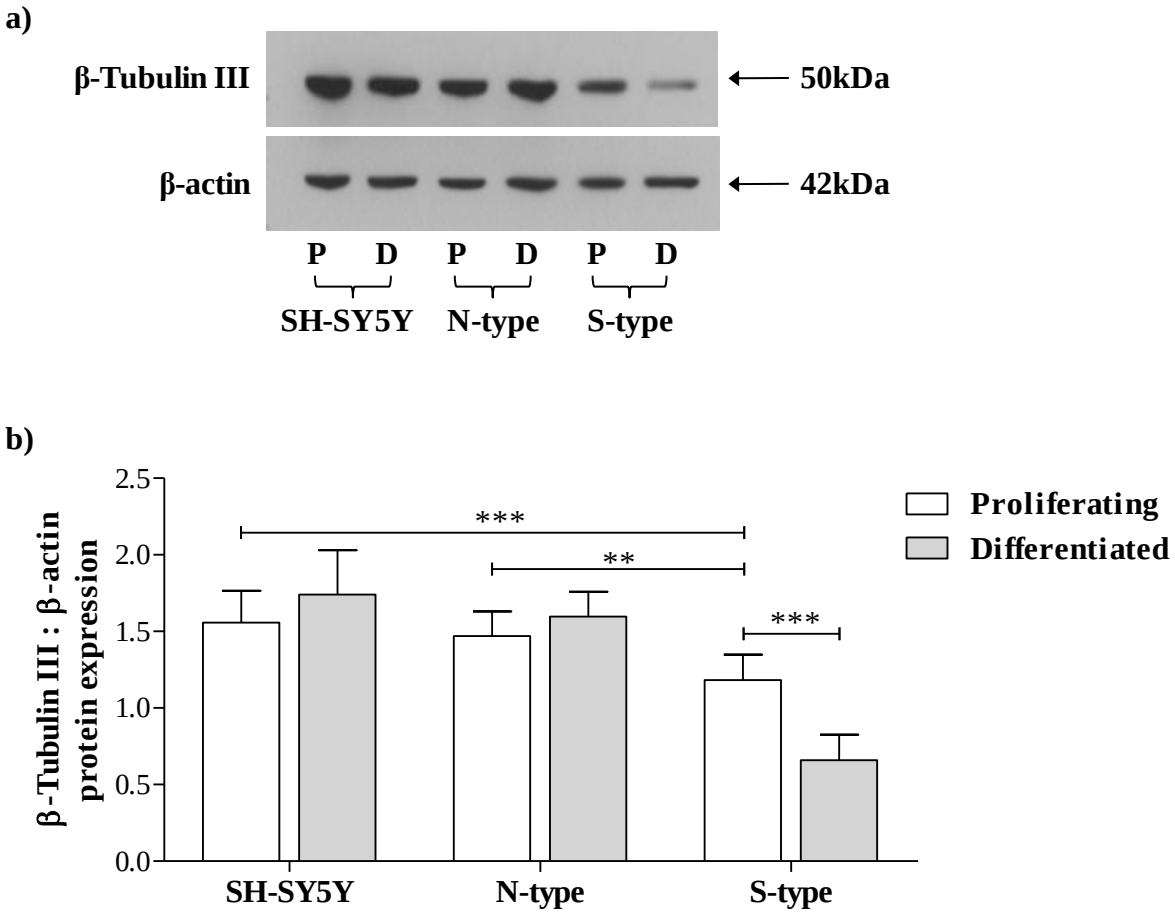

Figure 3.11 β-Tubulin III is expressed in SH-SY5Y, N-type and S-type cells

Western blots were performed on protein extracted from SH-SY5Y, N-type and S-type cells following 7 days EtOH (proliferating = **P**) or 9*c*RA (differentiated = **D**) treatment. **a**) Blots were probed with anti-β-Tubulin III antibody which detected a band at 50kDa. Blots were then re-probed with anti-β-actin antibody, used as a loading control, which detected a band of 42kDa. **b**) Quantitative measurements of bands were performed using densitometry (ImageJ software, Methods 2.6.4). β-Tubulin III was then expressed as a ratio of β-actin. β-Tubulin III expression does not change following 9*c*RA treatment in SH-SY5Y (P=0.1672) or N-type cells (P=0.1175) compared to their respective proliferating controls. However β-Tubulin III expression becomes significantly reduced in S-type cells following 9*c*RA treatment compared to proliferating controls, $P<0.0001^{***}$. β-Tubulin III expression is also significantly lower in proliferating S-type cell populations compared to SH-SY5Y ($P=0.0009^{***}$) and N-type ($P=0.0017^{**}$) proliferating cell populations. For SH-SY5Y cells $n=8$, for N-type cells $n=9$ and for S-type cells $n=9$.

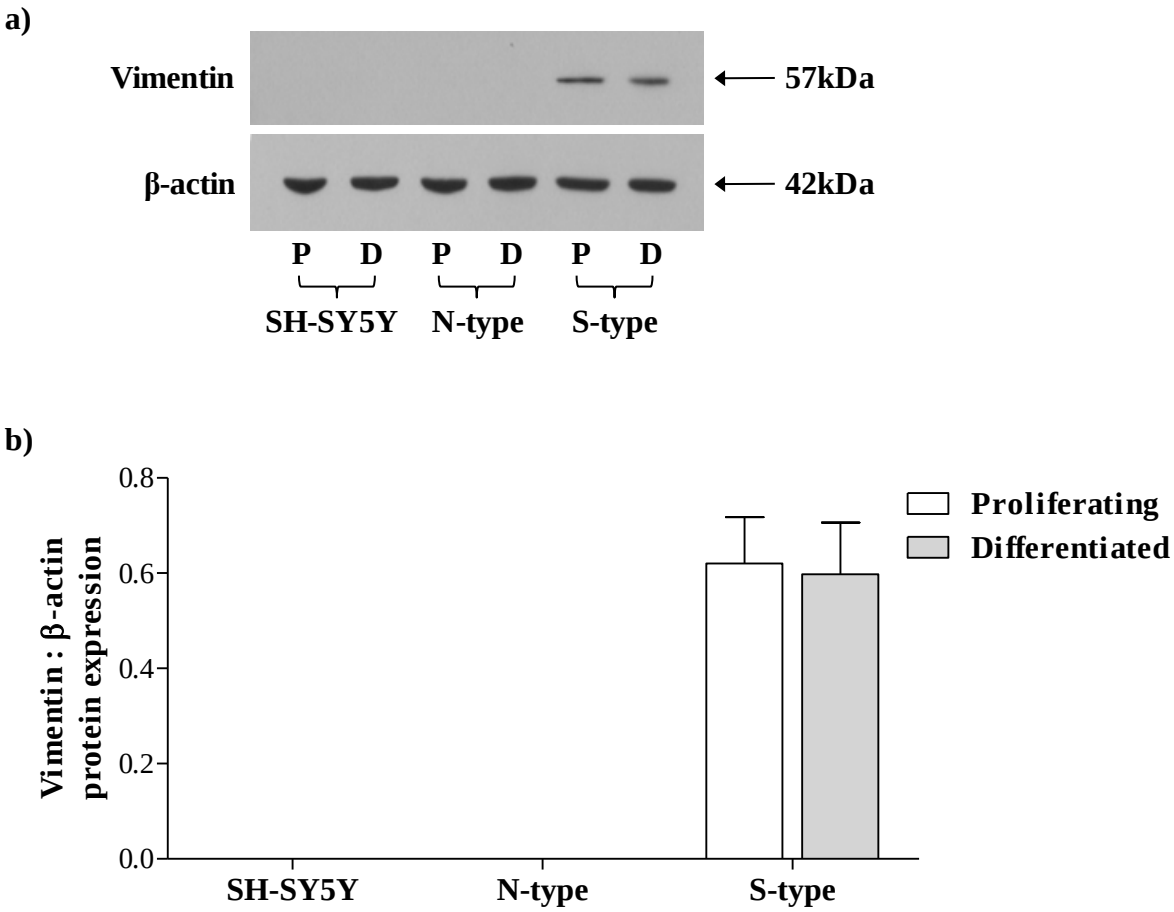

Figure 3.12 Vimentin is only expressed in S-type cells

Western blots performed on protein extracted from SH-SY5Y, N-type and S-type cells following 7 days EtOH (proliferating = **P**) or 9*c*RA (differentiated = **D**) treatment.
a) Blots were probed with anti-vimentin antibody which detected a band at 57kDa. Blots were then re-probed with anti-β-actin antibody, used as a loading control, which detected a band of 42kDa. **b**) Quantitative measurements of bands were performed using densitometry (ImageJ software, Methods 2.6.4). Vimentin was then expressed as a ratio of β-actin. Vimentin expression is not detected in SH-SY5Y or N-type cell populations. Vimentin is expressed in S-type cells, the level of which does not change following 9*c*RA treatment; P=0.8792. For SH-SY5Y cells *n*=8, for N-type cells *n*=8 and for S-type cells *n*=8.

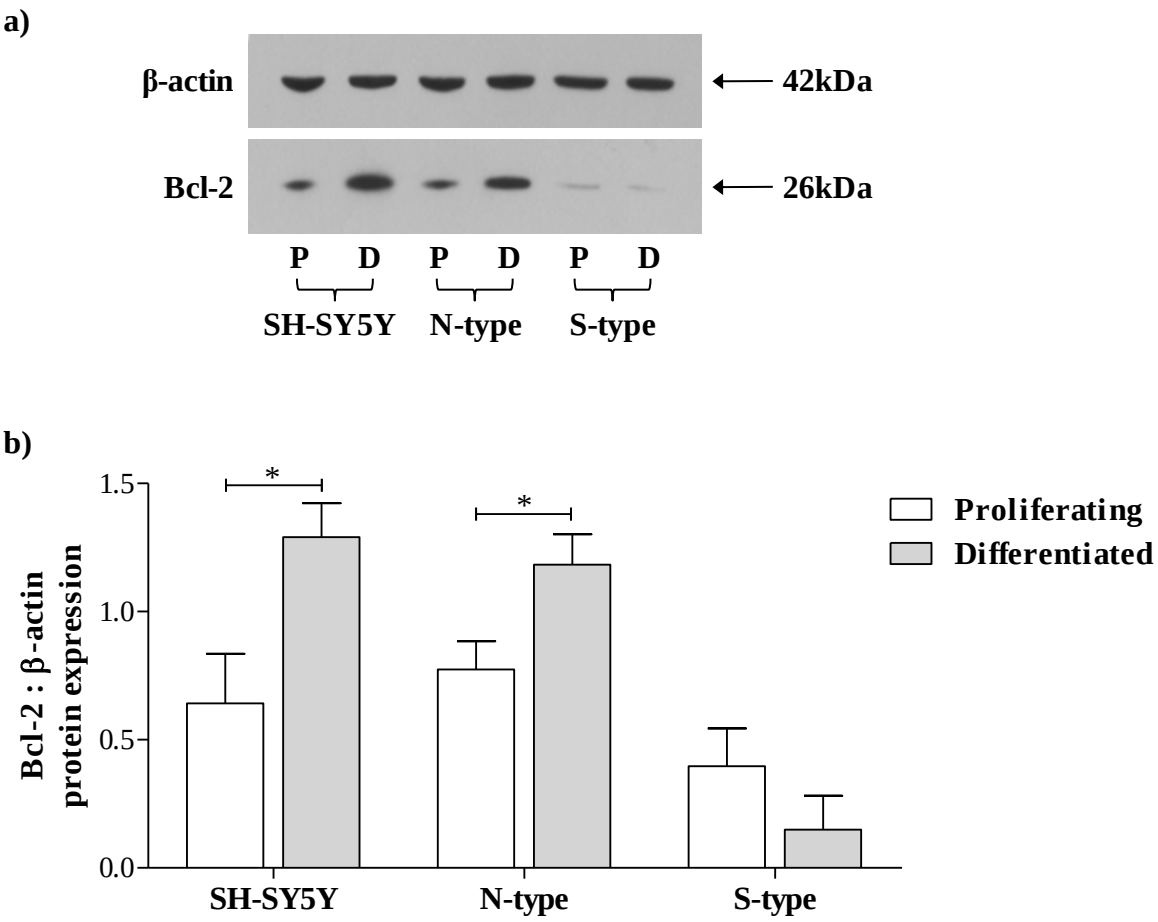

Figure 3.13 Bcl-2 expression in SH-SY5Y, N-type and S-type cells

Western blots performed on protein extracted from SH-SY5Y, N-type and S-type cells following 7 days EtOH (proliferating = **P**) or 9*c*RA (differentiated = **D**) treatment. **a**) Blots were probed with anti-Bcl-2 antibody which detected a band of 26kDa. Western blots were then re-probed with anti-β-actin antibody, used as a loading control, which detected a band of 42kDa. **b**) Quantitative measurements of bands were performed using densitometry (ImageJ software, Methods 2.6.4). Bcl-2 was then expressed as a ratio of β-actin. Bcl-2 expression significantly increases with 9*c*RA treatment in SH-SY5Y cells; P=0.0198* and N-type cells; P=0.0271*. Bcl-2 protein expression is not significantly different between proliferating and differentiated S-type cell population; P=0.2325. For SH-SY5Y cells *n*=6, for N-type cells *n*=7 and for S-type cells *n*=7.

3.3 Discussion

SH-SY5Y cells were induced to differentiate by treatment with 9*c*RA for 7 days (Figure 3.1). Following 1 day treatment there was a significant increase in the number of differentiated cells compared to proliferating controls (Figure 3.2). This result has also been observed by others (Cheung *et al*., 2009). Changes in gene expression can occur within a few hours of RA treatment (LaRosa *et al*., 1988), consistent with the effects of RA being observed following only 1 day treatment. By 7 days 9*c*RA treatment ~35% of cells were classed as differentiated (Figure 3.2). The proportion of differentiated cells did not exceed ~35%, even following 8 or more days 9*c*RA treatment, although this is possibly an underestimation of the actual number of differentiated cells as only cells with fully visible neurite extensions were classed as differentiated. However it is clear that not all cells respond to 9*c*RA treatment as some cells still continue to proliferate. The response to RA is therefore heterogeneous for two reasons, firstly because some cells respond more quickly than others and secondly because some cells do not respond at all. The heterogeneous response of SH-SY5Y cells to 9*c*RA has previously been observed (Brown *et al*., 2005).

The reasons underlying heterogeneity are unknown but one possibility is a cell-phenotype dependent sensitivity to RA. The SH-SY5Y cell line is comprised of two distinct cell phenotypes derived from the embryonic neural crest. The neuroblastic N-type cells, precursors to sympathetic neurons and cells of the adrenal medulla and the non-neuronal S-type cells, precursors to glial, Schwann and melanocytic cells (Introduction 1.2). Following 9*c*RA treatment N-type cells differentiate into neuronal-like cells and S-type cells differentiate into epithelial-like cells (Figure 3.5). S-type cells were not included in the cell counts performed to determine percent differentiation (Methods 2.4) and therefore the results obtained show that heterogeneity is a feature of the N-type cells. However, a third cell phenotype has also been identified in neuroblastoma cell lines. I-type cells have been hypothesised to be a cancer stem cell as they have the ability of self renewal and they express both N- and S-type markers, making them potential progenitors for both the N- and S-type cells (Ciccarone *et al*., 1989; Ross *et al*., 1995, 2007). They are morphologically difficult to distinguish from N-type cells (Messi *et al*., 2008; Acosta *et al*., 2009) and therefore could be present in the SH-SY5Y cell line. Studies have suggested that I-type cells, the most malignant of

the 3 cell phenotypes (Ross *et al*., 2003, 2007), may mediate RA resistance in neuroblastoma tumours and cell lines. Therefore, one possible explanation for the heterogeneous response observed following 9*c*RA treatment is that I-type cells are present in the SH-SY5Y cell line and it is these cells that fail to differentiate. RA resistant I-type cells have been identified within the SK-N-SH neuroblastoma cell line, the parental cell line of SH-SY5Y cells (Messi *et al.*, 2008). However, the N-type neuroblastoma cell line IMR-32 is also resistant to RA (Lasorella *et al*., 1995) and therefore regardless of cell phenotype other mechanisms must also be involved in RA resistance and sensitivity. RA exerts most of its effects by altering gene transcription through activation of RARs and RXRs (Niles, 2000) and therefore variability in activation and/or expression of RARs and RXRs may also provide an explanation for the heterogenic response observed.

As well as inducing differentiation of cells, 9*c*RA is used in the treatment of neuroblastoma due to its anti-proliferative effects. This effect was observed in this study and has also been observed by many others in the SH-SY5Y cell line (Reynolds *et al*., 1991; Lovat *et al*., 1994; Redfern *et al*., 1995; Lasorella *et al*., 1995; Brown *et al*., 2005). RA may mediate its anti-proliferative effects through repression of the growth stimulating transcription factor AP1 (Leder *et al*., 1990; Chambon, 1996; Altucci & Gronemeyer, 2011).

N- and S-type cell populations were enriched from the SH-SY5Y cell line (Figure 3.4), possible due to differences in substrate adherence properties where N-type cells are weakly adherent and S-type cells are strongly adherent (Ciccarone *et al*., 1989; Ross *et al*., 1995; Gaitonde *et al*., 2001). Although N- and S-type cells have clearly distinct morphologies, cell types were also defined biochemically. β-Tubulin III is a component of microtubules in neuronal cell types (Draberova *et al*., 1998; Katsetos *et al*., 2003; Shin *et al*., 2010) and was identified in both proliferating and differentiated N-type cells (Figures 3.7, 3.8 and 3.11). Expression of β-Tubulin III did not change following 9*c*RA treatment. It was expected that β-Tubulin III expression may increase as cells became more neuronal-like, as has been observed with neurofilament-68 (Messi *et al*., 2008). However, the expression of other neuronal markers, such as neurofilament-200 also remain unchanged following RA treatment of SH-SY5Y cells (Encinas *et al*., 2000; Cheung *et al*., 2009).

β-Tubulin III staining, albeit weak, was also surprisingly identified in both proliferating and differentiated S-type cells. Yet S-type cells have also been found to stain positively for the neuronal marker NF-68 (Messi *et al*., 2008; Acosta *et al*., 2009). Possibly the S-type cells stain positive for neuronal proteins as they have only recently committed to an S-type cell fate through the process of transdifferentiation. Interestingly, β-Tubulin III expression became significantly down-regulated following 9*c*RA-induced differentiation (Figure 3.11). S-type cells clearly change morphology following 9*c*RA treatment, becoming more epithelial-like (Figures 3.6 & 3.10). Following RA treatment S-type cells have been found to differentiate into Schwann cells (Tsokos *et al*., 1987) and melanocytic cells (Slack *et al*., 2002). The down-regulation in β-Tubulin III expression may therefore be due to S-type cells moving further away from a neuronal phenotype.

S-type cells stained positive for vimentin, the expression of which did not change following 9*c*RA-induced differentiation (Figure 3.13). Vimentin is an intermediate filament protein found in non-neuronal cells, it was not detected in N-type cells using western blotting (Figure 3.12). However some neurite extensions of some N-type cells stained positively for vimentin in immunofluorescence studies (Figure 3.9). Vimentin has been shown to be a transient requirement in the initiation of neurite outgrowth (neuritogenesis). In NB2a/d1 neuroblastoma cells (Shea *et al*., 1993) and in hippocampal neurons (Boyne *et al*., 1996), knockdown of vimentin significantly inhibited neurite initiation. Expression of vimentin rapidly declines as cells become post-mitotic and is replaced by neurofilament proteins (Shea *et al*., 1993; Boyne *et al*., 1996; Yabe *et al*., 2003; Dubey *et al*., 2004).

An increase in Bcl-2 protein expression was observed in SH-SY5Y (Figures 3.3 and 3.13) and N-type cells (Figure 3.13) following 7 days 9*c*RA treatment. This result has also been observed in this laboratory (Riddoch *et al*., 2007) and by others (Lasorella *et al*., 1995). There was no change in Bcl-2 expression in S-type cells following 7 days 9*c*RA treatment which also stained weakly for Bcl-2 (Figure 3.13). In SH-SY5Y cells Bcl-2 expression became significantly up-regulated compared to proliferating controls after 5 days 9*c*RA treatment. Lasorella *et al*., 1995 observed a significant increase in Bcl-2 expression in SH-SY5Y cells following 6 days RA treatment. An increase in Bcl-2 expression has also been observed in neuroblastoma cells differentiated with phorbol

ester (Hanada *et al*., 1993), which suggests that the increase in Bcl-2 is an effect of differentiation itself. Consistent with this notion, Bcl-2 is widely expressed in the developing and adult nervous system (Merry *et al*., 1994) and neurons removed from *Bcl-2* deficient mouse embryos grow at a slower rate compared to controls (Hilton *et al*., 1997). Bcl-2 is known to play a key role in controlling neuronal cell survival, via its regulation of both caspase-dependent and caspase-independent cell death pathways (Akhtar *et al.*, 2004; Merry and Korsmeyer, 1997). This may explain in part the temporal relationship between the increase in Bcl-2 expression (day 5) and morphological differentiation (day 1). Bcl-2 was used as a biochemical marker of differentiation for N-type cells only as expression was not altered in 9*c*RA differentiated S-type cells (Figure 3.13).

With the use of morphological and biochemical markers for N- and S- type cells, it was possible to investigate both Ca^{2+} signalling and differentiation responses that were specific to cell phenotype.

Chapter 4

Results II - SOCE in SH-SY5Y, N- and S-type cells

4.1 Introduction

Previous studies from this laboratory have shown that SOCE becomes down-regulated in SH-SY5Y cells following 9*c*RA-induced differentiation (Brown *et al*., 2005). SOCE is the process whereby external Ca^{2+} enters cells via SOCs located on the PM in response to depletion of ER Ca^{2+} stores (Introduction 1.6).

The SH-SY5Y cell line is heterogeneous (Chapter 3) and although predominantly composed of N-type cells, S-type cells are present typically at a level of ~5-15%.

The aims of this chapter were to characterise SOCE in SH-SY5Y, N- and S-type cells following 9*c*RA-induced differentiation in order to determine the extent that N- and S-type cells contribute to SOCE down-regulation. This was achieved by measuring SOCE in SH-SY5Y, N- and S-type cell populations following 9*c*RA-induced differentiation. N- and S-type cells were enriched from the SH-SY5Y cell line (Methods 2.2).

4.2 Results

4.2.1 SOCE in SH-SY5Y cells

SH-SY5Y cells were treated with 1µM 9*c*RA (differentiated) or the equivalent volume of vehicle EtOH (proliferating) for 7 days. To measure SOCE cells were loaded with the Ca^{2+} sensitive fluorescent indicator dye fura-2/AM, which enabled continuous measurement of cytosolic Ca^{2+}. Loaded cells, maintained in Ca^{2+}-free buffer, were then stimulated with TG in order to deplete ER Ca^{2+} stores. TG binds to and inhibits the SERCA pump located on the ER membrane causing a leak of Ca^{2+} from the ER into the cytosol. Depletion of ER Ca^{2+} stores activates SOCE whereby external Ca^{2+} enters the cytosol in order to replenish depleted stores. The addition of Ca^{2+} to the Ca^{2+}-free buffer, in what is termed an 'add-back' experiment, enabled the measurement of Ca^{2+} influx and therefore the activity of the SOCE pathway.

Calibrated fluorescence traces (i.e. showing $\Delta[Ca^{2+}]_i$) from proliferating and differentiated SH-SY5Y cell populations suggested that store depletion in response to TG addition (200nM) was similar between proliferating and differentiated cells (Figure 4.1). Subsequent Ca^{2+} entry following the addition of Ca^{2+} (2mM) suggested however that SOCE was reduced in differentiated cells compared to proliferating cells.

In order to quantify Ca^{2+} entry into the cell cytosol the area from under TG and Ca^{2+} responses was calculated from calibrated fluorescence traces (Methods 2.7) and presented in graphs as mean ± SEM of *n* determinations. Store depletion (TG response) was not significantly different between proliferating (10.72±1.6µMs) and differentiated (10.05±2.42µMs) SH-SY5Y cells, P=0.8253 (Figure 4.2). SOCE (Ca^{2+} response) following store depletion was however significantly down-regulated in 9*c*RA differentiated cells (10.23±2.5µMs) compared to proliferating cells (19.63±3.1µMs) by ~48%, P=0.0308. 9*c*RA-induced differentiation of SH-SY5Y cells therefore causes down-regulation of SOCE, as previously observed by Brown *et al*., 2005.

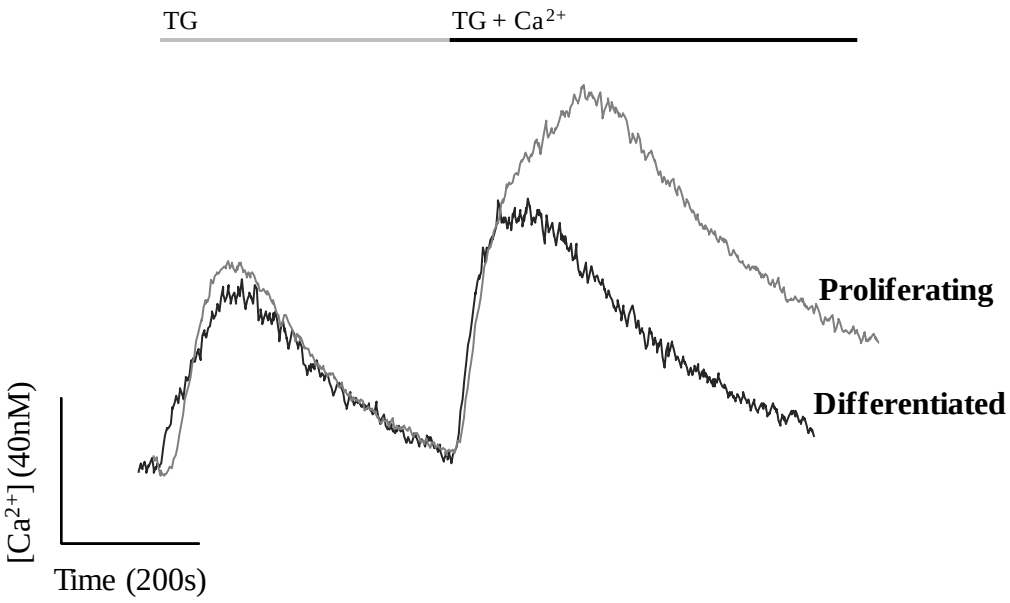

Figure 4.1 Ca^{2+} add-back traces from SH-SY5Y cells

Typical calibrated fluorescence traces showing $\Delta[Ca^{2+}]_i$ in proliferating and differentiated SH-SY5Y cells. The addition of TG (200nM) causes an increase in $[Ca^{2+}]_i$ as Ca^{2+} is depleted from ER stores. The addition of Ca^{2+} (2mM) to the Ca^{2+}-free buffer causes an increase in $[Ca^{2+}]_i$ as Ca^{2+} enters the cytosol via the SOCE pathway. Store depletion appears to be similar between proliferating and differentiated cells. SOCE appears to be reduced in differentiated cells compared to proliferating cells.

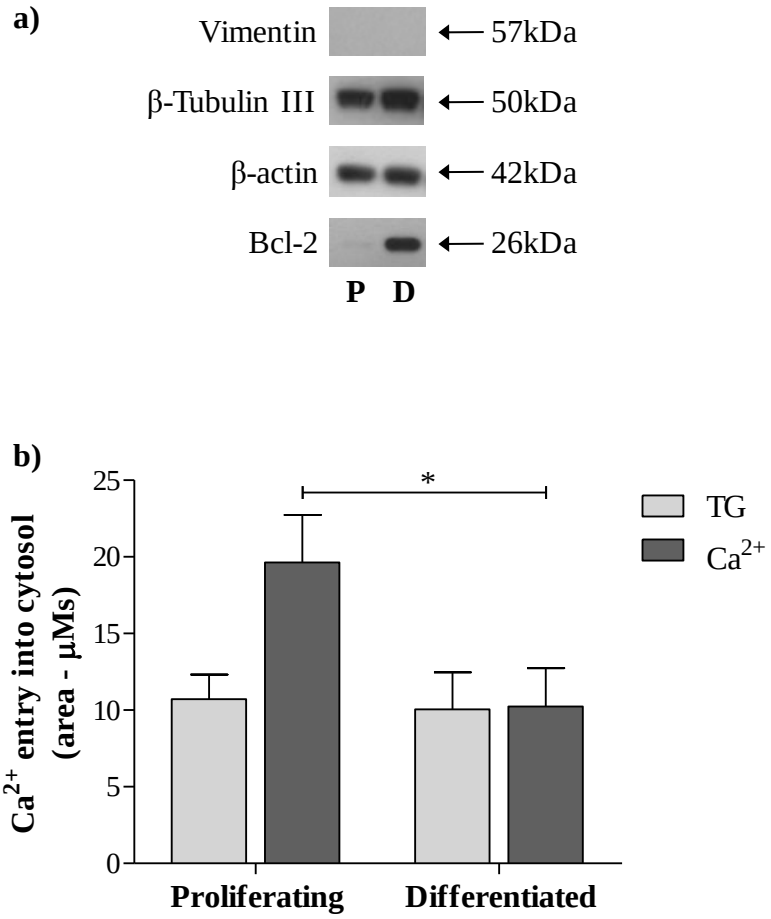

Figure 4.2 SOCE in SH-SY5Y cells

SH-SY5Y cells were treated with either EtOH (proliferating) or 9*c*RA (differentiated) for 7 days. **a)** Blots were performed on protein extracts from the cells fluorimetry experiments were performed on. In SH-SY5Y cells vimentin is not detected, β-Tubulin III is present, β-actin is used as a loading control and Bcl-2, a biochemical marker of differentiation, increases following 9*c*RA treatment. **b)** Graph shows Ca^{2+} entry into the cytosol following ER store depletion in response to stimulation with TG (200nM) and subsequent Ca^{2+} entry via the SOCE pathway following the addition of Ca^{2+} (2mM) in proliferating and differentiated cells. Store depletion was not significantly different between proliferating and differentiated cells, P=0.8253. SOCE was however significantly down-regulated by ~48% in differentiated cells compared to proliferating cells, P=0.0308*. For proliferating cells *n*=8, for differentiated cells *n*=9.

4.2.2 SOCE in N-type cells

The SH-SY5Y cell line is predominantly composed of N-type cells (Introduction 1.3), it was therefore expected that the down-regulation of SOCE observed in SH-SY5Y cells following 9*c*RA-induced differentiation (Figure 4.2) would also be observed in N-type cells. N-type cells are of a neuronal cell lineage, precursors to neuronal cells of the SNS. Following enrichment cells were treated with EtOH or 9cRA (1µM) for 7 days to provide proliferating and differentiated cell populations respectively.

Calibrated fluorescence traces from proliferating and differentiated N-type populations (N8) suggested that store depletion in response to TG addition (200nM) was similar between proliferating and differentiated cells (Figure 4.3). Subsequent Ca^{2+} entry following the addition of Ca^{2+} (2mM) suggested however that SOCE was reduced in differentiated cells compared to proliferating cells. As with the SH-SY5Y cells (Figure 4.1) there was a visible reduction in SOCE in N-type cells following 9*c*RA-induced differentiation.

The area from under TG and Ca^{2+} responses was calculated in order to quantify Ca^{2+} entry into the cell cytosol. Store depletion (TG response) was not significantly different between proliferating (9.45±0.78µMs) and differentiated (7.5±0.76µMs) cells, P=0.0883 (Figure 4.4). SOCE (Ca^{2+} response) following store depletion was however significantly down-regulated in 9*c*RA differentiated cells (7.64±1.83µMs) compared to proliferating cells (14.85±1.74µMs) by ~49%, P=0.0018. Therefore, as with the SH-SY5Y cells (Figure 4.2), 9*c*RA-induced differentiation of N-type cells is accompanied by down-regulation of SOCE.

4.2.2.1 Enrichment of N-type cells

Reference to ‘N-type cells’ throughout this thesis refers to N-type cells enriched for from the SH-SY5Y cell line 8 times, i.e. S8 (Methods 2.2.1). N-type (N8) cells were enriched from a typical SH-SY5Y population consisting of an N- to S-type cell ratio of ~90:10%. SH-SY5Y cells and N-type (N8) cells had very similar SOCE profiles (Figures 4.2 and 4.4 respectively). Further experiments revealed that N4 cells (also enriched from a typical SH-SY5Y population) also had a similar SOCE profile to SH-

SY5Y cells where SOCE was down-regulated by ~62% (Figure 4.5a). N12 cells also showed a similar profile with a ~43% down-regulation in SOCE (Figure 4.5b).

However, the importance of enrichment was seen when a batch of SH-SY5Y cells with an unusually high percentage of S-type cells was used. The batch contained ~50% S-type cells and an enrichment of N4 was not sufficient to obtain a typical SOCE profile of SH-SY5Y cells (Figure 4.6a). SOCE was not affected by 9*c*RA treatment, showing a similar profile to S-type cell populations (4.2.3). An enrichment of N8 however, showed ~52% down-regulated SOCE in response to 9*c*RA (Figure 4.6b), comparable to a typical SOCE profile of SH-SY5Y cells. An enrichment of N8 was therefore determined an acceptable level of enrichment to attribute responses to N-type cells.

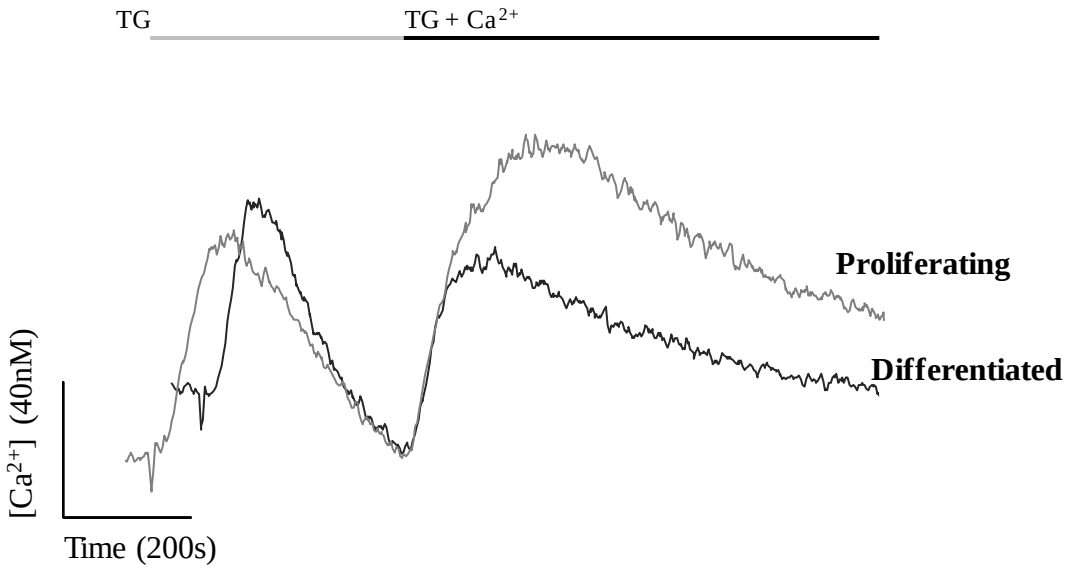

Figure 4.3 Ca^{2+} add-back traces from N-type cells

Typical calibrated fluorescence traces showing $\Delta[Ca^{2+}]_i$ in proliferating and differentiated N-type cells (N8). The addition of TG (200nM) causes an increase in $[Ca^{2+}]_i$ as Ca^{2+} is depleted from ER stores. The addition of Ca^{2+} (2mM) to the Ca^{2+}-free buffer reveals Ca^{2+} entry into the cytosol via the SOCE pathway. Store depletion appears to be similar between proliferating and differentiated cells. SOCE appears to be reduced in differentiated cells compared to proliferating cells.

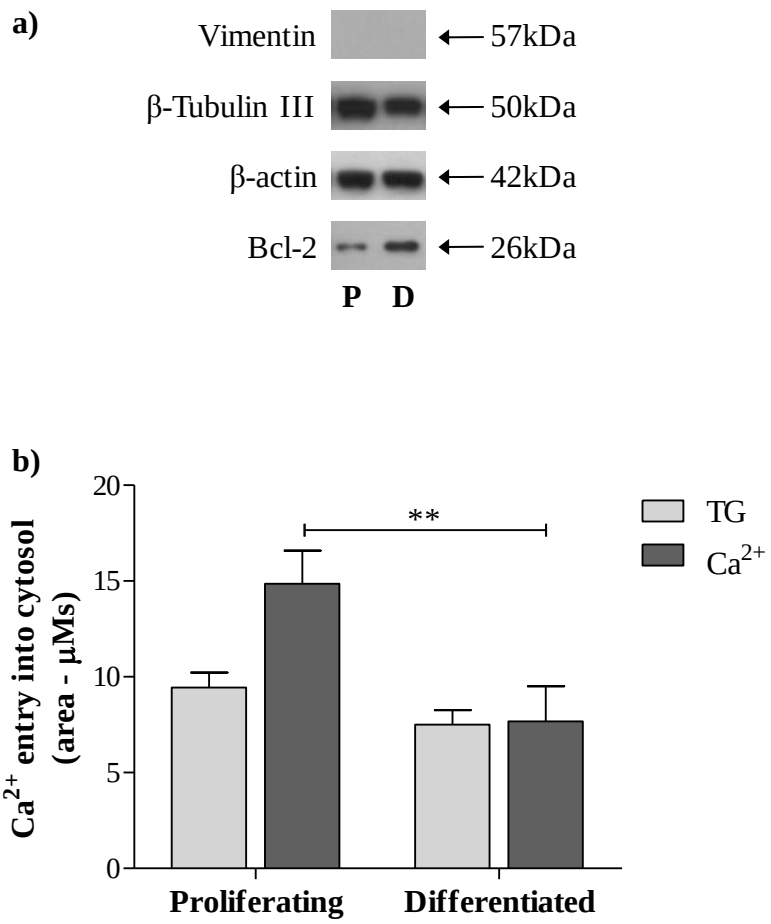

Figure 4.4 SOCE in N-type cells

N-type cells (N8) were enriched from the SH-SY5Y cell line. Cells were then treated with either EtOH (proliferating) or 9*c*RA (differentiated) for 7 days. **a)** Blots were performed on protein extracts from the cells that fluorimetry experiments were performed on. In N-type cells vimentin is not detected, β-Tubulin III is present, β-actin is used as a loading control and Bcl-2, a biochemical marker of differentiation, increases following 9*c*RA treatment. **b)** Graph shows Ca^{2+} entry into the cytosol following ER store depletion in response to stimulation with TG (200nM) and subsequent Ca^{2+} entry via the SOCE pathway following the addition of Ca^{2+} (2mM) in proliferating and differentiated cells. Store depletion was not significantly different between proliferating and differentiated cells, P=0.0883. SOCE was however significantly down-regulated by ~49% in differentiated cells compared to proliferating cells, P=0.0018**. For proliferating cells *n*=24, for differentiated cells *n*=18.

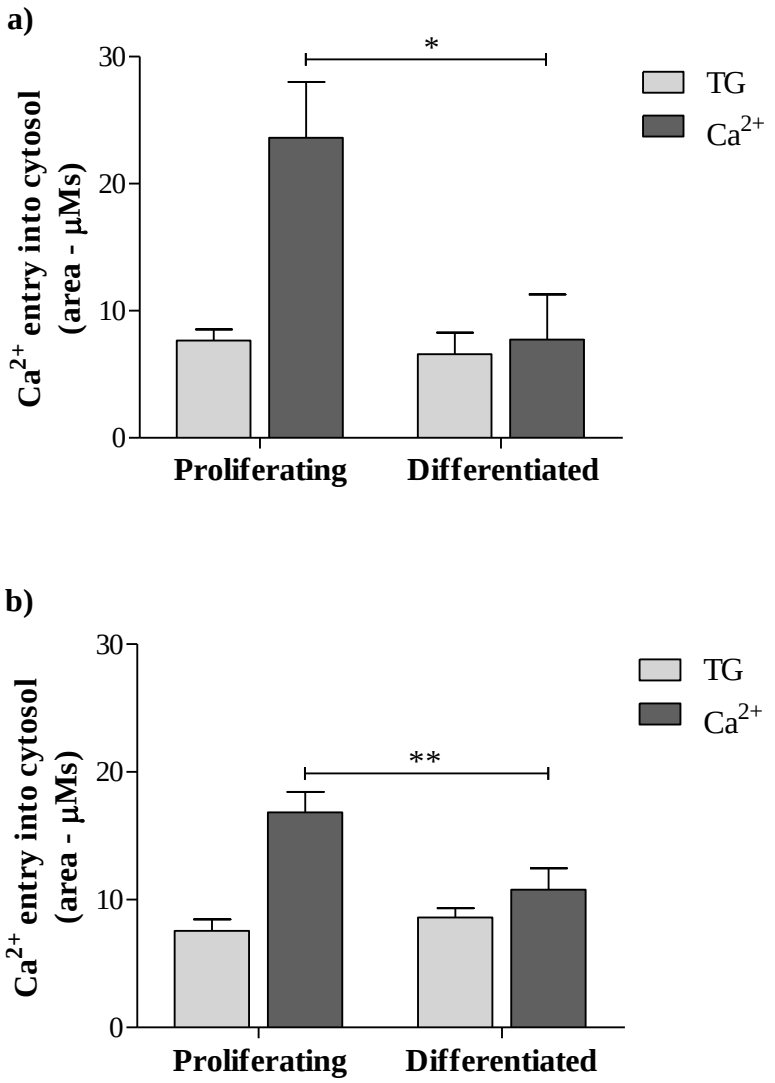

Figure 4.5 SOCE in N4 and N12 cells

N-type cells (N4 and N12) were enriched from a typical SH-SY5Y cell population. Cells were then treated with either EtOH (proliferating) or 9*c*RA (differentiated) for 7 days. **a)** N4 cells. Store depletion in response to stimulation with TG (200nM) was not significantly different between proliferating and differentiated cells, P=0.5919. SOCE was however significantly down-regulated by ~62% in differentiated cells compared to proliferating cells, P=0.0082**. For proliferating cells *n*=15 for differentiated cells *n*=17. **b)** N12 cells. Store depletion in response to stimulation with TG (200nM) was not significantly different between proliferating and differentiated cells, P=0.3762. SOCE was however significantly down-regulated by ~43% in differentiated cells compared to proliferating cells, P=0.0049**. For proliferating cells *n*=13 for differentiated cells *n*=16.

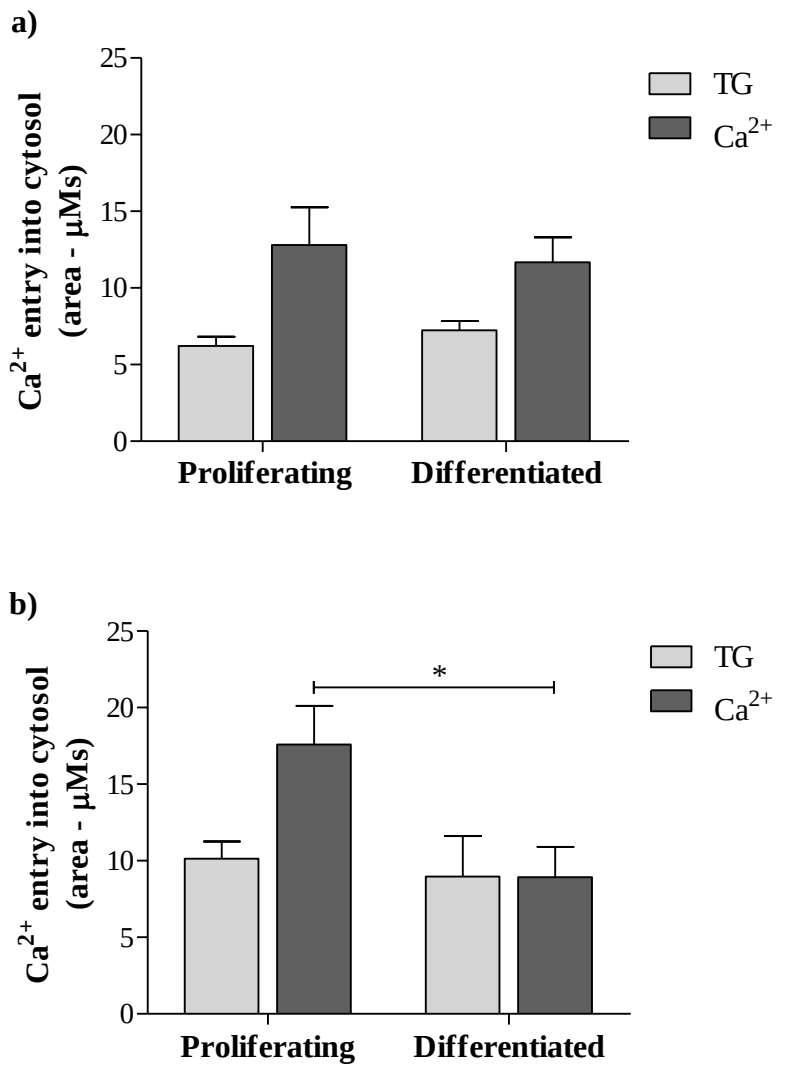

Figure 4.6 SOCE in N4 and N8 cells from (high S-type cell %)

N-type cells (N4 and N8) enriched from a batch of SH-SY5Y cells with an unusually high percentage of S-type cells (~50%). Cells were then treated with either EtOH (proliferating) or 9*c*RA (differentiated) for 7 days. **a)** N-type cells were enriched from the SH-SY5Y cell line four times (N4). Store depletion (TG, 200nM) was not significantly different between proliferating and differentiated cells, P=0.2530. Ca^{2+} entry (Ca^{2+}, 2mM) was also not significantly different between proliferating and differentiated cells, P=0.7108. *n*=8. **b)** N8 cells. Store depletion in response to stimulation with TG (200nM) was not significantly different between proliferating and differentiated cells, P=0.7015. Subsequent Ca^{2+} entry via the SOCE pathway following the addition of Ca^{2+} (2mM) was also not significantly different between proliferating and differentiated cells, P=0.0350*. *n*=4.

4.2.3 SOCE in S-type cells

S-type cells are of a non-neuronal cell lineage, precursors to glial type cells of the SNS. Following enrichment cells were treated with EtOH or 9cRA (1µM) for 7 days to provide proliferating and differentiated cell populations respectively.

Calibrated fluorescence traces from proliferating and differentiated S-type cell populations suggested that store depletion in response to TG addition (200nM) was similar between proliferating and differentiated cells (Figure 4.7). Subsequent Ca^{2+} entry following the addition of Ca^{2+} (2mM) also suggested that SOCE was similar between proliferating and differentiated cells.

Store depletion (TG response) was not significantly different between proliferating (6.63±0.77µMs) and differentiated (6.50±1.10µMs) cells, P=0.9245 (Figure 4.8). SOCE (Ca^{2+} response) following store depletion was also not significantly different between proliferating (10.15±1.48µMs) and differentiated (11.74±3.14µMs) cells, P=0.6574. Therefore, 9cRA-induced differentiation of S-type cells has no effect on SOCE.

4.2.3.1 Enrichment of S-type cells

Reference to 'S-type cells' throughout this thesis refers to S-type cells enriched for from the SH-SY5Y cell line 8 times, i.e. S8 (Methods 2.2.2). An enrichment of S8 was chosen in order to correspond with the selection of N8 cells as discussed in section 4.2.2.1. However an enrichment of S4 (Figure 4.9a) produced a similar result to S8 cells (Figure 4.8) whereby both store depletion were not significantly different between proliferating and differentiated cells. An S-type population can therefore be successfully obtained after only 4 enrichments. S12 cells also showed a similar profile to S8 cells (Figure 4.9b).

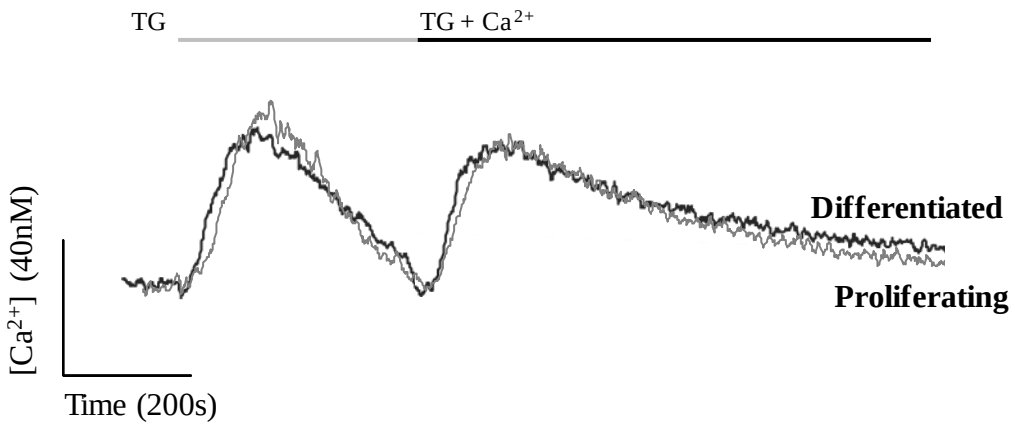

Figure 4.7 Ca^{2+} add-back traces from S-type cells

Typical calibrated fluorescence traces showing $\Delta[Ca^{2+}]_i$ in proliferating and differentiated S-type cells. The addition of TG (200nM) causes an increase in $[Ca^{2+}]_i$ as Ca^{2+} is depleted from the ER stores. The addition of Ca^{2+} (2mM) to the Ca^{2+}-free buffer reveals Ca^{2+} entry into the cytosol via the SOCE pathway. As can be seen from the traces both store depletion (TG response) and resultant SOCE (Ca^{2+} response) appear to be similar between proliferating and differentiated cells.

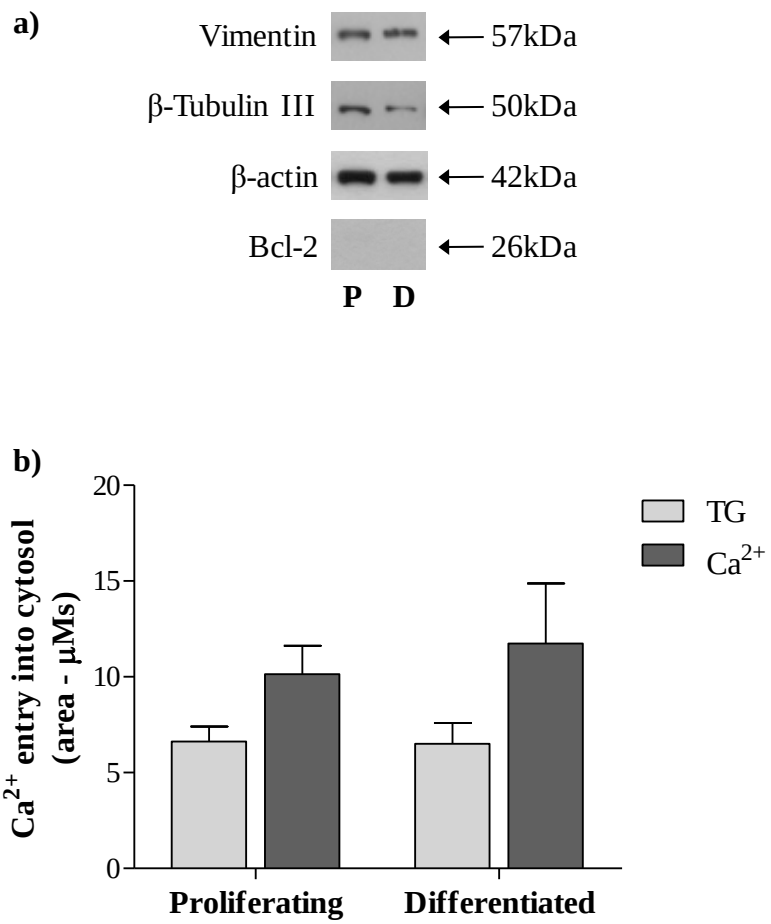

Figure 4.8 SOCE in S-type cells

S-type cells (S8) were enriched from the SH-SY5Y cell. Cells were then treated with either EtOH (Proliferating) or 9*c*RA (Differentiated) for 7 days. **a)** Blots were performed on protein extracts from the cells that fluorimetry experiments were performed on. In S-type cells vimentin is present, β-Tubulin III is down-regulated in 9*c*RA differentiated cells, β-actin is used as a loading control and Bcl-2 was not detected. **b)** Graph shows Ca^{2+} entry into the cytosol following ER store depletion in response to stimulation with TG (200nM) and subsequent Ca^{2+} entry via the SOCE pathway following the addition of Ca^{2+} (2mM) in proliferating and differentiated cells. Store depletion was not significantly different between proliferating and differentiated cells, P=0.9245. SOCE was not significantly different between proliferating and differentiated cells, P=0.6574. For proliferating cells *n*=15, for differentiated cells *n*=16.

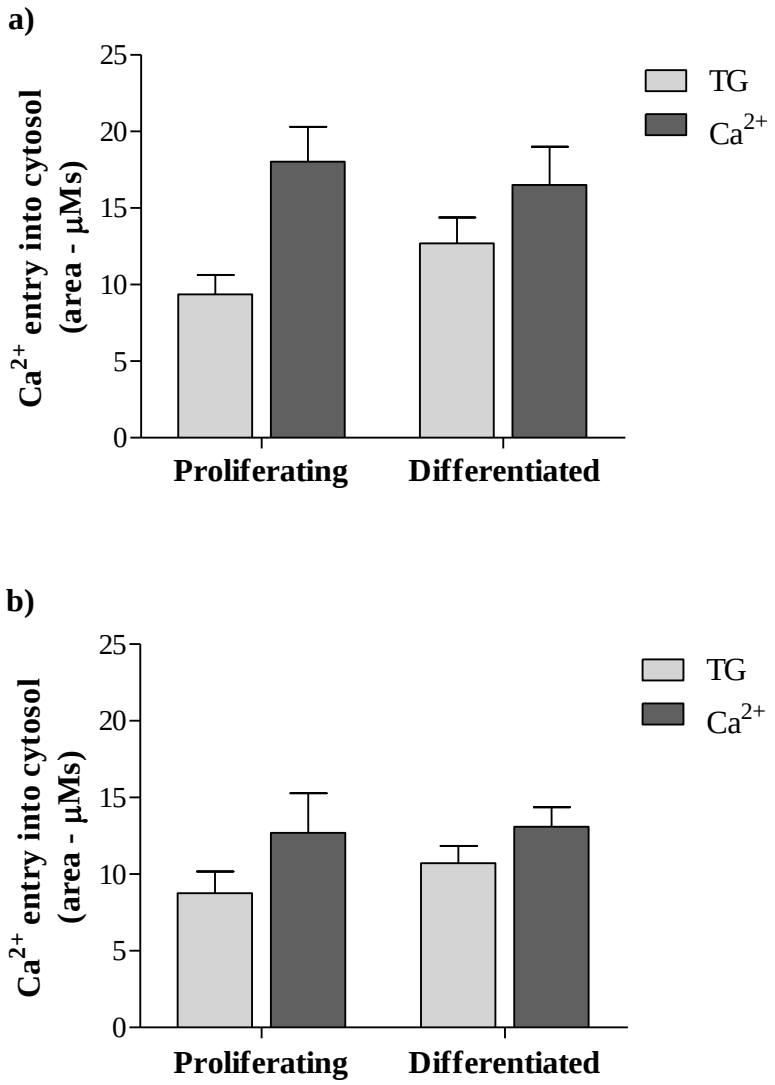

Figure 4.9 SOCE in S4 and S12 cells

S-type cells (S4 and S12) were enriched from SH-SY5Y cells. Cells were then treated with either EtOH (Proliferating) or 9*c*RA (Differentiated) for 7 days. Stores were depleted by the addition of TG (200nM) and subsequent Ca^{2+} entry occurred following the addition of Ca^{2+} (2mM) **a)** S4 cells. Store depletion was not significantly different between proliferating and differentiated cells, P=0.1207. SOCE was not significantly different between proliferating and differentiated cells, P=0.6607. For proliferating cells *n*=14 for differentiated cells *n*=10. **b)** S12 cells. Store depletion was not significantly different between proliferating and differentiated cells, P=0.2868. SOCE was not significantly different between proliferating and differentiated cells, P=0.8898. For proliferating cells *n*=23 for differentiated cells *n*=23.

4.3 Discussion

A previous study from this laboratory (Brown *et al.*, 2005) reported that 9*c*RA-induced differentiation of SH-SY5Y cells was accompanied by a down-regulation in SOCE. The aim of the work presented in this chapter was to determine whether this down-regulation was a feature of N-type cells, S-type cells or both cell types. N- and S-type cells were enriched from the SH-SY5Y cell line (Results 3.2).

The results show that 9*c*RA-induced down-regulation of SOCE is a feature of N-type cells (Figure 4.4). Although an enrichment of N4 (Figure 4.5a) was usually sufficient to observe the SOCE down-regulation profile that matched that of a standard SH-SY5Y cell population (Figures 4.2), this was not always the case. Some batches of mixed population cells contained higher proportions of S-type cells; in these batches enrichment of N-type cells to N8 was required to observe the SOCE down-regulation profile (Figure 4.6b). It was therefore determined that when preparing enriched N-type cells an enrichment to N8 would be used throughout the remainder of this thesis.

Enrichment for S-type populations provided the opportunity to compare SOCE between N- and S-type cells to determine the level of contribution of each cell type to the down-regulation in SOCE measured in SH-SY5Y cells. SOCE in S-type cells (S8) was unaffected following 9*c*RA-induced differentiation (Figure 4.8). As with the N-type cells, S-type cells were also enriched to S4 and S12, to determine the level of enrichment required to obtain an S-type population. SOCE was unchanged in both S4 and S12 cells (Figure 4.9) indicating that it is possible to obtain an S-type population following only 4 enrichments. An enrichment of S8 however was used for the remainder of this thesis to correspond with the level of enrichment selected for N-type cells.

Due to the ability of cell types to transdifferentiate (Introduction 1.2), both N- and S-type cells remain present in enriched populations. Yet the results show that there is a clear difference in the SOCE profile between N- and S-enriched cell populations. The enrichment for N- and S-type cells successfully enabled the differences between N- and S-type cells to be identified: down-regulation of SOCE observed in SH-SY5Y cells

following 9*c*RA-induced differentiation is a feature of N-type cells and not of S-type cells.

9*c*RA treatment of N-type cells induces differentiation of these neuronal precursor cells into more neuronal-like cells. 9*c*RA treatment of S-type cells induces differentiation of these non-neuronal multi-potent precursor cells (Schwann, glial cells and melanocytes) into more epithelial-like cells (Chapter 3). It is not surprising that SOCE remains unchanged in S-type cells as SOCE is an essential and universal form of Ca^{2+} signalling in non-excitable cells (Berridge *et al*., 2000; Parekh and Putney, 2005). The present results reveal therefore that SOCE down-regulation is a feature of neuronal cells only and suggest that as the cells reach a neuronal fate their Ca^{2+} signalling profile changes.

Ca^{2+} signals are known to play a key role in neuronal development. A down-regulation in SOCE has been observed during neural retina development (Sakaki *et al*., 1997) and also in differentiating NG 108-15X glioma cells (Ichikawa *et al*., 1998). Similarly, a non-voltage dependent Ca^{2+} entry pathway with characteristics of SOCE was lost during differentiation of embryonic rat cortical neurons (Maric *et al.*, 2000). The key point connecting the present findings with all of these studies is the suggestion that SOCE occurs more intensely in proliferating cells compared with differentiated cells.

Unpublished data from this laboratory by Dr Victoria Hann showed that N-type cells grow as normal in low Ca^{2+} media (0.001mM), however they are unable to differentiate following 9*c*RA treatment (7 day, 1µM), as determined by lack of neurite growth and lack of down-regulated SOCE. This suggests that Ca^{2+} entry into the cells is a requirement for differentiation to occur. However, it appears that entry is only required for the first 3 days of the 7 day differentiation process as at this point switching the cells from normal Ca^{2+} media (1.8mM) to low Ca^{2+} media (0.001mM) did not prevent the differentiation process (as deemed by neurite outgrowth and down-regulation of SOCE). These results raise the possibility that down-regulation of SOCE could be required for maintenance of the differentiated state. This possibility is examined further in subsequent chapters in this thesis.

The mechanism(s) underlying the down-regulation of SOCE in N-type cells is not clear. One possibility that can be excluded is a decrease in the size of the thapsigargin-sensitive Ca^{2+} store, since this store remains fully intact after 9*c*RA-treatment (Figures 4.3 and 4.4b). One limitation of the SOCE measurements is they are measured using cell populations. It remains unclear therefore whether differentiated cells have a fully down-regulated SOCE pathway (with the measured SOCE being a property of the contaminating proliferating cells) or whether a SOCE pathway may still be present and functioning in differentiated cells, albeit at a decreased level. Such a pathway may have alterations in its spatial and/or temporal characteristics such that the signal may only be detected using high resolution imaging techniques (Bootman *et al.,* 2001). However, given that the SOCE pathway in N-type cells is substantially down-regulated, a more likely possibility is that expression of one or more proteins involved in the pathway become down-regulated. There is a report of an increase in TG-stimulated Ca^{2+} influx accompanied by up-regulation of TRPC after differentiation of human stem cells to platelets (den Dekker *et al.,* 2001). The observation of a down-regulation of SOCE in the present study may reflect the down-regulation (or absence) of a particular SOCE protein in 9*c*RA-differentiated cells, which is present in proliferating cells. This possibility was examined in subsequent chapters in which the level of expression of the proteins STIM1 (Chapter 5), Orai1 (Chapter 6) and TRPC1 (Chapter 7) were investigated.

Chapter 5
Results III - STIM1

5.1 Introduction

The proteins STIM1, Orai1 and TRPC1 have been demonstrated to be involved in SOCE (Introduction 1.6). This chapter focuses on the involvement of STIM1 in SOCE and also in differentiation of N-type cells. 9*c*RA-induced differentiation resulted in a significant down-regulation of SOCE in N-type cells whereas SOCE remained unaffected in S-type cells (Chapters 4).

As STIM1 is proposed to sense ER Ca^{2+} levels and signal store depletion to SOCs, the relationship between STIM1 expression, SOCE and also differentiation was investigated in N-type cells. In order to do this STIM1 protein expression was both knocked down using siRNA transfection and overexpressed using plasmid DNA transfection in N-type cells (Methods 2.3). Manipulation of STIM1 expression was quantified by western blot (Methods 2.6). The effects on SOCE were measured using Ca^{2+} imaging experiments (Methods 2.8) and the effects on differentiation were determined morphologically by analysis of DIC images (Methods 2.4) and biochemically by measurement of Bcl-2 expression.

5.2 Results

5.2.1 STIM1 in SH-SY5Y, N- and S-type cells before and after 9*c*RA-induced differentiation

SOCE becomes down-regulated in SH-SY5Y and N-type cells following 9*c*RA-induced differentiation, it however remains unchanged in S-type cells (Chapter 4). In order to determine any changes in STIM1 protein expression associated with the observed changes in SOCE, western blots were performed on protein extracted from SH-SY5Y, N- and S-type cells before and after 9*c*RA-induced differentiation (Methods 2.6).

STIM1 is expressed in proliferating (7 day EtOH treated) and differentiated (7 day 9*c*RA treated) SH-SY5Y, N- and S-type cells as determined by a band detected at 84kDa by an anti-STIM1 antibody (Figure 5.1a). Blots were re-probed with β-actin, used as a loading control, and STIM1 was expressed as a ratio of β-actin in order to quantify changes in band intensity (Figure 5.1b).

STIM1 protein expression decreased in SH-SY5Y cells by ~53% and in N-type cells by ~49% following 9*c*RA-induced differentiation. The extent of down-regulation of SOCE for SH-SY5Y cells was ~48% (Figure 4.2) and for N-type cells was ~49% (Figure 4.4). The changes observed in SOCE are consistent with those seen in STIM1 expression and suggest that STIM1 is involved in the process of SOCE in SH-SY5Y and N-type cells. The level of STIM1 protein expression in S-type cells remained unchanged following 9*c*RA-induced differentiation (Figure 5.1). This is consistent with the level of SOCE in S-type cell populations following 9*c*RA-induced differentiation which also remained unchanged following treatment (Figure 4.8).

When looking at STIM1 expression, gels were run for 1 hour 15 minutes. This showed a double band in SH-SY5Y and N-type proliferating cells. The upper (Figure 5.1c) and lower (Figure 5.1d) STIM1 band were analysed individually. The upper band showed no significant difference in STIM1 expression following 9*c*RA treatment ($P>0.05$) whereas the lower band showed significant down-regulation of STIM1expression ($P<0.05$). This would suggest STIM1 exists in two different states. STIM1 knockdown (Figure 5.2 and 5.5) and overexpression (Figure 5.8) gels were run for 1 hour which did not show separation of bands.

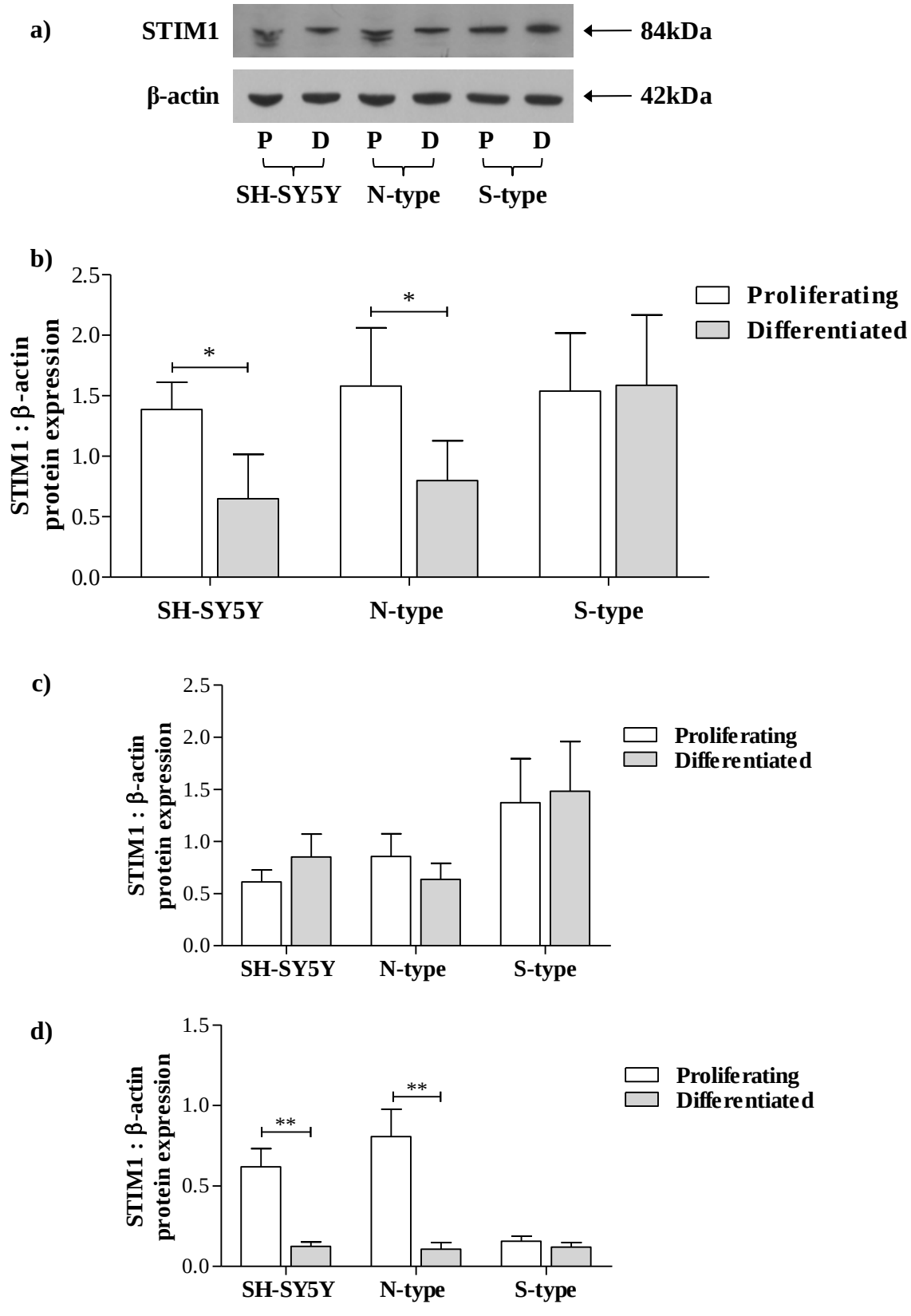

Figure 5.1 STIM1 expression decreases in SH-SY5Y and N-type cells following 9*c*RA-induced differentiation

Cells were treated with EtOH (proliferating - **P**) or 9*c*RA (differentiated - **D**) for 7 days following which cells were harvested for protein. **a)** Western blots were performed on protein extracts from SH-SY5Y, N- and S-type cells. Blots were probed with anti-STIM1 antibody which detected a band at 84kDa. Blots were re-probed with anti-β-actin antibody which detected a band at 42kDa. The band detected by the β-actin antibody was used as a loading control. **b)** Quantitative measurements of bands were performed using densitometry (ImageJ software, Methods 2.6.9). STIM1 was expressed as a ratio of β-actin expression. STIM1 protein expression becomes significantly reduced in 9*c*RA-differentiated SH-SY5Y cells, P=0.0142 and also N-type cells, P=0.0364 compared to proliferating controls. STIM1 protein expression remained unchanged in S-type cells following 9*c*RA treatment, P=0.9053. **c**) Quantitative analysis of upper STIM1 band.STIM1 expression was not significantly different following 9*c*RA treatment in SH-SY5Y (P=0.3749) cells and N-type (P=0.4439) cells. **d**) Quantitative analysis of lower STIM1 band. STIM1 expression was significantly down-regulated following 9*c*RA treatment in SH-SY5Y (P=0.0053**) cells and N-type (P=0.0075**) cells. *n*=4.

5.2.2 Knockdown of STIM1 in N-type cells down-regulates SOCE but does not induce differentiation

9*c*RA-induced differentiation of both SH-SY5Y and N-type cells resulted in the down-regulation of SOCE (Figures 4.2 and 4.4) and also STIM1 protein expression (Figure 5.1). No changes in either SOCE (Figure 4.8) or STIM1 protein expression (Figure 5.1) were observed in S-type cell populations following 9*c*RA-induced differentiation and therefore these cells were not studied further. SH-SY5Y cells and N-type cells so far have shown the same results as one another. This confirms that the SH-SY5Y cell line is predominantly composed of N-type cells. N-type cells were therefore used for the remainder of studies in this chapter.

To investigate whether down-regulation of STIM1 could be responsible for down-regulation of SOCE, STIM1 protein expression was knocked down in untreated (i.e. proliferating) N-type cells (Figure 5.2). STIM1 protein expression was knocked down by transfecting the cells with STIM1 siRNA for 48 hours (Methods, 2.3.1). Control cells were treated with a scrambled sequence not targeted to a specific gene (control siRNA). STIM1 siRNA transfection of N-type cells successfully resulted in the knockdown of STIM1 protein expression as observed by the reduced STIM1 band intensity (84kDa band) in response to anti-STIM1 antibody in comparison to control siRNA transfected cells (Figure5.2a). β-actin protein expression was used as a loading control to enable quantification of STIM1 knockdown (Figure 5.2b). STIM1 was expressed as a ratio of β-actin protein expression. STIM1 protein expression was significantly down-regulated by ~50% in STIM1 siRNA transfected cells compared to control siRNA transfected cells, P=0.0386

Bcl-2 protein expression was used as a measure of biochemical differentiation (Figure 5.2a) and was quantified by the expression of Bcl-2 as a ratio of β-actin expression (Figure 5.2c). Bcl-2 protein expression was not significantly different between control siRNA and STIM1 siRNA transfected cells, P=0.9910.

Following transfection of cells and the subsequent knockdown of STIM1 protein, Ca^{2+} add-back experiments were performed to measure SOCE and DIC images were taken to determine the extent of morphological differentiation.

Ca^{2+} add-back experiments revealed that store depletion (TG response) was not significantly different between control siRNA (14.75±1.83μMs) and STIM1 siRNA (12.96±1.95μMs) transfected cells, P=0.5117 (Figure 5.3). SOCE (Ca^{2+} response) following store depletion was however significantly down-regulated in STIM1 siRNA transfected cells (12.13±1.78μMs) compared to control siRNA transfected cells (30.80±4.13μMs), P=0.0005. This suggests STIM1 plays an important role in SOCE in proliferating N-type cells as STIM1 knockdown down-regulates SOCE by ~60%.

DIC images were taken of the cells to correspond with the protein samples and the Ca^{2+} add-back experiments to see whether there was any affect on differentiation as determined by neurite length (≥50μm) (Figure 5.4). DIC images of control siRNA cells revealed cellular differentiation to be 3.21±0.35% compared to STIM1 siRNA cells which were 4.67±0.87%, P=0.1721. Knockdown of STIM1 for 48 hours in N-type cells does not significantly affect the extent of morphological differentiation.

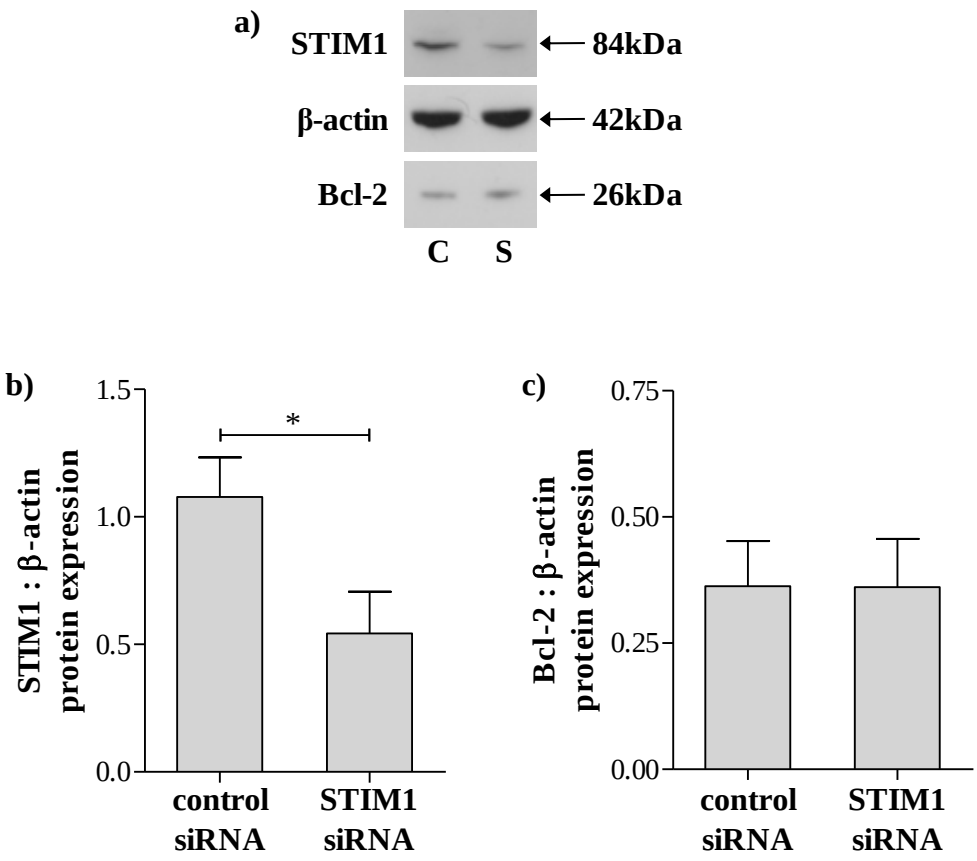

Figure 5.2 Knockdown of STIM1 in N-type cells

N-type cells were transfected with either control siRNA or STIM1 siRNA for 48 hours. **a**) Western blots were performed on protein extracted from control siRNA (**C**) and STIM1 siRNA (**S**) transfected cells. A band at 84kDa was detected with anti-STIM1 antibody. Blots were re-probed with anti-β-actin antibody (42kDa), used as a loading control. Blots were then re-probed with anti-Bcl-2 antibody (26kDa), used as a biochemical marker of differentiation. **b**) Quantitative measurements of bands were performed using densitometry (ImageJ software, Methods 2.6.9). STIM1 was significantly down-regulated following STIM1 siRNA transfection compared to control siRNA transfected cells; $P=0.0386^{*}$. **c**) Quantitative measurements of Bcl-2 protein expression show that Bcl-2 expression was not significantly different between control siRNA and STIM1 siRNA transfected cells; P=0.9910. *n*=6.

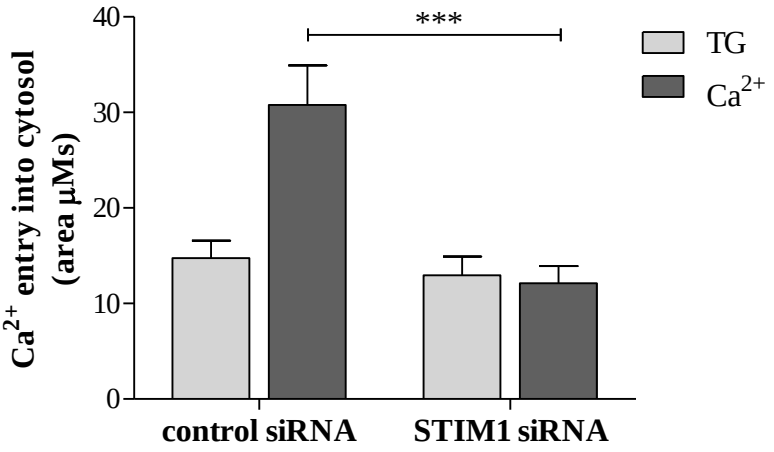

Figure 5.3 Knockdown of STIM1 in N-type cells down-regulates SOCE

N-type cells were transfected with either control siRNA or STIM1 siRNA for 48 hours. Ca^{2+} add-back experiments were performed on cells following treatment. Store depletion in response to the addition of TG (200nM) was not significantly different between control siRNA and STIM1 siRNA transfected cell (P=0.51117). However, SOCE in response to the addition of Ca^{2+} (2mM) was significantly down-regulated in STIM1 siRNA transfected cells compared to control siRNA transfected cells ($P=0.0005^{***}$). For control siRNA transfected cells *n*=16 and for STIM1 siRNA transfected cells *n*=14.

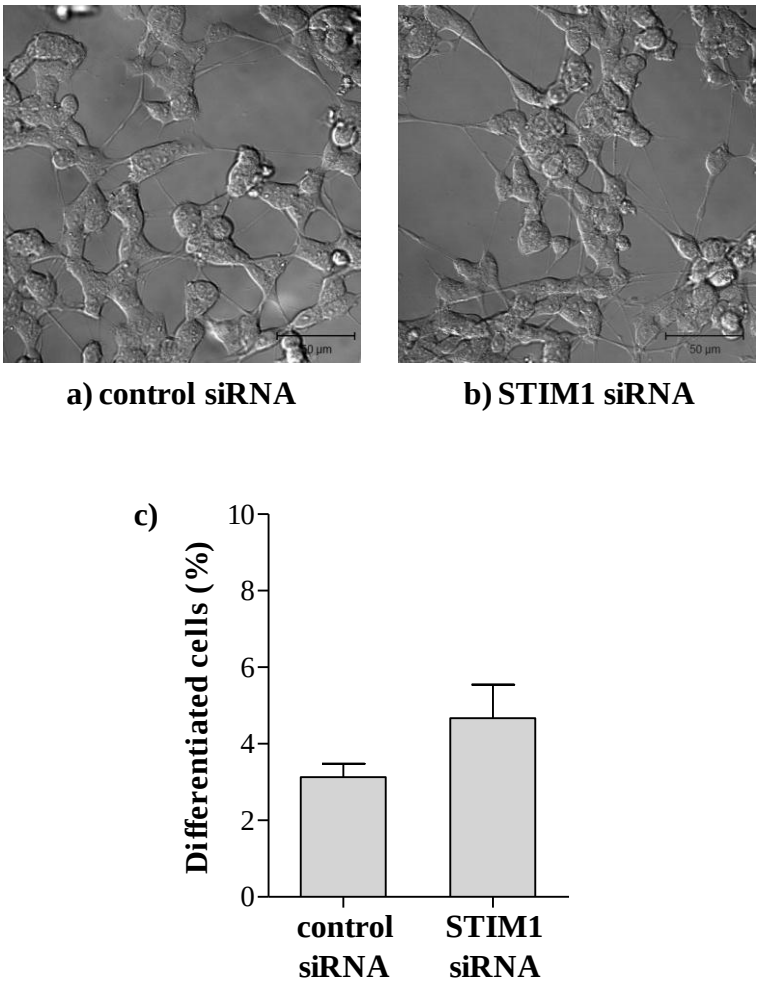

Figure 5.4 Knockdown of STIM1 in N-type cells does not induce morphological differentiation

Cells were transfected with either control siRNA or STIM1 siRNA for 48 hours. DIC image of N-type cells transfected with **a**) control siRNA and **b**) STIM1 siRNA. Scale bars equal 50µm. **c**) Quantification of DIC images; differentiated cells (neurite extensions ≥50µm) were counted and expressed as a percentage of the total cell population. For control siRNA ~3% of cells were classed as differentiated (66/2190 cells). For STIM1 siRNA almost 5% of cells were classed as differentiated (110/2355 cells), There was no significant difference in the extent of morphological differentiation between control siRNA and STIM1 siRNA transfected cells, P=0.1721. *n*=4.

5.2.3 Knockdown of STIM1 followed by 9*c*RA treatment down-regulates SOCE but does not affect differentiation

Knockdown of STIM1 did not itself induce differentiation (Figure 5.4). In the next series of experiments it was investigated as to whether knockdown of STIM1 affected the ability of 9*c*RA to induce differentiation of N-type cells.

STIM1 was knocked down in N-type cells by transfection with STIM1 siRNA for 48 hours (Methods 2.3). Following knockdown cells were then treated with either EtOH or 9*c*RA for a further 3 days. In total this amounts to 5 days treatment; 48 hours of transfection followed by 3 days of EtOH or 9*c*RA treatment. Data from our laboratory have shown that effects of 9*c*RA on SOCE (i.e. down-regulation) are apparent following 3 days of treatment; 3 days treatment is therefore a suitable time scale to determine whether knockdown of STIM1 has any affect on SOCE or differentiation of 9*c*RA treated cells.

Three sets of cells were used; two sets were transfected with control siRNA for 48 hours, one was then treated with EtOH and the other with 9*c*RA for 3 days. The final set was transfected with STIM1 siRNA for 48 hours followed by 9*c*RA treatment for 3 days. Henceforth cells transfected with control siRNA followed by EtOH treatment will be referred to as control EtOH cells, those transfected with control siRNA followed by 9*c*RA treatment will be referred to as control 9*c*RA cells and those transfected with STIM1 siRNA followed by 9*c*RA treatment will be referred to as STIM1 knockdown cells.

Western blot analysis showed the expression of STIM1, as identified by the presence of a band at 84kDa in response to anti-STIM1 antibody, in control EtOH, control 9*c*RA and STIM1 knockdown cells (Figure 5.5). There is a visible reduction in band intensity in control 9*c*RA cells and STIM1 knockdown cells compared to control EtOH cells. This was quantified by expressing STIM1 as a ratio of β-actin expression, which revealed a significant decrease in STIM1 protein expression by ~46% in control 9*c*RA cells and ~58% in STIM1 knockdown cells, P=0.0332 and P=0.0193 respectively**.**

Bcl-2 expression (Figure 5.5a) was quantified by expression of Bcl-2 as a ratio of β-actin expression (Figure 5.5c). Bcl-2 protein expression was not significantly up-

regulated in control 9*c*RA cells and STIM1 knockdown cells compared to control EtOH cells, P>0.05. Bcl-2 expression was not significantly up-regulated in SH-SY5Y cells until day 5 9*c*RA treatment.

Following transfection of cells and the subsequent knockdown of STIM1 protein, Ca^{2+} add-back experiments were performed to measure SOCE and DIC images were taken to determine the extent of morphological differentiation.

Ca^{2+} add-back experiments revealed that there was no significant difference in store depletion between control EtOH (12.56±1.89µMs), control 9*c*RA (11.75±0.76µMs) and STIM1 knockdown cells (12.43±1.12µMs), P>0.05. SOCE was down-regulated in control 9*c*RA cells (13.25±1.77µMs) compared to control EtOH cells (21.52±1.11µMs), P<0.05 (Figure 5.6). This result shows a similar relationship to 7 day EtOH and 9*c*RA treated cells (Figure 4.4), confirming that following 3 days 9*c*RA treatment SOCE becomes significantly down-regulated. SOCE measured in STIM1 knockdown cells (9.88±1.64µMs) was also significantly down-regulated compared to control EtOH cells (P<0.01).

DIC images were taken of the cells to correspond with the protein samples and the Ca^{2+} add-back experiments performed in order to see whether there was any affect on morphological differentiation (Figure 5.7). Images of control EtOH cells revealed cellular differentiation to be 1.25±0.12% compared to control 9*c*RA cells which were classed as 6.91±0.35% differentiated; P<0.001. This confirmed that the transfection procedure did not affect the ability of the cells to differentiate as the extent of differentiation was comparable to 3 day 9*c*RA treated cells (Figure 3.2). STIM1 knockdown cells were determined to be 7.33±0.68% differentiated (P<0.001 against control EtOH). This demonstrates that knockdown of STIM1 in N-type cells does not affect the ability of the cell to differentiate in response to 9*c*RA as values seen are comparable to control 9*c*RA cells, P>0.05.

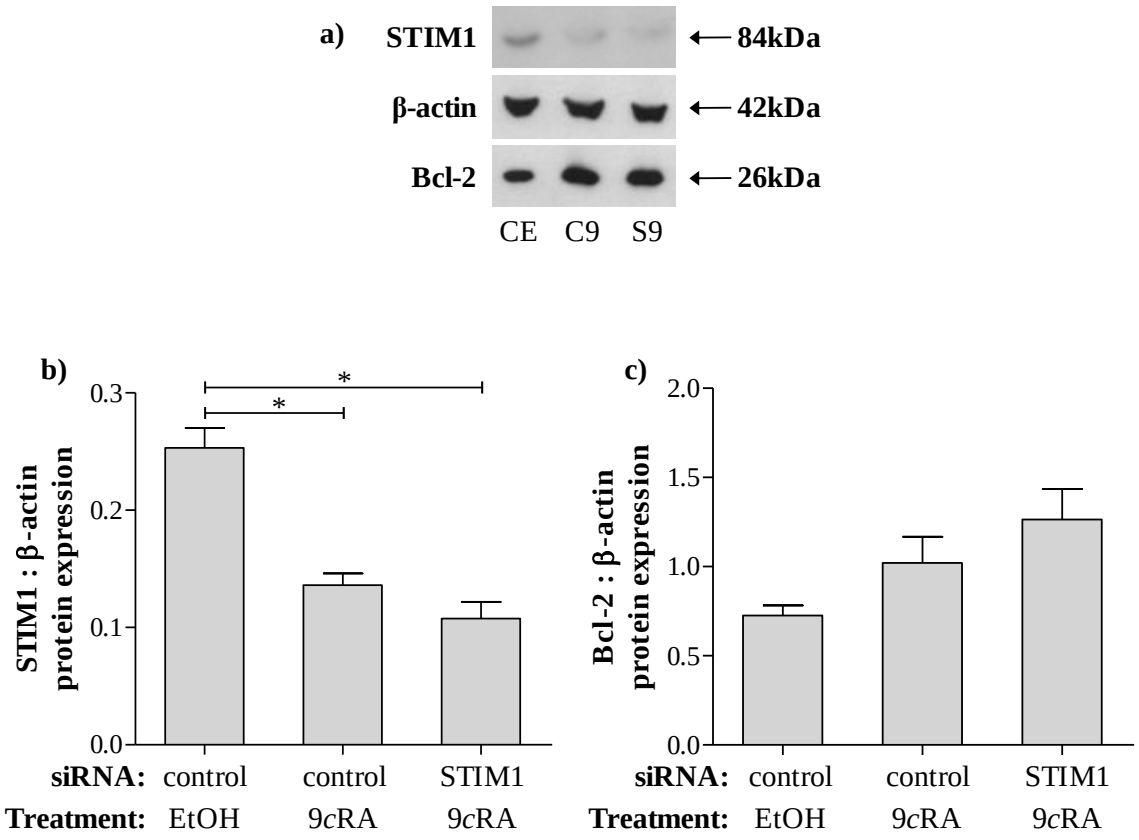

Figure 5.5 Knockdown of STIM1 in N-type cells followed by 9*c*RA treatment

N-type cells were transfected with either control siRNA or STIM1 siRNA for 48 hours and then treated with either EtOH or 9*c*RA for a further 3 days. **a**) Western blots were performed on protein extracted from control EtOH (CE), control 9*c*RA (C9) and STIM1 knockdown (S9) cells. A band at 84kDa was detected with anti-STIM1 antibody. Blots were re-probed with anti-β-actin antibody (42kDa), used as a loading control and with anti-Bcl-2 antibody (26kDa), used as a biochemical marker of differentiation. **b**) Quantitative measurements of bands were performed using densitometry (ImageJ software, Methods 2.6.9). STIM1 was significantly knocked down in control 9*c*RA cells and STIM1 knockdown cells compared to control EtOH cells, $P<0.05^{*}$ **c**) Quantitative measurements of Bcl-2 protein expression revealed that Bcl-2 expression was not significantly up-regulated in either 9*c*RA control or STIM1 knockdown cells compared to EtOH treated cells, $P>0.05$. $n=3$.

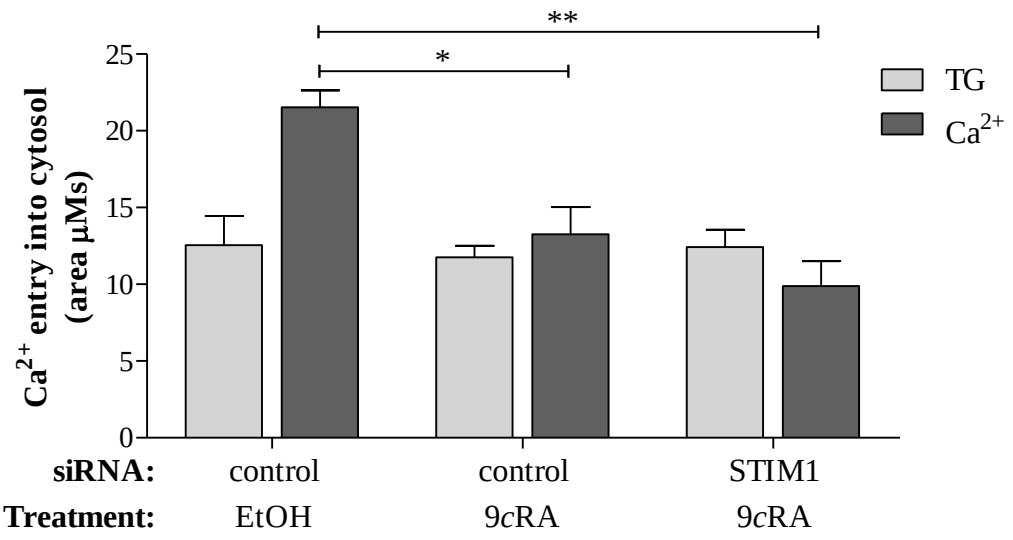

Figure 5.6 Knockdown of STIM1 in N-type cells followed by 9*c*RA treatment down-regulates SOCE

N-type cells were transfected with either control siRNA or STIM1 siRNA for 48 hours, followed by EtOH or 9*c*RA treatment for 3 days. Ca^{2+} add-back experiments were performed on cells following treatment. Store depletion in response to TG (200nM) was not significantly different between control EtOH, control 9*c*RA and STIM1 knockdown cells ($P>0.05$). SOCE in response to the addition of Ca^{2+} (2mM) was significantly down-regulated in control 9*c*RA cells compared to control EtOH cells, $P<0.05^{*}$. SOCE in STIM1 knockdown cells was also significantly down-regulated compared to control EtOH cells, $P<0.01^{**}$ and not significantly different to control 9cRA cells, $P>0.05$. For control EtOH cells $n=3$, control 9*c*RA cells $n=5$ and for STIM1 knockdown cells $n=6$.

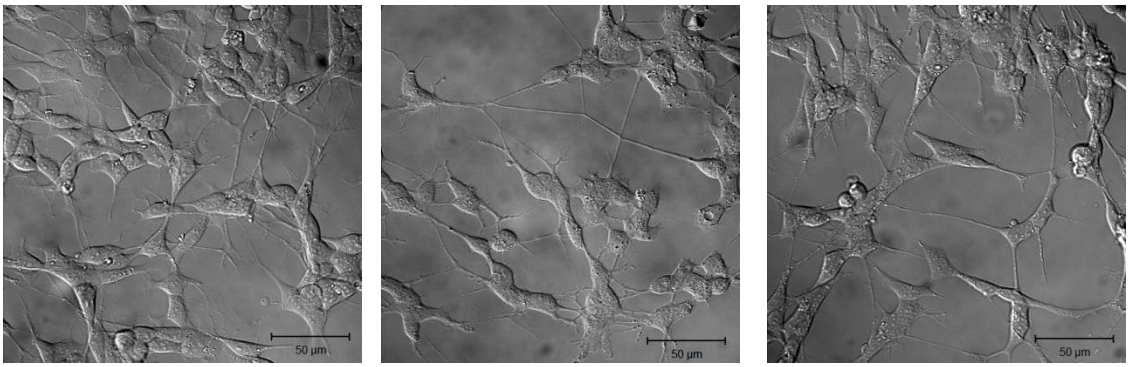

a) control siRNA EtOH **b)** control siRNA 9*c*RA **c)** STIM1 siRNA 9*c*RA

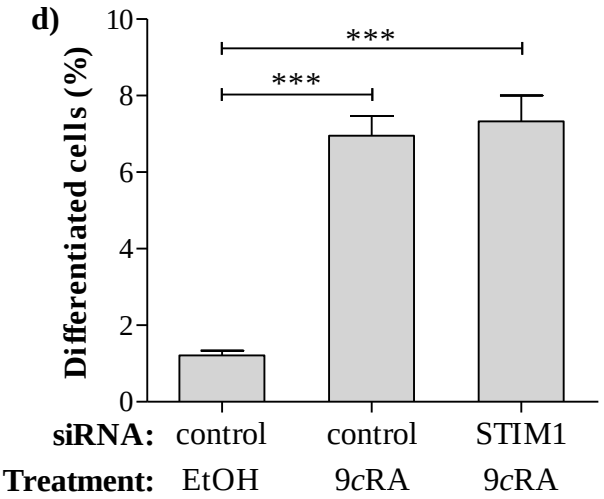

Figure 5.7 Knockdown of STIM1 in N-type cells followed by 9*c*RA treatment does not affect morphological differentiation

Cells were transfected with either control siRNA or STIM1 siRNA for 48 hours and then treated with EtOH or 9*c*RA for 3 days. DIC image of N-type cells transfected with **a**) control siRNA followed by EtOH treatment, **b**) control siRNA followed by 9*c*RA treatment and **c**) STIM1 siRNA followed by 9*c*RA treatment. Scale bars represent 50µm. **d**) Quantification of DIC images; differentiated cells (neurite extensions ≥50µm) were counted and expressed as a percentage of the total cell population. For control EtOH ~1% of cells were classed as differentiated (88/7399 cells), *n*=8. For control 9*c*RA ~7% of cells were classed as differentiated (330/4674 cells), *n*=10. For STIM1 knockdown ~7% of cells were classed as differentiated (349/4980 cells), *n*=12. There was a significant increase in the number of differentiated cells in control 9*c*RA and STIM1 knockdown cells compared to control EtOH treated cells, P<0.001***.

5.2.4 Overexpression of STIM1 in 9*c*RA-differentiated cells restores SOCE and decreases the extent of morphological differentiation

SOCE is down-regulated in 7 day 9*c*RA-differentiated N-type cells (Figure 4.4) as is the protein STIM1 (Figure 5.1). Furthermore, knockdown of the STIM1 protein in untreated (i.e. proliferating) N-type cells resulted in the down-regulation of SOCE (Figure 5.3). As knockdown of STIM1 resulted in the down-regulation of SOCE the next step was to investigate whether overexpression of STIM1 in 9*c*RA-differentiated cells (i.e. cells in which STIM1 and SOCE is down-regulated) would restore SOCE to levels seen in proliferating cells.

Three sets of cells were used, one set was treated with EtOH for 7 days and the other two sets were treated with 9*c*RA for 7 days. Following this the EtOH and one of the 9*c*RA treated sets were transfected with control vector (pcDNA 3.1) for 24 hours and the other 9*c*RA treated set was transfected with Cherry-STIM1 for 24 hours (Methods 2.3.2). Cells treated with EtOH for 7 days and then transfected with the control vector for 24 hours will be referred to as EtOH control cells. Cells treated with 9*c*RA for 7 days and then transfected with the control vector for 24 hours will be referred to as 9*c*RA control cells. Cells treated with 9*c*RA for 7 days and then transfected with Cherry-STIM1 will be referred to as STIM1 overexpressed cells.

Following treatment and transfection cells were harvested for protein, Ca^{2+} add-back experiments were performed and corresponding DIC images were taken.

STIM1 was present in EtOH control, 9*c*RA control and STIM1 overexpressed cells as identified by the presence of a band at 84kDa in response to anti-STIM1 antibody (Figure 5.8a). As expected, STIM1 expression was significantly down-regulated in 9*c*RA control cells compared to EtOH control cells, $P<0.05$. The band detected at ~104kDa indicates overexpression of STIM1 (the band is higher than the molecular weight of STIM1 due to the presence of the cherry tag). STIM1 expression was significantly increased in STIM1 overexpressed cells compared to EtOH and 9*c*RA control cells, $P<0.001$.

The protein Bcl-2 is up-regulated in 9*c*RA controls and in STIM1 overexpressed cells in comparison to EtOH control cells, as determined by a band detected at 26kDa in response to anti-Bcl-2 antibody. This indicates that biochemical differentiation of the cells had occurred in response to 9*c*RA treatment and this had not been affected by STIM1 protein overexpression (Figure 5.8a and c).

Ca^{2+} add-back experiments revealed store depletion in response to TG (200nM) was not significantly different between EtOH control (12.96±1.38µMs), 9*c*RA control (9.90±2.14µMs) and STIM1 overexpressed cells (9.89±0.95µMs), $P>0.05$. As expected however, SOCE in response to the addition of Ca^{2+} (2mM) was significantly down-regulated in 9*c*RA control cells (15.06±1.10µMs) compared to EtOH control cells (23.06±1.11µMs), $P<0.01$. This result is consistent with previous data where 7 day 9*c*RA treatment of N-type cells down-regulated SOCE (Figures 4.4). SOCE in response to the addition of Ca^{2+} in STIM1 overexpressed cells (20.35±1.33µMs) was not significantly different to EtOH control cells, $P>0.05$. Overexpression of STIM1 in 9*c*RA-differentiated cells has the ability to restore SOCE in cells which previously had down-regulated SOCE. This further supports a role for STIM1 in SOCE in N-type cells.

Corresponding DIC images revealed that, as expected, 9*c*RA control cells were significantly more differentiated compared to EtOH control cells; 36.14±3.88% compared to 2.33±0.46%, $P<0.001$ (Figure 5.10). This result is similar to previous data where 7 days 9*c*RA treatment saw a significant increase in the extent of morphological differentiation compared to EtOH treated cells (Figure 3.2). The extent of cellular differentiation in STIM1 overexpressed cells was 21.27±4.35%, although significantly higher than EtOH controls, $P<0.05$ this was also significantly lower compared to 9*c*RA controls, $P<0.05$. Overexpression of STIM1 therefore reduces the level of differentiation normally seen following 9*c*RA treatment suggesting that STIM1 drives the cells toward a proliferating state.

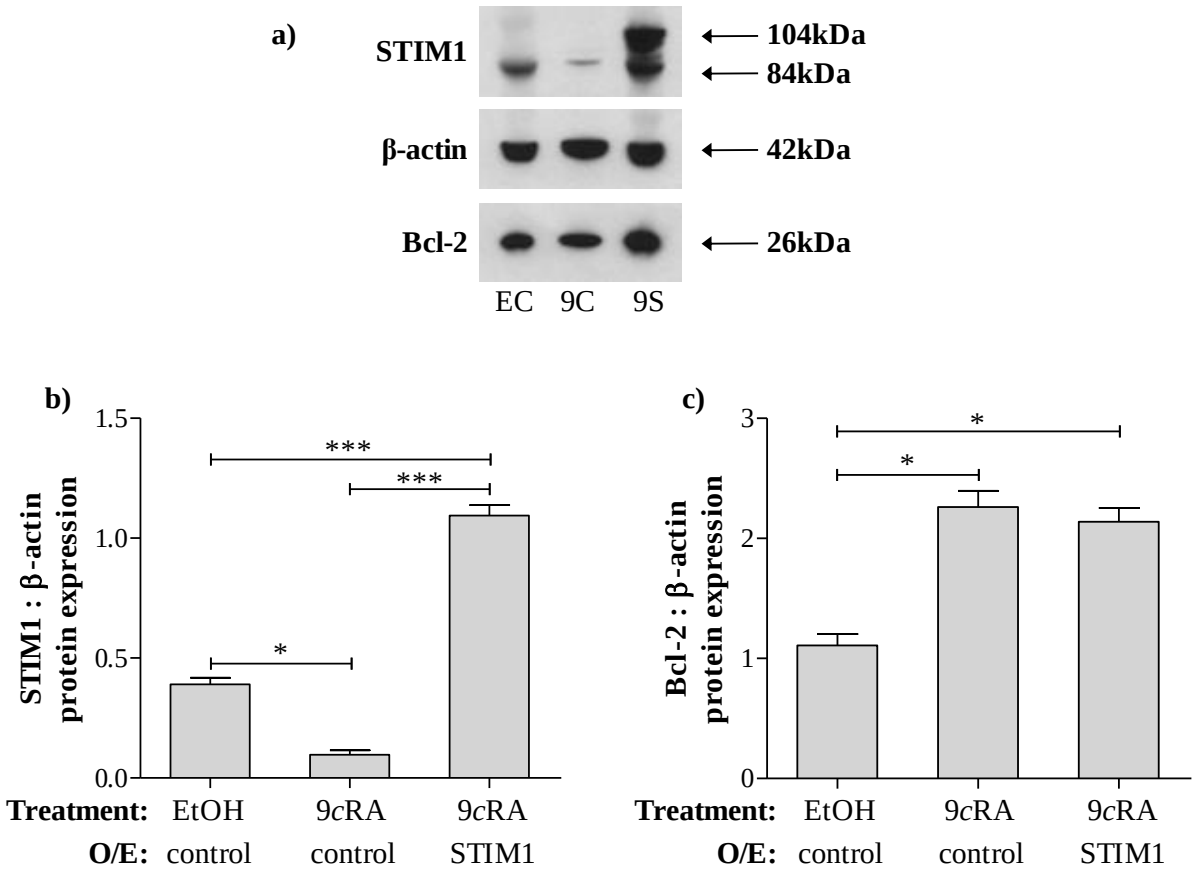

Figure 5.8 Overexpression of STIM1 in N-type cells

Cells were treated with EtOH or 9*c*RA for 7 days followed by transfection with either control vector or cherry-STIM1 for 24 hours. O/E: Overexpression **a**) STIM1 is expressed in EtOH control cells (EC), 9*c*RA control cells (9C) and STIM1 overexpressed cells (9S) as identified by the presence of a band at 84kDa in response to anti-STIM1 antibody and for STIM1 overexpressed cells at ~104kDa due to the presence of the cherry tag. Blots were re-probed with anti-β-actin antibody (42kDa), used as a loading control and with anti-Bcl-2 antibody (26kDa), used as a biochemical marker of differentiation. **b**) Quantitative measurements of bands were performed using densitometry (ImageJ software, Methods 2.6.9) where STIM1 was expressed as a ratio of β-actin. STIM1 protein expression was significantly down-regulated in 9*c*RA control cells compared to EtOH control cells, $P<0.05^{*}$ and was significantly up-regulated in STIM1 overexpressed cells compared to EtOH and 9*c*RA control cells ($P<0.001^{***}$). **c**) Quantification of Bcl-2 protein expression revealed Bcl-2 was significantly increased in 9*c*RA control and STIM1 overexpressed cells compared to EtOH control cells, $P<0.05^{*}$. *n*=4.

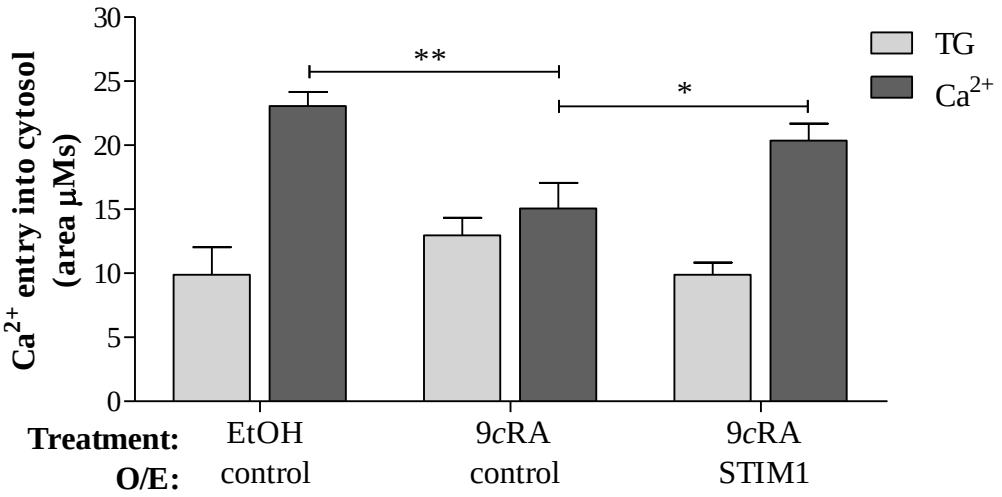

Figure 5.9 Overexpression of STIM1 in 9*c*RA-differentiated N-type cells restores SOCE

Cells were treated with EtOH or 9*c*RA for 7 days followed by transfection with either control vector or Cherry-STIM1. O/E: Overexpression. Store depletion in response to the addition of TG (200nM) was not significantly different between EtOH control, 9*c*RA control and STIM1 overexpressed cells (P>0.05). SOCE in response to the addition of Ca^{2+} (2mM) was significantly down-regulated in 9*c*RA control cells compared to EtOH control cells, P<0.01**. SOCE in STIM1 overexpressed cells was significantly up-regulated compared to 9*c*RA control cells, P<0.05* and not significantly different to EtOH control cells, P>0.05. *n*=11.

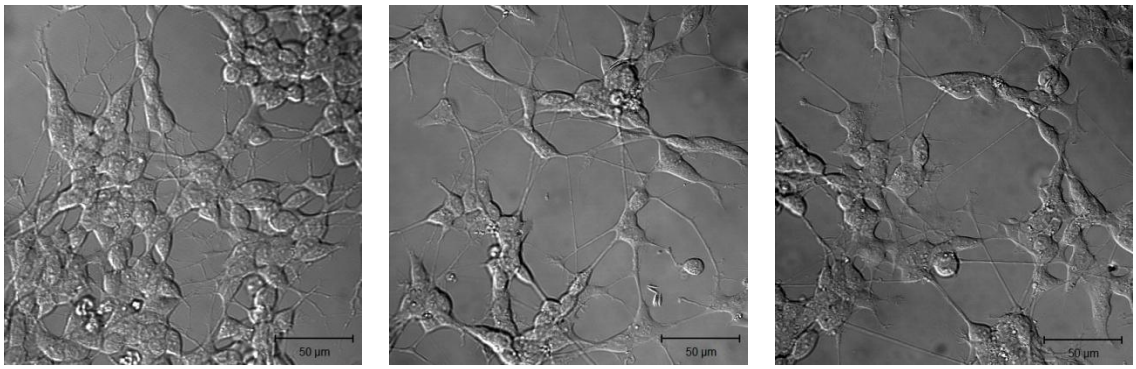

a) EtOH control O/E **b)** 9*c*RA control O/E **c)** 9*c*RA STIM1 O/E

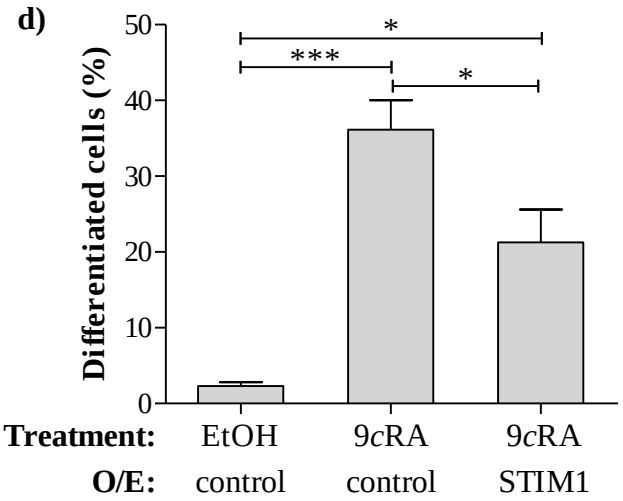

Figure 5.10 Overexpression of STIM1 in 9*c*RA-differentiated cells decreases morphological differentiation

Cells were treated with EtOH or 9cRA for 7 days and then transfected with either control vector or Cherry-STIM1 for 24 hours. O/E: Overexpression. DIC image of N-type cells treated with **a**) EtOH followed by transfection with control vector, **b**) 9*c*RA followed by transfection with control vector and **c**) 9*c*RA followed by transfection with Cherry-STIM1. Scale bars represent 50µm. **d**) Quantification of DIC images; differentiated cells (neurite extensions ≥50µm) were expressed as a percentage of the total cell population. The percent differentiation in EtOH control cells was ~2% (51/2036 cells), *n*=6, in 9*c*RA control cells was ~36% (504/1752 cells), *n*=12 and in STIM1 overexpressed cells ~21% (171/786 cells), *n*=6. The extent of differentiation was significantly higher in 9*c*RA control cells, $P<0.001^{***}$ and STIM1 overexpressed cells, $P<0.05^{*}$ compared to EtOH control cells. However, differentiation was significantly reduced in STIM1 overexpressed cells compared to 9*c*RA control cells, $P<0.05^{*}$.

5.3 Discussion

A down-regulation in SOCE was observed in 9*c*RA-differentiated SH-SY5Y and N-type cells (Chapter 4). The down-regulation in SOCE was accompanied by a down-regulation in STIM1 protein expression (Figure 5.1), consistent with a role for STIM1 in SOCE (Roos *et al*., 2005; Liou *et al*., 2005; Zhang *et al*., 2005).

To investigate the role of STIM1 in proliferating N-type cells, STIM1 was knocked down (Figure 5.2) and the effects on SOCE and differentiation were determined. Knockdown of STIM1 in proliferating N-type cells resulted in down-regulated SOCE (Figure 5.3), again consistent with a role for STIM1 in SOCE. Knockdown of STIM1 did not induce biochemical (Figure 5.2) or morphological (Figure 5.4) differentiation in proliferating N-type cells, suggesting that the down-regulation in STIM1 alone is not sufficient to induce the differentiation of cells that is observed following 9*c*RA treatment.

To investigate whether the down-regulation of STIM1 seen in 9*c*RA-differentiated N-type cells plays a role in the 9*c*RA-induced switch from proliferation to differentiation, STIM1 was knocked down in proliferating cells. These cells were then induced to differentiate by the addition of 9*c*RA (Figure 5.5). Knockdown of STIM1 in proliferating N-type cells down-regulated SOCE to a similar level observed in control 9*c*RA cells (Figure 5.6). SOCE is therefore not further down-regulated by 9*c*RA treatment following STIM1 knockdown suggesting that 9*c*RA treatment down-regulates STIM1 to a level that has already been achieved by knockdown. Knockdown of STIM1 in proliferating N-type cells did not prevent 9*c*RA-induced differentiation where the extent of differentiation was comparable to control 9*c*RA cells (Figure 5.7). That premature down-regulation of STIM1 did not prevent 9*c*RA-induced differentiation suggests that normal levels of STIM1 are not required for 9*c*RA to induce differentiation.

Next it was investigated as to whether down-regulation of STIM1 was required to maintain down-regulated SOCE and the differentiated state of N-type cells. STIM1 was overexpressed in 9*c*RA-differentiated N-type cells (Figure 5.8). Overexpression of STIM1 restored SOCE to levels comparable to that of proliferating cells (Figure 5.9).

This result shows that, although not normally observed in differentiated N-type cells, these cells are capable of supporting a SOCE response involving STIM1. Interestingly, overexpression of STIM1 in 9*c*RA-differentiated N-type cells reduced the number of differentiated cells compared to 9*c*RA controls (Figure 5.10), as determined morphologically. SOCE and STIM1 appear to be associated with a proliferative state in N-type cells and raises the possibility that STIM1 down-regulation is part of the molecular mechanism by which cells remain in the differentiated state.

The observation that in proliferating N-type cells knockdown of STIM1 down-regulates SOCE has also been observed in many other cell types, including endothelial progenitor cells (Kuang *et al*., 2010; Shi *et al*., 2010), proliferating endothelial cells (Abdullaev *et al*., 2008), vascular smooth muscle cells (Aubart *et al*., 2009; Portier *et al*., 2009), myoblasts (Darbellay *et al*., 2009; 2010) and adipocytes (Graham *et al*., 2009).

Also consistent with these findings in N-type SH-SY5Y cells, knockdown of STIM1 in HEK293 cells inhibited SOCE and did not itself induce differentiation (El Boustany *et al*., 2010). In other cell types however knockdown of STIM1 expression alone appears sufficient to influence differentiation. For example, knockdown of STIM1 decreased differentiation in myoblasts (Darbellay *et al*., 2009, 2010), but increased differentiation in adipocytes (Graham *et al*., 2009).

STIM1 down-regulation in N-type SH-SY5Y cells is not alone sufficient to induce differentiation, however overexpression studies indicated that normal down-regulation could be required to maintain the differentiated state. A similar result was found in adipoctyes, where overexpression of STIM1 increased SOCE and also hindered the ability of the cells to differentiate (Graham *et al*., 2009). The reduction in differentiation observed in STIM1 overexpressing N-type cells suggests that STIM1 favours proliferation of cells. In other cell types STIM1 has been found to be involved in proliferation. For example, STIM1 becomes upregulated in proliferating vascular smooth muscle cells (Aubart *et al*., 2009; Portier *et al*., 2009) and is also transiently up-regulated during the initial phase of myogenesis of C2C12 cells (Kiviluoto *et al*., 2011). Further evidence consistent with results obtained in this study, STIM1 expression decreases over the course of osteoclast differentiation (Zhou *et al*., 2011) and RA

treatment of rat mesangial cells down-regulated SOCE and STIM1 protein expression which was associated with decreased proliferation (Zhang *et al*., 2007).

It is noteworthy that 9*c*RA-induced STIM1 down-regulation was confined to N-type SH-SY5Y cells. N-type cells are progenitors to neurons of the SNS (Introduction 1.2). Excitable cells (such as neuronal cells) possess alternative families of PM Ca^{2+} channels, notably VOCs, which may provide alternative Ca^{2+} entry pathways through which ER Ca^{2+} stores can be replenished (Berridge, 1998). A previous study from the laboratory (Brown *et al*., 2005) has shown that an up-regulation in VOCE may occur in 9*c*RA-differentiated SH-SH5Y cells. In S-type cells SOCE was unaltered following 9*c*RA-induced differentiation (Chapter 4). Consistent with no change in SOCE, there was no change in STIM1 expression following 9*c*RA treatment (Figure 5.1). S-type cells are precursors to non-neuronal cell types, which are non-electrically excitable. It is well established that SOCE is essential for the generation of Ca^{2+} signals in the majority of non-excitable cells (Parekh and Putney, 2005). It is therefore not surprising that S-type cells retain SOCE in both proliferating and differentiated states.

In summary, these finding provide a possible molecular mechanism underlying the down-regulation of SOCE observed in N-type SH-SY5Y cells (Chapter 4). The effects on SOCE observed following both knockdown and overexpression of STIM1 in N-type SH-SY5Y cells, are consistent with a role for STIM1 in SOCE and contribute to the large body of evidence indicating that STIM1 is the ER Ca^{2+} sensor that mediates SOCE (Introduction 1.6.1). Knockdown studies of STIM1 in proliferating N-type cells did not support a role for STIM1 in the induction of differentiation that is observed following 9*c*RA treatment. However, overexpression of STIM1 in differentiated N-type cells suggests that STIM1 may play a role in maintaining cells in a proliferative state and therefore that the 9*c*RA-induced down-regulation of STIM1 may be required to maintain cells in a differentiated state.

Chapter 6
Results IV - Orai1

6.1 Introduction

The proteins STIM1, Orai1 and TRPC1 have been demonstrated to be involved in SOCE (Introduction, 1.6). This chapter focuses on the involvement of Orai1 in SOCE and also in differentiation of N-type cells. 9*c*RA-induced differentiation resulted in a significant down-regulation in SOCE (Chapter 4) and in the expression of STIM1 (Chapter 5) in N-type cells. SOCE and the expression of STIM1 remained unaffected in S-type cells (Chapters 4 and 5 respectively).

As Orai1 is proposed to form the SOC that STIM1 activates in response to store depletion, the relationship between Orai1 expression, SOCE and also differentiation was investigated in N-type cells. In order to do this Orai1 protein expression was both knocked down (using siRNA transfection) and overexpressed (using plasmid DNA transfection) in N-type cells (Methods 2.3). Manipulation of Orai1 expression was quantified by western blot (Methods 2.6). The effects on SOCE were measured using Ca^{2+} imaging experiments (Methods 2.8) and the effects on differentiation were determined morphologically by analysis of DIC images (Methods 2.4) and also biochemically by measurement of Bcl-2 expression.

6.2 Results

6.2.1 Orai1 in SH-SY5Y, N- and S-type cells before and after 9*c*RA-induced differentiation

SOCE becomes down-regulated in SH-SY5Y and N-type cells following 9*c*RA-induced differentiation, it however remains unchanged in S-type cells (Chapter 4). In order to determine any changes in Orai1 protein expression associated with the observed changes in SOCE, western blots were performed on protein extracted from SH-SY5Y, N- and S-type cells before and after 9*c*RA-induced differentiation.

Orai1 is expressed in proliferating (7 day EtOH treated) and differentiated (7 day 9*c*RA treated) SH-SY5Y, N-type and S-type cells as determined by a band detected at 47kDa by an anti-Orai1 antibody (Figure 6.1a). Blots were re-probed with β-actin, used as a loading control, and Orai1 was then expressed as a ratio of β-actin in order to quantify changes in band intensity (Figure 6.1b).

Orai1 protein expression was significantly decreased in SH-SY5Y cells by ~60% (P=0.0415) and in N-type cells by ~64% (P=0.0379) following 9*c*RA-induced differentiation. The extent of down-regulation of SOCE for SH-SY5Y cells was ~48% (Figure 4.2) and for N-type cells was ~49% (Figure 4.4). The changes observed in SOCE are similar to those seen in Orai1 protein expression and are consistent with the involvement of Orai1 in the process of SOCE in SH-SY5Y and N-type cells. The level of Orai1 protein expression in S-type cell populations remained unchanged following 9*c*RA-induced differentiation (P=0.6605, Figure 6.1b). This is consistent with the level of SOCE in S-type cells following 9*c*RA-induced differentiation, which also remained unchanged after treatment (Figure 4.6).

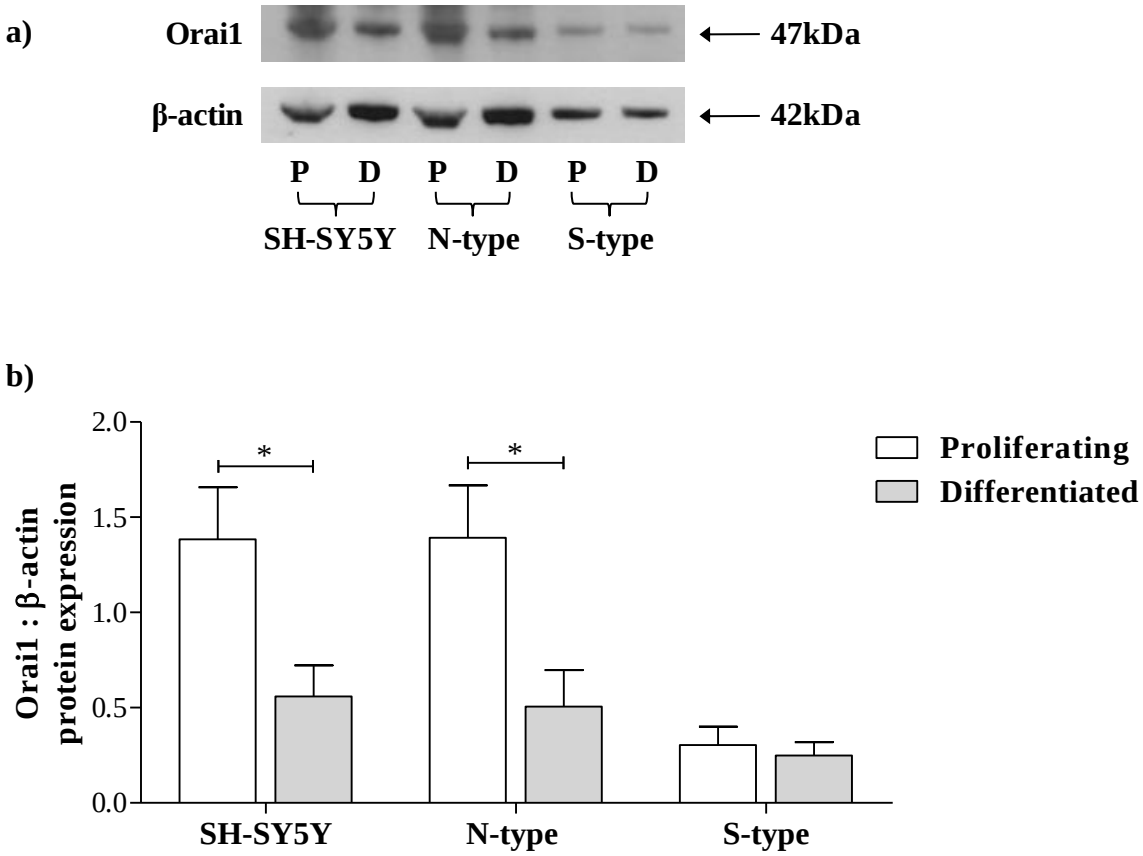

Figure 6.1 Orai1 expression decreases in SH-SY5Y and N-type cells following 9*c*RA-induced differentiation

SH-SY5Y, N-type and S-type cells were treated with EtOH (proliferating - **P**) or 9*c*RA (differentiated - **D**) for 7 days. Following treatment cells were harvested for protein. **a)** Western blot performed on protein extracts. Blots were probed with anti-Orai1 antibody which detected a band at 47kDa. Blots were re-probed with anti-β-actin antibody which detected a band at 42kDa. **b)** Quantitative analysis of Orai1 expression as determined by densitometry using ImageJ software (Methods 2.6.9); Orai1 was expressed as a ratio of β-actin expression (loading control). Orai1 protein expression was significantly reduced in 9*c*RA-differentiated SH-SY5Y cells, P=0.0415* and also N-type cells, P=0.0379* compared to proliferating controls. Orai1 protein expression was unchanged in S-type cells following 9*c*RA treatment, P=0.6605. *n*=4.

6.2.2 Knockdown of Orai1 in N-type cells down-regulates SOCE and induces morphological differentiation

9*c*RA-induced differentiation of both SH-SY5Y and N-type cells results in the down-regulation of SOCE (Figures 4.2 and 4.4 respectively) and also Orai1 protein expression (Figure 6.1). In S-type cells no changes were seen in either SOCE (Figure 4.8) or Orai1 protein expression (Figure 6.1) following 9*c*RA-induced differentiation and therefore these cells were not studied further. SH-SY5Y cells and N-type cells had similar levels of Orai1 expression, which confirmed that the SH-SY5Y cell line used in this study were predominantly composed of N-type cells. N-type cells were therefore used for the remainder of experiments in this chapter.

To investigate whether down-regulation of Orai1 could be responsible for down-regulation of SOCE, Orai1 protein expression was knocked down in untreated (i.e. proliferating) N-type cells (Figure 6.2). Orai1 protein expression was knocked down by transfecting the cells with Orai1 siRNA for 48 hours (Methods, 2.3.1). Control cells were transfected with a scrambled sequence not targeted to a specific gene (control siRNA). Transfection of N-type cells with Orai1 siRNA successfully resulted in the knockdown of Orai1 protein expression as observed by the reduced band intensity at 47kDa as detected by anti-Orai1 antibody in comparison to control siRNA transfected cells (Figure 6.2a). β-actin protein expression was used as a loading control to enable quantification of Orai1 knockdown, where Orai1 was expressed as a ratio of β-actin protein expression (Figure 6.2b). Orai1 protein expression was significantly knocked down by ~62% in Orai1 siRNA transfected cells compared to control siRNA transfected cells, $P=0.0131$.

Bcl-2 protein expression was used as a measure of biochemical differentiation (Figure 6.2a) and was quantified by the expression of Bcl-2 as a ratio of β-actin expression (Figure 6.2c). Bcl-2 protein expression was not significantly different between control siRNA and Orai1 siRNA transfected cells, $P=0.3268$.

Following transfection of cells and the subsequent knockdown of Orai1 protein, Ca^{2+} add-back experiments were performed to measure SOCE and DIC images were taken to determine the extent of morphological differentiation.

Ca^{2+} add-back experiments revealed that store depletion (TG response) was not significantly different between control siRNA (6.85±0.83μMs) and Orai1 siRNA (5.86±0.71μMs) transfected cells, P=0.3714 (Figure 6.3). SOCE (Ca^{2+} response) following store depletion was however significantly down-regulated in Orai1 siRNA transfected cells (6.30±1.48μMs) compared to control siRNA transfected cells (13.67±1.49μMs), P=0.0015. Knockdown of the Orai1 protein down-regulated SOCE by ~54% revealing the role that Orai1 plays in SOCE in proliferating N-type cells.

DIC images were taken of the cells to correspond with the protein samples and the Ca^{2+} add-back experiments to see whether there was any affect on differentiation as determined by neurite length (≥50μm) (Figure 6.4). DIC images of control siRNA transfected cells revealed cellular differentiation to be 3.21±0.35% compared to Orai1 siRNA transfected cells which were 8.13±1.36%, P=0.0127. Knockdown of Orai1 in N-type cells has therefore significantly induced morphological differentiation. This would suggest that the Orai1 protein plays a key role in the switch from proliferation to differentiation in N-type cells as knockdown of Orai1 is sufficient to induce morphological differentiation. Knockdown of Orai1 had no effect on proliferation as determined by the mean number of cells counted from each coverslip; control siRNA; 527.25±45.95, *n*=4 vs. Orai1 siRNA; 486.50±20.75, *n*=4, P=0.4498. The increase in differentiated cells as determined by morphological differentiation was not consistent with biochemical differentiation as measured by Bcl-2 protein expression which remained similar to control siRNA cells (Figure 6.2c).

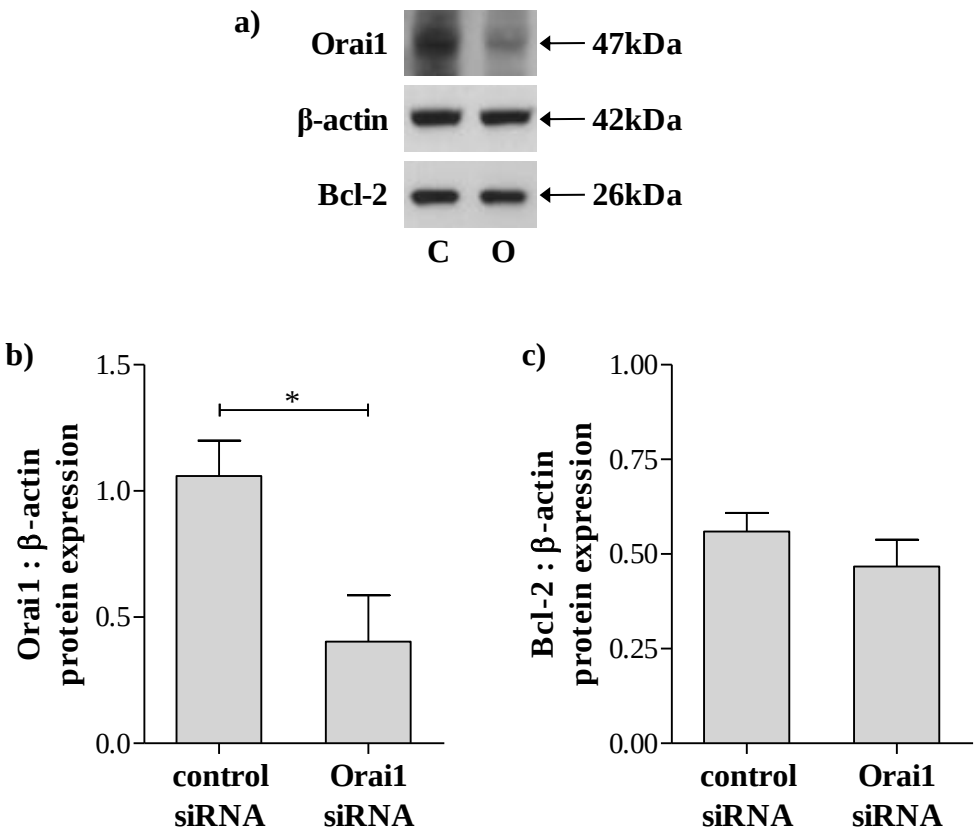

Figure 6.2 Knockdown of Orai1 in N-type cells

N-type cells were transfected with either control siRNA or Orai1 siRNA for 48 hours. **a**) Western blot performed on protein extracted from control siRNA (**C**) and Orai1 siRNA (**O**) transfected cells. A band at 47kDa was detected with anti-Orai1 antibody. Blots were re-probed with anti-β-actin antibody (42kDa), used as a loading control and with anti-Bcl-2 antibody (26kDa), used as a biochemical marker of differentiation. **b**) Quantitative measurements were performed on western blots by densitometry (using ImageJ software, Methods 2.6.9). Orai1 was significantly down-regulated following Orai1 siRNA transfection compared to control siRNA transfected cells; P=0.0131. **c**) Quantitative measurements of Bcl-2 protein expression show that Bcl-2 expression was not significantly different between control siRNA and Orai1 siRNA transfected cells; P=0.3268. *n*=4.

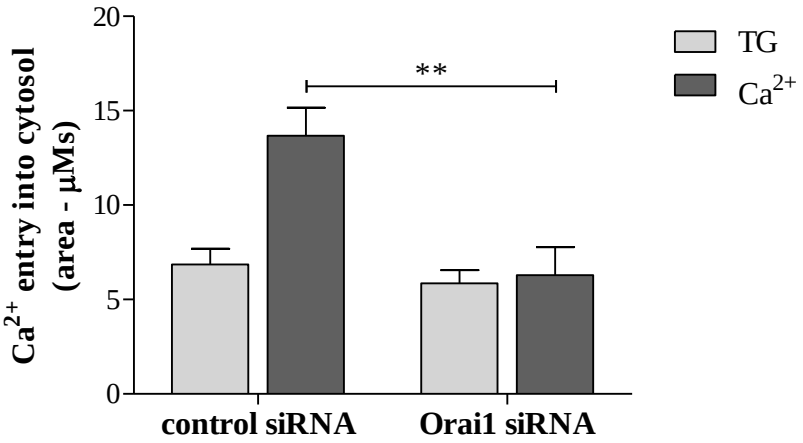

Figure 6.3 Knockdown of Orai1 in N-type cells down-regulates SOCE

N-type cells were transfected with either control siRNA or Orai1 siRNA for 48 hours following which Ca^{2+} add-back experiments were performed. Store depletion in response to the addition of TG (200nM) was not significantly different between control siRNA and Orai1 siRNA transfected cells, P=0.3714. SOCE in response to the addition of Ca^{2+} (2mM) was significantly down-regulated in Orai1 siRNA transfected cells compared to control siRNA transfected cells (P=0.0015**). For control siRNA transfected cells *n*=15 and for Orai1 siRNA transfected cells *n*=15.

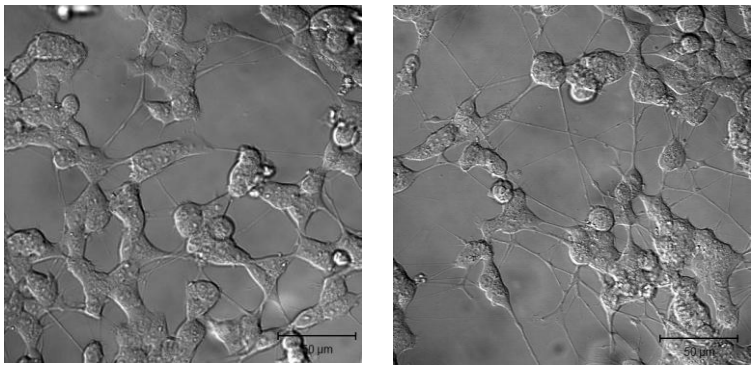

a) control siRNA **b) Orai1 siRNA**

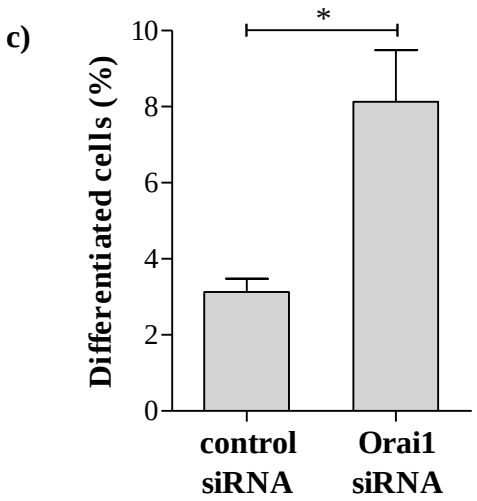

Figure 6.4 Knockdown of Orai1 in N-type cells induces morphological differentiation

Cells were transfected with either control siRNA or Orai1 siRNA for 48 hours. DIC image of N-type cells transfected with **a**) control siRNA and **b**) Orai1 siRNA. Scale bars equal 50µm. **c**) Quantification of DIC images; differentiated cells (neurite extensions ≥50µm) were counted and expressed as a percentage of the total cell population. For control siRNA ~3% of cells were classed as differentiated (66/2109 cells). For Orai1 siRNA ~8% of cells were classed as differentiated (159/1946 cells). There was a significant increase in the extent of morphological differentiation in Orai1 siRNA transfected cells compared to control siRNA transfected cells, P=0.0127*. *n*=4.

6.2.3 Knockdown of Orai1 in N-type cells followed by 9*c*RA treatment down-regulates SOCE and enhances morphological differentiation

The knockdown of Orai1 alone in N-type cells down-regulated SOCE (Figure 6.3) and also significantly induced morphological differentiation (Figure 6.4). In the next series of experiments it was investigated whether knockdown of Orai1 affected the ability of 9*c*RA to further induce differentiation of N-type cells.

Orai1 was knocked down in N-type cells by transfection with Orai1 siRNA for 48 hours. Following knockdown cells were then treated with either EtOH or 9*c*RA for a further 3 days. In total this amounts to 5 days treatment; 48 hours of transfection followed by 3 days of EtOH or 9*c*RA treatment. Three sets of cells were used; two sets were transfected with control siRNA for 48 hours, one was then treated with EtOH and the other with 9*c*RA for 3 days. The final set was transfected with Orai1 siRNA for 48 hours followed by 9*c*RA treatment for 3 days. Henceforth cells transfected with control siRNA followed by EtOH treatment will be referred to as control EtOH cells, those transfected with control siRNA followed by 9*c*RA treatment will be referred to as control 9*c*RA cells and those transfected with Orai1 siRNA followed by 9*c*RA treatment will be referred to as Orai1 knockdown cells.

Western blot analysis showed the expression of Orai1, as identified by the presence of a band at 47kDa in response to anti-Orai1 antibody, in control EtOH, control 9*c*RA and Orai1 knockdown cells (Figure 6.5). Expression of Orai1 as a ratio of β-actin expression revealed a knockdown in Orai1 protein expression by ~41% in control 9*c*RA cells and ~35% in Orai1 knockdown cells**.**

Bcl-2 protein expression was used as a biochemical measure of differentiation (Figure 6.5a and c). Bcl-2 protein expression was increased in control 9*c*RA cells and Orai1 knockdown cells compared to EtOH control cells.

Following transfection of cells and the subsequent knockdown of Orai1 protein, Ca^{2+} add-back experiments were performed to measure SOCE and DIC images were taken to determine the extent of morphological differentiation.

Ca^{2+} add-back experiments revealed that there was no significant difference in store depletion between control EtOH (12.56±1.89μMs), control 9*c*RA (11.75±0.76μMs) and Orai1 knockdown cells (12.65±0.77μMs), P>0.05. SOCE was down-regulated in control 9*c*RA cells (13.25±1.77μMs) compared to control EtOH cells (21.52±1.11μMs), P<0.05 (Figure 6.6). This result shows a similar relationship to 7 day EtOH and 9*c*RA treated cells (Figure 4.4), confirming that following 3 days 9*c*RA treatment SOCE becomes significantly down-regulated. SOCE measured in Orai1 knockdown cells (15.65±1.03μMs) was also significantly down-regulated compared to control EtOH cells (P<0.05) but not to control 9*c*RA cells (P>0.05).

DIC images were taken of the cells to correspond with the protein samples and the Ca^{2+} add-back experiments performed in order to see whether there was any affect on morphological differentiation (Figure 6.7). Images of control EtOH cells revealed morphological differentiation to be 1.21±0.12% compared to control 9*c*RA cells which were classed as 6.95±0.52% differentiated; P<0.001. This confirmed that the transfection procedure did not affect the ability of the cells to differentiate as the extent of differentiation was comparable to 3 day 9*c*RA treated cells (Figure 3.2). Orai1 knockdown cells were determined to be 14.44±0.94%, significantly more differentiated than both control EtOH and control 9*c*RA cells, P<0.001. These results demonstrate that knockdown of Orai1 in N-type enhances morphological differentiation induced by 9*c*RA treatment without enhancing biochemical differentiation as judged by Bcl-2 expression. This is consistent with the effects on untreated cells where Orai1 knockdown induced morphological differentiation (Figure 6.4) independently of Bcl-2 expression (Figure 6.2).

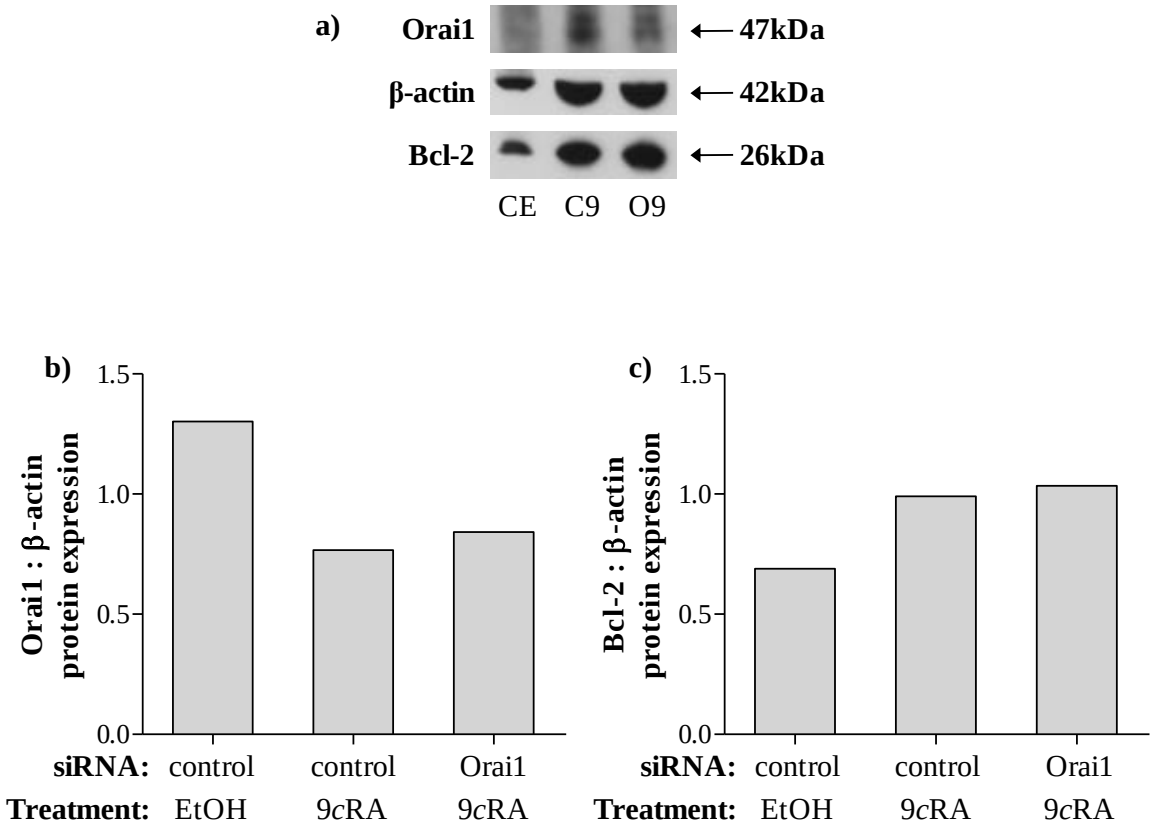

Figure 6.5 Knockdown of Orai1 in N-type cells followed by 9*c*RA treatment

N-type cells were transfected with either control siRNA or Orai1 siRNA for 48 hours and then treated with either EtOH or 9*c*RA for a further 3 days. **a**) Western blots were performed on protein extracted from control EtOH (CE), control 9*c*RA (C9) and Orai1 knockdown (O9) cells. A band at 47kDa was detected with anti-Orai1 antibody. Blots were re-probed with anti-β-actin antibody (42kDa), used as a loading control and with anti-Bcl-2 antibody (26kDa), used as a biochemical marker of differentiation. **b**) Quantitative measurements were performed on western blots by densitometry (using ImageJ software, Methods 2.6.9). Orai1 was decreased in control 9*c*RA cells and Orai1 knockdown cells compared to control EtOH cells. **c**) Quantitative measurements of Bcl-2 protein expression show that Bcl-2 expression was increased in both 9cRA treated cells and Orai1 knockdown cells compared to control EtOH cells, *n*=1.

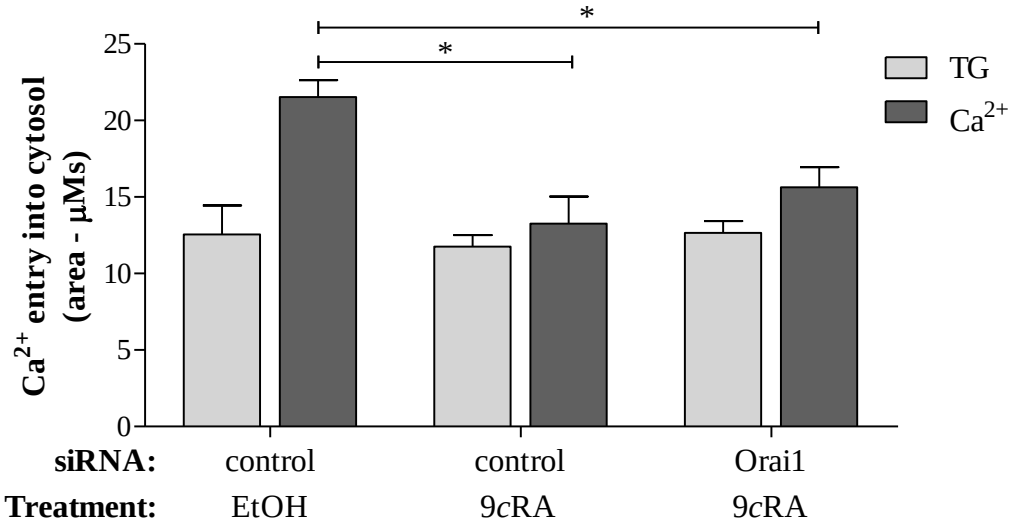

Figure 6.6 Knockdown of Orai1 in N-type cells followed by 9*c*RA treatment down-regulates SOCE

N-type cells were transfected with either control siRNA or Orai1 siRNA for 48 hours, followed by EtOH or 9*c*RA treatment for 3 days. Ca^{2+} add-back experiments were performed on cells following treatment. Store depletion in response to the addition of TG (200nM) was not significantly different between control EtOH, control 9*c*RA and Orai1 knockdown cells, P>0.05. SOCE in response to the addition of Ca^{2+} (2mM) was significantly down-regulated in control 9*c*RA cells compared to control EtOH cells ($P<0.05^{*}$). SOCE in Orai1 knockdown cells was also significantly down-regulated compared to control EtOH cells, $P<0.05^{*}$ but not to control 9*c*RA cells, P>0.05. For control EtOH cells *n*=3, control 9*c*RA cells *n*=5 and for Orai1 knockdown cells *n*=8.

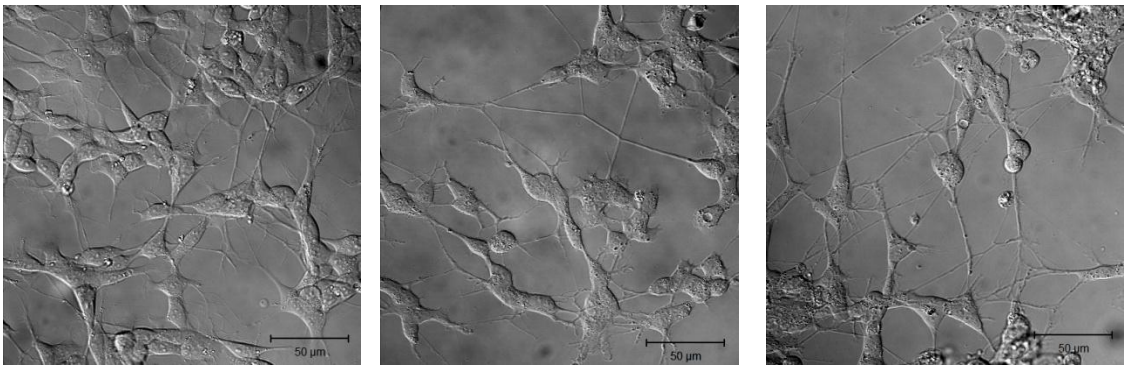

a) control siRNA EtOH **b)** control siRNA 9*c*RA **c)** Orai1 siRNA 9*c*RA

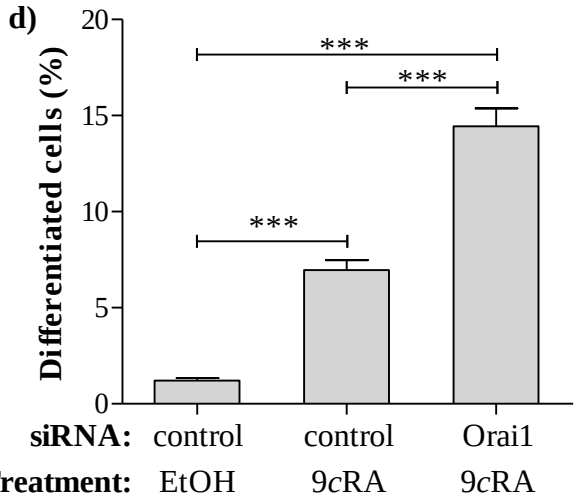

Figure 6.7 Knockdown of Orai1 in N-type cells followed by 9*c*RA treatment enhances morphological differentiation

Cells were transfected with either control siRNA or Orai1 siRNA for 48 hours and then treated with EtOH or 9*c*RA for 3 days. DIC image of N-type cells transfected with **a**) control siRNA followed by EtOH treatment, **b**) control siRNA followed by 9*c*RA treatment and **c**) Orai1 siRNA followed by 9*c*RA treatment. Scale bars represent 50µm. **d**) Quantification of DIC images; differentiated cells (neurite extensions ≥50µm) were counted and expressed as a percentage of the total cell population. For control EtOH ~1% of cells were classed as differentiated (88/7399 cells) *n*=8. For control 9*c*RA ~7% of cells were classed as differentiated (330/4674 cells) *n*=10. For Orai1 knockdown ~14% of cells were classed as differentiated (586/4152 cells) *n*=12. The extent of differentiation was significantly higher in 9*c*RA control cells and Orai1 knockdown cells compared to control EtOH cells, $P<0.001^{***}$ and was significantly higher in Orai1 knockdown cells compared to control 9*c*RA cells, $P<0.001^{***}$.

6.2.4 Overexpression of Orai1 in 9*c*RA-differentiated cells restores SOCE and decreases the extent of morphological differentiation

SOCE is down-regulated in 7 day 9*c*RA-differentiated N-type cells (Figure 4.4) as is the protein Orai1 (Figure 6.1). Furthermore, knockdown of Orai1 in untreated (i.e. proliferating) N-type cells resulted in the down-regulation of SOCE (Figure 6.3). As knockdown of Orai1 resulted in the down-regulation of SOCE the next step was to investigate whether overexpression of Orai1 in 9*c*RA-differentiated cells (i.e. cells in which Orai1 and SOCE is down-regulated) would restore SOCE to levels seen in proliferating cells.

Three sets of cells were used, one set was treated with EtOH for 7 days and the other two sets were treated with 9*c*RA for 7 days. Following this the EtOH and one of the 9*c*RA treated sets were transfected with control vector (pcDNA 3.1) for 24 hours and the other 9*c*RA treated set was transfected with GFP-Orai1 for 24 hours (Methods 2.3.2). Cells treated with EtOH for 7 days and then transfected with the control vector pcDNA 3.1 for 24 hours will henceforth be referred to as EtOH control cells. Cells treated with 9*c*RA for 7 days and then transfected with the control vector pcDNA 3.1 for 24 hours will be referred to as 9*c*RA control cells. Cells treated with 9*c*RA for 7 days and then transfected with the GFP-Orai1 will be referred to as Orai1 overexpressed cells.

Following treatment and transfection cells were harvested for protein, Ca^{2+} add-back experiments were performed and corresponding DIC images were taken.

Orai1 was present in EtOH control, 9*c*RA control and Orai1 overexpressed cells as identified by the presence of a band at 47kDa in response to anti-Orai1 antibody (Figure 6.8a). As expected, Orai1 expression was significantly decreased in 9*c*RA control cells compared to EtOH control cells, $P<0.05$. The band detected at ~65kDa indicates overexpression of Orai1 (the band is higher than the molecular weight of Orai1 due to the presence of the GFP tag). Orai1 expression was significantly increased in Orai1 overexpressed cells compared to EtOH control and 9*c*RA control cells, $P<0.001$.

The protein Bcl-2, used as a biochemical marker of differentiation, was significantly increased in 9*c*RA controls and Orai1 overexpressed cells compared to EtOH control cells, $P<0.05$ (Figure 6.8a and c).

Ca^{2+} add-back experiments revealed store depletion in response to TG (200nM) was not significantly different between EtOH control (10.16±1.12µMs), 9*c*RA control (9.79±1.54µMs) and Orai1 overexpressed (9.44±0.99µMs) cells, $P>0.05$. As expected, SOCE in response to the addition of Ca^{2+} (2mM) was significantly down-regulated in 9*c*RA control cells (14.50±1.97µMs) compared to EtOH control cells (24.60±3.48µMs), $P<0.001$. This result is consistent with previous data where 7 day 9*c*RA treatment down-regulated SOCE in N-type cells (Figure 4.4). SOCE in response to the addition of Ca^{2+} in Orai1 overexpressed cells (22.66±2.27µMs) was however significantly up-regulated compared to 9*c*RA control cells, $P<0.001$ and not significantly different to EtOH control cells, $P>0.05$. Overexpression Orai1 in 9*c*RA-differentiated cells has the ability to restore SOCE in cells which previously had down-regulated SOCE. This further supports the important role Orai1 plays in SOCE in these cells.

Corresponding DIC images revealed that, as expected, 9*c*RA control cells were significantly more differentiated compared to EtOH control cells; 36.14±3.88% compared to 2.33±0.46%, $P<0.001$ (Figure 6.10). This result is similar to previous data where 7 days 9*c*RA treatment saw a significant increase in the extent of morphological differentiation compared to EtOH treated cells (Figure 3.2). The extent of cellular differentiation in Orai1 overexpressed cells was 22.53±2.98%, although significantly higher than EtOH control cells, $P<0.05$ the extent of differentiation was significantly lower compared to 9*c*RA controls, $P<0.05$. Therefore in Orai1 overexpressed cells a greater number of cells were proliferating suggesting Orai1 expression drives cells toward a proliferating state.

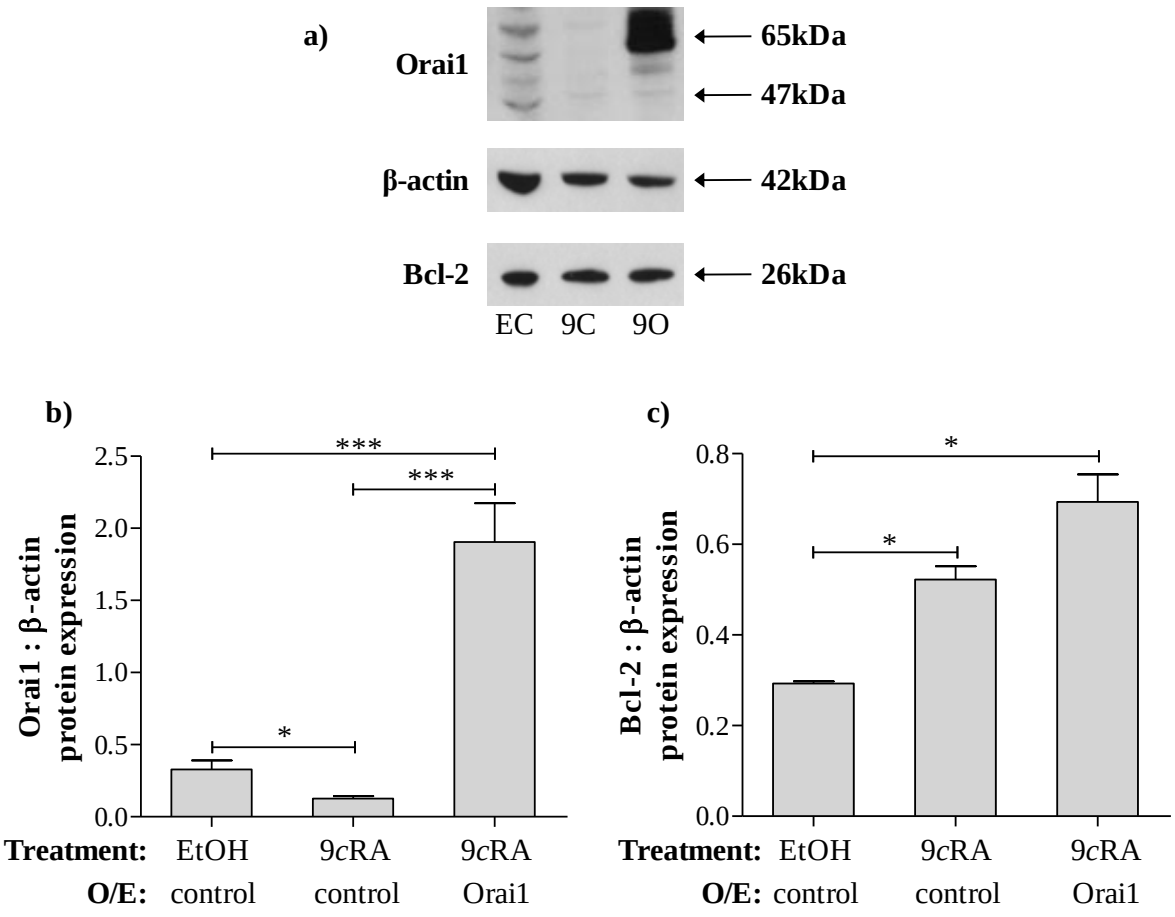

Figure 6.8 Overexpression of Orai1 in N-type cells

Cells were treated with EtOH or 9*c*RA for 7 days followed by transfection with either control vector or GFP-Orai1. O/E: Overexpression. **a**) Orai1 is expressed in EtOH control cells (EC), 9*c*RA control cells (9C) and Orai1 overexpressed cells (9O) as identified by the presence of a band at 47kDa in response to anti-Orai1 antibody and for Orai1 overexpressed cells at ~65kDa due to the presence of the GFP tag. **b**) Quantification of Orai1 protein expression was performed using densitometry (ImageJ software, Methods 2.6.9) where Orai1 was expressed as a ratio of β-actin (42kDa), used as a loading control. Orai1 protein expression was significantly decreased in 9*c*RA control cells compared to EtOH control cells, $P<0.05^{*}$ and was significantly increased in Orai1 overexpressed cells compared 9*c*RA control cells and EtOH control cells ($P<0.05^{*}$), $n=4$ **c**) Quantification of Bcl-2 protein expression reveals Bcl-2, a marker of biochemical differentiation, was significantly increased in 9*c*RA control (P=0.0108) and Orai1 overexpressed cells (P=0.0193) compared to EtOH control cells, $n=3$.

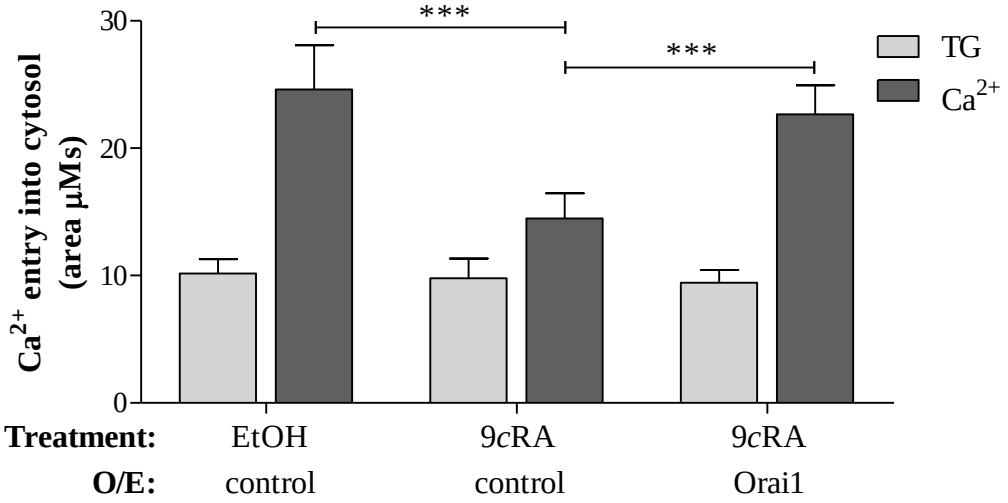

Figure 6.9 Overexpression of Orai1 in 9*c*RA-differentiated N-type cells restores SOCE

Cells were treated with EtOH or 9*c*RA for 7 days followed by transfection with either control vector or GFP-Orai1. O/E: Overexpression. Store depletion in response to the addition of TG (200nM) was not significantly different between EtOH control, 9*c*RA control and Orai1 overexpressed cells, P>0.05. SOCE in response to the addition of Ca^{2+} (2mM) was significantly down-regulated in 9*c*RA control cells compared to EtOH control cells, P<0.001***. SOCE in Orai1 overexpressed cells was significantly up-regulated compared to 9*c*RA control cells, P<0.001*** and not significantly different to EtOH control cells, P>0.05. For EtOH control cells *n*=14, for 9*c*RA control cells *n*=12, for Orai1 overexpressed cells *n*=11.

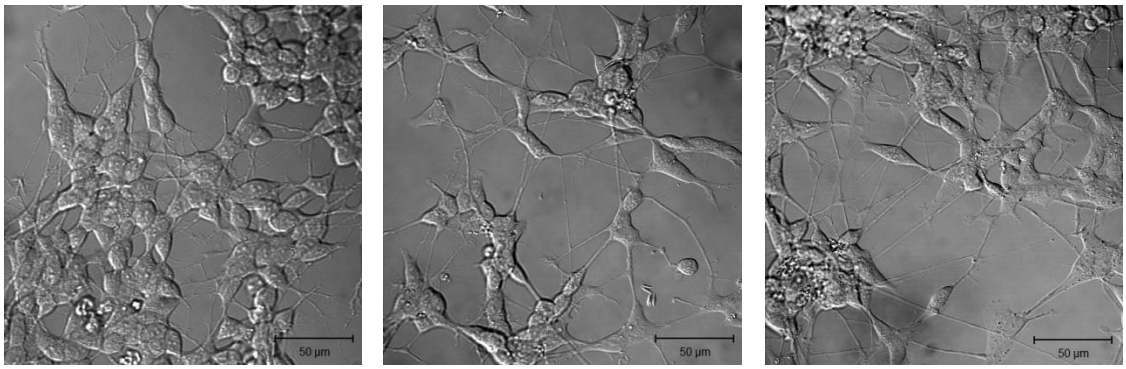

a) EtOH control O/E **b**) 9*c*RA control O/E **c)** 9*c*RA Orai1 O/E

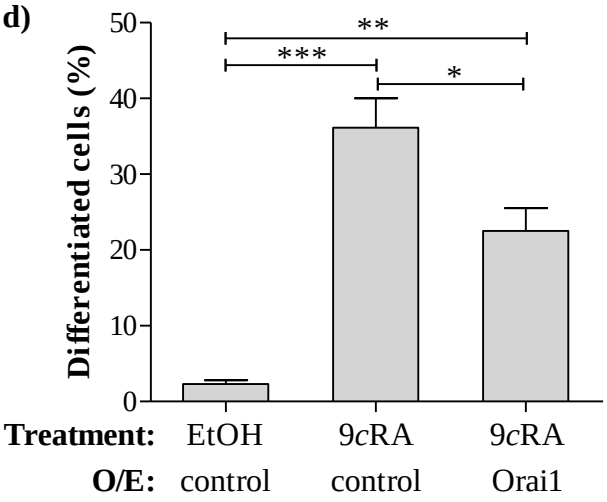

Figure 6.10 Overexpression of Orai1 in 9*c*RA-differentiated cells decreases morphological differentiation

Cells were treated with EtOH or 9*c*RA for 7 days and then transfected with either control vector or Cherry-STIM1 for 24 hours. O/E: Overexpression. DIC image of N-type cells treated with **a**) EtOH followed by transfection with control vector, **b**) 9*c*RA followed by transfection with control vector and **c**) 9*c*RA followed by transfection with GFP-Orai1. Scale bars represent 50µm. **d**) Quantification of DIC images; differentiated cells (neurite extensions ≥50µm) were expressed as a percentage of the total cell population. The percent differentiation in EtOH control cells was ~2% (51/2036 cells), *n*=6, in 9*c*RA control cells was ~36% (504/1752 cells), *n*=12 and in Orai1 overexpressed cells ~23% (141/588 cells), *n*=6. The extent of differentiation was significantly higher in 9*c*RA control cells, $P<0.001^{***}$ and Orai1 overexpressed cells, $P<0.01^{**}$ compared to EtOH control cells. However, differentiation was significantly reduced in Orai1 overexpressed cells compared to 9*c*RA control cells, $P<0.05^{*}$.

6.3 Discussion

A down-regulation in SOCE was observed in SH-SY5Y and N-type cells following 9*c*RA-induced differentiation (Chapter 4). The down-regulation in SOCE was accompanied by a down-regulation in STIM1 protein expression (Chapter 5), consistent with a role for STIM1 in SOCE. Results presented in this chapter show that Orai1 protein expression also becomes down-regulated following 9*c*RA-induced differentiation of SH-SY5Y and N-type cells (Figure 6.1), consistent with a role for Orai1 in SOCE.

To investigate the role of Orai1 in proliferating N-type cells, Orai1 was knocked down (Figure 6.2) and the effects on SOCE and differentiation were determined. Knockdown of Orai1 in proliferating N-type cells resulted in down-regulated SOCE (Figure 6.3), again consistent with a role for Orai1 in SOCE. However, whereas knockdown of STIM1 in proliferating cells did not itself induce differentiation (Chapter 5), knockdown of Orai1 in proliferating N-type cells induced a significant increase in the number of differentiated N-type cells (Figure 6.4). This result suggests that unlike STIM1, the down-regulation in Orai1 may be directly involved in the induction of differentiation that is observed following 9*c*RA treatment. One possibility is that Orai1 may be a negative regulator of differentiation.

To investigate this possibility further we examined whether the down-regulation of Orai1 plays a role in the 9*c*RA-induced switch from proliferation to differentiation. Orai1 was knocked down in proliferating N-type cells, these cells were then induced to differentiate by the addition of 9*c*RA (Figure 6.5). Knockdown of Orai1 in proliferating cells down-regulated SOCE to a similar level observed in control 9*c*RA cells (Figure 6.6). SOCE is therefore not further down-regulated by 9*c*RA treatment following Orai1 knockdown, suggesting that 9*c*RA treatment down-regulates Orai1 to a level that has already achieved by knockdown. However, whereas knockdown of STIM1 in a similar experiment had no effect on the extent 9*c*RA-induced differentiation (Chapter 5), N-type cells with Orai1 knockdown were significantly more differentiated that control 9*c*RA cells (Figure 6.7). Thus, not only does down-regulation of Orai1 expression itself induce differentiation, down-regulation also enhances the extent of differentiation

induced by 9*c*RA treatment. This result is also consistent with the notion that Orai1 may be a negative regulator of differentiation.

To further investigate whether Orai1 may be a negative regulator of differentiation we examined whether overexpression of Orai1 in 9*c*RA-differentiated cells could restore SOCE and drive cells towards proliferation. Orai1 was overexpressed in 9*c*RA-differentiated N-type cells (Figure 6.8). Overexpression of Orai1 restored SOCE to levels comparable to that of proliferating cells (Figure 6.9). This result is again consistent with a role for Orai1 in SOCE. Overexpression of Orai1 in 9*c*RA-differentiated N-type cells reduced the number of differentiated cells compared to 9*c*RA controls, as determined morphologically (Figure 6.10). This result shows that an increased expression of Orai1 drives N-type cells toward proliferation, further supporting the notion that Orai1 is a negative regulator of differentiation in these cells.

Knockdown of Orai1 has been shown to down-regulate SOCE in many cell types (Introduction 1.6.2). The role of Orai1 in SOCE was first identified in patients with SCID with impaired I_{CRAC} which was traced to a single point mutation in Orai1. Interestingly, both T and B cells from SCID patients displayed dysfunctional proliferation (Feske *et al*., 2006), thus also highlighting a potential role for Orai1 in proliferation. Subsequent studies have confirmed this role as knockdown of Orai1 has been reported to inhibit proliferation in endothelial cells (Abdullaev *et al*., 2008), vascular smooth muscle cells (Portier *et al*., 2009), arterial smooth muscle cells (Baryshnikov *et al*., 2009) and HEK293 cells (El Boustany *et al.*, 2010). Furthermore, an increase in Orai1 has been observed following vascular smooth muscle cell injury associated with an increased requirement for cellular proliferation (Zhang *et al*., 2011) and also during proliferation of airways smooth muscle cells (Zou *et al*., 2011).

These data suggest that SOCE channels with Orai1 at their core are required for proliferation and that silencing of the protein results in a decrease in proliferation rate. In N-type cells, knockdown of Orai1 is required to drive the cells down a differentiation pathway. The mechanisms by which Orai1 is able to influence the balance between proliferation and differentiation are unknown. An interaction between a cell cycle component and a Ca^{2+} channel protein has been described previously: the complex

cdc2/cyclin B1 regulates IP_3R activity (Malathi *et al.,* 2005). Orai1 may interfere with a cell cycle component to induce N-type SH-SY5Y cell proliferation.

It is noteworthy that Orai1 protein expression was unaltered (i.e. not down-regulated) following 9*c*RA-induced differentiation of S-type cells. STIM1 expression was also unaltered upon 9*c*RA-treatment of S-type cells (Chapter 5). These findings would explain the observation that SOCE was not down-regulated in 9*c*RA-differentiated S-type cells (Chapter 4). Interestingly, the level of expression of Orai1 in S-type cells (Figure 6.1) was considerably lower than the level of expression STIM1 (Figure 5.1). This raises the possibility that Orai1 may not be the only putative SOCE channel protein in S-type cells.

In summary, Orai1 forms an element of SOCE in proliferating N-type cells, along with STIM1 (Chapter 5). In addition, evidence suggests that the decrease in Orai1 expression observed following 9*c*RA differentiation is a key enabling step in the differentiation process. Orai1 therefore plays a direct role in the switch from proliferation to differentiation. This is in contrast to STIM1, which has no direct role in the switch from proliferation to differentiation but which may play a role in maintaining the differentiated state. Prostate cancer cells with down-regulated Orai1 were more resistant to apoptosis (Flourakis *et al*., 2010). The current standard treatment protocol for high-risk neuroblastoma in the UK includes the use of retinoic acid, after chemotherapy and bone-marrow transplantation (Matthay *et al.,* 1999). However RA-differentiated neuroblastoma cells are more resistant to the apoptosis-inducing effects of chemotherapeutic drugs (Lasorella *et al.,* 1995), this is a limitation in the use of conventional retinoids for neuroblastoma therapy. Whether this resistance could be due down-regulation of Orai1 needs to be determined.

Chapter 7
Results V - TRPC1

7.1 Introduction

The proteins STIM1, Orai1 and TRPC1 have been demonstrated to be involved in SOCE (Introduction, 1.6). This chapter focuses on the involvement of TRPC1 in SOCE and also in differentiation of N-type cells. 9*c*RA-induced differentiation of N-type cells down-regulated SOCE (Chapter 4) and the levels of STIM1 (Chapter 5) and Orai1 (Chapter 6) expression. In S-type cells SOCE and the level of STIM1 and Orai1 expression remained unaffected (Chapters 4, 5 and 6 respectively).

As TRPC1 has been implicated in SOCE, possibly as a SOC itself or as part of a complex with STIM1 and Orai1, the relationship between TRPC1 expression, SOCE and also differentiation was investigated in N-type cells. In order to do this TRPC1 protein expression was knocked down (using siRNA transfection) in N-type cells (Methods 2.3.1). The effects on SOCE were measured using Ca^{2+} imaging experiments (Methods 2.7) and the effects on differentiation were determined morphologically by analysis of DIC images (Methods 2.4).

7.2 Results

7.2.1 TRPC1 in SH-SY5Y, N- and S-type cells before and after 9*c*RA-induced differentiation

SOCE is down-regulated in SH-SY5Y and N-type cells following 9*c*RA-induced differentiation, however it remains unchanged in S-type cells (Chapter 4). In order to determine any changes in TRPC1 protein expression associated with the observed changes in SOCE, western blots were performed on protein extracted from SH-SY5Y, N-type and S-type cells before and after 9*c*RA-induced differentiation (Methods 2.6).

TRPC1 is expressed in proliferating (7 day EtOH treated) and differentiated (7 day 9*c*RA treated) SH-SY5Y and N-type cells, as determined by a band detected at 90kDa by an anti-TRPC1 antibody (Figure 7.1a). Blots were re-probed with β-actin, used as a loading control; TRPC1 was then expressed as a ratio of β-actin in order to quantify changes in band intensity (Figure 7.1b). TRPC1 protein expression increased in SH-SY5Y cells by ~48% and in N-type cells by ~53% following 9*c*RA-induced differentiation. SOCE in SH-SY5Y and N-type cells was down-regulated following 9*c*RA induced differentiation (Chapter 4). This would suggest that TRPC1 is not a SOC in SH-SY5Y or N-type cells. TRPC1 was not detected in S-type cells suggesting that TRPC1 does not play a role in Ca^{2+} signalling in these cells. Unfortunately due to problems with the TRPC1 antibody used this experiment was only performed once. TRPC1 protein expression has however previously been shown in our laboratory to increase in SH-SY5Y cells following 9*c*RA-induced differentiation (Figure 7.2).

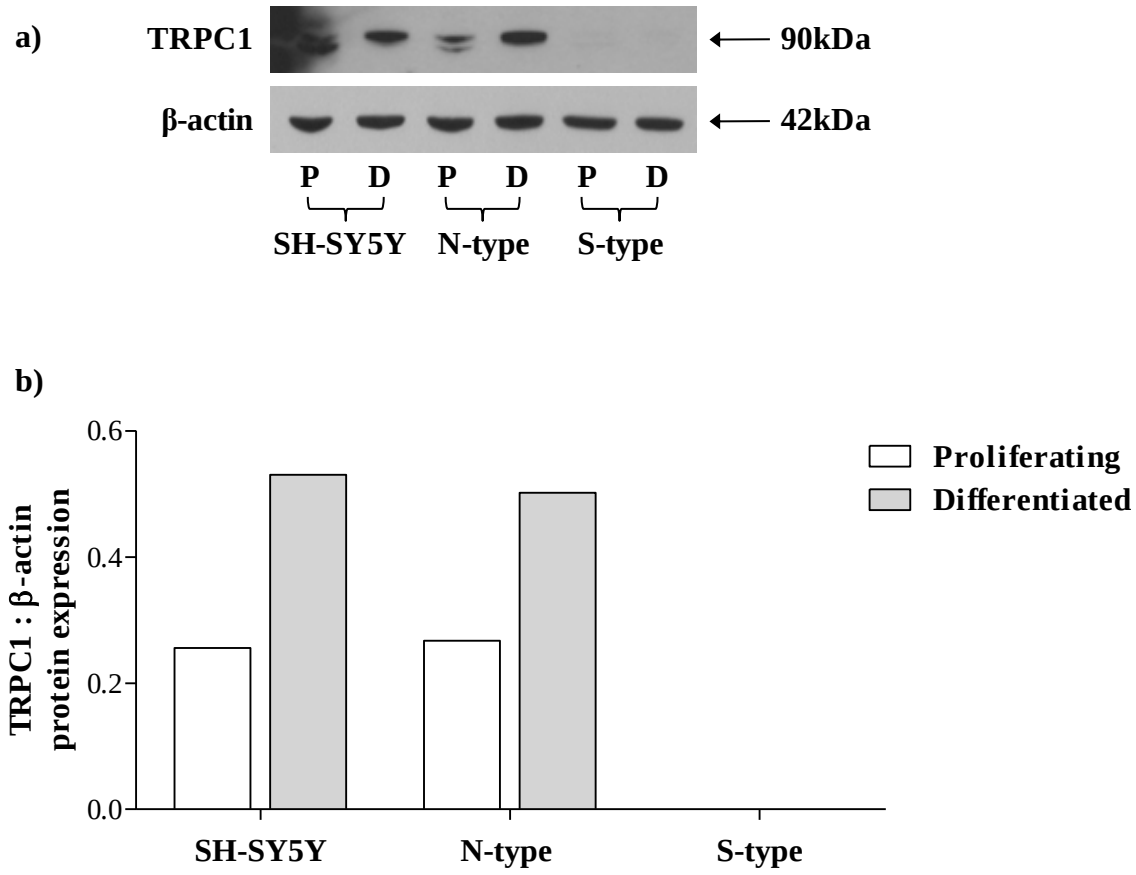

Figure 7.1 TRPC1 expression increases in SH-SY5Y and N-type cells following 9*c*RA-induced differentiation

Cells were treated with EtOH (proliferating - **P**) or 9*c*RA (differentiated - **D**) for 7 days. Following treatment cells were harvested for protein. **a)** Western blots were performed on protein extracts from SH-SY5Y, N-type and S-type cell populations. Blots were probed with anti-TRPC1 antibody which detected a band at 90kDa. Blots were re-probed with anti-β-actin antibody which detected a band at 42kDa. The band detected by the β-actin antibody was used as a loading control. **b)** Quantitative analysis of TRPC1 expression as determined by densitometry using ImageJ software (Methods 2.6.9); TRPC1 was expressed as a ratio of β-actin expression. TRPC1 protein expression appears to up-regulated in 9*c*RA-differentiated SH-SY5Y and N-type cells compared to proliferating controls. TRPC1 is not expressed in S-type cells. *n*=1.

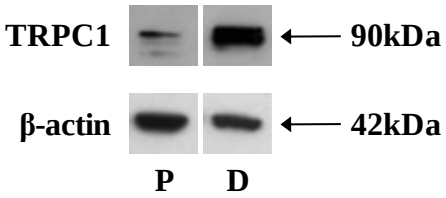

Figure 7.2 TRPC1 expression increases in SH-SY5Y following 9*c*RA-induced differentiation

SH-SY5Y cells were treated with EtOH (proliferating - **P**) or 9*c*RA (differentiated - **D**) for 7 days. Following treatment cells were harvested for protein and western blots were performed on protein extracts. Blots were probed with anti-TRPC1 antibody which detected a band at 90kDa. Blots were re-probed with anti-β-actin antibody used as a loading control (42kDa). TRPC1 expression was up-regulated in 9*c*RA-differentiated SH-SY5Y cells.

The blot presented in this figure (7.2) was performed by Dr Victoria Hann.

7.2.2 Knockdown of TRPC1 in proliferating N-type cells does not affect SOCE or induce differentiation

9*c*RA-induced differentiation of both SH-SY5Y and N-type cells results in the down-regulation of SOCE (Figures 4.2 and 4.4) and the up-regulation of TRPC1 protein expression (Figure 7.1). TRPC1 expression was not detected in S-type cells (Figure 7.1) and therefore these cells were not studied further. SH-SY5Y cells and N-type cells so far have shown the same results as one another. As in Chapters 5 and 6, N-type cells were used for the remainder of studies in this chapter.

Following transfection of cells and the subsequent knockdown of TRPC1 protein, Ca^{2+} add-back experiments were performed to measure SOCE. DIC images were taken to determine the extent of morphological differentiation.

Ca^{2+} add-back experiments revealed that store depletion (TG response) was not significantly different between control siRNA (12.53±1.22 µMs) and TRPC1 siRNA (13.58±1.23µMs) transfected cells, P=0.5767 (Figure 7.3). SOCE (Ca^{2+} response) following store depletion was also not significantly different between control siRNA (20.94±1.61µMs) and TRPC1 siRNA (21.45±2.34µMs) transfected cells, P=0.8536. That knockdown of TRPC1 protein did not affect SOCE suggests that TRPC1 is not involved in the SOCE pathway in proliferating N-type cells.

DIC images of the cells were taken to correspond with the Ca^{2+} add-back experiments to see whether there was any affect on differentiation as determined by neurite length (≥50µm) (Figure 7.4). DIC images of control siRNA cells revealed morphological differentiation to be 3.21±0.35% compared to TRPC1 siRNA cells which were 3.42±0.38%, P=0.7013. Knockdown of TRPC1 for 48 hours in N-type cells does not significantly affect the extent of morphological differentiation. Knockdown of TRPC1 had no effect on proliferation as determined by the mean number of cells counted from each coverslip; control siRNA; 527.25±45.95, *n*=4 vs. TRPC1 siRNA; 491.75±31.74, *n*=4, P=0.5485.

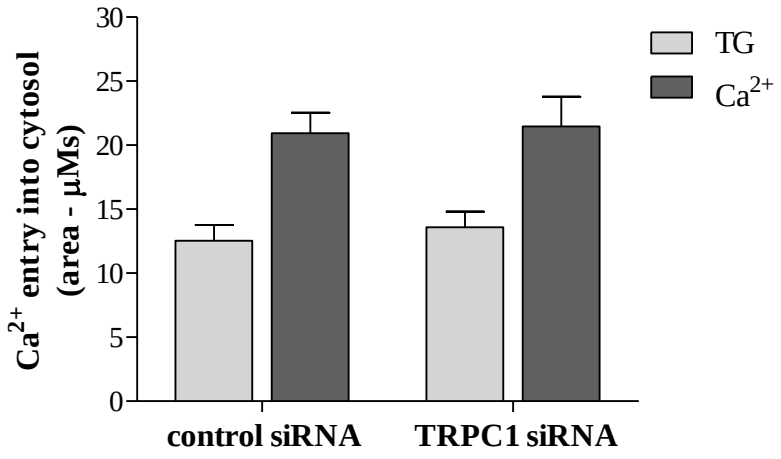

Figure 7.3 Knockdown of TRPC1 in N-type cells does not affect SOCE

N-type cells were transfected with either control siRNA or TRPC1 siRNA for 48 hours. Ca^{2+} add-back experiments were performed on cells following transfection. Store depletion in response to the addition of TG (200nM) was not significantly different between control siRNA and TRPC1 siRNA transfected cells (P=0.5767). SOCE in response to the addition of Ca^{2+} (2mM) was also not significantly different between control siRNA and TRPC1 siRNA transfected cells (P=0.8536). For control siRNA transfected cells *n*=15 and for TRPC1 siRNA transfected cells *n*=9.

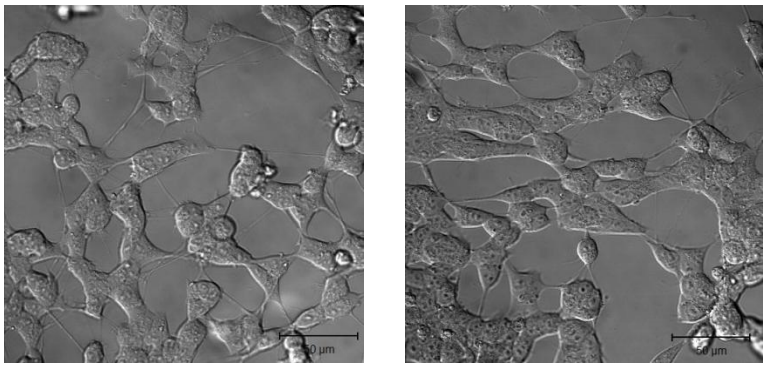

a) control siRNA **b) TRPC1 siRNA**

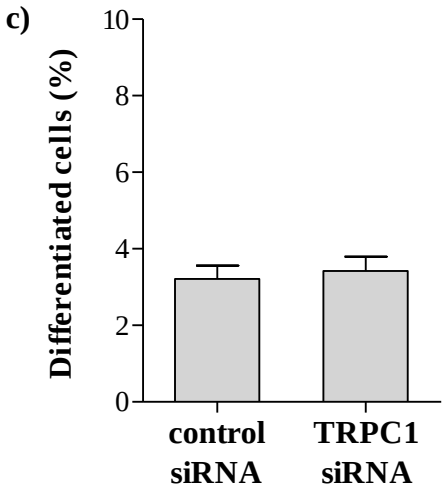

Figure 7.4 Knockdown of TRPC1 in N-type cells does not induce morphological differentiation

Cells were transfected with either control siRNA or TRPC1 siRNA for 48 hours. DIC image of N-type cells transfected with **a**) control siRNA and **b**) TRPC1 siRNA. Scale bars equal 50µm. **c**) Quantification of DIC images; differentiated cells (neurite extensions ≥50µm) were counted and expressed as a percentage of the total cell population. For control siRNA ~3% of cells were classed as differentiated (66/2190 cells), *n*=4. For TRPC1 siRNA almost ~3% of cells were classed as differentiated (66/1967 cells), *n*=4. There was no significant difference in the extent of morphological differentiation between control siRNA and TRPC1 siRNA transfected cells, P=0.7013.

7.2.3 Knockdown of TRPC1 prevents SOCE down-regulation and reduces the extent of morphological differentiation induced by 9*c*RA treatment

Knockdown of TRPC1 did not inhibit SOCE in proliferating cells (Figure 7.3) or induce differentiation (Figure 7.4). In the next series of experiments it was investigated as to whether knockdown of TRPC1 affected the ability of 9*c*RA to down-regulate SOCE or induce differentiation of N-type cells.

TRPC1 was knocked down in N-type cells by transfection with TRPC1 siRNA for 48 hours (Methods 2.3.1). Following knockdown cells were then treated with either EtOH or 9*c*RA for a further 3 days. In total this amounts to 5 days treatment; 48 hours of transfection followed by 3 days of EtOH or 9*c*RA treatment. Data from our laboratory have shown that effects of 9*c*RA on SOCE (i.e. down-regulation) are apparent following 3 days of treatment; 3 days treatment is therefore a suitable time scale to determine whether knockdown of TRPC1 has any affect on differentiation of 9*c*RA treated cells.

Three sets of cells were used; two sets were transfected with control siRNA for 48 hours, one was then treated with EtOH and the other with 9*c*RA for 3 days. The final set was transfected with TRPC1 siRNA for 48 hours followed by 9*c*RA treatment for 3 days. Henceforth cells transfected with control siRNA followed by EtOH treatment will be referred to as control EtOH cells, those transfected with control siRNA followed by 9*c*RA treatment will be referred to as control 9*c*RA cells and those transfected with TRPC1 siRNA followed by 9*c*RA treatment will be referred to as TRPC1 knockdown cells.

Following transfection of cells and the subsequent knockdown of TRPC1 protein, Ca^{2+} add-back experiments were performed to measure SOCE and DIC images were taken to determine the extent of morphological differentiation.

Ca^{2+} add-back experiments performed on the cells revealed that there was no significant difference in store depletion between control EtOH (12.56±1.89µMs), control 9*c*RA (11.75±0.76µMs) and TRPC1 knockdown (12.87±0.94µMs) cells, $P>0.05$. SOCE was down-regulated in control 9*c*RA cells (13.25±1.77µMs) compared to control EtOH cells

(21.52±1.11µMs), P<0.05 (Figure 7.5). This result shows a similar relationship to 7 day EtOH and 9*c*RA treated cells N-type cells (Figure 4.4), confirming that following 3 days 9*c*RA treatment SOCE becomes significantly down-regulated. However, SOCE measured in TRPC1 knockdown cells (19.39±2.35µMs) was not significantly different compared to control EtOH cells (P>0.05). Knockdown of TRPC1 prevented 9*c*RA-induced SOCE down-regulation which suggests that TRPC1 does have a role in SOCE.

DIC images of the cells were taken to correspond with the Ca^{2+} add-back experiments performed in order to determine any effects on morphological differentiation (Figure 7.6). Images of control EtOH cells revealed cellular differentiation to be 1.21±0.12% compared to control 9*c*RA cells which were classed as 6.95±0.52% differentiated; P<0.001. This confirmed that the transfection procedure did not affect the ability of the cells to differentiate as the extent of differentiation was comparable to 3 day 9*c*RA treated cells (Figure 3.2). TRPC1 knockdown cells were determined to be 5.35±0.53% differentiated, significantly higher than control EtOH cells, P<0.001. Notably however, the extent of differentiation in TRPC1 knockdown cells was also significantly lower than control 9*c*RA cells (P<0.05). This suggests that knockdown of TRPC1 in N-type cells affects the ability of the cells to differentiate in response to 9*c*RA and that TRPC1 may play a role in the switch from proliferation to differentiation.

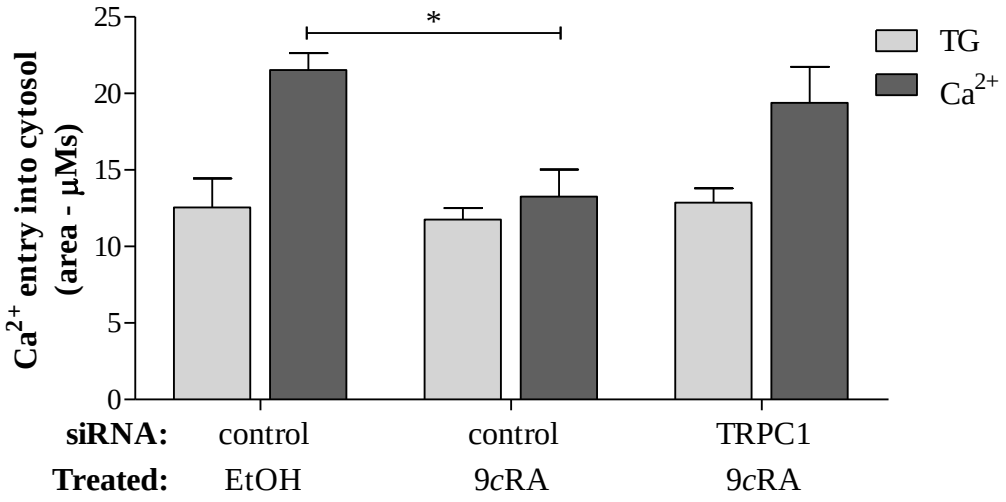

Figure 7.5 Knockdown of TRPC1 in N-type cells prevents SOCE down-regulation induced by 9*c*RA treatment

N-type cells were transfected with either control siRNA or TRPC1 siRNA for 48 hours, followed by EtOH or 9*c*RA treatment for 3 days. Ca^{2+} add-back experiments were performed on cells following treatment. Store depletion in response to the addition of TG was not significantly different between control EtOH, control 9*c*RA and TRPC1 knockdown cells, P>0.05. SOCE in response to the addition of Ca^{2+} was significantly down-regulated in control 9*c*RA cells compared to control EtOH cells ($P<0.05^{*}$). SOCE in TRPC1 knockdown cells was not significantly different compared to control EtOH cells (P>0.05). For control EtOH cells *n*=3, control 9*c*RA cells *n*=5 and for TRPC1 knockdown cells *n*=9.

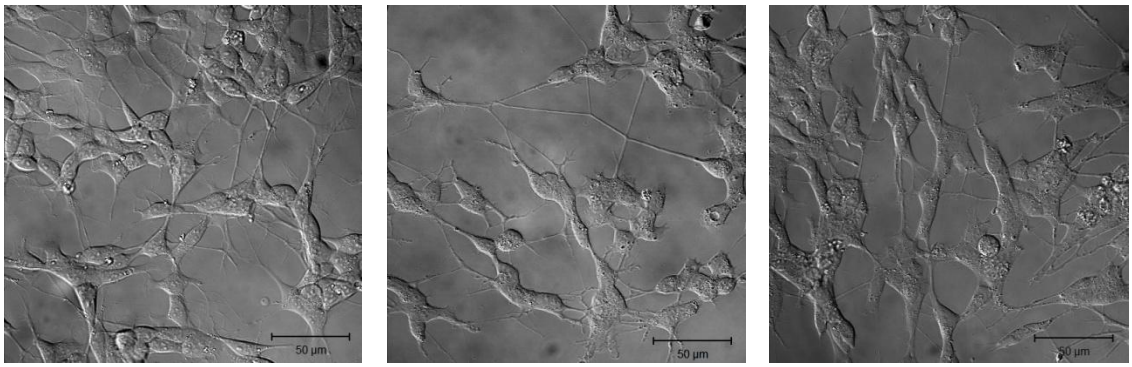

a) control siRNA EtOH **b)** control siRNA 9*c*RA **c)** TRPC1 siRNA 9*c*RA

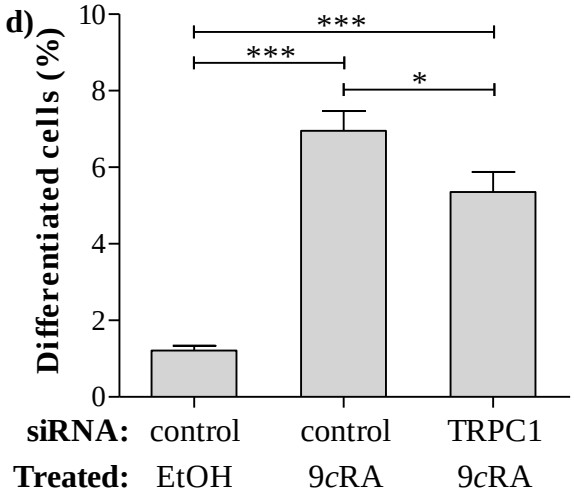

Figure 7.6 Knockdown of TRPC1 in N-type cells followed by 9*c*RA treatment affects morphological differentiation

Cells were transfected with either control siRNA or TRPC1 siRNA for 48 hours and then treated with EtOH or 9*c*RA for 3 days. DIC image of N-type cells transfected with **a**) control siRNA followed by EtOH treatment, **b**) control siRNA followed 9*c*RA treatment and **c**) TRPC1 siRNA followed by 9*c*RA treatment. Scale bars represent 50µm. **d**) Quantification of DIC images; differentiated cells (neurite extensions ≥50µm) were counted and expressed as a percentage of the total cell population. The percent differentiation in control EtOH cells was ~1% (88/7399 cells), *n*=8, in control 9*c*RA cells ~7% (330/4674 cells), *n*=10 and in TRPC1 knockdown ~5% (174/3514 cells), *n*=9. Morphological differentiation was significantly higher in control 9*c*RA and TRPC1 knockdown cells compared to control EtOH cells $P<0.001^{***}$. However, morphological differentiation was significantly lower in TRPC1 knockdown cells compared to control 9*c*RA cells, $P<0.05^{*}$.

7.3 Discussion

A down-regulation in SOCE was observed in 9*c*RA-differentiated SH-SY5Y and N-type cells (Chapter 4). SOCE down-regulation in these cell types was accompanied by a down-regulation in the levels of STIM1 (Chapter 5) and of Orai1 (Chapter 6), consistent with the involvement of these proteins in the SOCE pathway. A key finding in the present chapter is that, unlike STIM1 and Orai1 which have decreased expression, the level of TRPC1 protein expression increases in 9*c*RA-differentiated SH-SY5Y and N-type cells (Figures 7.1 and 7.2). This suggests that TRPC1 does not form a SOC in 9*c*RA-differentiated SH-SY5Y or N-type cells and instead points to a potential role in proliferating cells and/or in the 9*c*RA-induced switch between proliferation and differentiation. TRPC1 was not detected in S-type cells (Figure 7.1) and therefore does not form a SOC in S-type cells.

To investigate a potential role for TRPC1 in proliferating N-type cells, TRPC1 was knocked down. Knockdown of TRPC1 in proliferating cells did not affect SOCE (Figure 7.3) or itself induce morphological differentiation (Figure 7.4), suggesting that resting levels of TRPC1 do not form a SOC in proliferating N-type cells or themselves influence differentiation.

To investigate whether the increase in TRPC1 levels seen in response to 9*c*RA-treatment plays a key role in the 9*c*RA-induced switch from proliferation to differentiation, TRPC1 was knocked down in proliferating cells. These cells were then induced to differentiate by addition of 9*c*RA. Knockdown of TRPC1 in proliferating N-type cells prevented the level of down-regulation in SOCE normally seen following 9*c*RA treatment: SOCE in TRPC1 knockdown cells was comparable to that of control EtOH cells (Figure 7.5). In addition, knockdown of TRPC1 affected 9*c*RA-induced morphological differentiation: the extent of differentiation was significantly lower in TRPC1 knockdown cells compared to control 9*c*RA cells (Figure 7.6). All these data suggest that, although not a SOC in these cells, the increase in TRPC1 expression observed following 9*c*RA differentiation is necessary for cells to display a fully differentiated phenotype. TRPC1 seems likely therefore to play a role in the switch from proliferation to differentiation.

The reasons as to why increased expression of TRPC1 favours differentiation in N-type SH-SY5Y cells are unclear. In hippocampal neurons a dramatic increase in TRPC1 protein expression was observed following differentiation, though this was also associated with an increase in SOCE (Wu *et al*., 2004). Results from TRPC1 knockdown studies indicate that the role of TRPC1 in SOCE is variable between cell types. For example, in ECs (Abdullaev *et al*., 2008) and VSMCs (Potier *et al*., 2009) no effect on SOCE was observed following knockdown of TRPC1, however a decrease in SOCE was observed in myoblasts (C2C12), (Louis *et al*., 2008). The up-regulation of TRPC1 in differentiated N-type and SH-SY5Y cells could be due to an increase in the expression of the protein to act as a ROC in order to compensate for the loss of the down-regulated SOCE pathway. The function of TRPC1 as a SOC has been found to be regulated in a STIM1 dependent manner where STIM1 heteromultimerizes TRPC1 channels to determine their function as SOCs (Yuan *et al*., 2007). Furthermore STIM1 has been found to covert TRPC1 from a ROC to a SOC by inserting TRPC1 into LRDs where TRPC1 functions as a SOC only when inserted into LRDs (Alicia *et al*., 2008).

The relationship between 9*c*RA-induced TRPC1 up-regulation and 9*c*RA-induced STIM1 (Chapter 5) and/or Orai1 (Chapter 6) down-regulation is unknown. Overexpression of TRPC1 in myoblast (C2C12) cells has been shown to suppress STIM1 expression (Louis *et al*., 2008), providing a potential molecular mechanism by which TRPC1 could indirectly influence the level of SOCE. Certainly TRPC1 has been shown to interact with STIM1 and Orai1 (Introduction 1.6.3). These studies determined regions of interaction that would indicate the involvement of TRPC1 in SOCE through ternary complexes with STIM1 and Orai1, these sites of interaction may also be how TRPC1 could mediate inhibitory affects (Ong *et al*., 2007; Ambudkar *et al*., 2007b; Liao *et al*., 2007, 2008, 2009).

Perhaps STIM1 is down-regulated prior to TRPC1 and the removal of STIM1 inhibition allows TRPC1 expression to increase. TRPC1 has been shown to only act as a SOC when in the complex and with both STIM1 and Orai1and otherwise is not involved in SOCE (Jardin *et al*., 2008a).

Clearly, whether the increase in TRPC1 expression observed in 9*c*RA-differentiated cells occurs before or after the down-regulation in STIM1 and/or Orai1 expression

needs to be investigated. TRPC1 overexpression studies may also be informative. Overexpression of TRPC1 in proliferating cells may promote a switch towards differentiation which would further support a key role for TRPC1 in controlling differentiation in these cells. Lack of availability of a reliable TRPC1 antibody and lack of time prevented completion of these experiments.

In summary, TRPC1 does not appear to form a SOC in either proliferating or differentiated N-type cells. The increase in TRPC1 expression observed following 9*c*RA differentiation appears may be important in allowing cells to obtain a fully differentiated phenotype. Decreased expression of TRPC1 seems to favour SOCE and proliferation whereas increased expression seems to favour down-regulated SOCE and differentiation.

Chapter 8
Final Discussion

8.1 Summary of Findings

The aim of this study was to investigate the role of Ca^{2+} signalling in differentiation of neuroblastoma cells. N- and S-type cell populations enriched from the SH-SY5Y cell line were characterised both morphologically and biochemically.

Morphologically N-type cells are small cells with many short neurite-like processes emanating from their cell bodies, whereas S-type cells are slightly larger and flatter and do not exhibit neurite extensions (Figure 3.4). Following 9*c*RA-induced differentiation both N- and S-type cells change morphology, with N-type cells becoming more neuronal-like, with neurite-like extensions of ≥50μm in length and S-type cells becoming more epithelial-like with increased cytoplasmic content and transparency (Figure 3.6).

β-Tubulin III was detected in both proliferating and differentiated N- and S-type cells (Table 8.1). The expression of β-Tubulin III remained unchanged following 9*c*RA-induced differentiation of N-type cells. β-Tubulin III does not distinguish between immature and mature neuronal cells and therefore appears to be a indicator solely of neuronal cell type, in N-type cells at least. Surprisingly β-Tubulin III was present in S-type cells, as a neuronal protein this was not expected. However both N- and S-type cells are immature cells derived from the neural crest, precursors of multipotent lineages that are still able to transdifferentiate into one another. It is therefore possible that the S-type cells have not fully moved toward a non-neuronal cell type. Consistent with this notion is that following 9*c*RA-induced differentiation, as the cells become more epithelial-like, β-Tubulin III decreases. Due to variable expression of β-Tubulin III between N- and S-type cells it was still deemed a suitable marker to distinguish between the two cell phenotypes. Vimentin was not detected in N-type cells by western blot, which was expected as the protein is specific to non-neuronal cell types. Though immunofluorescence studies revealed that vimentin was occasionally detected in developing neurites of N-type cells (Figure 3.9), however a temporary role for vimentin has been identified in neuritogenesis. Vimentin was expressed in both proliferating and differentiated S-type cells (Table 8.1). Vimentin was deemed a suitable marker to distinguish between N- and S-type cells. Bcl-2 was expressed in proliferating and differentiated N-type cells, but was barely detectable in S-type cells (Table 8.1). Bcl-2

expression increases following RA-induced differentiation of N-type cells, as previously observed in SH-SY5Y cells (Hanada *et al*., 1993; Lasorella *et al*., 1995; Riddoch *et al*., 2007), Bcl-2 was therefore used as a biochemical marker of differentiation in SH-SY5Y and N-type cells.

SOCE was characterised in N- and S-type cells by measuring changes in $[Ca^{2+}]_i$ in fura-2 loaded cells (Chapter 4). Differentiation of N-type cells toward a more neuronal-like cell type following 9*c*RA treatment was associated with a down-regulation in SOCE. Excitable cells have other means of Ca^{2+} signal generation, such as through VOCs, it has been proposed that as cells become more neuronal-like they rely less on SOCE as a means of generating Ca^{2+} signals and to replenish depleted stores (Berridge, 1998). In SH-SY5Y cells 9*c*RA-induced differentiation resulted in an increase in voltage-dependent Ca^{2+} entry (Brown *et al.*, 2005). S-type cells however showed no change in SOCE, though they adapted a more epithelial-like appearance following 9*c*RA-induced differentiation. As non-excitable cells, S-type cells likely rely on SOCE as a major pathway to generate Ca^{2+} signals and replenish depleted ER Ca^{2+} stores. It had previously been observed in this laboratory that 9*c*RA-induced differentiation of SH-SY5Y cells resulted in down-regulated SOCE (Brown *et al*., 2005). This response can now be attributed to N-type cells and not S-type cells.

The level of expression of the three key Ca^{2+} signalling proteins, STIM1, Orai1 and TRPC1, was measured in the 9*c*RA-induced switch from proliferation to differentiation by western blot in N- and S-type cells (Table 8.1), to determine the relationship between expression and SOCE as these proteins have been implicated in SOCE in numerous studies. In N-type cells STIM1 and Orai1 were associated with down-regulated SOCE as both STIM1 and Orai1 became down-regulated following 9*c*RA-induced differentiation (Figures 5.1 and 6.1). However, TRPC1 became up-regulated (Figures 7.1 and 7.2), suggesting that TRPC1 does not form SOCs in N-type cells. 9*c*RA-induced differentiation of SH-SY5Y cells up-regulates a non-SOCE pathway (Brown *et al*., 2005). Whether TRPC1 represents the non-SOCE channel protein in differentiated cells needs to be elucidated. In S-type cells the expression of STIM1 and Orai1 following 9*c*RA-induced differentiation remained unaltered, consistent with no change in SOCE. TRPC1 was not detected in S-type cells and therefore S-type cells do not mediate SOCE through TRPC1 channels.

	N-type cells		S-type cells	
	Proliferating	**Differentiated**	**Proliferating**	**Differentiated**
β-Tubulin III	↑↑	↑↑	↑	↓
Vimentin	×*	×*	↑	↑
Bcl-2	↑	↑↑	×	×
STIM1	↑	↓	↑	↑
Orai1	↑	↓	↓	↓
TRPC1	↓	↑	×	×

Table 8.1 Summary of proteins expressed in N- and S-type cells

Protein expression measured in proliferating and 9*c*RA-differentiated N- and S-type cells. ↑; protein was detected, ↑↑; protein was detected at an increased level than previously observed, ↓; protein was detected but the level of expression was low ×; protein was not/barely detectable. * Vimentin was not detected in proliferating or differentiated N-type cells by western blot (Figure 3.12) but was detected in some neurite extensions in immunofluorescence experiments (Figure 3.9).

The absolute level of STIM1 and Orai1 expression was variable between N- and S-type cells. S-type cells had similar levels of STIM1 compared to proliferating N-type cells, yet Orai1 protein expression was reduced compared to proliferating N-type cells. Although expression of Orai1 in S-type cells is low, a role for Orai1 as a SOC remains, though perhaps there is another SOC functioning in these cell types. S-type cells showed no changes in SOCE or Ca^{2+} signalling protein expression following 9*c*RA-induced differentiation and therefore S-type cells were not studied further. The expression of STIM1, Orai1 and TRPC1 was however manipulated in N-type cells to determine a role for these proteins in SOCE and differentiation. Data obtained throughout this thesis was consistent with a role for STIM1 and Orai1 in SOCE and a role for STIM1, Orai1 and TRPC1 in differentiation.

Knockdown of STIM1 and Orai1 in proliferating N-type cells resulted in down-regulated SOCE (Table 8.2). Inhibition of SOCE by knockdown of STIM1 has previously been observed in SH-SY5Y cells (Roos *et al*., 2005), though down-regulation of SOCE following Orai1 knockdown has not previously been reported in SH-SY5Y cells. Clearly STIM1 and Orai1 are involved in SOCE in N-type cells and appear to have similar role in SOCE down-regulation. However, Orai1 appears to have an additional role in the differentiation response of N-type cells. This conclusion was based on the observation that knockdown of Orai1 alone induced differentiation of N-type cells and that knockdown of Orai1 followed by 9*c*RA treatment enhanced differentiation compared to 9*c*RA treatment alone (Table 8.2). In N-type neuroblastoma cells Orai1 therefore appears to be a negative regulator of differentiation. Consistent with this role is that overexpression of Orai1 in 9*c*RA-differentiated cells reduced the level of differentiation compared to 9*c*RA control cells. In contrast, knockdown of STIM1 alone did not induce differentiation or enhance differentiation induced by 9*c*RA, arguing against an addition role for STIM1 in regulating differentiation. However, overexpression of STIM1 in 9*c*RA-differentiated cells reduced the extent of differentiation (in addition to restoring SOCE) (Table 8.2). This raises the possibility that down-regulation of STIM1 in 9*c*RA-differentiated cells is required to maintain the differentiated state. Knockdown of TRPC1 in proliferating N-type cells had no effect on SOCE or on differentiation but reduced the extent of SOCE down-regulation and differentiation induced by 9*c*RA. TRPC1 expression may therefore be required for a fully functional differentiated phenotype.

Protein	Expression		Knockdown (in proliferating cells)			Overexpression (in 9*c*RA-differentiated cells)	
	Proliferating cells	Differentiated cells	SOCE	Induction of differentiation	9*c*RA-induced differentiation	SOCE	9*c*RA-induced differentiation
STIM1	↑	↓	Down-regulates	No	No effect	Restores	Reduces
Orai1	↑	↓	Down-regulates	Yes	Enhances	Restores	Reduces
TRPC1	↓	↑	No effect	No	Reduces	-	-

Table 8.2 Summary of the results obtained from Ca^{2+} signalling studies using N-type cells in this thesis

Based on these results, a model of Ca^{2+} entry pathways in proliferating and differentiated N-type cells can be hypothesised (Figure 8.1).

In proliferating N-type cells activation of a G-protein-coupled receptor in the PM results in Ca^{2+} release from the ER via the phosphoinostide signalling pathway and in some cells via ryanodine receptors (Riddoch *et al*., 2005). Depletion of ER Ca^{2+} causes redistribution of STIM1 to ER-PM junctions where STIM1 interacts with Orai1, which forms the SOC in proliferating N-type cells, to allow extracellular Ca^{2+} to enter the cell cytosol to replenish depleted ER stores (Putney, 2009). Proliferating cells do not express TRPC1.

In differentiated N-type cells STIM1 and Orai1 are not present (or are expressed at very low levels) and TRPC1 is upregulated. Depleted ER stores are replenished through Ca^{2+} entry via a non-SOCE mechanism. The non-SOCE mechanism may constitute a diacylglycerol-activated Ca^{2+} entry pathway (Tesfai *et al.*, 2001) that has been postulated to involve members of the TRP protein family (Ma *et al.*, 2000). An alternative possibility is that the non-SOCE pathway represents a form of the arachidonic acid-activated Ca^{2+} entry pathway (Broad *et al.*, 2009) or the arachidonate-regulated Ca^{2+} current [$I_{ARC,}$ Mignen & Shuttleworth, 2000] (Luo *et al.*, 2001; Peppiatt *et al.*, 2004). In differentiated N-type cells Ca^{2+} release from the ER is propagated along neurites (Riddoch *et al*., 2007). A non-SOCE pathway provides a potential mechanism whereby more remote neuritic elements of ER can refill with Ca^{2+} in readiness for a subsequent stimulus.

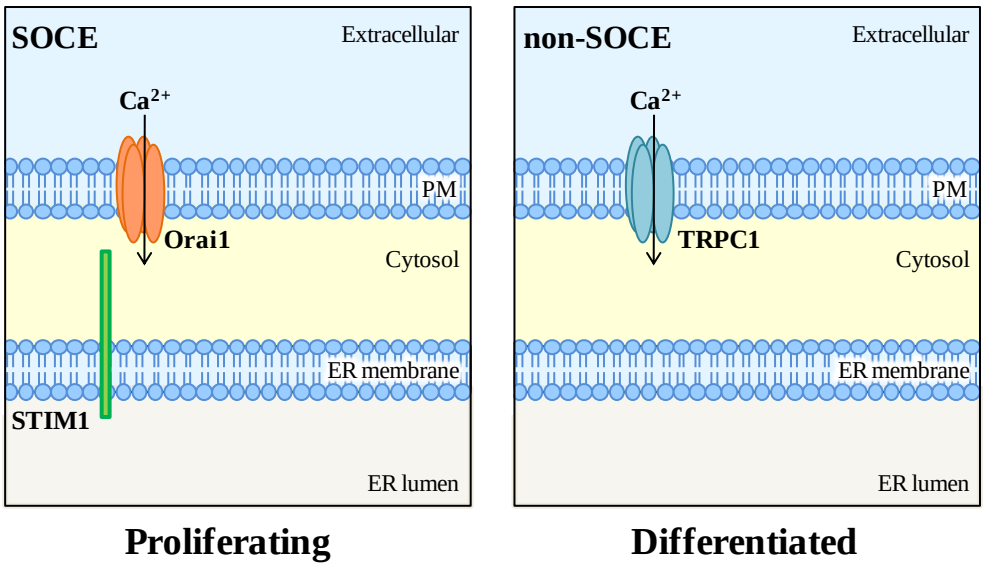

Figure 8.1 Ca^{2+} signalling and the switch from proliferation to differentiation in N-type SH-SY5Y cells

Schematic diagram showing how the results presented in this thesis contribute to the understanding of Ca^{2+} signalling in N-type SH-SY5Y cells. In proliferating cells, depletion of ER Ca^{2+} stores activates SOCE via a complex involving STIM1 in the ER membrane and Orai1 in the PM, enabling the ER to refill with Ca^{2+}. In differentiated cells STIM1 and Orai1 are down-regulated, replaced by an up-regulation of TRPC1. Depletion of ER Ca^{2+}stores activates a non-SOCE pathway via TRPC1 channels.

8.2 Future Studies

The key results from this thesis have revealed that following 7 day 9*c*RA-induced differentiation of proliferating N-type cells the expression of STIM1, Orai1 and TRPC1 are altered. Due to time constraints, the sequence of change in protein expression was not determined. Measuring the expression of these proteins throughout the 7 days of 9*c*RA treatment will be required to determine the relationship between STIM1, Orai1 and TRPC1. For example, the up-regulation of TRPC1 may precede STIM1 and Orai1 down-regulation and therefore TRPC1 may be a negative regulator of STIM1 and Orai1. This could be tested by overexpressing TRPC1 in proliferating cells and determining the effect on STIM1 and Orai1 expression, SOCE and differentiation.

Interestingly, non-SOCE (I_{ARC}) and SOCE pathways have been reported to operate in a reciprocal manner, such that in the absence of SOCE, non-SOCE becomes the predominant pathway for Ca^{2+} entry (Mignen *et al.*, 2001; Luo *et al.*, 2001; Moneer & Taylor, 2001; Peppiatt *et al.*, 2004). The notion that non-SOCE could be actively attenuated by SOCE (Mignen *et al.*, 2001; Luo *et al.*, 2001) would be consistent with an alternative protein expression profile in which STIM1 and/or Orai1 down-regulation is a driver for TRPC1 up-regulation. STIM1 has been shown to determine the function of TRPC1 (Alicia *et al.*, 2008); a decrease in STIM1 expression may therefore allow TRPC1 to increase. Orai1 has been found to mediate the interaction between STIM1 and TRPC1 (Ong *et al.*, 2007; Cheng *et al.*, 2008), perhaps down-regulation in Orai1 expression is the enabling step and this then affects STIM1 and TRPC1 expression. This would be consistent with the suggestion in this thesis that Orai1 is a negative regulator of differentiation in these cells. Ultimately there are many possible interactions between the three key Ca^{2+} signalling proteins that could result in down-regulated STIM1 and Orai1 and up-regulated TRPC1 expression. Determining these interactions and their timelines will be key to understanding the molecular mechanisms involved in the switch from proliferation to differentiation.

The increase in Bcl-2 expression observed in differentiated SH-SY5Y cells is associated with an increased resistance to apoptosis (Lasorella *et al.*, 1995). Bcl-2 expression is high in neuroblasts which show low rates of spontaneous apoptosis and low in substrate-adherent cells which show high rates of spontaneous apoptosis (Piacentini *et*

al., 1996). Overexpression of Bcl-2 has been reported to down-regulate SOCE (Pinton *et al.*, 2000; Vanden Abeele *et al.*, 2002). It will be interesting to know whether the increased expression of Bcl-2 following 9*c*RA-induced differentiation plays a role in down-regulating STIM1 and/or Orai1 in N-type cells.

8.3 Conclusion

Neuroblastoma tumours are predominantly composed of continually proliferating neuroblasts. RA induces differentiation and inhibits proliferation of neuroblastoma cells (Sidell, 1982). This effect underlies the use of RA in the treatment of neuroblastoma (Matthay *et al*., 1999, 2009; Reynolds *et al*., 2003). In the treatment of cancer, three key considerations are inhibition of proliferation, induction of differentiation and induction of apoptosis (Bergner *et al*., 2008). Understanding changes involved in the switch from proliferation to differentiation are therefore essential in the treatment of neuroblastoma as this provides further understanding of how to move proliferating cells towards a differentiated state (i.e. neurons) to enable the conversion of malignant tumours into benign tumours. The results obtained in this thesis have revealed that changes in Orai1 and TRPC1 expression are involved in the switch from proliferation to differentiation and that changes in STIM1 expression may act to stabilise the differentiated state.

In airway smooth muscle cells SOCE mediated by STIM1 and Orai1 was identified as playing a key role in proliferation. It was proposed that STIM1/Orai1 could represent a new drug target in the treatment of chronic asthma patients to attenuate proliferation and subsequent airway remodelling (Zou *et al*., 2011).

Likewise in the treatment of neuroblastoma, Orai1, STIM1 and TRPC1 could represent new drug targets in the induction of differentiation. Drugs designed to inhibit Orai1 and stimulate TRPC1 expression would promote differentiation. Furthermore inhibition of STIM1 may further help the cells retain a differentiated state. On the contrary drugs designed to stimulate Orai1 and STIM1 expression and inhibit TRPC1 expression could be used to promote differentiation if so required.

Further understanding of the relationship between these proteins as discussed (8.2 Future work) is required to reveal priority drug targets (e.g. Orai1). Certainly in the proliferating airway smooth muscle cells mentioned above a much higher increase in Orai1 mRNA than STIM1 mRNA was associated with increased proliferation (Zou *et al*., 2011).

Chapter 9

References

Abdullaev, I. F., Bisaillon, J. M., Potier, M., Gonzalez, J. C., Motiani, R. K. and Trebak, M. (2008) 'Stim1 and Orai1 mediate CRAC currents and store-operated calcium entry important for endothelial cell proliferation', *Circ Res*, 103, (11):1289-1299.

Abemayor, E. and Sidell, N. (1989) 'Human neuroblastoma cell lines as models for the in vitro study of neoplastic and neuronal cell differentiation', *Environ Health Perspect*, 80:3-15.

Acosta, S., Lavarino, C., Paris, R., Garcia, I., de Torres, C., Rodriguez, E., Beleta, H. and Mora, J. (2009) 'Comprehensive characterization of neuroblastoma cell line subtypes reveals bilineage potential similar to neural crest stem cells', *BMC Dev Biol*, 9:12.

Akhtar, R. S., Ness, J. M. and Roth, K. A. (2004) 'Bcl-2 family regulation of neuronal development and neurodegeneration', *Biochim Biophys Acta*, 1644, (2-3):189-203.

Alicia, S., Angelica, Z., Carlos, S., Alfonso, S. and Vaca, L. (2008) 'STIM1 converts TRPC1 from a receptor-operated to a store-operated channel: moving TRPC1 in and out of lipid rafts', *Cell Calcium*, 44, (5):479-491.

Ambudkar, I. S. (2007a) 'TRPC1: a core component of store-operated calcium channels', *Biochem Soc Trans*, 35, (Pt 1):96-100.

Ambudkar, I. S., Ong, H. L., Liu, X., Bandyopadhyay, B. C. and Cheng, K. T. (2007b) 'TRPC1: the link between functionally distinct store-operated calcium channels', *Cell Calcium*, 42, (2):213-223.

Aubart, F. C., Sassi, Y., Coulombe, A., Mougenot, N., Vrignaud, C., Leprince, P., Lechat, P., Lompre, A. M. and Hulot, J. S. (2009) 'RNA interference targeting STIM1 suppresses vascular smooth muscle cell proliferation and neointima formation in the rat', *Mol Ther*, 17, (3):455-462.

Baba, Y., Hayashi, K., Fujii, Y., Mizushima, A., Watarai, H., Wakamori, M., Numaga, T., Mori, Y., Iino, M., Hikida, M. and Kurosaki, T. (2006) 'Coupling of STIM1 to store-operated Ca^{2+} entry through its constitutive and inducible movement in the endoplasmic reticulum', *Proc Natl Acad Sci U S A*, 103, (45):16704-16709.

Baryshnikov, S. G., Pulina, M. V., Zulian, A., Linde, C. I. and Golovina, V. A. (2009) 'Orai1, a critical component of store-operated Ca^{2+} entry, is functionally associated with Na^{+}/Ca^{2+}

exchanger and plasma membrane Ca^{2+} pump in proliferating human arterial myocytes', *Am J Physiol Cell Physiol,* 297, (5):C1103-1112.

Bergner, A. and Huber, R. M. (2008) 'Regulation of the endoplasmic reticulum Ca^{2+}-store in cancer', *Anticancer Agents Med Chem,* 8, (7):705-709.

Berridge, M. J., Bootman, M. D. and Lipp, P. (1998) 'Calcium - a life and death signal', *Nature,* 395, (6703):645-648.

Berridge, M. J. (1998) 'Neuronal calcium signaling', *Neuron,* 21, (1):13-26.

Berridge, M., Lipp, P. and Bootman, M. (1999) 'Calcium signalling', *Curr Biol,* 9, (5):R157-159.

Berridge, M. J., Lipp, P. and Bootman, M. D. (2000) 'The versatility and universality of calcium signalling', *Nat Rev Mol Cell Biol,* 1, (1):11-21.

Berridge, M. J. (2009) 'Inositol trisphosphate and calcium signalling mechanisms', *Biochim Biophys Acta,* 1793, (6):933-940.

Bez, A., Corsini, E., Curti, D., Biggiogera, M., Colombo, A., Nicosia, R. F., Pagano, S. F. and Parati, E. A. (2003) 'Neurosphere and neurosphere-forming cells: morphological and ultrastructural characterization', *Brain Res*, 993, (1-2):18-29.

Biedler, J. L., Helson, L. and Spengler, B. A. (1973) 'Morphology and growth, tumorigenicity, and cytogenetics of human neuroblastoma cells in continuous culture', *Cancer Res,* 33, (11):2643-2652.

Biedler, J. L., Spengler, B. A., Lyser, K. M. (1975) 'Morphological Interconversion of Human Neuroblastoma Cells' *In Vitro,* 10:380

Biedler, J. L., Roffler-Tarlov, S., Schachner, M. and Freedman, L. S. (1978) 'Multiple neurotransmitter synthesis by human neuroblastoma cell lines and clones', *Cancer Res,* 38, (11 Pt 1):3751-3757.

Bootman, M. D., Collins, T. J., Peppiatt, C. M., Prothero, L. S., MacKenzie, L., De Smet, P., Travers, M., Tovey, S. C., Seo, J. T., Berridge, M. J., Ciccolini, F. and Lipp, P. (2001) 'Calcium signalling - an overview', *Semin Cell Dev Biol*, 12, (1):3-10.

Boyne, L. J., Fischer, I. and Shea, T. B. (1996) 'Role of vimentin in early stages of neuritogenesis in cultured hippocampal neurons', *Int J Dev Neurosci*, 14, (6):739-748.

Brandman, O., Liou, J., Park, W. S. and Meyer, T. (2007) 'STIM2 is a feedback regulator that stabilizes basal cytosolic and endoplasmic reticulum Ca^{2+} levels', *Cell*, 131, (7):1327-1339.

Broad, L. M., Cannon, T. R. and Taylor, C. W. (1999) 'A non-capacitative pathway activated by arachidonic acid is the major Ca^{2+} entry mechanism in rat A7r5 smooth muscle cells stimulated with low concentrations of vasopressin', *J Physiol*, 517 (Pt 1):121-134.

Brodeur, G. M. (1995) 'Molecular Basis for Heterogeneity in Human Neuroblastomas', *Eur J Cancer*, 31A (4):505-510.

Brodeur, G. M., Castleberry, R. P. (1997) 'Neuroblastoma', *Principles and Practices of Pediatric Oncology*, 3rd ed. Philadelphia, PA: Lippincott-Raven, 761-797.

Brown, A. M., Riddoch, F. C., Robson, A., Redfern, C. P. and Cheek, T. R. (2005) 'Mechanistic and functional changes in Ca^{2+} entry after retinoic acid-induced differentiation of neuroblastoma cells', *Biochem J*, 388, (Pt 3):941-948.

Calcraft, P. J., Ruas, M., Pan, Z., Cheng, X., Arredouani, A., Hao, X., Tang, J., Rietdorf, K., Teboul, L., Chuang, K. T., Lin, P., Xiao, R., Wang, C., Zhu, Y., Lin, Y., Wyatt, C. N., Parrington, J., Ma, J., Evans, A. M., Galione, A. and Zhu, M. X. (2009) 'NAADP mobilizes calcium from acidic organelles through two-pore channels', *Nature*, 459, (7246):596-600.

Cheng, K. T., Liu, X., Ong, H. L. and Ambudkar, I. S. (2008) 'Functional requirement for Orai1 in store-operated TRPC1-STIM1 channels', *J Biol Chem*, 283, (19):12935-12940.

Cheung, Y. T., Lau, W. K., Yu, M. S., Lai, C. S., Yeung, S. C., So, K. F. and Chang, R. C. (2009) 'Effects of all-trans-retinoic acid on human SH-SY5Y neuroblastoma as in vitro model in neurotoxicity research', *Neurotoxicology*, 30, (1):127-135.

Ciccarone, V., Spengler, B. A., Meyers, M. B., Biedler, J. L. and Ross, R. A. (1989) 'Phenotypic diversification in human neuroblastoma cells: expression of distinct neural crest lineages', *Cancer Res,* 49, (1):219-225.

Cotterill, S. J., Pearson, A. D., Pritchard, J., Kohler, J. A. and Foot, A. B. (2001) 'Late relapse and prognosis for neuroblastoma patients surviving 5 years or more: a report from the European Neuroblastoma Study Group "Survey"', *Med Pediatr Oncol,* 36, (1):235-238.

Darbellay, B., Arnaudeau, S., Konig, S., Jousset, H., Bader, C., Demaurex, N. and Bernheim, L. (2009) 'STIM1- and Orai1-dependent store-operated calcium entry regulates human myoblast differentiation', *J Biol Chem,* 284, (8):5370-5380.

Darbellay, B., Arnaudeau, S., Ceroni, D., Bader, C. R., Konig, S. and Bernheim, L. (2010) 'Human muscle economy myoblast differentiation and excitation-contraction coupling use the same molecular partners, STIM1 and STIM2', *J Biol Chem,* 285, (29):22437-22447.

DeHaven, W. I., Smyth, J. T., Boyles, R. R. and Putney, J. W., Jr. (2007) 'Calcium inhibition and calcium potentiation of Orai1, Orai2, and Orai3 calcium release-activated calcium channels', *J Biol Chem,* 282, (24):17548-17556.

DeHaven, W. I., Jones, B. F., Petranka, J. G., Smyth, J. T., Tomita, T., Bird, G. S. and Putney, J. W., Jr. (2009) 'TRPC channels function independently of STIM1 and Orai1', *J Physiol,* 587, (Pt 10):2275-2298.

Demaurex, N. and Frieden, M. (2003) 'Measurements of the free luminal ER Ca^{2+} concentration with targeted "cameleon" fluorescent proteins', *Cell Calcium,* 34, (2):109-119.

den Dekker, E., Molin, D. G., Breikers, G., van Oerle, R., Akkerman, J. W., van Eys, G. J. and Heemskerk, J. W. (2001) 'Expression of transient receptor potential mRNA isoforms and Ca^{2+} influx in differentiating human stem cells and platelets', *Biochim Biophys Acta,* 1539, (3):243-255.

Dubey, M., Hoda, S., Chan, W. K., Pimenta, A., Ortiz, D. D. and Shea, T. B. (2004) 'Reexpression of vimentin in differentiated neuroblastoma cells enhances elongation of axonal neurites', *J Neurosci Res,* 78, (2):245-249.

El Boustany, C., Katsogiannou, M., Delcourt, P., Dewailly, E., Prevarskaya, N., Borowiec, A. S. and Capiod, T. (2010) 'Differential roles of STIM1, STIM2 and Orai1 in the control of cell proliferation and SOCE amplitude in HEK293 cells', *Cell Calcium*, 47, (4):350-359.

Encinas, M., Iglesias, M., Liu, Y., Wang, H., Muhaisen, A., Cena, V., Gallego, C. and Comella, J. X. (2000) 'Sequential treatment of SH-SY5Y cells with retinoic acid and brain-derived neurotrophic factor gives rise to fully differentiated, neurotrophic factor-dependent, human neuron-like cells', *J Neurochem*, 75, (3):991-1003.

Feske, S., Prakriya, M., Rao, A. and Lewis, R. S. (2005) 'A severe defect in CRAC Ca^{2+} channel activation and altered K^{+} channel gating in T cells from immunodeficient patients', *J Exp Med*, 202, (5):651-662.

Feske, S., Gwack, Y., Prakriya, M., Srikanth, S., Puppel, S. H., Tanasa, B., Hogan, P. G., Lewis, R. S., Daly, M. and Rao, A. (2006) 'A mutation in Orai1 causes immune deficiency by abrogating CRAC channel function', *Nature*, 441, (7090):179-185.

Flourakis, M., Lehen'kyi, V., Beck, B., Raphael, M., Vandenberghe, M., Abeele, F. V., Roudbaraki, M., Lepage, G., Mauroy, B., Romanin, C., Shuba, Y., Skryma, R. and Prevarskaya, N. (2010) 'Orai1 contributes to the establishment of an apoptosis-resistant phenotype in prostate cancer cells', *Cell Death Dis*, 1:e75.

Gaitonde, S. V., Qi, W., Falsey, R. R., Sidell, N. and Martinez, J. D. (2001) 'Morphologic conversion of a neuroblastoma-derived cell line by E6-mediated p53 degradation', *Cell Growth Differ*, 12, (1):19-27.

Galione, A., Morgan, A. J., Arredouani, A., Davis, L. C., Rietdorf, K., Ruas, M. and Parrington, J. 'NAADP as an intracellular messenger regulating lysosomal calcium-release channels', *Biochem Soc Trans*, 38, (6):1424-1431.

Garcia, I., Martinou, I., Tsujimoto, Y. and Martinou, J. C. (1992) 'Prevention of programmed cell death of sympathetic neurons by the bcl-2 proto-oncogene', *Science*, 258, (5080):302-304.

Goodman, M. T., Gurney, J. G., Smith, M. A., Olshan, A. F. (1999) 'Sympathetic Nervous System Tumours', *National Cancer Institute, SEER Pediatric Monograph (1975-1995)*, ICCC IV:65-72.

Graham, S. J., Black, M. J., Soboloff, J., Gill, D. L., Dziadek, M. A. and Johnstone, L. S. (2009) 'Stim1, an endoplasmic reticulum Ca^{2+} sensor, negatively regulates 3T3-L1 pre-adipocyte differentiation', *Differentiation,* 77, (3):239-247.

Grynkiewicz, G., Poenie, M. and Tsien, R. Y. (1985) 'A new generation of Ca^{2+} indicators with greatly improved fluorescence properties', *J Biol Chem,* 260, (6):3440-3450.

Gurney, J. G., Smith, M. A., Ross, J. A. (1999) 'Cancer Among Infants', *National Cancer Institute, SEER Pediatric Monograph (1975-1995*), XII:149-156.

Gwack, Y., Srikanth, S., Feske, S., Cruz-Guilloty, F., Oh-hora, M., Neems, D. S., Hogan, P. G. and Rao, A. (2007) 'Biochemical and functional characterization of Orai proteins', *J Biol Chem,* 282, (22):16232-16243.

Hanada, M., Krajewski, S., Tanaka, S., Cazals-Hatem, D., Spengler, B. A., Ross, R. A., Biedler, J. L. and Reed, J. C. (1993) 'Regulation of Bcl-2 oncoprotein levels with differentiation of human neuroblastoma cells', *Cancer Res,* 53, (20):4978-4986.

Hilton, M., Middleton, G. and Davies, A. M. (1997) 'Bcl-2 influences axonal growth rate in embryonic sensory neurons', *Curr Biol,* 7, (10):798-800.

Huang, G. N., Zeng, W., Kim, J. Y., Yuan, J. P., Han, L., Muallem, S. and Worley, P. F. (2006) 'STIM1 carboxyl-terminus activates native SOC, Icrac and TRPC1 channels', *Nat Cell Biol,* 8, (9):1003-1010.

Ichikawa, J., Fukuda, Y. and Yamashita, M. (1998) 'In vitro changes in capacitative Ca^{2+} entry in neuroblastoma X glioma NG108-15 cells', *Neurosci Lett,* 246, (2):120-122.

Ishola, T. A. and Chung, D. H. (2007) 'Neuroblastoma', *Surg Oncol,* 16, (3):149-156.

Jardin, I., Lopez, J. J., Salido, G. M. and Rosado, J. A. (2008a) 'Orai1 mediates the interaction between STIM1 and hTRPC1 and regulates the mode of activation of hTRPC1-forming Ca^{2+} channels', *J Biol Chem,* 283, (37):25296-25304.

Jardin, I., Salido, G. M. and Rosado, J. A. (2008b) 'Role of lipid rafts in the interaction between hTRPC1, Orai1 and STIM1', *Channels (Austin),* 2, (6):401-403.

Jardin, I., Lopez, J. J., Redondo, P. C., Salido, G. M. and Rosado, J. A. (2009) 'Store-operated Ca^{2+} entry is sensitive to the extracellular Ca^{2+} concentration through plasma membrane STIM1', *Biochim Biophys Acta,* 1793, (10):1614-1622.

Katsetos, C. D., Herman, M. M. and Mork, S. J. (2003) 'Class III beta-tubulin in human development and cancer', *Cell Motil Cytoskeleton,* 55, (2):77-96.

Kiviluoto, S., Decuypere, J. P., De Smedt, H., Missiaen, L., Parys, J. B. and Bultynck, G. (2011) 'STIM1 as a key regulator for Ca^{2+} homeostasis in skeletal-muscle development and function', *Skelet Muscle,* 1, (1):16.

Kuang, C. Y., Yu, Y., Guo, R. W., Qian, D. H., Wang, K., Den, M. Y., Shi, Y. K. and Huang, L. (2010) 'Silencing stromal interaction molecule 1 by RNA interference inhibits the proliferation and migration of endothelial progenitor cells', *Biochem Biophys Res Commun,* 398, (2):315-320.

LaRosa, G. J. and Gudas, L. J. (1988) 'An early effect of retinoic acid: cloning of an mRNA (Era-1) exhibiting rapid and protein synthesis-independent induction during teratocarcinoma stem cell differentiation', *Proc Natl Acad Sci U S A,* 85, (2):329-333.

Lasorella, A., Iavarone, A. and Israel, M. A. (1995) 'Differentiation of neuroblastoma enhances Bcl-2 expression and induces alterations of apoptosis and drug resistance', *Cancer Res,* 55, (20):4711-4716.

Lewis, R. S. (2007) 'The molecular choreography of a store-operated calcium channel', *Nature,* 446, (7133):284-287.

Li, Z., Lu, J., Xu, P., Xie, X., Chen, L. and Xu, T. (2007) 'Mapping the interacting domains of STIM1 and Orai1 in Ca^{2+} release-activated Ca^{2+} channel activation', *J Biol Chem,* 282, (40):29448-29456.

Liao, Y., Erxleben, C., Yildirim, E., Abramowitz, J., Armstrong, D. L. and Birnbaumer, L. (2007) 'Orai proteins interact with TRPC channels and confer responsiveness to store depletion', *Proc Natl Acad Sci U S A,* 104, (11):4682-4687.

Liao, Y., Erxleben, C., Abramowitz, J., Flockerzi, V., Zhu, M. X., Armstrong, D. L. and Birnbaumer, L. (2008) 'Functional interactions among Orai1, TRPCs, and STIM1

suggest a STIM-regulated heteromeric Orai/TRPC model for SOCE/Icrac channels', *Proc Natl Acad Sci U S A*, 105, (8):2895-2900.

Liao, Y., Plummer, N. W., George, M. D., Abramowitz, J., Zhu, M. X. and Birnbaumer, L. (2009) 'A role for Orai in TRPC-mediated Ca^{2+} entry suggests that a TRPC:Orai complex may mediate store and receptor operated Ca^{2+} entry', *Proc Natl Acad Sci U S A*, 106, (9):3202-3206.

Liou, J., Kim, M. L., Heo, W. D., Jones, J. T., Myers, J. W., Ferrell, J. E., Jr. and Meyer, T. (2005) 'STIM is a Ca^{2+} sensor essential for Ca^{2+}-store-depletion-triggered Ca^{2+} influx', *Curr Biol*, 15, (13):1235-1241.

Liou, J., Fivaz, M., Inoue, T. and Meyer, T. (2007) 'Live-cell imaging reveals sequential oligomerization and local plasma membrane targeting of stromal interaction molecule 1 after Ca^{2+} store depletion', *Proc Natl Acad Sci U S A*, 104, (22):9301-9306.

Liu, X., Cheng, K. T., Bandyopadhyay, B. C., Pani, B., Dietrich, A., Paria, B. C., Swaim, W. D., Beech, D., Yildrim, E., Singh, B. B., Birnbaumer, L. and Ambudkar, I. S. (2007) 'Attenuation of store-operated Ca^{2+} current impairs salivary gland fluid secretion in TRPC1(-/-) mice', *Proc Natl Acad Sci U S A*, 104, (44):17542-17547.

Lopez, J. J., Salido, G. M., Pariente, J. A. and Rosado, J. A. (2006) 'Interaction of STIM1 with endogenously expressed human canonical TRP1 upon depletion of intracellular Ca^{2+} stores', *J Biol Chem*, 281, (38):28254-28264.

Louis, M., Zanou, N., Van Schoor, M. and Gailly, P. (2008) 'TRPC1 regulates skeletal myoblast migration and differentiation', *J Cell Sci*, 121, (Pt 23):3951-3959.

Lovat, P. E., Lowis, S. P., Pearson, A. D., Malcolm, A. J. and Redfern, C. P. (1994) 'Concentration-dependent effects of 9-cis retinoic acid on neuroblastoma differentiation and proliferation in vitro', *Neurosci Lett*, 182, (1):29-32.

Lovat, P. E., Irving, H., Malcolm, A. J., Pearson, A. D. and Redfern, C. P. (1997a) '9-cis retinoic acid - a better retinoid for the modulation of differentiation, proliferation and gene expression in human neuroblastoma', *J Neurooncol*, 31, (1-2):85-91.

Lovat, P. E., Irving, H., Annicchiarico-Petruzzelli, M., Bernassola, F., Malcolm, A. J., Pearson, A. D., Melino, G. and Redfern, C. P. (1997b) 'Retinoids in neuroblastoma therapy: distinct biological properties of 9-cis- and all-trans-retinoic acid', *Eur J Cancer,* 33, (12):2075-2080.

Luik, R. M., Wu, M. M., Buchanan, J. and Lewis, R. S. (2006) 'The elementary unit of store-operated Ca^{2+} entry: local activation of CRAC channels by STIM1 at ER-plasma membrane junctions', *J Cell Biol,* 174, (6):815-825.

Luik, R. M. and Lewis, R. S. (2007) 'New insights into the molecular mechanisms of store-operated Ca^{2+} signaling in T cells', *Trends Mol Med,* 13, (3):103-107.

Luo, D., Broad, L. M., Bird, G. S. and Putney, J. W., Jr. (2001) 'Mutual antagonism of calcium entry by capacitative and arachidonic acid-mediated calcium entry pathways', *J Biol Chem,* 276, (23):20186-20189.

Ma, H. T., Patterson, R. L., van Rossum, D. B., Birnbaumer, L., Mikoshiba, K. and Gill, D. L. (2000) 'Requirement of the inositol trisphosphate receptor for activation of store-operated Ca^{2+} channels', *Science,* 287, (5458):1647-1651.

Malathi, K., Li, X., Krizanova, O., Ondrias, K., Sperber, K., Ablamunits, V. and Jayaraman, T. (2005) 'Cdc2/cyclin B1 interacts with and modulates inositol 1,4,5-trisphosphate receptor (type 1) functions', *J Immunol,* 175, (9):6205-6210.

Manji, S. S., Parker, N. J., Williams, R. T., van Stekelenburg, L., Pearson, R. B., Dziadek, M. and Smith, P. J. (2000) 'STIM1: a novel phosphoprotein located at the cell surface', *Biochim Biophys Acta,* 1481, (1):147-155.

Maric, D., Maric, I. and Barker, J. L. (2000) 'Developmental changes in cell calcium homeostasis during neurogenesis of the embryonic rat cerebral cortex', *Cereb Cortex,* 10, (6):561-573.

Maris, J. M., Hogarty, M. D., Bagatell, R. and Cohn, S. L. (2007) 'Neuroblastoma', *Lancet,* 369, (9579):2106-2120.

Matthay, K. K., Villablanca, J. G., Seeger, R. C., Stram, D. O., Harris, R. E., Ramsay, N. K., Swift, P., Shimada, H., Black, C. T., Brodeur, G. M., Gerbing, R. B. and Reynolds, C.

P. (1999) 'Treatment of high-risk neuroblastoma with intensive chemotherapy, radiotherapy, autologous bone marrow transplantation, and 13-cis-retinoic acid. Children's Cancer Group', *N Engl J Med,* 341, (16):1165-1173.

Matthay, K. K., Reynolds, C. P., Seeger, R. C., Shimada, H., Adkins, E. S., Haas-Kogan, D., Gerbing, R. B., London, W. B. and Villablanca, J. G. (2009) 'Long-term results for children with high-risk neuroblastoma treated on a randomized trial of myeloablative therapy followed by 13-cis-retinoic acid: a children's oncology group study', *J Clin Oncol,* 27, (7):1007-1013.

Mercer, J. C., Dehaven, W. I., Smyth, J. T., Wedel, B., Boyles, R. R., Bird, G. S. and Putney, J. W., Jr. (2006) 'Large store-operated calcium selective currents due to co-expression of Orai1 or Orai2 with the intracellular calcium sensor, Stim1', *J Biol Chem,* 281, (34):24979-24990.

Merry, D. E., Veis, D. J., Hickey, W. F. and Korsmeyer, S. J. (1994) 'Bcl-2 protein expression is widespread in the developing nervous system and retained in the adult PNS', *Development,* 120, (2):301-311.

Merry, D. E. and Korsmeyer, S. J. (1997) 'Bcl-2 gene family in the nervous system', *Annu Rev Neurosci,* 20:245-267.

Mertens, A. C., Yasui, Y., Neglia, J. P., Potter, J. D., Nesbit, M. E., Jr., Ruccione, K., Smithson, W. A. and Robison, L. L. (2001) 'Late mortality experience in five-year survivors of childhood and adolescent cancer: the Childhood Cancer Survivor Study', *J Clin Oncol,* 19, (13):3163-3172.

Messi, E., Florian, M. C., Caccia, C., Zanisi, M. and Maggi, R. (2008) 'Retinoic acid reduces human neuroblastoma cell migration and invasiveness: effects on DCX, LIS1, neurofilaments-68 and vimentin expression', *BMC Cancer,* 8:30.

Mignen, O. and Shuttleworth, T. J. (2000) 'I_{ARC}, a novel arachidonate-regulated, noncapacitative Ca^{2+} entry channel', *J Biol Chem,* 275, (13):9114-9119.

Mignen, O., Thompson, J. L. and Shuttleworth, T. J. (2001) 'Reciprocal regulation of capacitative and arachidonate-regulated noncapacitative Ca^{2+} entry pathways', *J Biol Chem,* 276, (38):35676-35683.

Mignen, O., Thompson, J. L. and Shuttleworth, T. J. (2007) 'STIM1 regulates Ca^{2+} entry via arachidonate-regulated Ca^{2+}-selective (ARC) channels without store depletion or translocation to the plasma membrane', *J Physiol,* 579, (Pt 3):703-715.

Mignen, O., Thompson, J. L. and Shuttleworth, T. J. (2008a) 'Both Orai1 and Orai3 are essential components of the arachidonate-regulated Ca^{2+}-selective (ARC) channels', *J Physiol,* 586, (1):185-195.

Mignen, O., Thompson, J. L. and Shuttleworth, T. J. (2008b) 'Orai1 subunit stoichiometry of the mammalian CRAC channel pore', *J Physiol,* 586, (2):419-425.

Mignen, O., Thompson, J. L. and Shuttleworth, T. J. (2009) 'The molecular architecture of the arachidonate-regulated Ca^{2+}-selective ARC channel is a pentameric assembly of Orai1 and Orai3 subunits', *J Physiol,* 587, (Pt 17): 4181-4197.

Miller, W. H., Jr. (1998) 'The emerging role of retinoids and retinoic acid metabolism blocking agents in the treatment of cancer', *Cancer,* 83, (8):1471-1482.

Moneer, Z. and Taylor, C. W. (2002) 'Reciprocal regulation of capacitative and non-capacitative Ca^{2+} entry in A7r5 vascular smooth muscle cells: only the latter operates during receptor activation', *Biochem J,* 362, (Pt 1):13-21.

Muik, M., Frischauf, I., Derler, I., Fahrner, M., Bergsmann, J., Eder, P., Schindl, R., Hesch, C., Polzinger, B., Fritsch, R., Kahr, H., Madl, J., Gruber, H., Groschner, K. and Romanin, C. (2008) 'Dynamic coupling of the putative coiled-coil domain of ORAI1 with STIM1 mediates ORAI1 channel activation', *J Biol Chem,* 283, (12):8014-8022.

Nakagawara, A. and Ohira, M. (2004) 'Comprehensive genomics linking between neural development and cancer: neuroblastoma as a model', *Cancer Lett,* 204, (2):213-224.

Nakayama, S. and Kretsinger, R. H. (1994) 'Evolution of the EF-hand family of proteins', *Annu Rev Biophys Biomol Struct,* 23:473-507.

Ng, L. C., McCormack, M. D., Airey, J. A., Singer, C. A., Keller, P. S., Shen, X. M. and Hume, J. R. (2009) 'TRPC1 and STIM1 mediate capacitative Ca^{2+} entry in mouse pulmonary arterial smooth muscle cells', *J Physiol,* 587, (Pt 11):2429-2442.

Nicolini, G., Miloso, M., Zoia, C., Di Silvestro, A., Cavaletti, G. and Tredici, G. (1998) 'Retinoic acid differentiated SH-SY5Y human neuroblastoma cells: an in vitro model to assess drug neurotoxicity', *Anticancer Res*, 18, (4A):2477-2481.

Ong, H. L., Cheng, K. T., Liu, X., Bandyopadhyay, B. C., Paria, B. C., Soboloff, J., Pani, B., Gwack, Y., Srikanth, S., Singh, B. B., Gill, D. L. and Ambudkar, I. S. (2007) 'Dynamic assembly of TRPC1-STIM1-Orai1 ternary complex is involved in store-operated calcium influx. Evidence for similarities in store-operated and calcium release-activated calcium channel components', *J Biol Chem*, 282, (12):9105-9116.

Pahlman, S., Odelstad, L., Larsson, E., Grotte, G. and Nilsson, K. (1981) 'Phenotypic changes of human neuroblastoma cells in culture induced by 12-O-tetradecanoyl-phorbol-13-acetate', *Int J Cancer*, 28, (5):583-589.

Pahlman, S., Ruusala, A. I., Abrahamsson, L., Mattsson, M. E. and Esscher, T. (1984) 'Retinoic acid-induced differentiation of cultured human neuroblastoma cells: a comparison with phorbolester-induced differentiation', *Cell Differ*, 14, (2):135-144.

Pani, B., Ong, H. L., Liu, X., Rauser, K., Ambudkar, I. S. and Singh, B. B. (2008) 'Lipid rafts determine clustering of STIM1 in endoplasmic reticulum-plasma membrane junctions and regulation of store-operated Ca^{2+} entry (SOCE)', *J Biol Chem*, 283, (25):17333-17340.

Pani, B. and Singh, B. B. (2009a) 'Lipid rafts/caveolae as microdomains of calcium signaling', *Cell Calcium*, 45, (6):625-633.

Pani, B., Ong, H. L., Brazer, S. C., Liu, X., Rauser, K., Singh, B. B. and Ambudkar, I. S. (2009b) 'Activation of TRPC1 by STIM1 in ER-PM microdomains involves release of the channel from its scaffold caveolin-1', *Proc Natl Acad Sci U S A*, 106, (47):20087-20092.

Parekh, A. B. and Putney, J. W., Jr. (2005) 'Store-operated calcium channels', *Physiol Rev*, 85, (2):757-810.

Peinelt, C., Vig, M., Koomoa, D. L., Beck, A., Nadler, M. J., Koblan-Huberson, M., Lis, A., Fleig, A., Penner, R. and Kinet, J. P. (2006) 'Amplification of CRAC current by STIM1 and CRACM1 (Orai1)', *Nat Cell Biol*, 8, (7):771-773.

Penna, A., Demuro, A., Yeromin, A. V., Zhang, S. L., Safrina, O., Parker, I. and Cahalan, M. D. (2008) 'The CRAC channel consists of a tetramer formed by Stim-induced dimerization of Orai dimers', *Nature*, 456, (7218):116-120.

Peppiatt, C. M., Holmes, A. M., Seo, J. T., Bootman, M. D., Collins, T. J., McDonald, F. and Roderick, H. L. (2004) 'Calmidazolium and arachidonate activate a calcium entry pathway that is distinct from store-operated calcium influx in HeLa cells', *Biochem J*, 381, (Pt 3):929-939.

Piacentini, M., Piredda, L., Starace, D. T., Annicchiarico-Petruzzelli, M., Mattei, M., Oliverio, S., Farrace, M. G. and Melino, G. (1996) 'Differential growth of N- and S-type human neuroblastoma cells xenografted into scid mice. correlation with apoptosis', *J Pathol*, 180, (4):415-422.

Pinton, P., Ferrari, D., Magalhaes, P., Schulze-Osthoff, K., Di Virgilio, F., Pozzan, T. and Rizzuto, R. (2000) 'Reduced loading of intracellular Ca^{2+} stores and downregulation of capacitative Ca^{2+} influx in Bcl-2-overexpressing cells', *J Cell Biol*, 148, (5):857-862.

Ponthan, F., Borgstrom, P., Hassan, M., Wassberg, E., Redfern, C. P. and Kogner, P. (2001) 'The vitamin A analogues: 13-cis retinoic acid, 9-cis retinoic acid, and Ro 13-6307 inhibit neuroblastoma tumour growth in vivo', *Med Pediatr Oncol*, 36, (1):127-131.

Potier, M., Gonzalez, J. C., Motiani, R. K., Abdullaev, I. F., Bisaillon, J. M., Singer, H. A. and Trebak, M. (2009) 'Evidence for STIM1- and Orai1-dependent store-operated calcium influx through ICRAC in vascular smooth muscle cells: role in proliferation and migration', *FASEB J*, 23, (8):2425-2437.

Prakriya, M., Feske, S., Gwack, Y., Srikanth, S., Rao, A. and Hogan, P. G. (2006) 'Orai1 is an essential pore subunit of the CRAC channel', *Nature*, 443, (7108):230-233.

Putney, J. W., Jr. (1986) 'A model for receptor-regulated calcium entry', *Cell Calcium*, 7, (1):1-12.

Putney, J. W., Jr., Broad, L. M., Braun, F. J., Lievremont, J. P. and Bird, G. S. (2001) 'Mechanisms of capacitative calcium entry', *J Cell Sci*, 114, (Pt 12):2223-2229.

Putney, J. W. (2009) 'Capacitative calcium entry: from concept to molecules', *Immunol Rev*, 231, (1):10-22.

Redfern, C. P., Lovat, P. E., Malcolm, A. J. and Pearson, A. D. (1994) 'Differential effects of 9-cis and all-trans retinoic acid on the induction of retinoic acid receptor-beta and cellular retinoic acid-binding protein II in human neuroblastoma cells', *Biochem J*, 304 (Pt 1):147-154.

Redfern, C. P., Lovat, P. E., Malcolm, A. J. and Pearson, A. D. (1995) 'Gene expression and neuroblastoma cell differentiation in response to retinoic acid: differential effects of 9-cis and all-trans retinoic acid', *Eur J Cancer*, 31A, (4):486-494.

Reynolds, C. P., Kane, D. J., Einhorn, P. A., Matthay, K. K., Crouse, V. L., Wilbur, J. R., Shurin, S. B. and Seeger, R. C. (1991) 'Response of neuroblastoma to retinoic acid in vitro and in vivo', *Prog Clin Biol Res*, 366:203-211.

Reynolds, C. P., Wang, Y., Melton, L. J., Einhorn, P. A., Slamon, D. J. and Maurer, B. J. (2000) 'Retinoic-acid-resistant neuroblastoma cell lines show altered MYC regulation and high sensitivity to fenretinide', *Med Pediatr Oncol*, 35, (6):597-602.

Reynolds, C. P., Matthay, K. K., Villablanca, J. G. and Maurer, B. J. (2003) 'Retinoid therapy of high-risk neuroblastoma', *Cancer Lett*, 197, (1-2):185-192.

Riddoch, F. C., Rowbotham, S. E., Brown, A. M., Redfern, C. P. and Cheek, T. R. (2005) 'Release and sequestration of Ca^{2+} by a caffeine- and ryanodine-sensitive store in a sub-population of human SH-SY5Y neuroblastoma cells', *Cell Calcium*, 38, (2):111-120.

Riddoch, F. C., Brown, A. M., Rowbotham, S. E., Redfern, C. P. and Cheek, T. R. (2007) 'Changes in functional properties of the caffeine-sensitive Ca^{2+} store during differentiation of human SH-SY5Y neuroblastoma cells', *Cell Calcium*, 41, (3):195-206.

Roos, J., DiGregorio, P. J., Yeromin, A. V., Ohlsen, K., Lioudyno, M., Zhang, S., Safrina, O., Kozak, J. A., Wagner, S. L., Cahalan, M. D., Velicelebi, G. and Stauderman, K. A. (2005) 'STIM1, an essential and conserved component of store-operated Ca^{2+} channel function', *J Cell Biol*, 169, (3):435-445.

Ross, R. A., Spengler, B. A. and Biedler, J. L. (1983) 'Coordinate morphological and biochemical interconversion of human neuroblastoma cells', *J Natl Cancer Inst,* 71, (4):741-747.

Ross, R. A., Spengler, B. A., Domenech, C., Porubcin, M., Rettig, W. J. and Biedler, J. L. (1995) 'Human neuroblastoma I-type cells are malignant neural crest stem cells', *Cell Growth Differ,* 6, (4):449-456.

Ross, R. A., Biedler, J. L. and Spengler, B. A. (2003) 'A role for distinct cell types in determining malignancy in human neuroblastoma cell lines and tumors', *Cancer Lett,* 197, (1-2):35-39.

Ross, R. A. and Spengler, B. A. (2007) 'Human neuroblastoma stem cells', *Semin Cancer Biol,* 17, (3):241-247.

Sakaki, Y., Sugioka, M., Fukuda, Y. and Yamashita, M. (1997) 'Capacitative Ca^{2+} influx in the neural retina of chick embryo', *J Neurobiol,* 32, (1):62-68.

Shea, T. B., Beermann, M. L. and Fischer, I. (1993) 'Transient requirement for vimentin in neuritogenesis: intracellular delivery of anti-vimentin antibodies and antisense oligonucleotides inhibit neurite initiation but not elongation of existing neurites in neuroblastoma', *J Neurosci Res,* 36, (1):66-76.

Shi, Y., Song, M., Guo, R., Wang, H., Gao, P., Shi, W. and Huang, L. (2010) 'Knockdown of stromal interaction molecule 1 attenuates hepatocyte growth factor-induced endothelial progenitor cell proliferation', *Exp Biol Med (Maywood),* 235, (3):317-325.

Shuttleworth, T. J. 'STIM and Orai proteins and the non-capacitative ARC channels', *Front Biosci,* 17: 847-860.

Sidell, N. (1982) 'Retinoic acid-induced growth inhibition and morphologic differentiation of human neuroblastoma cells in vitro', *J Natl Cancer Inst,* 68, (4):589-596.

Sidell, N., Sarafian, T., Kelly, M., Tsuchida, T. and Haussler, M. (1986) 'Retinoic acid-induced differentiation of human neuroblastoma: a cell variant system showing two distinct responses', *Exp Cell Biol,* 54, (5-6):287-300.

Slack, R., Lach, B., Gregor, A., al-Mazidi, H. and Proulx, P. (1992) 'Retinoic acid- and staurosporine-induced bidirectional differentiation of human neuroblastoma cell lines', *Exp Cell Res*, 202, (1):17-27.

Soboloff, J., Spassova, M. A., Hewavitharana, T., He, L. P., Xu, W., Johnstone, L. S., Dziadek, M. A. and Gill, D. L. (2006a) 'STIM2 is an inhibitor of STIM1-mediated store-operated Ca^{2+} Entry', *Curr Biol*, 16, (14):1465-1470.

Soboloff, J., Spassova, M. A., Tang, X. D., Hewavitharana, T., Xu, W. and Gill, D. L. (2006b) 'Orai1 and STIM reconstitute store-operated calcium channel function', *J Biol Chem*, 281, (30):20661-20665.

Spassova, M. A., Soboloff, J., He, L. P., Xu, W., Dziadek, M. A. and Gill, D. L. (2006) 'STIM1 has a plasma membrane role in the activation of store-operated Ca^{2+} channels', *Proc Natl Acad Sci U S A*, 103, (11):4040-4045.

Stathopulos, P. B., Li, G. Y., Plevin, M. J., Ames, J. B. and Ikura, M. (2006) 'Stored Ca^{2+} depletion-induced oligomerization of stromal interaction molecule 1 (STIM1) via the EF-SAM region: An initiation mechanism for capacitive Ca^{2+} entry', *J Biol Chem*, 281, (47):35855-35862.

Stathopulos, P. B., Zheng, L., Li, G. Y., Plevin, M. J. and Ikura, M. (2008) 'Structural and mechanistic insights into STIM1-mediated initiation of store-operated calcium entry', *Cell*, 135, (1):110-122.

Tesfai, Y., Brereton, H. M. and Barritt, G. J. (2001) 'A diacylglycerol-activated Ca^{2+} channel in PC12 cells (an adrenal chromaffin cell line) correlates with expression of the TRP-6 (transient receptor potential) protein', *Biochem J*, 358, (Pt 3):717-726.

Tsokos, M., Scarpa, S., Ross, R. A. and Triche, T. J. (1987) 'Differentiation of human neuroblastoma recapitulates neural crest development. Study of morphology, neurotransmitter enzymes, and extracellular matrix proteins', *Am J Pathol*, 128, (3): 484-496.

Vanden Abeele, F., Skryma, R., Shuba, Y., Van Coppenolle, F., Slomianny, C., Roudbaraki, M., Mauroy, B., Wuytack, F. and Prevarskaya, N. (2002) 'Bcl-2-dependent modulation of

Ca^{2+} homeostasis and store-operated channels in prostate cancer cells', *Cancer Cell*, 1, (2):169-179.

Vig, M., Peinelt, C., Beck, A., Koomoa, D. L., Rabah, D., Koblan-Huberson, M., Kraft, S., Turner, H., Fleig, A., Penner, R. and Kinet, J. P. (2006a) 'CRACM1 is a plasma membrane protein essential for store-operated Ca^{2+} entry', *Science*, 312, (5777):1220-1223.

Vig, M., Beck, A., Billingsley, J. M., Lis, A., Parvez, S., Peinelt, C., Koomoa, D. L., Soboloff, J., Gill, D. L., Fleig, A., Kinet, J. P. and Penner, R. (2006b) 'CRACM1 multimers form the ion-selective pore of the CRAC channel', *Curr Biol*, 16, (20):2073-2079.

Walton, J. D., Kattan, D. R., Thomas, S. K., Spengler, B. A., Guo, H. F., Biedler, J. L., Cheung, N. K. and Ross, R. A. (2004) 'Characteristics of stem cells from human neuroblastoma cell lines and in tumors', *Neoplasia*, 6, (6):838-845.

Wessel, D. and Flugge, U. I. (1984) 'A method for the quantitative recovery of protein in dilute solution in the presence of detergents and lipids', *Anal Biochem*, 138, (1):141-143.

Williams, R. T., Manji, S. S., Parker, N. J., Hancock, M. S., Van Stekelenburg, L., Eid, J. P., Senior, P. V., Kazenwadel, J. S., Shandala, T., Saint, R., Smith, P. J. and Dziadek, M. A. (2001) 'Identification and characterization of the STIM (stromal interaction molecule) gene family: coding for a novel class of transmembrane proteins', *Biochem J*, 357, (Pt 3):673-685.

Williams, R. T., Senior, P. V., Van Stekelenburg, L., Layton, J. E., Smith, P. J. and Dziadek, M. A. (2002) 'Stromal interaction molecule 1 (STIM1), a transmembrane protein with growth suppressor activity, contains an extracellular SAM domain modified by N-linked glycosylation', *Biochim Biophys Acta*, 1596, (1):131-137.

Wu, M. M., Buchanan, J., Luik, R. M. and Lewis, R. S. (2006) 'Ca^{2+} store depletion causes STIM1 to accumulate in ER regions closely associated with the plasma membrane', *J Cell Biol*, 174, (6):803-13.

Wu, X., Zagranichnaya, T. K., Gurda, G. T., Eves, E. M. and Villereal, M. L. (2004) 'A TRPC1/TRPC3-mediated increase in store-operated calcium entry is required for

differentiation of H19-7 hippocampal neuronal cells', *J Biol Chem,* 279, (42):43392-43402.

Yabe, J. T., Chan, W. K., Wang, F. S., Pimenta, A., Ortiz, D. D. and Shea, T. B. (2003) 'Regulation of the transition from vimentin to neurofilaments during neuronal differentiation', *Cell Motil Cytoskeleton,* 56, (3):193-205.

Yamashita, M., Navarro-Borelly, L., McNally, B. A. and Prakriya, M. (2007) 'Orai1 mutations alter ion permeation and Ca^{2+}-dependent fast inactivation of CRAC channels: evidence for coupling of permeation and gating', *J Gen Physiol,* 130, (5):525-540.

Yeromin, A. V., Zhang, S. L., Jiang, W., Yu, Y., Safrina, O. and Cahalan, M. D. (2006) 'Molecular identification of the CRAC channel by altered ion selectivity in a mutant of Orai', *Nature,* 443, (7108):226-229.

Yuan, J. P., Zeng, W., Huang, G. N., Worley, P. F. and Muallem, S. (2007) 'STIM1 heteromultimerizes TRPC channels to determine their function as store-operated channels', *Nat Cell Biol,* 9, (6):636-645.

Zeng, W., Yuan, J. P., Kim, M. S., Choi, Y. J., Huang, G. N., Worley, P. F. and Muallem, S. (2008) 'STIM1 gates TRPC channels, but not Orai1, by electrostatic interaction', *Mol Cell,* 32, (3):439-448.

Zhang, S. L., Yeromin, A. V., Zhang, X. H., Yu, Y., Safrina, O., Penna, A., Roos, J., Stauderman, K. A. and Cahalan, M. D. (2006) 'Genome-wide RNAi screen of Ca^{2+} influx identifies genes that regulate Ca^{2+} release-activated Ca^{2+} channel activity', *Proc Natl Acad Sci U S A,* 103, (24):9357-9362.

Zhang, S. L., Yu, Y., Roos, J., Kozak, J. A., Deerinck, T. J., Ellisman, M. H., Stauderman, K. A. and Cahalan, M. D. (2005) 'STIM1 is a Ca^{2+} sensor that activates CRAC channels and migrates from the Ca^{2+} store to the plasma membrane', *Nature,* 437, (7060):902-905.

Zhang, S. L., Kozak, J. A., Jiang, W., Yeromin, A. V., Chen, J., Yu, Y., Penna, A., Shen, W., Chi, V. and Cahalan, M. D. (2008) 'Store-dependent and -independent modes regulating Ca^{2+} release-activated Ca^{2+} channel activity of human Orai1 and Orai3', *J Biol Chem,* 283, (25):17662-17671.

Zhang, W., Meng, H., Li, Z. H., Shu, Z., Ma, X. and Zhang, B. X. (2007) 'Regulation of STIM1, store-operated Ca^{2+} influx, and nitric oxide generation by retinoic acid in rat mesangial cells', *Am J Physiol Renal Physiol*, 292, (3):F1054-1064.

Zheng, L., Stathopulos, P. B., Li, G. Y. and Ikura, M. (2008) 'Biophysical characterization of the EF-hand and SAM domain containing Ca^{2+} sensory region of STIM1 and STIM2', *Biochem Biophys Res Commun*, 369, (1):240-246.

Zheng, L., Stathopulos, P. B., Schindl, R., Li, G. Y., Romanin, C. and Ikura, M. 'Auto-inhibitory role of the EF-SAM domain of STIM proteins in store-operated calcium entry', *Proc Natl Acad Sci U S A*, 108, (4):1337-1342.

Zhou, Y., Lewis, T. L., Robinson, L. J., Brundage, K. M., Schafer, R., Martin, K. H., Blair, H. C., Soboloff, J. and Barnett, J. B. (2011) 'The role of calcium release activated calcium channels in osteoclast differentiation', *J Cell Physiol*, 226, (4):1082-1089.

Zhu, M. X., Ma, J., Parrington, J., Calcraft, P. J., Galione, A. and Evans, A. M. 'Calcium signaling via two-pore channels: local or global, that is the question', *Am J Physiol Cell Physiol*, 298, (3):C430-441.

Zou, J. J., Gao, Y. D., Geng, S. and Yang, J. (2011) 'Role of STIM1/Orai1-mediated store-operated Ca^{2+} entry in airway smooth muscle cell proliferation', *J Appl Physiol*, 110, (5):1256-1263.